UNIVERSITÀ DEGLI STUDI DI MILANO

Scuola di Dottorato in Scienze Biologiche e Molecolari

XXIV Ciclo

Bypass of UV-induced DNA lesions in *Saccharomyces cerevisiae:* experimental analysis and "*in silico*" modeling

Flavio Amara

PhD Thesis

Scientific tutors: Prof. Paolo Plevani

Prof. Marco Muzi-Falconi

Dott. Daniela Besozzi

Academic Year 2011-2012

SSD: BIO/11

Thesis performed at the ex Department of Biomolecular Sciences and Biotechnology now Department of Biosciences of the University of Milan. In collaboration with the University of Milano Bicocca, the IGM-CNR of Pavia and the Centre for computational and Systems Biology (CoSBi) of Trento.

Index

List of frequently used abbreviations

DDR: DNA Damage Response

NER: Nucleotide Excision Repair

PRR: Post-Replication Repair

DDT: DNA Damage Tolerance

TS: Template Switching

TLS: Translesion DNA Synthesis

CPD: Cyclobutane Pyrimidine Dimer

6-4 PP: 6-4 Photoproduct or 6-4 Pyrimidine-Pyrimidone

PART I

ABSTRACT

My research activity has been supported by the bioinformatic platform of the Fondazione Cariplo NOBEL Project named "Understanding DNA damage checkpoint and repair". The aim of this platform was to investigate the molecular mechanisms involved in the DNA Damage Response (DDR), through a Systems Biology approach.

Among the DDR pathways, the focus of my research was the DNA Damage Tolerance (DDT) pathway called Post-Replication Repair (PRR) using *Saccharomyces cerevisiae* cells as a model system. This pathway leads to the bypass of UV-induced DNA lesions through a mechanism, which is poorly characterized at molecular level in comparison with the Nucleotide Excision Repair (NER) process, the mechanism leading to the effective repair of UV-induces DNA lesions. The data presented in this thesis led to the production of the first mathematical model of PRR in eukaryotic cells.

In the work carried out in this thesis I had the difficult task to manage both *in silico* and *in vivo* aspects of a Systems Biology project. Given the complexity of the PRR pathway and the lack of critical experimental data, the attempt to build a mathematical model of PRR was an ambitious aim not free from difficulties.

Before this study, the crosstalk between PRR and other DDR pathways were unknown and, indeed, the discrepancy between the *in vivo* data and the *in silico* simulations, observed under certain experimental conditions, led to additional experiments that uncovered new unpublished aspects of PRR and others that need to be done.

Abstract

In this way the so called “Circle of Systems Biology” applied to PRR can be considered closed and promising for the future: the limit of the model to particular experimental conditions is leading to a new batch of experiments to do and new hypothesis to test.

STATE OF THE ART

UV-induced DNA damage

Sun radiation is one of the elements, which allowed and continues to support life on the earth. However, its energy is so strong that we can easily identify a second essential element for life in our planet: the ozonosphere, a layer of ozone enveloping earth in the stratosphere, which is absorbing part of this energy. Life on earth depends upon a sort of equilibrium between sun radiation and its protection by the ozone layer. This layer is subjected to periodic reduction, but since the half of the seventies we know that this reduction is increasing because of the increase of Chloro Fluoro Carbon (CFC) gases in the atmosphere. The reduction of the ozone layer is decreasing the shielding against sun radiation, which ranges from infrared to ultraviolet (UV) wavelength (3000 to 100 nm, respectively). Inside the UV region three sub-regions can be distinguished: the UV-A (400-315 nm), the UV-B (315-280 nm) and the UV-C (280-100 nm).

The physiological relevance of this project arises from the damaging effects of UV radiations present particularly in the lower region of the spectrum. UV radiations act on biologic materials, in particular DNA, so enhancing mutagenesis, affecting genome stability in living organisms and, ultimately, they increase cancerogenesis in human skin.

UV radiations cause covalent DNA modifications, such as Cyclobutane Pyrimidine Dimers (CPDs) and 6-4 photoproducts (6-4 PPs). CPDs are usually the most abundant lesions: the CPDs: 6-4 PPs ratio is on average about 3:1 (Friedberg et al., 2005), however, it may change in different

organisms. Moreover, 6-4 PPs can be converted into their Dewar isomers by sunlight induced photo-isomerization (Taylor and Cohrs, 1987; Taylor et al., 1990) and the carcinogenicity of the last UV-induced DNA lesion on human cells is still under investigation.

The level of CPDs/Kbp of DNA has been calculated for UV-A, UV-B and UV-C: the first relevant aspect of these studies was the linearity between the UV dose and the number of UV-induced lesions on DNA. It was discovered that UV-C radiations were about 100 times more effective than UV-B and 100000 more effective than UV-A in inducing CPDs on DNA (Kuluncsics et al., 1999). The physiological DNA damage caused by shielded sunlight (which is a mixture of about 6% UV-A, 0.8% UV-B, 44.5% visible light, 48.7% infrared and no UV-C) could be due only to UV-B (Kuluncsics et al., 1999). Most of the experimental data on the effects of UV radiations produced during the last 20-30 years (including those published by my lab) made use of 254 nm UV-C germicidal lamps to irradiate various types of living cells. Only very recently, some labs are trying to more directly test the effect of sunlight on the DDR by irradiating cells with low acute or chronic UV-C doses, or by using shielded UV-B lamps.

In the experiments described in this thesis, I used low acute or high acute UV-C irradiation, and preliminary dose-response set up experiments established that the threshold (minimal UV dose) to monitor the biological readout of my system, namely PCNA ubiquitylation, was an UV dose of 5 J/m^2; therefore all the experiments carried out in this thesis have been performed at UV doses $\geq$ of 5 J/m^2 (see main results of the thesis at page 44).

Inside the chemistry of UV-induced DNA lesions

In the case of CPDs, UV radiations induce photochemical reactions, which modify two adjacent pyrimidines. One CPD contains a four carbon ring coming from the covalent bond between the carbons in positions 5 and 6 (Fig. 1). These dimers can theoretically form with the configurations cis-syn, cys-anti, trans-syn, trans-anti; however, CPDs exist mainly in the cys-syn form (Friedberg et al., 2005). A 6-4 PP, also called 6-4 pyrimidine-pyrimidone, links the C6 position of the 5' pyrimidine in an adjacent pair to the C4 position of the 3' pyrimidine, (Friedberg et al., 2005), (Fig. 1).

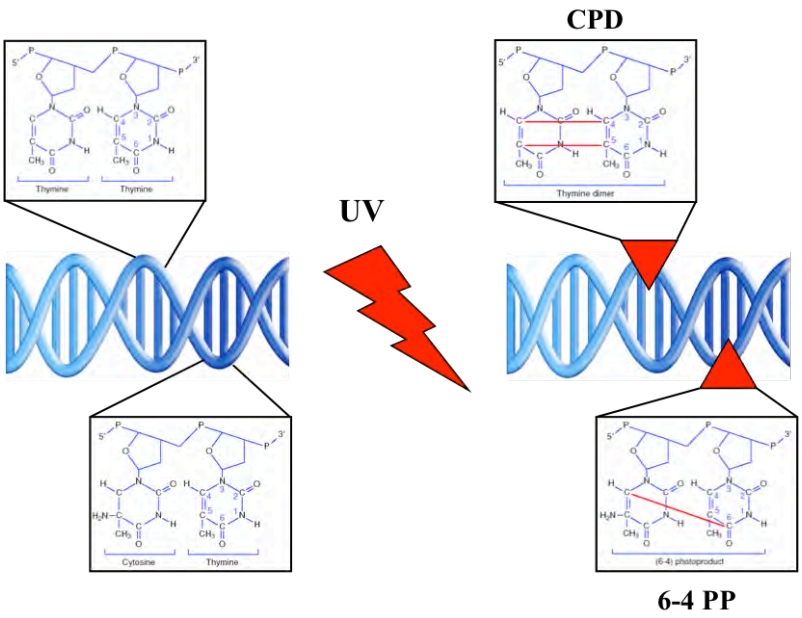

Fig. 1. The chemistry of UV-induced CPDs and 6-4 PPs.

These modifications produce distortions in the DNA helix. Most of the UV-induced lesions are sensed by cells and repaired through the activity of an efficient repair pathway, called NER. Cells respond to these lesions in a complex way, generally called DDR, that includes sensing, signaling/checkpoint, repair and/or bypass. In the next paragraphs, I will briefly discuss each aspect of DDR in *S.cerevisiae*, with a particular emphasis on UV lesions bypass, because it represents the focus of my research. I would like to stress that the mechanisms I am going to described are not limited to yeast cells, but are extremely conserved in all eukaryotic organisms from yeast to human.

Sensing and repair of UV-induced DNA lesions

In *S.cerevisiae* and higher eukaryotes, CPDs and 6-4 PPs are repaired by essentially the same mechanism called NER (McCready and Cox, 1992) (Fig. 2), although with different kinetics. Indeed, 6-4 PPs, which are more cytotoxic are removed more rapidly than CPDs (McCready and Cox, 1992).

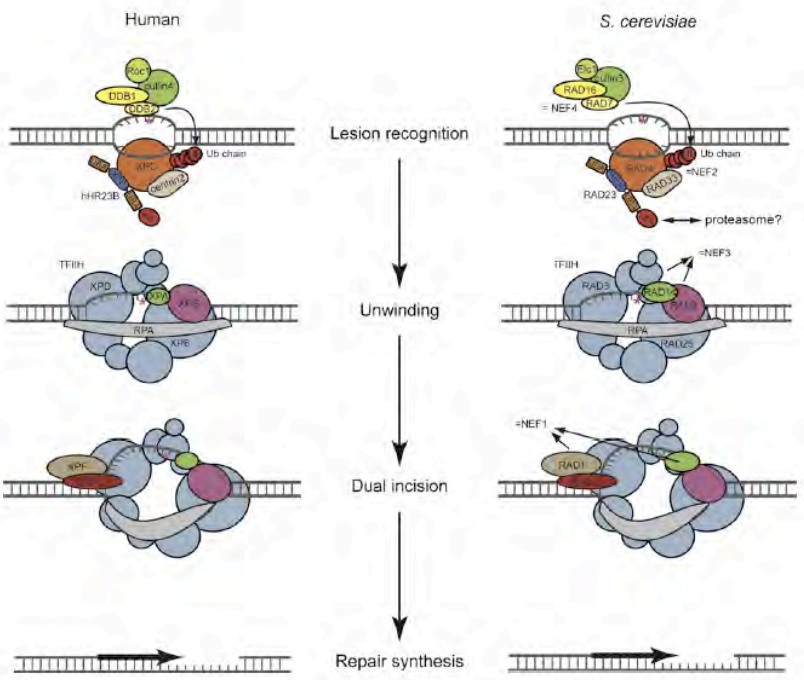

Fig. 2. The NER pathway is highly conserved between human and budding yeast (Dantuma et al., 2009).

The NER senses UV lesions and based on the physical location of the lesions on the genome, it can be divided into two sub-pathways: the Transcription Coupled NER (TC-NER), acts on lesions present on

actively transcribed regions of the genome, while the Global Genome NER (GG-NER), acts predominantly on t he untranscribed part of the genome (Friedberg et al., 2005). Once the lesion is sensed, a pre-incision complex is assembled at the damage site. Next, asymmetric endonucleolytic incisions 5' and 3' from the lesion in combination with a helicase activity produces a short single stranded DNA (ssDNA) gap of ~ 30 nucleotides (nts) covered by Replication Protein A (RPA); this gap is then rapidly refilled through the activity of DNA polymerases (about 3700 nts/min) (Morin et al., 2008; Novarina et al., 2010).

The molecular mechanism of NER is the same across the cell cycle, but its modulation and/or its downstream effect may change from one cell cycle phase to another and, partially, from one organism to another.

For example, in non cycling budding yeast cells, irradiation with medium/high UV doses and the subsequent production of ssDNA gaps trigger the activation of DNA damage checkpoint, because these gaps fail to be quickly refilled through repair synthesis (Novarina et al., 2010). This checkpoint stops or slows down cell cycle progression till UV-induced DNA lesions are completely removed from the genome, ensuring genome integrity (Lazzaro et al., 2009). It is important to highlight that in G_1 or G_2 arrested wild-type yeast cells the DNA damage checkpoint is not activated at UV doses from 5 to 10 J/m^2 (Giannattasio et al., 2010), likely because a low level of UV-induced DNA lesions in the genome are efficiently repaired, if NER is working properly. However, the presence of cells, which actively replicate DNA in a logarithmically growing cell population, makes it sensitive to UV-induced DNA damage, even at lower UV doses. Indeed, the Mec1/Rad53-dependent DNA damage

checkpoint is just activated when cycling budding yeast cells are UV irradiated with 4, 5, 10 J/m^2 (Fig. 3).

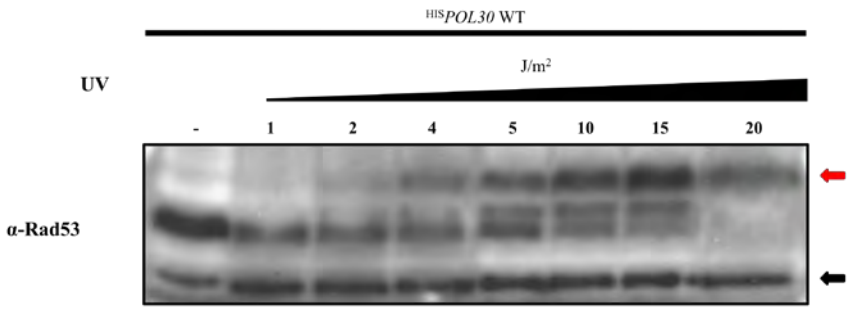

Fig. 3. Checkpoint activation in logarithmically growing wild-type yeast cells. Dose-response curve after low acute UV irradiation. Cells were UV irradiated, collected 30' after UV irradiation and subjected to TCA protein extraction, SDS-Page and western blot as published in Giannattasio et al., 2004. The red arrow indicates the position of the hyperphosphorylated low migrating Rad53 protein, which represents the biochemical readout of the activation of the DNA damage checkpoint. The black arrow indicates an aspecific band used as a loading control.

In G_1 and G_2 arrested cells the UV damaged genome is "static", thus it can be easily "cut and repaired" by NER and DNA synthesis. Conversely in logarithmically growing yeast cells, many of them are in S phase, where the DNA is replicated through the activation of ~ 228 replicons (Nieduszynski et al., 2006) theoretically acting at the same time. When a replication fork hits an UV-induced DNA lesion on the DNA template, it stalls because replicative DNA polymerases (Pol-δ for the lagging strand and Pol-ε for the leading strand) are unable to incorporate any nucleotide in front of such a kind of DNA lesion. Moreover, the NER activity near a moving replication fork could be dangerous because DNA incisions by NER coupled to incoming DNA synthesis may generate Double Strand Breaks (DSBs) on the genome (Ulrich and Walden, 2010), which are

potentially lethal for the cell if not repaired (Sandell and Zakian, 1993). An alternative solution to avoid replication fork collapse after stalling is the bypass of the UV-induced DNA lesions through PRR.

Bypass of UV-induced DNA lesions

The bypass of UV-induced DNA lesions (but also of lesions caused by other DNA damaging agents) is carried out by the PRR pathway. In budding yeast, this pathway is also known as the *RAD6* epistasis group. Members of this group are the genes coding for the following proteins: Rad6, Rad5, Mms2, Ubc13, Rad30, Rev1, Rev3, Rev7, and Srs2. These proteins include:

- two Ubiquitin conjugating enzymes (E2), Rad6 and Ubc13
- one Ubiquitin conjugating enzyme variant (UEV), Mms2
- two Ubiquitin ligases (E3), Rad18 and Rad5
- three Translesion DNA polymerases, Pol-η (Rad30) and Rev1, belonging to the Y family of polymerases; Pol-ζ, formed by the Rev3 and Rev7 subunits and belonging to the B family of polymerases; Rev1 can act as an adaptor for Pol-ζ.
- One anti-recombinogenic DNA helicase, Srs2.

The Proliferating Cell Nuclear Antigen (PCNA)

All the above listed proteins physically and/or functionally interact with the master regulator of PRR: PCNA (codified in budding yeast by the *POL30* gene).

PCNA is a ring-like protein discovered in 1985 and involved in essentially all DNA transactions, including DNA replication, Mismatch Repair (MMR), Base Excision Repair (BER), NER, prevention of re-replication, prevention of sister chromatid recombination, chromatin assembly, sister chromatid cohesion, transcription, cell cycle control and

survival (Moldovan et al., 2007). In eukaryotic cells the functional PCNA is a homo-trimer of 780 aminoacids (aa) with two domains/subunit. It belongs to the structurally and functionally conserved DNA sliding clamps family. Despite the low level of aa sequence conservation among the members of this family, PCNA shows an extremely conserved 3D structure (Krishna et al., 1994). These clamps form RING shaped complexes with pseudo esaedric symmetry when they encircle DNA. PCNA monomers have two globular domains linked by a long flexible loop called inter-domain connecting loop and they are not covalently bound through a head-tail orientation (Fig. 4).

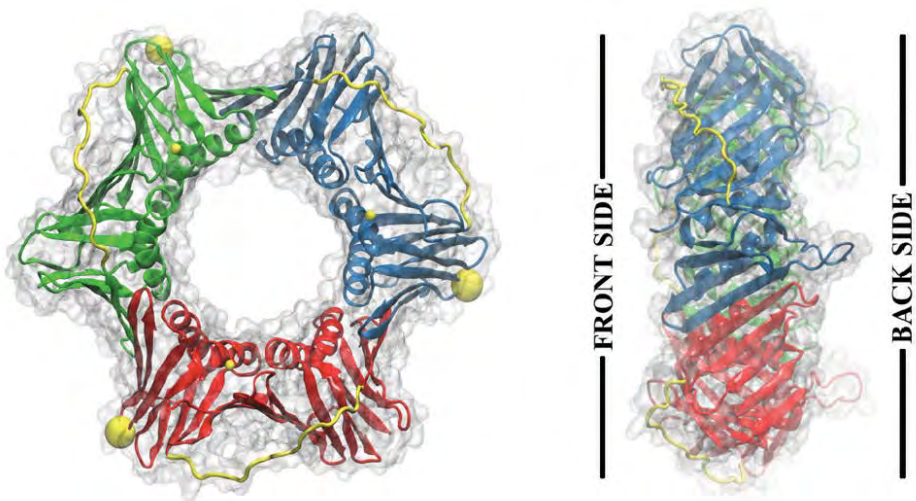

Fig. 4. Front (left) and side (right) views of PCNA: the three monomers are coloured in red, green and blue; the inter-domain connecting loop is coloured in yellow, and lysines 164 are designed with big yellow balls (Stoimenov and Helleday, 2009).

PCNA is loaded onto DNA through the action of the Replication Factor C (RFC) complex (Majka and Burgers, 2004). Briefly, PCNA forms a stable complex with RFC and one molecule of ATP; the binding of PCNA with

DNA causes the hydrolysis of ATP and the release of RFC (Gomes and Burgers 2001; Yao et al., 2006; Chen et al., 2009). RFC binds PCNA on the so called "C side" (the region where are localized the C-terminal domains of the three monomers) and it loads this region pointing the 3' end of DNA. This particular orientation ensures that DNA polymerases, which bind the C side, are correctly oriented on the growing end of the DNA. The binding of DNA polymerases on the C side of PCNA increases thousand times their processivity. The C side is also the region where PCNA interacts with most of its partners, through the so called PCNA-Interaction Protein box or PIP domain, an evolutionary conserved region found in all PCNA interacting proteins (Fig. 5).

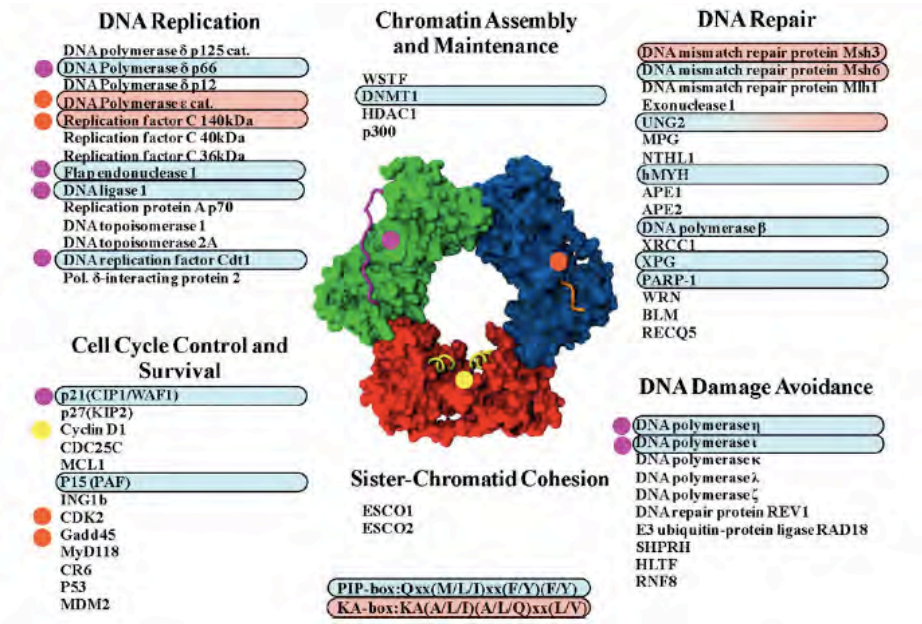

Fig. 5. PCNA interacting proteins. Characteristic interfaces on PCNA are emphasized: inter-domain connecting loop (purple), C-terminal tail (orange) and inner α-helices (yellow). Different interacting proteins are grouped by function, their PCNA-interactive domains are denoted by coloured boxes, and the respective PCNA interface (if known) is presented as a coloured circle (Stoimenov and Helleday, 2009).

Since all the PCNA partners containing the PIP domain interact with the C side of PCNA the binding of these factors is usually competitive and mutually exclusive on t he same subunit; however, because functional PCNA has a homo-trimeric structure, we cannot exclude that different partners are able to bind PCNA at the same time, on different subunits.

Enzymology of the *RAD6* epistasis group

All the members of the *RAD6* epistasis group can be further divided into two sub-classes:

- PCNA modifiers: Rad6, Ubc13, Mms2, Rad18 and Rad5. These proteins act upstream the UV-induced DNA lesion bypass, as soon as the replication fork stalls. These proteins post-translationally modify PCNA through the covalent binding of ubiquitin moieties (a process called ubiquitylation) to make it proficient for the binding of the members of the next sub-class.

- Bypass effectors/regulators: Pol-η, Rev1, Pol-ζ and Srs2. The binding of these proteins to PCNA occurs after its ubiquitylation and they regulate the mechanisms involved in bypassing UV-induced DNA lesions. This class of proteins is likely to be incomplete, since other effectors of ubiquitylated PCNA remain to be characterized. For example, Mgs1 was identified as a probable member of this class of proteins in a very recent study (Saugar et al., 2012).

Rad6 and Rad18

The *RAD6* and *RAD18* genes were identified in a screening for UV sensitive mutants in *S.cerevisiae* (Cox and Parry, 1968). Further analysis highlighted that yeast strains carrying deletions of these genes show an increase in spontaneous mutagenesis and a decrease in UV induced mutagenesis (Lawrence and Christensen 1976; Armstrong et al., 1994). The Rad6 protein is one of the 13 E2 enzymes in budding yeast and it is involved in many cellular processes, such as PRR, induced mutagenesis, sporulation, silencing and N-end rule protein degradation (Raboy et al., 1999). Rad6 receives the activated ubiquitin moiety from the unique ubiquitin-activating enzyme (E1) Uba1 and transfers it to the target protein through an E3 ubiquitin ligase, which provides the target specificity. During post-replicative repair, the E3 ubiquitin ligase for PCNA is Rad18 (Hibbert et al., 2011).

Rad18 is a RING finger E3 enzyme with ATPase activity and ssDNA binding properties (Bailly et al., 1997). Deletions of *RAD6* or *RAD18* causes sensitivity not only to UV irradiation, but also to X-rays, γ-rays, alkylating agents like Methyl Metan Sulphonate (MMS), UV mimetic drugs like 4-Nitro Quinoline Oxide (4-NQO), anti-tumoral drugs (DNA damaging agents) like Bleomicin and Cysplatin.

Co-immunoprecipitation experiments showed that Rad6 and Rad18 are able to form stable dimer of hetero-dimers (Bailly et al., 1994; Bailly et al., 1997; Notenboom et al., 2007). Even if Rad18 has intrinsic ssDNA binding properties, its localization at the level of stalled replication forks requires interaction with RPA (Davies et al., 2008); therefore, both DNA damage checkpoint and PRR share the same activating substrate, namely RPA-coated ssDNA. The presence of Rad18 at the level of a s talled

replication fork targets Rad6, carrying an active ubiquitin moiety, on PCNA and through its RING domain promotes PCNA mono-ubiquitylation on K 164 (Hoege et al., 2002). Even if this complex was isolated as a stable hetero-dimer, a recent study explained that the most probable stoichiometry of the full-length Rad18-Rad6 complex is 2:1, respectively (Fig. 6). The asymmetry of the Rad18-Rad6 complex seems to force Rad6 to exclusively mono-ubiquitylate PCNA, by inhibiting the Rad6 degradative poly-ubiquitylation activity (Huang et al., 2011).

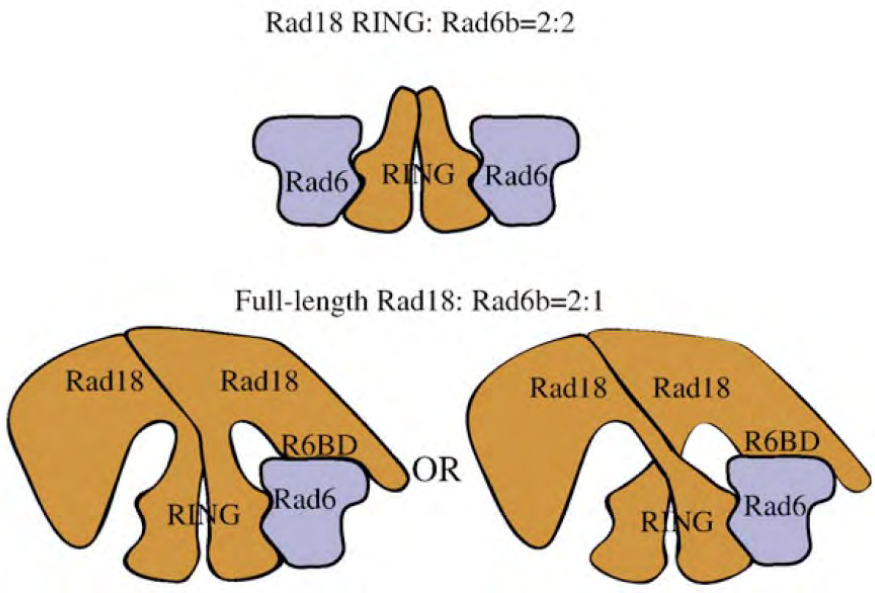

Fig. 6. The last published structure of the Rad18-Rad6 complex. The Rad18 RING alone is able to form a 2:2 dimer, but in full-length Rad18, only one Rad6 is bound. Two different possibilities for this asymmetric complex exist: left, Rad6b binds to Rad18 RING and Rad6 Binding Domain (R6BD) of the same monomer, and right, Rad6b binds to RING and R6BD domain of different monomers (Huang et al., 2011).

Ubc13-Mms2 and Rad5

These proteins are responsible for PCNA poly-ubiquitylation with a particular K63 linked polyubiquitin chain, which is not involved in protein degradation through proteasome (Zhao and Ulrich, 2010). This kind of post-translational modification is known to have a signaling function beyond targeting membrane proteins to the vacuolar/lysosome degradation pathway (Hicke and Dunn, 2003).

Ubc13, like Rad6, is an E2 enzyme, whose function in PRR requires the formation of a hetero-dimer with Mms2 (Hofmann and Pickart, 1999), which is an E2-like protein containing an Ubc variant domain (UEV). This domain shares high sequence and structural identity with the UBC domain, but it lacks of the catalytic cysteine necessary for ubiquitin conjugation.

These two proteins aggregate with a fast kinetics, so that the Ubc13-Mms2 complex is considered very stable (Ulrich, 2003). This complex is able to synthesize *in vitro* short K63 linked poly-ubiquitin chains (Hofmann and Pickart, 2001), and after its crystallization it was possible to understand the molecular mechanism. Ubc13 (as Rad6) receives an ubiquitin moiety from Uba1, so it carries the ubiquitin "acceptor". The function of Mms2 is to bind a molecule of a soluble ubiquitin (the "donor") and orientate it in the space so that its C-terminal domain is near the K63 of the acceptor (VanDemark et al., 2001).

In undamaged conditions the Ubc13-Mms2 complex is usually in the cytoplasm, but it is quickly translocated inside the nucleus after DNA damage, with a still unclear mechanism (Ulrich and Jentsch, 2000). Inside the nucleus, the intrinsic ubiquitin chain synthesis activity of Ubc13-Mms2 is targeted, through Rad5, to mono-ubiquitylated PCNA (from

Rad6-Rad18). In this way the ubiquitin chain on K164 is extended not exceeding 4 ubiquitin moieties (Windecker and Ulrich, 2008). This kind of specific K63 linked PCNA poly-ubiquitylation probably recruits a class of effectors not yet characterized, but Mgs1 could be one of them (Saugar et al., 2012).

Rad5 is a RING finger E3 enzyme with ubiquitin ligase, ATPase (Johnson et al., 1994) and helicase activities at level of replication fork (Blastyak et al., 2007); Rad5 plays also a structural role in PRR (Pagès et al., 2008). Its RING ubiquitin ligase domain is essential for the association with Ubc13-Mms2 through Ubc13 (Ulrich, 2003). The inactivation of ATPase activity confers modest UV sensitivity, whereas mutation of ubiquitin ligase causes a strong UV sensitivity. Inactivation of both ATPase and ubiquitin ligase activities causes, after UV irradiation, the same level of cell lethality caused by *RAD5* deletion, indicating that both activities are important for PRR efficiency (Gangavarapu et al., 2006).

Rad5 physically interacts with itself, PCNA and Rad18 (Ulrich and Jentsch, 2000; Chen et al., 2005). By immunofluorescence analysis it has been found that Rad18 and Rad5 independently co-localize in the same foci in response to UV DNA damage (Ulrich and Jentsch, 2000). All the interaction data published up to now show that various combinations of E2 and E3 enzymes can co-localize at the same time on a stalled PCNA homo-trimer. These combinations can produce different PCNA binding macro complexes in a dynamic equilibrium, as shown in Fig. 7.

Fig. 7. Possible combinations of aggregation of the PRR proteins, in budding yeast (modified picture from Ulrich and Jentsch, 2000).

The physiology of the Post-Replication Repair pathway

Based on how PCNA modifiers ubiquitylate PCNA, PRR can be divided in three sub-pathways (Xiao et al., 2000; Barbour and Xiao, 2003).

The first sub-pathway is an error-free Translesion DNA Synthesis (TLS): briefly, mono-ubiquitylation of PCNA on K164 by Rad6-Rad18 promotes polymerase switch from Pol-δ/ε (replicative DNA polymerases unable to continue replication over a damaged template), to the TLS DNA polymerase Pol-η, which correctly bypass the CPDs avoiding mutagenic bypass (Johnson et al., 1999; Washington et al., 2000). In the case of 6-4 PPs, as Pol-η is unable to efficiently bypass this lesion, an error-prone TLS, associated with the TLS DNA polymerase Pol-ζ (and/or Rev1-Pol-ζ), takes place still promoted by PCNA mono-ubiquitylation (Johnson et al., 2001). TLS DNA synthesis carried out by Pol-ζ often introduces wrong nucleotides opposite the DNA lesion, causing the fixation of mutation in the next S phase. For this reason this sub-pathway is considered mutagenic.

As indicated above, the choice between the two TLS sub-pathways seems to depend on t he type of UV-induced DNA lesion produced on t he genome. Alternatively, it is possible that the choice is indirectly driven by the levels of TLS polymerases, such as Rev1 that fluctuates during the

cell cycle, greatly increasing in G_2, while it disappears in G_1 (Wiltrout and Walker, 2011). This hypothesis implies a competition between Pol-η and Rev1-Pol-ζ at the level of mono-ubiquitylated PCNA during G_2 PRR.

The third and last sub-pathway is totally error-free, because it exploits a recombination based mechanism, called Template Switching (TS), to bypass the UV-induced DNA lesion (Higgins and Strauss, 1976; Branzei et al., 2004). TS is promoted by PCNA poly-ubiquitylation on K164, and becomes active only if mono-ubiquitylated PCNA by Rad6-Rad18 is further modified through the addition of other ubiquitin moieties by Ubc13-Mms2 and Rad5 (Torres-Ramos et al., 2002; Gangavarapu et al., 2006). This particular K63 linked ubiquitin chain extension promotes strand invasion of the growing filament on the undamaged sister filament, so DNA replication could continue on an undamaged template. The particular DNA structures produced by this mechanism (hemicatenanes) are resolved through the action of the Sgs1 helicase (Branzei et al., 2008). However, most of the molecular details of the TS pathway are still poorly defined.

It is quite clear that the choice among the three PRR sub-pathways depends on the state of PCNA ubiquitylation on K164; however it is not known the "driving force" directing the "PCNA modifiers" to prefer mono- versus poly-ubiquitylation or *vice versa*.

Some years ago, the mechanism of PCNA ubiquitylation in *S.cerevisiae* was clarified mainly through the work of HD Ulrich and collaborators (Parker and Ulrich, 2009). In particular, through various combinations of the PCNA modifiers, they identified the various steps leading to PCNA ubiquitylation. The major conclusion was that PCNA ubiquitylation occurs stepwise (Fig. 8A): PCNA is first mono-ubiquitylated by Rad6-

Rad18 at K164 and then Ubc13-Mms2-Rad5 adds one ubiquitin moiety at the time, leading to a linear K63 linked poly-ubiquitylated PCNA. That study excluded the possibility that both the E2 enzymes, Rad6 or Ubc13-Mms2 could poly-ubiquitylate PCNA "*en block*" (Fig. 8B), even if Rad6 is able to poly-ubiquitylate proteasomal targets (Raboy et al., 1999) and Ubc13-Mms2 can synthesize short free K63 linked polyubiquitin chains in solution (Hofmann and Pickart, 1999).

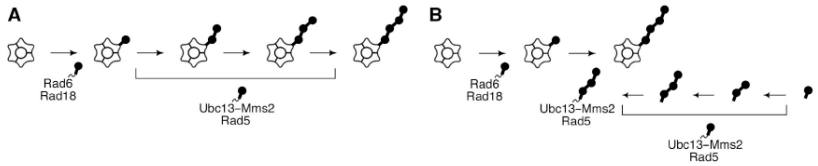

Fig. 8. Two alternative models for the formation of poly-ubiquitylated PCNA by Rad6-Rad18 and Ubc13-Mms2-Rad5. (A) Stepwise assembly. (B) Sequential action, with preformed chains (Parker and Ulrich, 2009).

In the last few years most of the studies on PRR have been focused in studying the timing and spacing of UV-induced DNA damage bypass.
For example, in both *S.cerevisiae* and human cells, it was discovered that DNA replication can be uncoupled from UV-induced DNA damage bypass (Daigaku et al., 2010; Karras and Jentsch, 2010; Diamant et al., 2011) and it was proposed that this bypass can happen in the G_2 phase through post-replicative gap filling. Altogether, these studies demonstrated that UV-induced DNA damage bypass is not limited to S phase, but it can occur also in G_2.

Covalent modifications of PCNA

Besides being ubiquitylated PCNA can also be SUMOylated and this modification is strictly connected with PRR for two reasons:

- PCNA SUMOylation occurs on a main residue, the K164 (the same used for the DNA damage induced ubiquitylation) and a secondary site, the K127.

- The downstream effector of PCNA SUMOylation is the Srs2 helicase, which has an inhibitory effect on any kind of recombinogenic bypass of UV-induced DNA lesions.

SUMOylation is catalyzed by two enzymes: the SUMO conjugating enzyme Ubc9 (E2) and the SUMO ligase Siz1 (E3), with the possibility that Ubc9 may SUMOylate its target without the need of the E3 (Windecker and Ulrich, 2008). As for ubiquitylation, PCNA SUMOylation needs loading of PCNA onto DNA (Parker et al., 2008). Given that the two modifications occur on the same residue (K164), it was assumed that ubiquitylation and SUMOylation of PCNA were two competing processes (Hoege et al., 2002). However, later studies found that poly-ubiquitylation of PCNA occurs largely independently from its SUMOylation and this is in agreement with the homo-trimeric nature of PCNA, which can be theoretically modified by ubiquitin and SUMO at the same time on different subunits through various combinations.

Regarding the physiological role of PCNA SUMOylation on K164, it was found that this modification can occur in S phase during an unperturbed cell cycle to avoid the deleterious effects of hyper-recombination and that

this process is reversible and controllable thanks to the SUMO lyase Ulp1 (Stelter and Ulrich, 2003). Moreover, mono-SUMOylation of PCNA induces spontaneous mutagenesis throughout Pol-ζ. In response to DNA damage, PCNA poly-SUMOylation is greatly enhanced similarly to what happens for ubiquitylation (Windecker and Ulrich, 2008).

The role of K164 SUMOylation in the DNA damage bypass was spatio-temporally clarified when it was demonstrated that such modification plays its functional role in the error-free DNA damage bypass, after strand invasion. K164 SUMOylated PCNA binds the DNA template and recruits the Srs2 helicase, which is able to disrupt the Rad51 protofilaments thus modulating the central steps of TS. Almost no information is available about the physiological role of PCNA SUMOylation on K127. If SUMOylation on K164 enhances the affinity of Srs2 for PCNA (*in vitro* and *in vivo*), the same modification on K127 enhances the affinity of the Eco1 acetylase for PCNA (Moldovan et al 2006). Such interaction was demonstrated only *in vitro* and we do not know its physiological role during DNA replication in an unperturbed cell cycle or in response to DNA damage. In a recent study it was found that PCNA SUMOylation is conserved between yeast and human; indeed human PCNA can be SUMOylated on the highly conserved K164 residue, but also at a secondary site, K254. This covalent modification prevents the formation of DSBs in the genome (Gali et al., 2012). Thanks to the particular phenotype of a yeast strain carrying a defect in DNA ligase I (the *cdc9-1* allele), it was discovered a new PCNA modification. Indeed, a peculiar ubiquitylation occurs on the K107 residue and it is catalyzed by Rad5, Mms2 and the E2 Ubc4, instead of Ubc13. Therefore, this new PCNA ubiquitylating pathway partially overlaps PRR. PCNA is

ubiquitylated on K 107 when DNA ligase I is unable to link Okazaki fragments. However, the physiological role of this modification in DNA damage conditions is totally unknown. The current view is that PCNA ubiquitylation on K 107 may be required for full activation of the DNA damage checkpoint after MMS treatment (Das-Bradoo et al., 2010).

A summary of PCNA modifications is shown in Fig. 9.

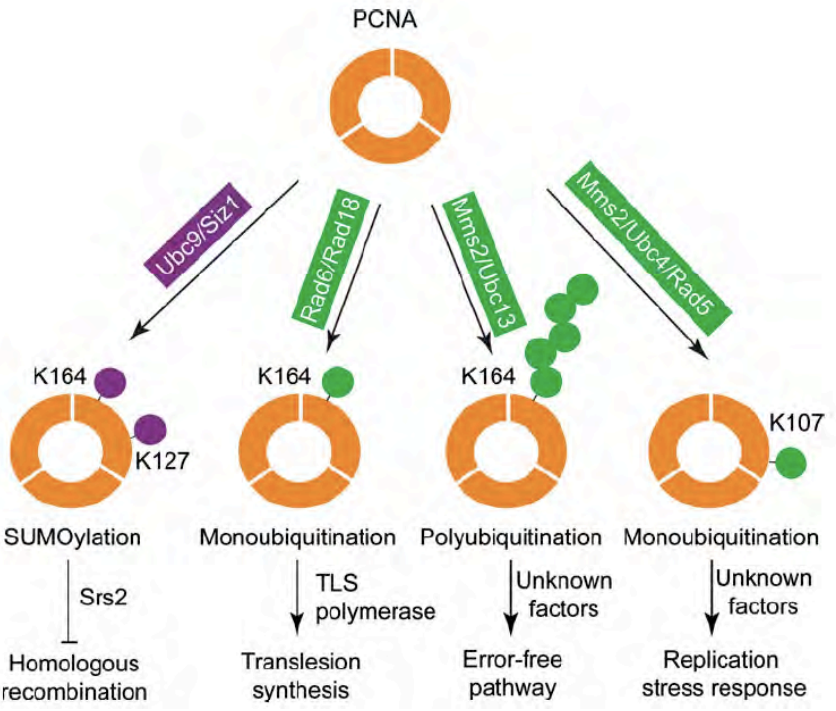

Fig. 9. PCNA ubiquitylation and SUMOylation pathways. PCNA can be modified by SUMO, mono-ubiquitin or ubiquitin chains at different sites. SUMOylation on PCNA can occur either on K164 or K127, which involves the inhibition of homologous recombination. Mono-ubiquitylation was observed on K164, which initiates TLS and K107, which is specific for DNA ligase I-deficiency. Poly-ubiquitylation on PCNA K164 is critical for an error-free DNA damage tolerance pathway (Chen et al., 2011).

AIM OF THE PROJECT

My thesis project represents the first attempt to investigate the PRR pathway through a Systems Biology approach by combining bioinformatics and experimental tools.

The first important thing to do was to collect and rationalize all the published data on *S.cerevisiae* PRR. The elaboration of literature data led to the definition of all the necessary parameters for a "r aw" implementation of the pathway into an opportune simulation software (the SSBS simulator). This software, a mono-compartmental simulator for biological pathways, was developed by Dr. Daniela Besozzi and her collaborators at the University of Milano and at the University of Milano Bicocca. I worked in tight connection with the same group to build up the *in silico* work package of the thesis project. The raw implementation of the PRR model took in consideration all the data about PRR derived from research papers, biological databases or their re-elaboration. It was built a protein-protein PRR interaction map, the list of the biochemical reactions involving these proteins, the list of their starting levels and it was defined the "binder" parameter between experimental results and computer simulations, which was the number of UV-induced DNA lesions/haploid yeast genome at a given UV dose.

The first big problem we had to face was the lack of knowledge in the scientific literature of the kinetics constants for the biochemical reactions identified in the PRR pathway. The optimization of any model needs the definition of these important kinetics parameters. Therefore, it was necessary to work at the bench to obtain the critical mass of robust experimental data required to extrapolate them. Simultaneously, the

computational work package was developed by the bioinformaticians collaborating with me during the entire project.

We decided to use PCNA mono- and poly-ubiquitylation as the biochemical readout of PRR. It was therefore necessary to set up a sensitive, reliable and reproducible protocol to detect such modifications *in vivo*. This was a difficult task, because the experimental set up is quite complicated and the overall procedure is time consuming. Moreover, once I succeeded in establishing the experimental conditions, I had to systematically analyze the only parameter kept free to vary: namely the UV dose.

The characterization of the *in vivo* dynamics of PCNA ubiquitylation after UV irradiation at various doses, allowed the bioinformaticians to develop the model by extrapolating the best set of kinetics constants from my experimental data.

The achievement of the first working mathematical model of PRR allowed me and the bioinformaticians to identify the limits of the model itself, find the critical parameters and reactions of PRR, make predictions and evaluate them experimentally. Indeed, some experiments suggested by the model open new scenarios about PRR, that can be tested in the future and make the actual model even more accurate.

MAIN RESULTS

Model topology and implementation

Data in the literature offer an idea of how PRR works in S.*cerevisiae*. However, it was necessary to translate all the published biological data into a format with a suitable syntax to simulate the pathway *in silico*. First, I collected all the physical interaction data among the PRR proteins (Fig. 1), obtaining a static picture of the pathway.

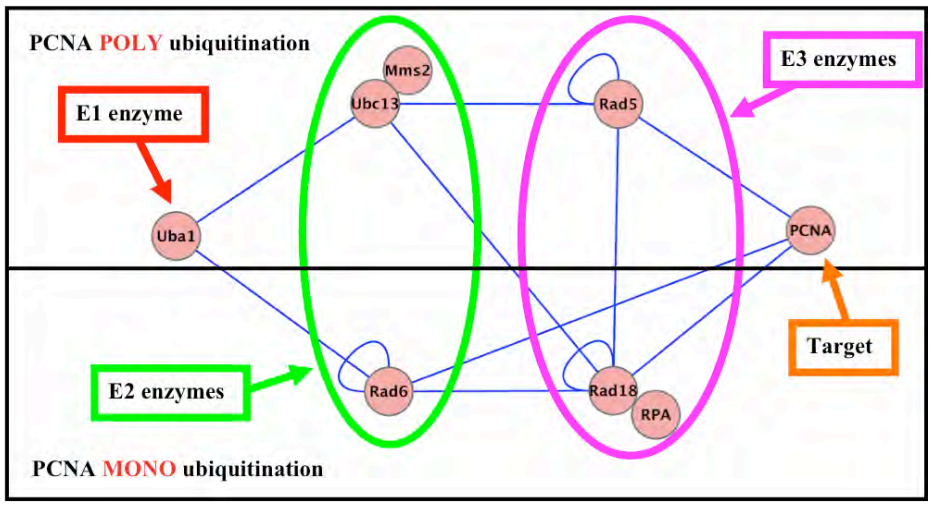

Fig. 1. Protein-Protein interaction map of the PRR pathway. The diagram was obtained through the Cytoscape software (Shannon et al., 2003).

For the initial topology of the model I considered the whole PCNA ubiquitylation pathway, from ubiquitin activation to PCNA modification (Fig. 2). However, I then decided to simplify the pathway leaving out two proteins: Uba1 and RPA.

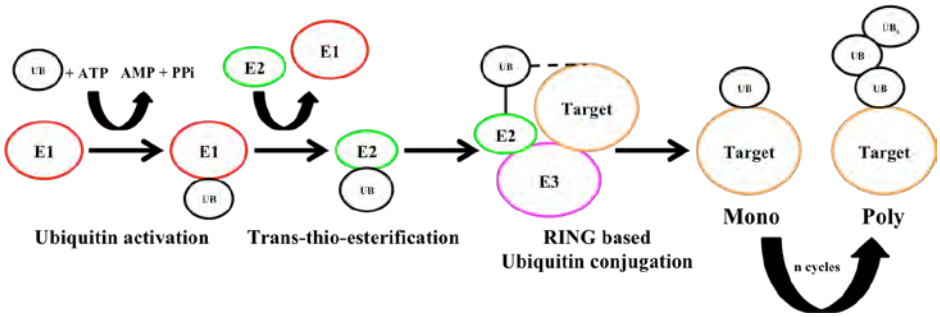

Fig. 2. The three steps of the RING based ubiquitylation processes. Colours are in agreement with Fig. 1.

The first one was not considered because the process of ubiquitin activation and trans-thio-esterification through this unique E1 enzyme were just finely characterized and it accounts for more than 20 biochemical reactions (Haas and Rose, 1982, for ubiquitin activation). Since we were interested in PRR, I decided not to consider them to simplify the model.

To do that, it was necessary to confirm that the ubiquitin activation, trans-thio-esterification and conjugation steps could be spatio-temporally separated also in PRR. For this purpose, I decided to *in silico* characterize the correct spatio-temporal formation of the protein complexes by exploiting a 3D molecular modeling approach developed some years ago (Ulrich, 2003; Lee and Schindelin, 2008). An important pre-requisite for this type of analysis rests on the structural conservation among the modeled proteins. This conservation was assumed in the previously cited references, but I decided to confirm it independently (Fig. 3 and Fig. 4). Through the structural analysis it was possible to suggest that PRR complexes Uba1-Rad6 and Rad18-Rad6 were mutually exclusive, like Uba1-Ubc13 and Rad5-Ubc13-Mms2 (see submitted manuscript at page 8: “structural modeling of uncharacterized protein-protein complexes”).

These findings temporally and physically separated the three steps of PCNA ubiquitylation and, therefore, I divided the "whole PRR" process in at least three sub-modules, which could be individually analyzed and simulated.

Moreover, even if RPA is essential for Rad18 localization at the level of a stalled replication fork, I excluded it from the model because I needed to know the number and the extension of the ssDNA gaps associated to stalled replisomes, an information, which is presently lacking.

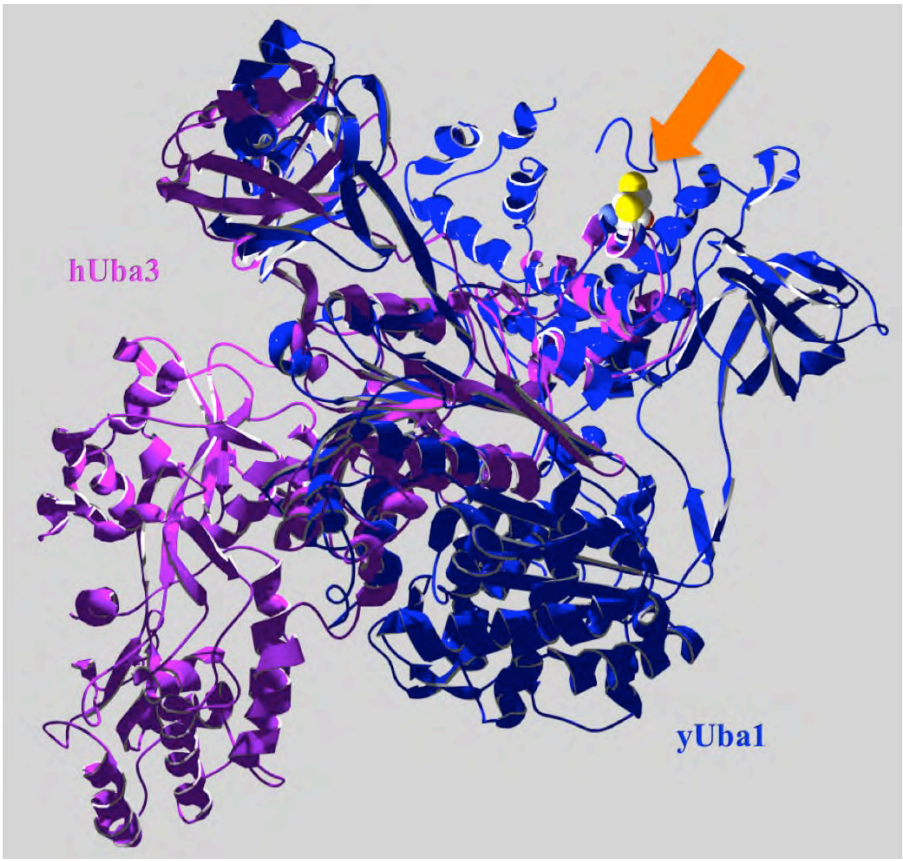

Fig. 3. Structural conservation between the human E1 enzyme, Uba3 (magenta) and the unique yeast E1 enzyme Uba1 (blue). The orange arrow highlights the active site.

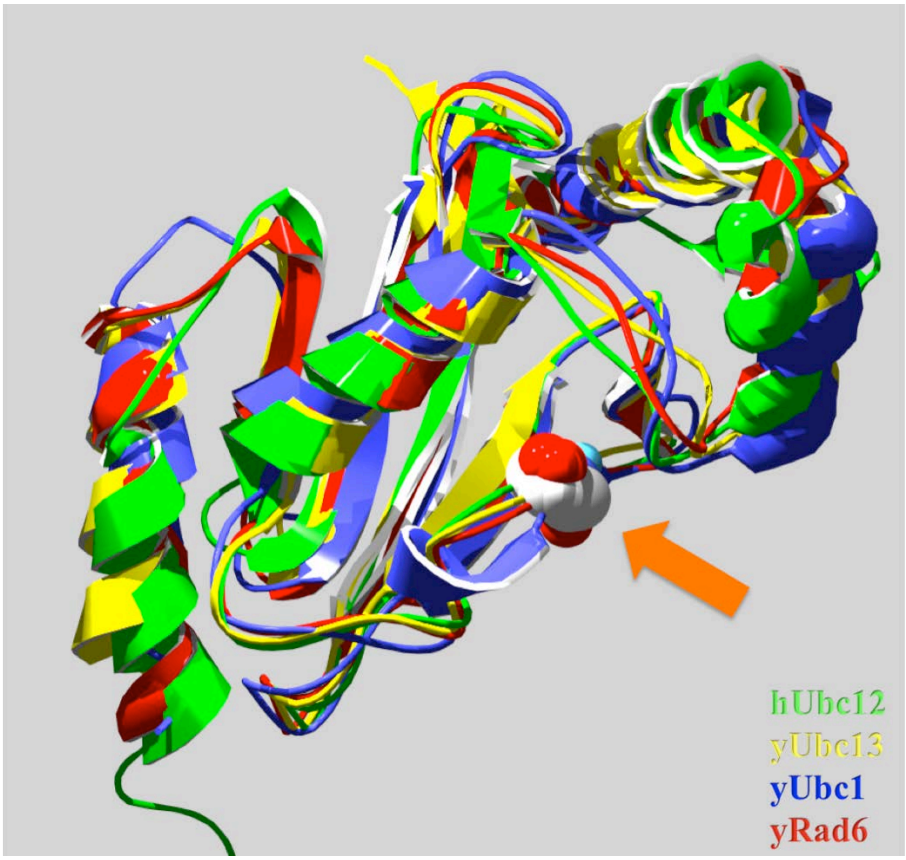

Fig. 4. Structural conservation between the human E2 enzyme Ubc12 (Green) and yeast E2 enzymes: Ubc13 (Yellow), Ubc1 (Blue) and Rad6 (Red). The orange arrow highlights the active site.

In conclusion, I decided to exclude the ubiquitin activation and summarize the trans-thio-esterification through two simple reaction, in order to focus my attention only on t he reactions, which directly ubiquitylate PCNA in response to UV-induced DNA damage (ubiquitin conjugation on PCNA).

The next step was to translate the previous static picture of PRR into a dynamic simulable pathway, through its implementation into the SSBS simulator (Besozzi et al., 2010). In particular, the critical module of

ubiquitin conjugation on PCNA was converted into a list of biochemical reactions keeping in account also the results of 3D molecular modeling and other useful literature data. The list of biochemical reactions (see submitted manuscript, at pages 28 and 29: Tab. 5, "Mechanistic model of the PRR in yeast") was supplemented with generic reactions of signal switch-off, because this effect was observed *in vivo* in budding yeast after UV irradiation (Daigaku et al., 2010) and in my time-course experiments at low acute UV doses. However, these switch-off reactions were not associated to specific proteins because it is still a matter of scientific debate.

The removal of the *stiff problem* (a problem of time…)

The actual list of the biochemical reactions of the model lacks the three formation steps of ubiquitylated/not ubiquitylated Ubc13-Mms2 complexes that were included in the first attempts to construct the model (see submitted manuscript at page 11: "Definition of the mechanistic model" and part III, additional file 8). To identify the kinetics constants of the biochemical reactions of the pathway (parameter estimation) that better fit the experimental data, it was necessary to carry out thousands of simulations by using a manual "trial and error" optimization of the reaction rate constants. By including in the model the three formation steps indicated above, the simulation time of a single iteration was about 20 minutes. Such a long time dramatically slowed down the feasibility of the project. Such a "*stiff problem*" remained unsolved till I hypothesized that a solution could be to use a different bioinformatic approach, which is capable to visualize and identify the exact step/steps (biochemical reaction/s) causing the slowing down of the entire simulation.

The system I decided to use is called Hybrid Petri Net (Nagasaki et al., 2004a). I translated all biochemical reactions presenting the *stiff problem* into a Hybrid Petri Net based simulation software: Cell Illustrator (Nagasaki et al., 2004b). Omitting the details of the Hybrid Petri Net approach, the most important aspect of this analysis is the critical opportunity to see in real time the "flowing" of all species in the pathway (called "tokens" in the Petri Net syntax) through the biochemical reactions. Thanks to this analysis I discovered that a large part of the tokens made "ping-pong" among the previously mentioned three

formation steps of ubiquitylated/not ubiquitylated Ubc13-Mms2 complexes, slowing down the entire simulation process.

I thus proposed to the bioinformaticians to substitute the three reactions with a single biologically equivalent reaction. When they tested this modification the quality of the simulation did not vary (see part III: additional file 8) and the speed of the whole optimization process changed from 20 minutes/simulation to less than one minute/simulation (at least for the simulations at 5 and 10 J/m^2).

The development of a reliable protocol for the quantitative analysis of PCNA ubiquitylation after UV irradiation

As the level of PCNA ubiquitylation drives the choice between TLS (mono-ubiquitylation) and TS (poly-ubiquitylation) we decided that the best biological readout of the model could be the ratio among the various ubiquitylated PCNA isoforms after UV-induced DNA damage. The manual optimization of the reaction kinetics constants of the model required the systematic characterization of the dynamics of PCNA ubiquitylation after irradiation at different UV doses and it was therefore necessary to go back to the bench to obtain such information.

To visualize and quantify PCNA ubiquitylation it was necessary to use a yeast strain carrying the ^{HIS}*POL30* allele, which led to the production of a N-terminal HIS tagged PCNA, detectable by western blotting with a suitable antibody (this strain is considered as my wild-type strain in all the experiments shown here and in the accompanying manuscripts). This strain was kindly provided by HD Ulrich (Windecker and Ulrich, 2008). She also sent me other two strains used as controls of PCNA ubiquitylation: the ^{HIS}*pol30*-K164R (unable to be ubiquitylated on K164) and the ^{HIS}*pol30*-K127R (unable to be SUMOylated on K127).

To better detect *in vivo* all the PCNA ubiquitylated isoforms after UV irradiation, I modified a published protocol (Ulrich and Davies, 2009) improving the efficiency of their detection ~ 10 fold.

The initial attempts to set up the protocol were made by treating cells growing in liquid YEPD for 30-40 minutes with the UV mimetic drug 4-

NQO; then, I began to use UV irradiated cells, using a standard protocol developed in the laboratory (Giannattasio et al., 2004).

To determine the amount of PCNA pulled down in each sample, the membrane was cut between the markers migrating at 32.5 and 47.5 kDa and then hybridized with monoclonal anti-ubiquitin antibody to detect ubiquitylated PCNA isoforms (upper part in Fig. 5) and with anti-HIS or polyclonal anti-PCNA (kindly given by HD Ulrich), to detect unmodified PCNA (bottom part in Fig. 5).

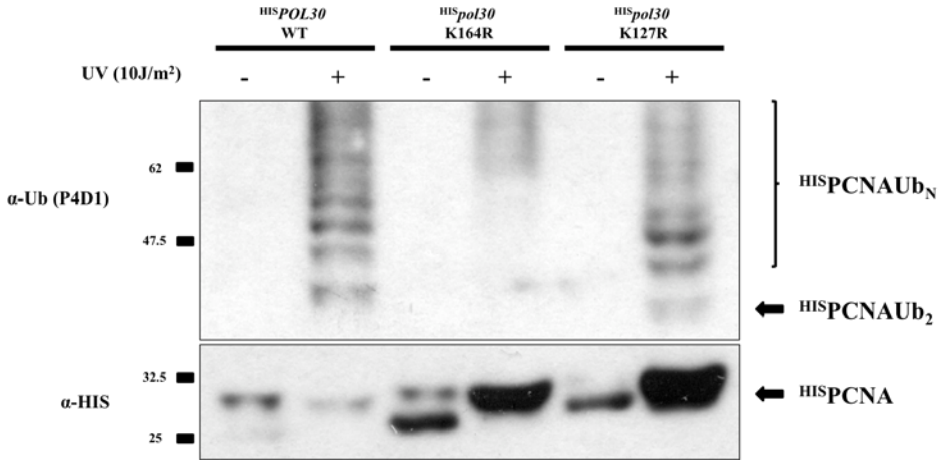

Fig. 5. *In vivo* detection of ubiquitylated PCNA after UV irradiation. Cells were UV irradiated as published in Giannattasio et al., 2004; 30 minutes after UV irradiation cells were harvested and processed as published in Ulrich and Davies, 2009. Nitrocellulose membranes were cut and the upper part was hybridized with monoclonal anti-ubiquitin antibody P4D1, while the bottom part was hybridized with monoclonal anti-HIS antibody.

In initial experiments we found a not homogeneous amounts of pulled down PCNA in all the samples (bottom part in Fig. 5). Since we needed a quantitative assay to collect robust data for mathematical modeling we tried to overcome this problem by integrating the denaturating pull-down

protocol with cell extracts normalization using a Biorad protein assay optimized for the lysis buffer used. In this way, all the samples loaded on the same gel were comparable and allowed a reliable and consistent quantification of the western blots by using as normalization factor the signal corresponding to unmodified PCNA detected in the lower part of the membrane. However, another technical problem was present that emerged also in previous studies (Hoege et al., 2002 and Windecker and Ulrich, 2008): all the commercial antibodies against ubiquitin (monoclonal and polyclonal) were unable to detect yeast mono-ubiquitylated PCNA, and this isoform was detectable only by using home-made polyclonal anti-PCNA antibodies and after very long ECL exposure. This technical problem could affect the whole "wet package" of the project, because we needed to detect the ECL signal on the same film in order to extrapolate the ratio among all ubiquitylated PCNA isoforms *in vivo*. The fact that mono-ubiquitylated PCNA was present on t he nitrocellulose membrane, but it was detectable only with anti-PCNA antibody, was called the "hidden epitope" problem.

The first attempt to solve this problem was to run the samples on a 10% SDS-urea PAGE, a procedure usually used for membrane proteins (Hafiz, 2004). The rationale was to use acrylamide gels containing both 8M urea and SDS to ensure the complete denaturation of protein species inside the gel. This protocol dramatically changed the electrophoretic mobility of the proteins, offering a higher correspondence between the molecular weight of the PCNA isoforms and the protein markers used. However, the main problem was not resolved: mono-ubiquitylated PCNA was still undetectable with any anti-ubiquitin antibody.

By carefully searching through the literature I found that the ECL ubiquitin signal on membrane could be increased up to ten fold by heat denaturating the nitrocellulose membranes and by coupling this treatment with a polyclonal peptidic antibody against ubiquitin (Swerdlow et al., 1986; Mimnaugh and Neckers, 2002). I thus autoclaved the membrane after protein transfer with a wet cycle of 30 minutes at 120°C and then I probed it with the 3933 peptidic anti-ubiquitin polyclonal antibody from Cell Signaling (TM). As shown in Fig. 6, the detection of mono-ubiquitylated PCNA with this protocol was dramatically improved. In fact, in the absence of the heat denaturation step the 3933 antibody was unable to detect this PCNA isoform on UV irradiated *mms2*Δ cells, where mono-ubiquitylated PCNA must be the only detectable form (Hoege et al., 2002). Therefore, the coupling of the 3933 antibody with the autoclaving step allowed the detection of the PCNA ubiquitylated isoforms.

The optimized protocol described above became a standard procedure in the laboratory and it has been used in other research projects where it is necessary to measure the activity of the PRR pathway by detecting the various PCNA ubiquitylated forms (see published paper I).

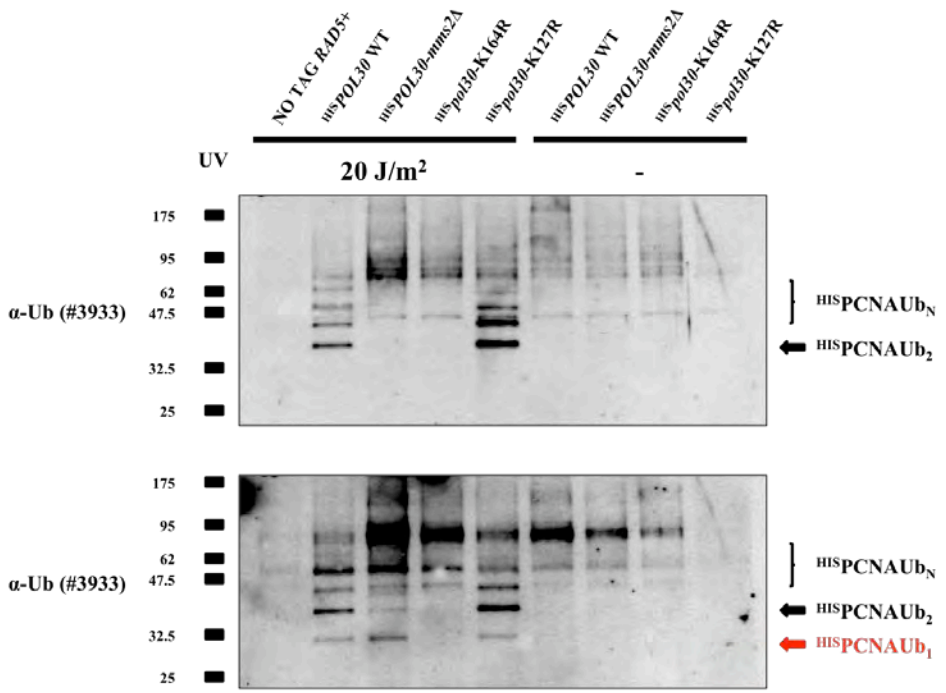

Fig. 6. Optimization of the *in vivo* detection of mono-ubiquitylated PCNA. Cells were UV irradiated with 20 J/m^2 as in Giannattasio et al., 2004. 30 minutes after UV irradiation cells were harvested and processed as in Ulrich and Davies, 2009. After denaturating pull-down, samples were run onto 10% SDS-urea PAGE and transferred into 0.2 μm nitrocellulose membrane. The membrane was first probed with polyclonal anti-ubiquitin antibody (Upper part). After ECL reaction, the membrane was washed in TBS and autoclaved at 120°C for 30 minutes. Autoclaved membrane was re-hybridized with the same anti-ubiquitin antibody (Bottom part).

Dose-response measurement of PCNA ubiquitylation after UV irradiation

After optimizing the detection protocol of PCNA ubiquitylation, I tested its sensitivity (threshold of detection) by UV-irradiating wild-type cells at different doses (from 1 to 100 J/m^2).

As shown in Fig. 7, I found that the PCNA ubiquitylation is undetectable below a dose of 5 J /m^2 notwithstanding the enhanced detection of ubiquitin. I chose 5 J /m^2 as the lower UV dose to be used in all my experiments. As the upper dose I chose 75 J/m^2 because, although it is a non-physiological dose, is near to the NER excision activity saturation dose in budding yeast (80 J/m^2) (Waters and Moustacchi, 1975).

It is worth mentioning the importance of the normalization step. In fact, unmodified PCNA, which represents the normalization bar for the pull-down assay, was more homogeneous in Fig. 7 than in Fig. 5. As a consequence, also the signal intensities of the samples in the upper parts of the blots were more comparable.

As fixed through the dose-response curve, all the experiments shown in the submitted manuscript ranged from 5 to 75 J /m^2 (see submitted manuscript, “Results and discussion” section starting from page 11 with the respective figures).

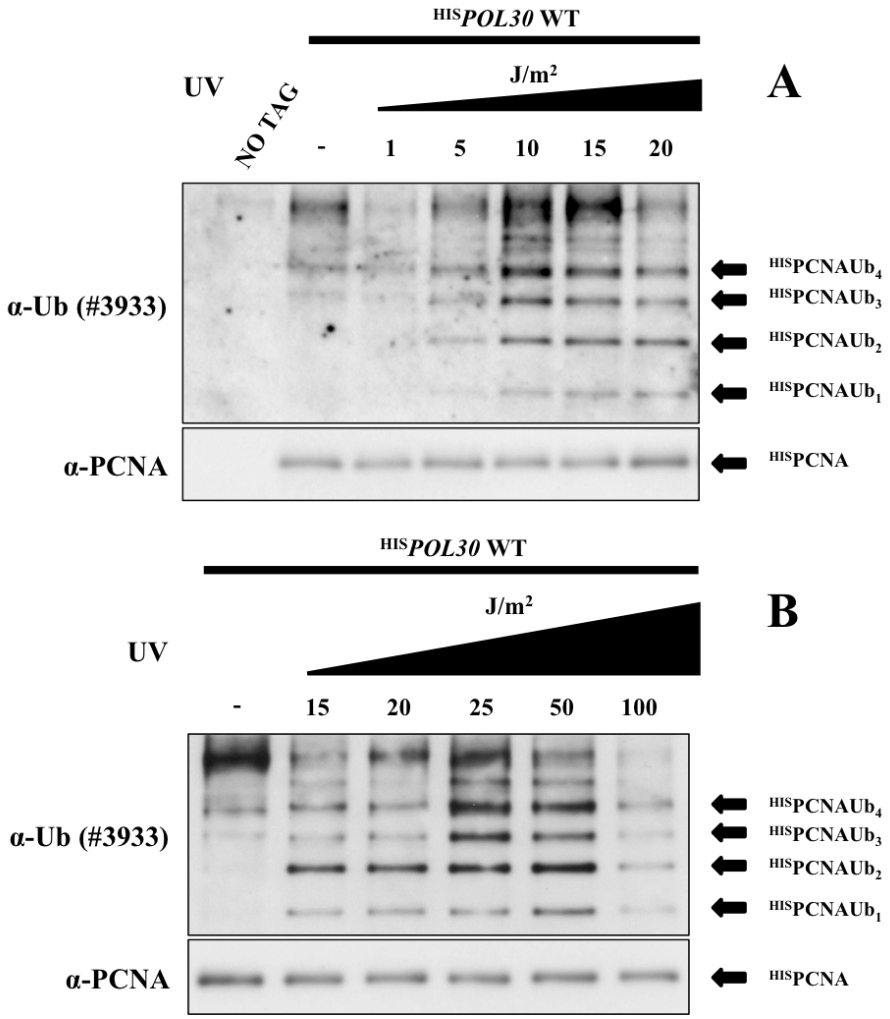

Fig. 7. PCNA ubiquitylation after UV-induced DNA damage: dose-response curve. I tested five low acute doses (A) and 5 high acute doses (B). PCNA ubiquitylation was undetectable below 5 J/m^2. After the autoclaving step, the upper part of the membrane was hybridized with polyclonal anti-ubiquitin antibody, while the bottom part was hybridized with polyclonal anti-PCNA antibody.

Time-course of PCNA ubiquitylation after UV-induced DNA damage

Although the dose-response curve was useful to establish the range of UV doses to use in my experiments, it was not the correct approach to produce *in vivo* data for mathematical modeling of PRR.

The correct approach to collect experimental data useful for the mathematical modeling of a biological pathway is the analysis of the evolution of the target species (in my case ubiquitylated PCNA isoforms) over the time (i.e. time-course experiments). First, I decided to try some preliminary short time-course experiments to evaluate the quality of the result at low UV doses (Fig. 8).

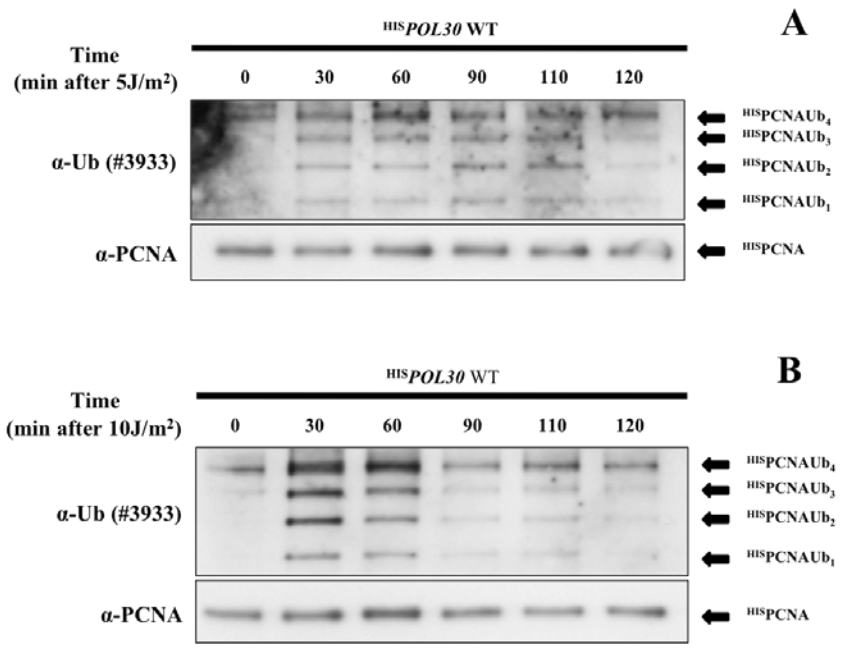

Fig. 8. PCNA ubiquitylation after UV-induced DNA damage: short time-course experiments. Cells were treated with 5 (A) and 10 (B) J/m^2 as in Fig. 7 (A) and harvested at the indicated time points. The experimental procedure is the same described in Fig. 7.

Although the quality of the experimental data was satisfactory to be transferred into the computational model, we observed that the PCNA ubiquitylation signals tended to switch-off after 120 minutes, as previously published (Daigaku et al., 2010). Therefore, the collection of the samples was extended up to 300 minutes after UV irradiation to observe essentially a complete switch-off of PCNA ubiquitylation, at least after low acute UV irradiation.

Then, I systematically characterized the dynamics of PCNA ubiquitylation at various UV doses (5, 10, 50 and 75 J/m^2) in duplicate experiments, to assess the reproducibility of the protocol and of the data. As shown in Fig. 9, in response to low acute UV irradiation (5 and 10 J/m^2, Fig. 9 A-B and C-D, respectively), the PCNA ubiquitylation signal switched-off within three hours, while at higher acute doses the signal was still detectable up to five hours. Indeed, it has been shown that the genome of yeast log cells contains ~ 25% of the UV lesions five hours after irradiation with a UV dose of 75 J/m^2 (McCready and Cox, 1993).

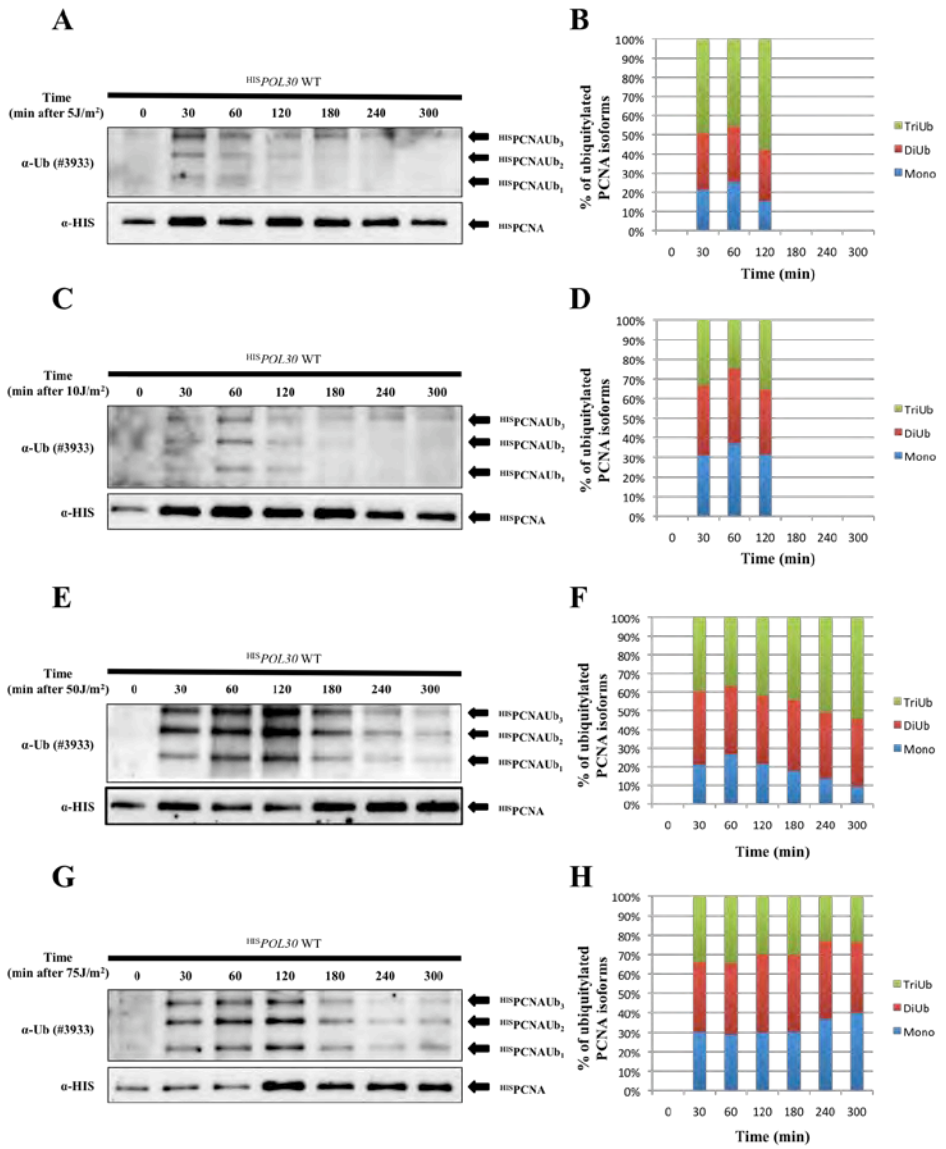

Fig. 9. PCNA ubiquitylation after UV-induced DNA damage: long time-course experiments. A, C, E, G, are representative western blots of the experiments at 5, 10, 50, 75 J/m^2, respectively. B, D, F, H are the quantifications of two independent experiments for each dose. Each plot represents the ratio among mono, di-, tri-ubiquitylated PCNA vs. time. The experimental conditions are as described in Fig. 7.

Main Results

All the time-course experiments where performed using wild-type logarithmically growing cells. In this condition, UV irradiated cells transiently stop cell cycle progression in response to DNA damage checkpoint activation and restart to cycle when the damage is repaired. The entity of this temporary stop depends on the amount of damage in the genome and, therefore, it correlates with the UV dose. Considering this aspect of the UV-induced DNA damage response, I tested the activation of the DNA damage checkpoint in log phase cells UV irradiated with 5, 10, 50 and 75 J/m^2, by analyzing the status of Rad53 phosphorylation, as the best biochemical marker to measure off DNA damage checkpoint activation. As shown in Fig. 10, at low acute (5 and 10 J/m^2) UV doses the DNA damage checkpoint was activated but it switched-off in 2 hour (Fig. 10A), while at high acute UV doses (50 and 75 J/m^2) Rad53 phosphorylation was still detectable after five hours (Fig. 10B).

By measuring cell growth and division by spectrophotometric measurements (data not shown) it was evident that UV irradiated log phase cells continued to sustain significant growth, especially when treated with low UV doses (5 and 10 J/m^2). This finding might affect interpretation of the data, because the dynamics of PCNA ubiquitylation is extrapolated on a dynamic cell population, raising the possibility that the switch-off signal observed at 5 and 10 J/m^2 might result from protein dilution in the growing cell population. The lack of such a control might affect the mathematical modeling.

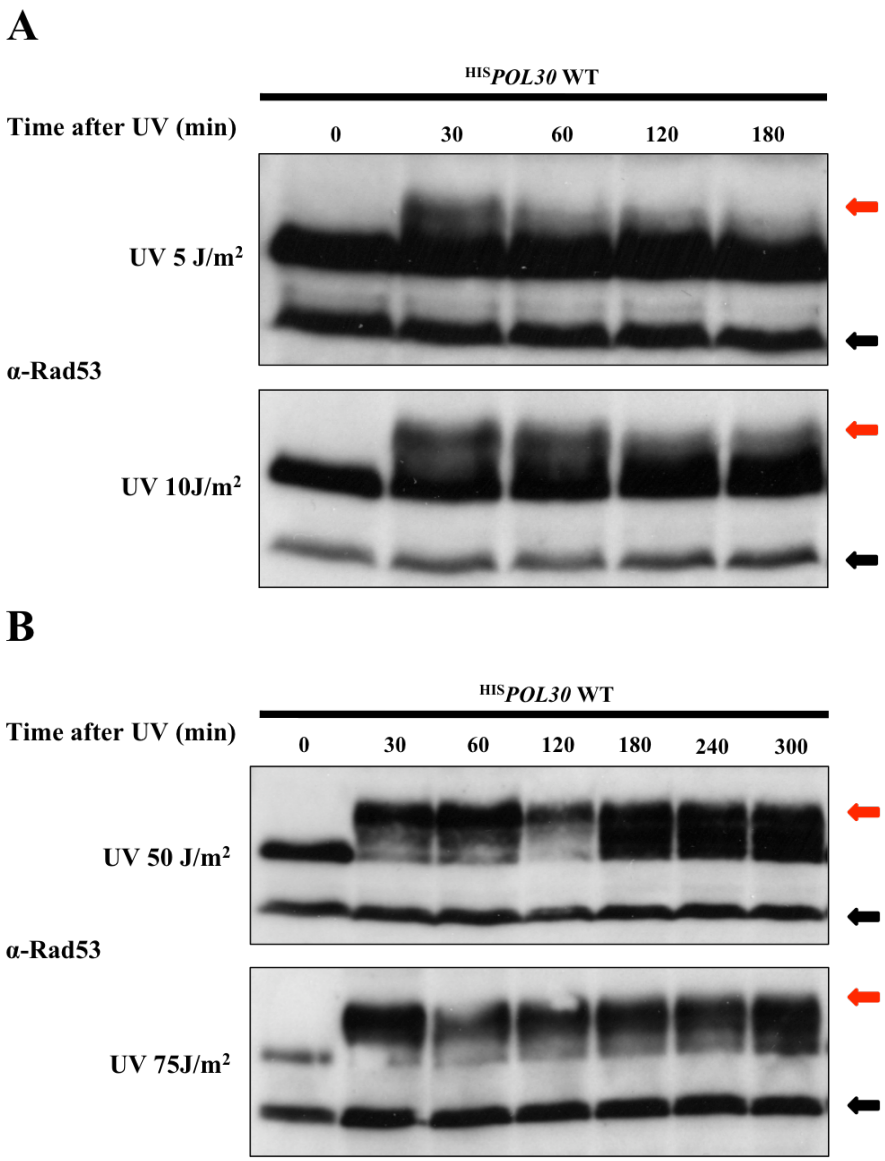

Fig. 10. UV-induced DNA damage checkpoint activation and switch-off in log phase cycling cells. Cells were UV irradiated, collected at the indicated time point after UV irradiation and subjected to TCA protein extraction, SDS-Page and western blot as previously described (Giannattasio et al. 2004) (A) Rad53 phosphorylation after low acute UV doses 5 and 10 J/m^2. (B) Rad53 phosphorylation after high acute UV doses 50 and 75 J/m^2. The red arrows correspond to hyperphosphorylated Rad53 protein, which is representative of checkpoint activation, while the black arrows correspond to an aspecific band used as a loading control.

Another weakness of the experimental approach described so far arose from the knowledge, present in the literature, that PRR genes are transcriptionally regulated in a dose dependent manner after UV irradiation and the magnitude of this transcriptional burst is gene-dependent as summarized in the following Tab. 1. In addition it is possible that the *in vivo* amount of the PRR proteins can be regulated at the translational level.

Because no data were available on the amount of PRR proteins after UV irradiation, and the only quantitative published data were extrapolated on undamaged log phase cells, a realistic mathematical model of PRR might consider the possibility of working with a non-fixed amount of proteins. The optimization of a mathematical model, where the level of the PRR proteins fluctuated in a dose-dependent manner and possibly with a dynamics, varying from protein to protein, made the study too complex considering the complete lack of experimental data on UV-induced *de novo* synthesis of PRR proteins.

Tab. 1. UV-induced transcriptional burst of PRR genes.

Gene	UV doses (J/m^2)	Time-peak of transcription (min)	Fold of Induction	Reference
RAD6	25, 37, 50	30-60	3.8-7.5	Madura et al, 1990
RAD18	37, 50, 70	30-60	1.75-2.5	Jones and Prakash, 1991
UBC13	50% of survival	150	5	Ulrich, 2001
MMS2	50% of survival	150	3	"

Summarizing the arguments I discussed above, I had to solve two problems. The first one was biological and to solve it I would need to irreversibly stop cell cycle progression of logarithmically growing cells immediately after UV irradiation, to avoid the protein dilution effect especially at low UV doses. The second problem was related to the

necessity of harmonizing the experimental data with the subsequent computational analysis, and to obtain such goal I needed to fix the PRR protein levels immediately after UV irradiation, avoiding the possible dependency of PCNA ubiquitylation dynamics on UV induced transcriptional/translational burst(s).

I decided to simultaneously bypass these two problems through an experimental trick, based on the use of cycloheximide (CHX), a drug able to stop both cell cycle and protein synthesis. CHX binds the 60S subunit of the eukaryotic ribosome and inhibits its associated peptidyl transferase activity.

Before using CHX in my experiments I performed a literature search and a set of pilot experiments to identify the minimal dose, which could stop both cell cycle progression and protein synthesis. It has been found that a dose of 10 μg/ml CHX inhibits ~ 91% of protein synthesis within 15 min in budding yeast (Hanna et al 2003) and that 0.2 μg/ml of CHX are able to arrest G_1 and G_2 phases of the yeast cell cycle (Popolo et al., 1982). Moreover, I performed a number of dose-response experiments to test the effect of various CHX doses on the arrest of cell cycle progression. By analyzing the FACS profiles of G_1 arrested cell after release in CHX, I chose 10 μg/ml as the best CHX dose to be used (see part III: additional file 1).

All the experimental data shown in the "Result and discussion" section starting from page 8 of the submitted manuscript, with the respective figures, and additional files (part III) were produced in presence of CHX.

Comparison of the dynamics of PCNA ubiquitylation plus/minus cycloheximide

The last test I performed before definitively using CHX in my experiments was to compare, on the same western blot, the dynamics of PCNA ubiquitylation in the presence or absence of 10 μg/ml of CHX at 5, 10, 50 and 75 J/m^2.

As shown in Fig. 11A and B, the presence of CHX did not affect PCNA ubiquitylation at low acute UV doses (Fig. 11A and B), while at high UV doses (Fig. 11C and D) a certain effect was observed. In fact, in the absence of CHX at 50 and 75 J/m^2 a faster disappearance of ubiquitylated PCNA isoforms was detectable four and five hours after UV irradiation with respect to cells treated with CHX. This effect could be due either to the protein dilution effect caused by cells re-starting to cycle after repair of DNA damage or to an UV-induced increased level of PRR proteins, which can bypass UV lesions faster in the absence of CHX.

This observations led us to re-do all the dynamics of PCNA ubiquitylation at all UV doses in the presence of CHX, at least in triplicate, while the minimal and maximal doses were analyzed four/five times. Such a systematic collection of biological data, was necessary to develop the computational work-package by the bioinformaticians of Milano Bicocca (see submitted manuscript from page 11: “Kinetics of PCNA ubiquitylation at low and high doses of UV irradiation” and respective figures).

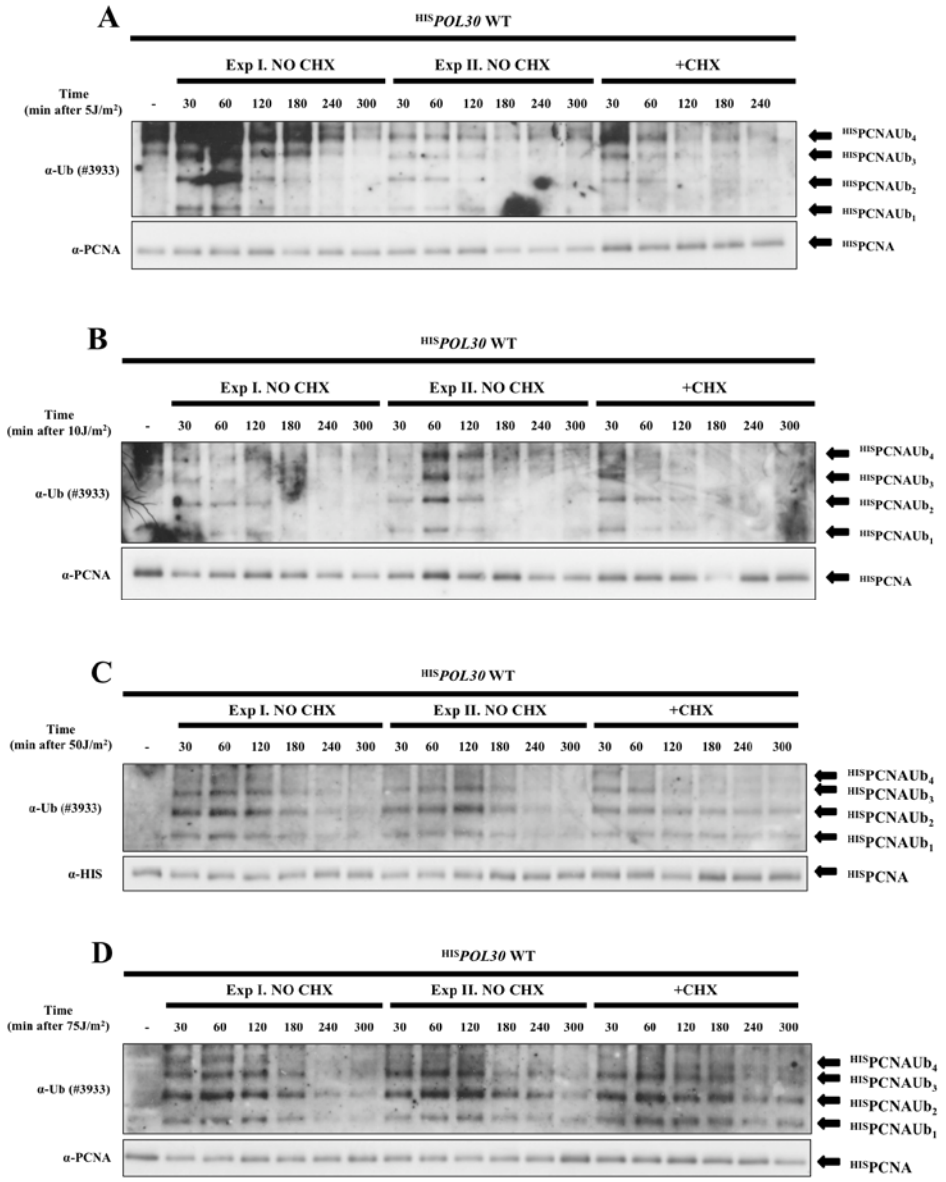

Fig. 11. Comparison of the dynamics of PCNA ubiquitylation in absence/presence of 10 μg/ml of CHX. A, B, C, D are respectively 5, 10 , 50 , 75 J/m^2.

CONCLUSIONS AND FUTURE PERSPECTIVES

My PhD project is the first attempt of the Plevani and Muzi-Falconi lab to analyze the response to UV-induced DNA damage by combining experimental and computational biology approaches. The final result is the first mathematical model of PRR in *S.cerevisiae:* the main body of the data are presented in the submitted manuscript and some of technical problems we had to solve have been described in the previous section.

The model we propose is suggesting new experiments and perspectives to improve our understanding of the PRR pathway. In fact, the simulations we carried out highlighted the limits of the model itself, which is very robust at low, near physiological UV doses and it is still reliable at doses approaching 30 J /m^2. Over this threshold we observed discrepancies between the *in vivo* and *in silico* dynamics of PCNA ubiquitylation. These inconsistencies are likely linked to an overestimation of the number of lesions / haploid genome at a certain UV dose and to the crosstalk between NER and PRR: in fact, our findings strongly indicate that the pathway responsible for repairing the UV lesions (NER) is playing an important role for optimal functioning of PRR in any cell cycle phase.

All the computational analyses required to build up t he model were performed below the critical dose of 30 J /m^2, where we highlighted the extreme importance of the ubiquitin concentration parameter: in fact, this protein can become a limiting factor in all the processes in which it is involved, including PRR. Since ubiquitin is a crucial player in a number of cellular pathways, the lack of a working mechanism of homeostasis,

(recycling through deubiquitylating enzymes or DUBs and *de novo* synthesis), could cause the malfunctioning of all ubiquitin dependent pathways, after the fast depletion of this protein from the cell.

When we tested, in the mathematical model of PRR, the effect of varying the concentration of free ubiquitin (see submitted paper at page 13: "Influence of ubiquitin concentration" and respective figure), we observed that the pathway was malfunctioning below a certain level of free ubiquitin; we thus decided to test this aspect *in vivo*. To do so, we impaired the availability of free ubiquitin for PRR by acting on its *de novo* synthesis, by impeding ubiquitin biosynthesis with CHX and by interfering with ubiquitin recycling by deleting *DOA4,* one of the DUBs coding genes, whose deletion confers mild UV sensitivity (Gong and Siede, 2011).

We observed that deletion of *DOA4* caused a strong reduction of PCNA ubiquitylation after UV irradiation and we correlated this behaviour to the reduced level of free ubiquitin in the cell. Indeed, it has been published that in the absence of Doa4 ~ 1/3 of the total cellular ubiquitin is present in logarithmically growing cells (Swaminathan et al., 1999). A similar impairment of PRR was observed when the *DOA1* gene, coding another DUB enzyme, was deleted (Lis and Romesberg, 2006).

In some collateral experiments I wanted to evaluate if the triple deletion of *DOA4 PEP4 PRB1*, which was able to rescue ~ 80% of the wild-type level of free ubiquitin (Swaminathan et al., 1999) had a positive effect on UV sensitivity, PCNA ubiquitylation or both. We found that the almost wild-type re-establishment of free cellular ubiquitin had no positive effect on PCNA ubiquitylation and the deletion of all the three genes was increasing the UV sensitivity.

The future extension and improvement of the present PRR model will mainly require a better characterization of the crosstalk between NER and PRR. The most important parameter to define will be the number of UV lesion as INPUT of the model. This amount cannot be calculated only through a linear regression of published dose-response data (see submitted manuscript at page 6: "Number of DNA lesions" and the respective Tables 3 and 4 at pages 27 and 28), but it must take into account how many UV lesions will be directly repaired by NER and how many lesions will go through PRR, generating PCNA ubiquitylation. Moreover, this parameter will likely be influenced by the cell cycle phases, since the way UV lesions are "contended" between NER and PRR changes in a cell cycle-dependent manner.

Another point of improvement is to better describe the switch-off module of the model. It is actually codified through three generic biochemical reactions of switch-off. Unfortunately, during the time of my PhD, I was unable to fully clarify the mechanisms leading to the disappearance of all ubiquitylated PCNA isoforms. We tried to interfere with the two most probable ways of signal switch-off, PCNA chromatin unloading and deubiquitylation, but we obtained only partial answers. An unexpected result was obtained by interfering with another pathway of PCNA modification, apparently disconnected with its UV-induced ubiquitylation. In fact, we found that deletion of the *UBC4* gene, caused a strong delay in PCNA ubiquitylation switch-off after high acute UV irradiation. The Ubc4 protein is an E2 enzyme involved in proteasomal protein degradation (Chuang and Madura, 2005) and it is responsible for K107 PCNA ubiquitylation in response to DNA ligase I defects (Das-Bradoo et al., 2010). As stated before, modification of PCNA on K107 is

carried out by the Rad5-Mms2 ubiquitylating proteins of the error-free PRR sub-pathway, with Ubc4 replacing Ubc13; however, how such modification affects PRR in budding yeast in response to UV irradiation still remains to be clarified.

The discovery of another PCNA residue (K107 in budding yeast, but still unknown in mammalian cells), that can be covalently modified beside K164 (ubiquitin and SUMO) and K127 (SUMO), together with other PCNA post-translational modifications (for example phosphorylation on Y211 or acetylation on K14 in human cells after UV treatment), suggest the intriguing possibility that a PCNA modification code may exist analogous to that found for histone molecules. Considering the homo-trimeric nature of PCNA and the fact that each subunit can be differently modified, the possible combinations may be extremely relevant. A Systems Biology approach could be helpful to shed some light on the existence and on the biological relevance of a PCNA post-translational modification code.

REFERENCES

Armstrong JD, Chadee DN, Kunz BA. 1994. Roles for the yeast RAD18 and RAD52 DNA repair genes in UV mutagenesis. *Mutat Res.*, 315(3):281-93.

Bailly V. Lamb,J, Sung P, Prakash S and Prakash L. 1994. Specific complex formation between yeast RAD6 and RAD18 proteins: a potential mechanism for targeting RAD6 ubiquitin-conjugating activity to DNA damage sites. *Gen. & Dev.*, 8:811-820.

Bailly V, Lauder S, Prakash S and Prakash L. 1997. Yeast DNA repair proteins Rad6 and Rad18 form a heterodimer that has ubiquitin conjugating, DNA binding, and ATP hydrolytic activities. *J. Biol. Chem.*, 272:23360-5.

Barbour L and Xiao W. 2003. Regulation of alternative replication bypass pathways at stalled replication forks and its effects on ge nome stability: a yeast model. *Mutat. Res.*, 532:137-155.

Besozzi D, Cazzaniga P, Mauri G, Pescini D, 2010. BioSimWare: a software for the modeling, simulation and analysis of biological systems. In Membrane Computing, 11th International Conference, CMC 2010, Jena, Germany. LNCS 6501, 2010:119-143.

References

Blastyak A, Pinter L, Unk I, Prakash L, Prakash S, Haracska L. 2007. Yeast Rad5 protein required for postreplication repair has a DNA helicase activity specific for replication fork regression. *Mol. Cell*, 28:167–175.

Branzei D, Seki M and Enomoto T. 2004. Rad18/Rad5/Mms2-mediated polyubiquitination of PCNA is implicated in replication completion during replication stress. *Genes Cells*, 9(11):1031-42.

Branzei D, Vanoli F, Foiani M. 2008. SUMOylation regulates Rad18-mediated template switch. *Nature*, 456(7224):915-20.

Chen J, Bozza W, Zhuang Z. 2011. Ubiquitination of PCNA and its essential role in eukaryotic translesion synthesis. *Cell Biochem. Biophys.*, 60(1-2):47-60.

Chen S, Davies A, Sagan D and Ulrich HD. 2005. The RING finger ATPase Rad5p of Saccharomyces cerevisiae contributes to DNA double-strand break repair in a ubiquitin-independent manner. *Nucleic acids research*, 33:5878-86.

Chen S, Levin MK, Sakato M, Zhou Y and Hingorani MM. 2009. Mechanism of ATP-Driven PCNA Clamp Loading by S.cerevisiae RFC. *J. Mol. Biol.*, 388:431-442.

References

Chuang SM and Madura K. 2005. Saccharomyces cerevisiae Ub-conjugating enzyme Ubc4 binds the proteasome in the presence of translationally damaged proteins. Genetics, 171(4):1477-84.

Cox BS and Parry JM. 1968. The isolation, genetics and survival characteristics of ultraviolet-light sensitive mutants in yeast. *Mutat. Res.* 6:37-55.

Daigaku Y, Davies AA and Ulrich HD. 2010. Ubiquitin-dependent DNA damage bypass is separable from genome replication. *Nature*, 465(7300):951-5.

Das-Bradoo S, Nguyen HD, Wood JL, Ricke RM, Haworth JC, Bielinsky AK. 2010. Defects in DNA ligase I trigger PCNA ubiquitylation at Lys 107. *Nat. Cell Biol.*, 12(1):74-9.

Dantuma NP, Heinen C, Hoogstraten D. 2009. The ubiquitin receptor Rad23: at the crossroads of nucleotide excision repair and proteasomal degradation. *DNA Repair (Amst)*, 8(4):449-60.

Davies A, Huttner D, Daigaku Y, Chen S and Ulrich HD. 2008. Activation of ubiquitin-dependent DNA damage bypass is mediated by replication protein. *Mol. Cell*, 29:625-36.

References

Diamant N, Hendel A, Vered I, Carell T, Reissner T, de Wind N, Geacinov N, Livneh Z. 2012. DNA damage bypass operates in the S and G2 phases of the cell cycle and exhibits differential mutagenicity. Nucleic Acids Res., 40(1):170-80.

Friedberg EC, Walker GC, Siede W, Wood RD, Schultz RA and Ellenberger TE. 2005. DNA repair and mutagenesis, 2nd ed. ASM Press, Washington, DC.

Gali H, Juhasz S, Morocz M, Hajdu I, Fatyol K, Szukacsov V, Burkovics P, Haracska L. 2012. Role of SUMO modification of human PCNA at stalled replication fork. *Nucleic Acids Res.*, 40(13):6049-59.

Gangavarapu V, Haracska L, Unk I, Johnson RE, Prakash S, Prakash L. 2006. Mms2-Ubc13-dependent and -independent roles of Rad5 ubiquitin ligase in post-replication repair and translesion DNA synthesis in Saccharomyces cerevisiae. *Mol. Cell Biol.*, 26(20):7783-90.

Giannattasio M, Lazzaro F, Longhese MP, Plevani P, Muzi-Falconi M. 2004. Physical and functional interactions between nucleotide excision repair and DNA damage checkpoint. *EMBO J.*, 23(2):429-38.

Giannattasio M, Follonier C, Tourrière H, Puddu F, Lazzaro F, Pasero P, Lopes M, Plevani P, Muzi-Falconi M. 2010. Exo1 competes with repair synthesis, converts NER intermediates to long ssDNA gaps, and promotes checkpoint activation. *Mol Cell.*, 40(1): 50-62.

References

Gomes XV and Burgers PM. 2001. ATP utilization by yeast replication factor C. I. ATP-mediated interaction with DNA and with proliferating cell nuclear antigen. *J. Biol. Chem.*, 276(37):34768-75.

Gong J and Siede W. 2011. Infuence of deubiquitinating enzymes on mutagenesis in Saccharomyces cerevisiae. *Internet J. Microb.*, 9(2).

Haas A and Rose I. 1982. The mechanism of ubiquitin activating enzyme. A kinetic and equilibrium analysis. *J. Biol. Chem.*, 257(17):10329-37.

Hafiz A. 2004. Principles and Reactions of Protein Extraction, Purification, and Characterization. CRC Press 2004.

Hanna J, Leggett D, Finley D. 2003. Ubiquitin depletion as a key mediator of toxicity by translational inhibitors. *Mol. Cell Biol.*, 23(24):9251-9261.

Hibbert RG, Huang A, Boelens R and Sixma TK. 2011. E3 ligase Rad18 promotes monoubiquitination rather than ubiquitin chain formation by E2 enzyme Rad6. *Proc Natl Acad Sci USA*, 108(14):5590-5.

Hicke L and Dunn R. 2003. Regulation of membrane protein transport by ubiquitin and ubiquitin-binding proteins. *Annu Rev Cell Dev Biol.*, 19:141-72.

References

Higgins NP, Kato K, Strauss B. 1976. A model for replication repair in mammalian cells. *J. Mol. Biol.*, 101(3):417-25.

Hoege C, Pfander B, Moldovan GL, Pyrowolakis G and Jentsch S. 2002. RAD6-dependent DNA repair is linked to modification of PCNA by ubiquitin and SUMO. *Nature*, 419:135-41.

Hofmann RM and Pickart CM. 1999. Ubiquitin-Conjugating Enzyme Functions in Assembly of Novel Polyubiquitin Chains for DNA Repair. *Cell*, 96:645-653.

Hofmann RM and Pickart CM. 2001. In vitro assembly and recognition of Lys-63 polyubiquitin chains. *J. Biol. Chem.*, 276:27936-43.

Huang A, Hibbert RG, De Jong RN, Das D, Sixma TK, Boelens R. 2011. Symmetry and asymmetry of the RING-RING dimer of Rad18. *J. Mol Biol.*, 410(3):424-35.

Johnson RE, Prakash S and Prakash L. 1994. Yeast DNA repair protein RAD5 that promotes instability of simple repetitive sequences is a DNA-dependent ATPase. *J. Biol. Chem.*, 269: 28259–28262.

Johnson RE, Prakash S, Prakash L. 1999. Efficient Bypass of a Thymine-Thymine Dimer by Yeast DNA Polymerase, Pol-zeta. *Science*, **283**:1001-1004.

References

Johnson RE, Haracska L, Prakash S and Prakash L. 2001. Role of DNA Polymerase-eta in the Bypass of a (6-4) TT Photoproduct. *Mol Cell Biol.*, 21(10):3558-63.

Jones JS and Prakash L. 1991. Transcript levels of the *Saccharomyces cerevisiae* DNA repair gene RAD18 increase in UV irradiated cells and during meiosis but not during the mitotic cell cycle. *Nucleic Acids Res.*, 19:893-8.

Karras GI and Jentsch S. 2010. The RAD6 DNA Damage Tolerance Pathway Operates Uncoupled from the Replication Fork and Is Functional Beyond S Phase. *Cell*, 141(2):255-67.

Krishna TS, Kong XP, Gary S, Burgers PM, Kuriyan J. 1994. Crystal structure of the eukaryotic DNA polymerase processivity factor PCNA. *Cell*, 79(7):1233-1243.

Kuluncsics Z, Perdiz D, Brulay E, Muel B, Sage E. 1999. Wavelength dependence of ultraviolet-induced DNA damage distribution: involvement of direct or indirect mechanisms and possible artefacts. *J Photochem Photobiol B.*, 49(1):71-80.

Lawrence CW, Christensen R. 1976. UV mutagenesis in radiation-sensitive strains of yeast. *Genetics*, 82(2):207-32.

References

Lazzaro F, Giannattasio M, Puddu F, Granata M, Pellicioli A, Plevani P, Muzi-Falconi M. 2009. Checkpoint mechanisms at the intersection between DNA damage and repair. *DNA Repair (Amst)*, 8(9):1055-67.

Lee I and Schindelin H. 2008. Structural insights into E1-catalyzed ubiquitin activation and transfer to conjugating enzymes. Cell, 134(2):268-278.

Lis ET and Romesberg FE. 2006. Role of Doa1 in the Saccharomyces cerevisiae DNA damage response. *Mol Cell Biol.*, 26(11):4122-33.

Madura K, Prakash S, Prakash L. 1990. Expression of the *Saccharomyces cerevisiae* DNA repair gene RAD6 that encodes a ubiquitin conjugating enzyme, increases in response to DNA damage and in meiosis but remains constant during the mitotic cell cycle. *Nucleic Acids Res.*, 18:771–778.

Majka J and Burgers PM. 2004. The PCNA-RFC families of DNA clamps and clamp loaders. *Prog. Nucleic Acid Res. Mol. Biol.*, 78:227-60.

McCready S and Cox B. 1993. Repair of 6-4 photoproducts in Saccharomyces cerevisiae. *Mutation research*, 293:233-40.

Mimnaugh EG and Neckers LM. 2002. Immunoblotting Methods for the Study of Protein Ubiquitination. *Methods in Mol. Biol.*, 194:179-203.

References

Moldovan GL, Pfander B, Jentsch S. 2006. PCNA controls establishment of sister chromatid cohesion during S phase. *Mol. Cell.*, 23(5):723-32.

Moldovan GL, Pfander B. and Jentsch S. 2007. PCNA, the maestro of the replication fork. *Cell*, 129:665-79.

Morin I, Ngo HP, Greenall A, Zubko MK, Morrice N and Lydall D. 2008. Checkpoint-dependent phosphorylation of Exo1 modulates the DNA damage response. *EMBO J.*, 27:2400–2410.

Nagasaki M, Doi A, Matsuno H, Miyano S. 2004a. A versatile Petri net based architecture for modeling and simulation of complex biological processes. *Genome Informatics*, 15(1):180-197.

Nagasaki M, Doi A, Matsuno H, Miyano S. 2004b. Genomic Object Net: a platform for modeling and simulating biopathways, *Applied Bioinformatics*, 2:181-184.

Nieduszynski C, Knox Y and Donaldson AD. 2006. Genome-wide identification of replication origins in yeast by comparative genomics. *Genes & development*, **20**, 1874-9.

Notenboom V, Hibbert RG, van Rossum-Fikkert SE, Olsen JV, Mann M, Sixma TK. 2007. Functional characterization of Rad18 domains for Rad6, ubiquitin, DNA binding and PCNA modification. *Nucleic Acids Res.*, 35(17):5819-30.

References

Novarina D, Amara F, Lazzaro F, Plevani P and Muzi-Falconi M. 2010. Mind the gap: Keeping UV lesions in check. *DNA repair*, 10(7):751-9.

Pagès V, Bresson A, Acharya N, Prakash S, Fuchs RP, Prakash L. 2008. Requirement of Rad5 for DNA polymerase zeta-dependent translesion synthesis in Saccharomyces cerevisiae. *Genetics*, 180(1):73-82.

Parker JL, Bucceri A, Davies AA, Heidrich K, Windecker H, Ulrich HD. 2008. SUMO modification of PCNA is controlled by DNA. *EMBO J.*, 27(18):2422-31.

Parker J and Ulrich HD. 2009. Mechanistic analysis of PCNA polyubiquitylation by the ubiquitin protein ligases Rad18 and Rad5. *EMBO J.*, 28(23):3657–3666.

Popolo L, Vanoni M, Alberghina L. 1982. Control of the yeast cell cycle by protein synthesis. *Exp. Cell Res.*, 142(1):69-78.

Raboy B, Marom A, Dor Y and Kulka GR. 1999. Heat-induced cell cycle arrest of Saccharomyces cerevisiae: involvement of the RAD6/UBC2 and WSC2 genes in its reversal. *Mol. Microbiol.,* 32:729-739.

Sandell LL and Zakian VA. 1993. Loss of a yeast telomere: Arrest, recovery, and chromosome loss. *Cell*, 75(4):729–739.

References

Saugar I, Parker JL, Zhao S and Ulrich HD. 2012. The genome maintenance factor Mgs1 is targeted to sites of replication stress by ubiquitylated PCNA. *Nucleic acids research*, 40:245-57.

Shannon P, Markiel A, Ozier O, Baliga NS, Wang JT, Ramage D, Amin N, Schwikowski B, Ideker T. 2003. Cytoscape: a software environment for integrated models of biomolecular interaction networks. *Genome Res.*, 13(11): 2498-504.

Stelter P and Ulrich HD. 2003. Control of spontaneous and damage-induced mutagenesis by SUMO and ubiquitin conjugation. *Nature*, 425(6954):188-91.

Stoimenov I and Helleday T. 2009. PCNA on the crossroad of cancer. *Biochem. Soc. Trans.*, 37(3):605-13.

Swaminathan S, Amerik A, Hochstrasser M. 1999. The Doa4 deubiquitinating enzyme is required for ubiquitin homeostasis in yeast. Mol. Cell Biol., 10(8):2583-2594.

Swerdlow PS, Finley D and Varshavsky A. 1986. Enhancement of immunoblot sensitivity by heating of hydrated filters. Anal. Biochem., 156:147-153.

Taylor JS and Cohrs MP. 1987. DNA, light and Dewar pyrimidinones: the structure and biological significance of TpT3. *J. Am. Chem. Soc.*, 109: 2834-2835.

References

Taylor JS, Lu HF, Kotyk JJ. 1990. Quantitative conversion of the (6-4) photoproduct of TpdC to its Dewar valence isomer upon e xposure to simulated sunlight. *Photochem. and Photobiol.*, 51(2):161–167.

Torres-ramos CA, Prakash S and Prakash L. 2002. Requirement of RAD5 and MMS2 for Postreplication Repair of UV-induced Damaged DNA in Saccharomyces cerevisiae. *Mol. Cell Biol.*, 22(7):2419–2426.

Ulrich HD and Jentsch S. 2000. Two RING finger proteins mediate cooperation between ubiquitin-conjugating enzymes in DNA repair. *EMBO J.*, 19(13):3388-97.

Ulrich HD. 2001. The *srs2* suppressor of UV sensitivity acts specifically on the *RAD5*- and *MMS2*-dependent branch of the *RAD6* pathway. *Nucleic Acids Res.*, 29:3487–3494.

Ulrich HD. 2003. Protein-protein interactions within an E2-RING finger complex. Implications for ubiquitin-dependent DNA damage repair. *J. Biol. Chem.*, 278:7051-8.

Ulrich HD and Davies AA. 2009. In vivo detection and characterization of sumoylation targets in Saccharomyces cerevisiae. *Methods Mol. Biol.*, 497(II):81-103.

Ulrich HD and Walden H. 2010. Ubiquitin signalling in DNA replication and repair. *Nat. Rev. Mol. Cell Biol.*, 11(7):479-89.

References

VanDemark P, Hofmann RM, Tsui C, Pickart CM and Wolberger C. 2001. Molecular insights into polyubiquitin chain assembly: crystal structure of the Mms2/Ubc13 heterodimer. *Cell* 105:711-20.

Washington MT, Johnson RE, Prakash S and Prakash L. 2000. Accuracy of thymine-thymine dimer bypass by Saccharomyces cerevisiae DNA polymerase eta. *Proc. Natl. Acad. Sci. USA*, 97:3094-9.

Waters R and Moustacchi E. 1975. Dose dependence of the excision of ultraviolet-induced pyrimidine dimers from nuclear deoxyribonucleic acids of haploid and diploid Saccharomyces cerevisiae. *J. Bacteriol.*, 121(3):901-6.

Wiltrout ME and Walker GC. 2011. Proteasomal regulation of the mutagenic translesion DNA polymerase, Saccharomyces cerevisiae Rev1. *DNA Repair,* **10**:169-175.

Windecker H and Ulrich HD. 2008. Architecture and Assembly of Poly-SUMO Chains on PCNA in Saccharomyces cerevisiae. *J. Mol. Biol.*, 376(1):221-31.

Xiao W, Chow BL, Broomfield S and Hanna M. 2000. Saccharomyces cerevisiae RAD6 group is composed of an Error-Prone and Two Error-Free Postreplication Repair Pathways. *Genetics*, 155:1633–1641.

References

Yao NY, Johnson A, Bowman GD, Kuriyan J and O'Donnell M. 2006. Mechanism of proliferating cell nuclear antigen clamp opening by replication factor C. *J. Biol. Chem.*, 281:17528-39.

Zhao S and Ulrich HD. 2010. Distinct consequences of posttranslational modification by linear versus K63-linked polyubiquitin chains. *Proc Natl Acad Sci USA*, 107:7704-9.

PART II

CONTENT

Published paper I

Lazzaro F, Novarina D, Amara F, Watt DL, Stone JE, Costanzo V, Burgers PM, Kunkel TA, Plevani P, Muzi-Falconi M. 2012. RNase H and postreplication repair protect cells from ribonucleotides incorporated in DNA. *Mol Cell.,*45(1):99-110.

Published paper II

Novarina D, Amara F, Lazzaro F, Plevani P, Muzi-Falconi M. 2011. Mind the gap: keeping UV lesions in check. *DNA Repair (Amst)*,10(7):751-9.

Published paper III

Muzi-Falconi M, Plevani P and Amara F. 2012. Cell cycle checkpoints. *Springer Reference*,
http://www.springerreference.com/index/chapterdbid/306217.
It will be a chapter of the Encyclopedia of Systems Biology. Dubitzky W, Wolkenhauer O, Yokota H, Cho KH. 2013.

Submitted manuscript (24 July 2012)

Amara F, Colombo R, Cazzaniga P, Pescini D, Csikasz-Nagy A, Muzi-Falconi M, Besozzi D and Plevani P. *In vivo* and *in silico* analysis of PCNA ubiquitylation in the activation of the Post-Replication Repair pathway in S.cerevisiae. *BMC Systems Biology*.

Published paper I

Use of the optimized protocol for *in vivo* detection of ubiquitylated PCNA in the presence of hybrid RNA-DNA structures in the genome

The optimized protocol I developed for the detection of ubiquitylated PCNA was used also in another project. In particular, Dr. Lazzaro was investigating the activation of PRR in the absence of RNAses H. The lack of this enzyme(s) causes the persistence of RNA in the genome, that must be bypassed during DNA replication. Dr. Lazzaro et al., provide a series of genetic data including the synthetic lethality obtained by combining mutations in the genes encoding RNAse H enzymes with certain genes of the *RAD6* epistasis group. Thanks to the protocol I developed and experiments that I carried out in the Lazzaro et al., paper is provided the biochemical evidence that cells lacking RNAse H, PCNA is ubiquitylated and PRR is chronically activated.

Molecular Cell
Article

RNase H and Postreplication Repair Protect Cells from Ribonucleotides Incorporated in DNA

Federico Lazzaro,[1] Daniele Novarina,[1] Flavio Amara,[1] Danielle L. Watt,[2] Jana E. Stone,[2] Vincenzo Costanzo,[3] Peter M. Burgers,[4] Thomas A. Kunkel,[2] Paolo Plevani,[1,*] and Marco Muzi-Falconi[1,*]
[1]Dipartimento di Scienze Biomolecolari e Biotecnologie, Università degli Studi di Milano, 20133 Milano, Italy
[2]Laboratory of Structural Biology and Laboratory of Molecular Genetics, National Institute of Environmental Health Sciences, National Institutes of Health, DHHS, Research Triangle Park, NC 27709, USA
[3]Genome Stability Unit, Clare Hall Laboratories, London Research Institute, Cancer Research UK, South Mimms, Hertfordshire EN6 3LD, UK
[4]Department of Biochemistry and Molecular Biophysics, Washington University School of Medicine, St. Louis, MO 63110, USA
*Correspondence: paolo.plevani@unimi.it (P.P.), marco.muzifalconi@unimi.it (M.M.-F.)
DOI 10.1016/j.molcel.2011.12.019

SUMMARY

The chemical identity and integrity of the genome is challenged by the incorporation of ribonucleoside triphosphates (rNTPs) in place of deoxyribonucleoside triphosphates (dNTPs) during replication. Misincorporation is limited by the selectivity of DNA replicases. We show that accumulation of ribonucleoside monophosphates (rNMPs) in the genome causes replication stress and has toxic consequences, particularly in the absence of RNase H1 and RNase H2, which remove rNMPs. We demonstrate that postreplication repair (PRR) pathways—*MMS2*-dependent template switch and Pol ζ-dependent bypass—are crucial for tolerating the presence of rNMPs in the chromosomes; indeed, we show that Pol ζ efficiently replicates over 1–4 rNMPs. Moreover, cells lacking RNase H accumulate mono- and polyubiquitylated PCNA and have a constitutively activated PRR. Our findings describe a crucial function for RNase H1, RNase H2, template switch, and translesion DNA synthesis in overcoming rNTPs misincorporated during DNA replication, and may be relevant for the pathogenesis of Aicardi-Goutières syndrome.

INTRODUCTION

The integrity of the eukaryotic cellular genome is preserved by surveillance mechanisms that coordinate DNA replication, repair, and recombination with cell-cycle progression (Muzi-Falconi et al., 2003; Lazzaro et al., 2009). The DNA nature of the chromosomes provides for an intrinsic stability as opposed to the fragility of RNA, which is due to the higher reactivity of ribose compared to deoxyribose. The incorporation of ribonucleotides (rNTPs) in place of deoxyribonucleotides (dNTPs) within genomic DNA is generally avoided by the high selectivity of DNA polymerases, largely due to a steric gate residue in the polymerase active site (Joyce, 1997). However, there are occasions when rNTPs can be linked to DNA chains, such as during the synthesis of Okazaki fragments or possibly during repair of double strand DNA breaks in G1 (Nick McElhinny and Ramsden, 2003; Zhu and Shuman, 2008). Recent work indicates that during normal DNA replication, DNA polymerases can also incorporate rNTPs in place of dNTPs (Nick McElhinny et al., 2010b). rNMPs embedded in DNA are expected to represent a problem for cycling cells, sensitizing the DNA backbone to spontaneous and/or enzymatic nicking. Indeed, the presence of rNMPs in the yeast genome elevates the rate of short deletions in repeated sequences through a mechanism depending on topoisomerase I (Nick McElhinny et al., 2010a; Clark et al., 2011; Kim et al., 2011). Furthermore, the presence of rNMPs alters DNA helix parameters. For example, structural studies (Egli et al., 1993; Jaishree et al., 1993; Ban et al., 1994a; Ban et al., 1994b; Wahl and Sundaralingam, 2000) indicate that rNMPs in dsDNA alter global conformation from B- to A-form, with most of the sugars adopting C3′-endo or closely related conformations. rNMPs must be removed prior to the next cell cycle or they will pose problems during subsequent rounds of replication; in fact, efficient and accurate synthesis by replicative DNA polymerases strongly depends on helix geometry, such that changes in sugar pucker could render a primer terminus more difficult to extend. Indeed, a recent study has shown that single rNMPs in DNA templates impede DNA synthesis by the yeast replicases (Watt et al., 2011). Altered helix geometry may be less problematic for polymerases specialized for translesion synthesis, e.g., DNA polymerase ζ, which can efficiently extend aberrant primer termini (Prakash et al., 2005). An important question is thus how cells cope with replicating chromosomes containing rNMPs that escape repair.

RNase H is a family of enzymes that cleave the RNA moiety in RNA:DNA hybrids, allowing the reconstruction of a dsDNA molecule. Eukaryotic cells possess RNase H1 and RNase H2 activities that have partially overlapping substrate specificity. While RNase H1 requires at least a tract of four rNMPs to cleave, RNase H2 can incise 5′ to a single rNMP incorporated within a DNA molecule (Cerritelli and Crouch, 2009). The in vivo roles of RNase H in eukaryotic cells are still not fully understood. In mammalian cells, RNase H1 is essential for mitochondrial DNA replication (Cerritelli et al., 2003); such function is not conserved in budding yeast cells. The role of the nuclear population of RNase H1 is still not clear. RNase H2 represents the major

RNase H activity in eukaryotic cells and is involved in several cellular processes (Cerritelli and Crouch, 2009). Evidence indicates that these enzymes can process Okazaki fragments during replication although, at least in budding yeast, such activity is redundant and Okazaki fragment processing can be carried out by Rad27 and Dna2 (Rydberg and Game, 2002; Ayyagari et al., 2003). Furthermore, removal of R-loops, which accumulate when a transcription bubble collides with a replication fork, can be achieved by overexpressing RNase H (Huertas and Aguilera, 2003). Mutations in any of the three subunits of human RNase H2 are the molecular cause of a human genetic syndrome known as Aicardi-Goutières syndrome (AGS) (Crow et al., 2006a). The mechanism(s) involved in the pathogenesis of AGS is under intense investigation but still uncertain (Crow et al., 2006b; Yang et al., 2007; Stetson et al., 2008; Rice et al., 2009; Crow and Rehwinkel, 2009).

Another enzyme that processes rNMPs in DNA is topoisomerase I. It was recently reported that, in the absence of RNase H2, rNTPs incorporated in DNA are targeted by topoisomerase I, which cleaves but fails to rejoin the DNA backbone, generating a ssDNA break (Sekiguchi and Shuman, 1997; Kim et al., 2011). Interestingly, not all genomic rNMPs are topoisomerase I targets (Kim et al., 2011), and cells lacking RNase H2 do not exhibit growth defects, suggesting that cells must have other pathways allowing them to replicate rNMP-containing chromosomes.

In this work, we investigate the processes permitting yeast cells to survive in the presence of elevated rNTPs incorporated within genomic DNA. We show that both RNase H1 and RNase H2 play a critical role in repairing rNMPs incorporated by replicative polymerases, and in the absence of RNase H activity residual genomic rNMPs cause replication problems in the following cell cycle. When the replicative DNA polymerases encounter rNMPs in the template strand, endogenous replication stress is generated, which sensitizes cells to mild treatments with exogenous replication stress-inducing agents. In this situation, postreplication repair mechanisms are effectively responsible for the survival of RNase H defective cells. We provide genetic and biochemical evidence that rNMPs-containing chromosomes can be fully replicated through the action of template switch and DNA polymerase ζ, which efficiently bypasses rNMPs in a DNA template.

Our data show unexpected mechanisms that preserve genome integrity in normally replicating cells, extend the role of PRR, and particularly that of Pol ζ, to the replication of rNMPs in genomic DNA, and reveal a synthetic interaction between PRR, RNase H activities, and replication stress that may have relevant consequences for human disease, identifying a possible family of modifier genes that may influence the penetrance of a set of AGS mutations.

RESULTS

Unrepaired rNMPs Incorporated in Genomic DNA during Replication Sensitize Cells to Replication Stress-Inducing Agents

The preferential incorporation of dNTPs over that of rNTPs is at least partially provided by a steric gate that prevents replicative DNA polymerases from using rNTPs during the elongation step (Joyce, 1997). Nonetheless, budding yeast DNA polymerase ε has been demonstrated (Nick McElhinny et al., 2010b) to incorporate large numbers of rNTPs into DNA. This effect is exacerbated in a Pol ε variant, Pol2-M644G, where a methionine adjacent to the steric gate residue (Y645) has been changed to glycine (Nick McElhinny et al., 2010a). A *pol2-M644G rnh201Δ* strain, where the mutation in Pol ε is combined with inactivation of RNase H2, which has been implicated in processing of rNMPs incorporated during DNA synthesis, exhibits slower progression through S phase (Nick McElhinny et al., 2010a), coupled to phosphorylated Rad53 checkpoint kinase (Figure S1C), suggestive of increased replication stress.

Low levels of replication stress-inducing agents (HU or MMS) are known to be toxic for cells with replication problems. To test whether the presence of rNMPs in the template strand affected DNA replication, we plated *pol2-M644G rnh201Δ* cells on medium containing low doses of HU or MMS, which in wild-type cells only mildly slow down cell-cycle progression. Figure 1A shows that a combination of the *pol2-M644G* and *rnh201Δ* mutations, leading to accumulation of elevated levels of rNMPs in genomic DNA, causes high sensitivity to low levels of HU and MMS (see also Figure S5 for quantitative survival data). Interestingly, loss of RNase H1 alone does not sensitize *pol2-M644G* cells to HU or MMS (Figure 1A). These phenotypes can be explained by the fact that, even though the substrate specificity of RNase H1 partially overlaps with that of RNase H2, and both enzymes cleave DNA containing four or more consecutive rNMPs, only RNase H2 cleaves at single rNMPs (Cerritelli and Crouch, 2009). These observations suggest that the presence of large amounts of single rNMPs within chromosomal DNA generates endogenous replication stress. When both RNase H1 and H2 enzymes are inactivated, virtually all single and multiple rNMPs incorporated during DNA synthesis will persist until the next round of replication. Strikingly, *pol2-M644G rnh201Δ* is synthetic lethal with the absence of RNase H1 (Figure 1B), indicating that RNase H1 plays an important role in repairing the rNTPs incorporated by Pol ε.

RNase H1 Cooperates with RNase H2 in the Removal of rNMPs from the Chromosomes Preserving Genome Integrity

The critical role of both RNase H enzymes is supported by the fact that double mutant *rnh1Δ rnh201Δ*, *rnh1Δ rnh202Δ*, and *rnh1Δ rnh203Δ* cells (*RNH202* and *RNH203* encode the two noncatalytic subunits of RNase H2) are sensitive to low levels of replication stress even in the presence of normal replicases (Figure 1C). Microscopic observation revealed that *rnh1Δ rnh201Δ* cells form small and irregular microcolonies on plates containing 25 mM HU while wild-type cells generate a regular colony (Figure 1D). FACS analysis of synchronous cultures incubated with low levels of HU or MMS shows that cells lacking RNase H arrest in G2-M after the bulk of genome replication has been completed (Figures 1E and S1A), and western blot analysis of Rad53 kinase revealed that mutant cells accumulate hyperphosphorylated Rad53 (Figures 1F and S1B). It is worth noting that cycling cells of mutants that accumulate elevated rNMP levels in the genome exhibit a constitutively phosphorylated Rad53, indicative of

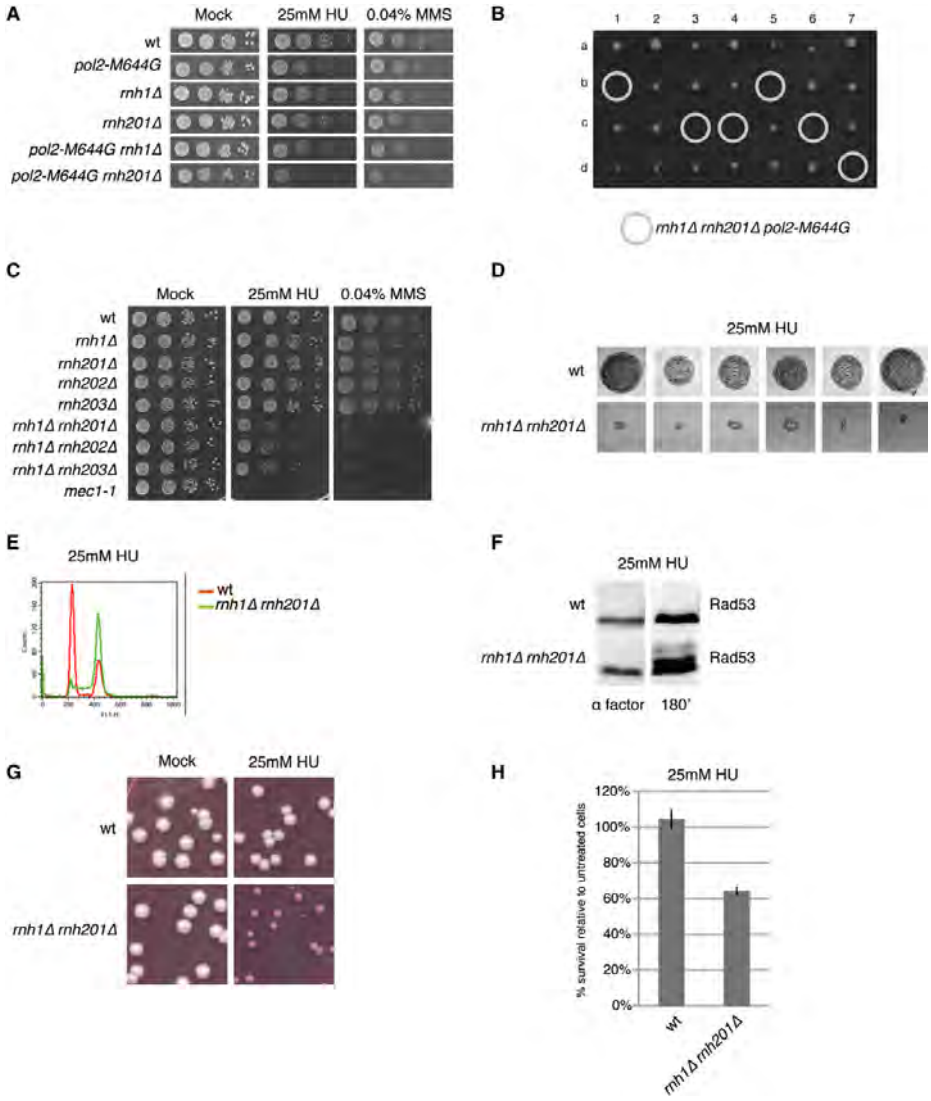

Figure 1. Abundant Incorporation of rNTPs into DNA Sensitizes Cells to Replication Stress and Is Lethal in Cells Lacking RNase H

(A) To test sensitivity to sublethal doses of HU or MMS, 10-fold serial dilutions of the indicated mutant strains were plated on YPD, YPD + 25 mM HU and YPD + 0.04% MMS. Pictures were taken after 3 days of incubation.

(B) Tetrads derived from a cross between *rnh1Δ rnh201Δ* and *rnh1Δ pol2-M644G* were dissected on YPD plates. Seven tetrads (1–7) are shown. The circles on the figure indicate the position of the original *rhn1Δ rnh201Δ pol2-M644G* spores.

(C) Sensitivity to HU and MMS of the indicated strains was tested as described in (A). A checkpoint-defective *mec1-1* strain was included as a positive control.

(D) Single cells were isolated on YPD plates and grown for 22 hr in the presence of 25 mM HU; colonies were visualized by microscopic analysis.

(E and F) wild-type and *rnh1Δ rn201Δ* cells were released in 25 mM HU after α factor arrest. After 180 min, cultures were analyzed by FACS, for DNA contents, and cell extracts were tested by western blotting with anti-Rad53 antibodies.

(G) Wild-type and *rnh1Δ rnh201Δ* cells were plated on YPD with or without 25 mM HU in the presence of Phloxine B, which stains in red colonies containing dead cells.

(H) Quantification of cell survival was obtained by plating G1 synchronized cells (100 cells per plate) on dishes containing 25 mM HU or mock. Colonies were counted after 3 days of incubation. The graph is representative of three independent experiments. Error bars describe standard deviation.

chronic replication stress (Figure S1C). These findings indicate that low doses of HU lead *rnh1Δ rnh201Δ* cells to block at the mitotic checkpoint and cause massive cell lethality, as suggested by the rugged shape of the microcolonies (Figure 1D) and further demonstrated by the fact that the small colonies eventually growing on 25 mM HU contain a large proportion of dead cells, which are stained by Phloxine B (Figure 1G). To estimate the extent of such lethality, we plated wild-type and *rnh1Δ rnh201Δ* cells in the absence or presence of 25 mM HU and calculated the percent survival on HU. Three independent experiments confirmed 40% lethality in cells lacking RNase H and exposed to low doses of HU (Figure 1H). Quantitative survival data for all the strains used throughout this study are shown in Figure S5. To test whether Rad53 phosphorylation and loss of cell viability derive from enzymatic processing of rNMP-containing DNA followed by chromosome breakage, we monitored phosphorylation of histone H2A on S129, a marker of DNA damage. Figure S1D shows that exposure of *rnh1Δ rnh201Δ* cultures to 25 mM HU does not induce H2A phosphorylation, suggesting that these cells do not accumulate double strand breaks, even when challenged with HU.

The sensitivity to HU observed upon loss of RNase H is unlikely to be due to the role of RNase H in Okazaki fragment processing or to a possible involvement in R-loop metabolism. Indeed, *rad27* mutated cells, which accumulate unprocessed Okazaki fragments (Ayyagari et al., 2003), are not sensitive to replication stress (Figure S2A). Moreover, combining *rnh1Δ rnh201Δ* with a mutation in *HPR1* gene, which leads to the accumulation of R-loops (Huertas and Aguilera, 2003), does not increase sensitivity to 25 mM HU and actually seems to mildly suppress the *rnh1Δ rnh201Δ* phenotype at this low dose, even though the mechanism is not known (Figure S2B). These findings strongly support the notion that RNase H activity is important to keeping genomic DNA free from rNMPs incorporated by DNA polymerases during replication and that sensitivity to replication stress-inducing drugs is a valid assay to track this process.

Survival of Cells with rNMPs-Containing Chromosomes Requires Translesion DNA Synthesis and Template Switch PRR Pathways

The survival of cells lacking RNase H activities indicates that yeast must have additional mechanisms to cope with the incorporation of rNTPs into the genome.

We investigated whether nucleotide excision repair (NER) or base excision repair (BER) play a role in the removal of rNMPs from the chromosomes. Abolishing NER (*rad14Δ*) or deleting *APN1*, which is responsible for $\geq$97% of AP endonuclease and 3′-diesterase activities required for BER (Popoff et al., 1990), does not sensitize *rnh1Δ rhn201Δ* cells to replication stress-inducing agents (Figure 2A). This result is consistent with data showing that rNMPs-containing DNA cannot be processed by NER and BER nucleases (Rydberg and Game, 2002). The observation that deletion of *APN2* in a *rnh1Δ rnh201Δ apn1Δ* causes an increase in sensitivity to 25 mM HU can be explained by the fact that simultaneous deletion of *APN1* and *APN2* causes an accumulation of elevated levels of endogenous lesions, increasing cellular stress (Leroy et al., 2001). We cannot exclude, though, that a secondary BER pathway may be able to process a minority of rNMPs.

Given that rNMPs in DNA templates impede DNA synthesis by the yeast replicases Pols ε and δ (Watt et al., 2011), lethality may result from failure to complete DNA replication. We thus investigated whether postreplication repair (PRR) mechanisms may allow full genome replication in *rnh1Δ rnh201Δ* cells. When DNA polymerases encounter replication-blocking lesions, PCNA is monoubiquitylated by Rad6-Rad18 triggering translesion DNA synthesis (TLS), while polyubiquitylation, carried out by Mms2-Ubc13-Rad5, promotes template switch (Ulrich, 2011).

We checked by spot assay whether deleting either branch of PRR would affect DNA replication in cells that do not remove rNMPs from genomic DNA, and cell lethality was quantitated as in Figure 1. Loss of only the template switch pathway (*mms2Δ*) or only translesion DNA synthesis (TLSΔ: corresponding to deletions of *REV1*, *REV3*, *REV7*, and *RAD30* genes encoding all TLS polymerases in budding yeast) does not sensitize cells lacking RNase H to HU. On the other hand, concomitant elimination of TLS and template switch results in almost no growth of *rnh1Δ rhn201Δ* cells in 25 mM HU, due to cell lethality (Figures 2B and 2C). These findings show that when *rnh1Δ rnh201Δ* cells are subjected to a low level of replication stress, survival depends almost entirely on either PRR pathway. This effect, although striking in the presence of HU, can also be detected in unperturbed conditions (bottom line, Figure 2B; see also Figures S3A and S3B). We conclude that cells devoid of RNase H1 and H2 can use TLS and template switch pathways to completely replicate their rNMPs-containing genome. Consistently, deletion of *RAD51*, which is required for a recombination-dependent PRR pathway (Gangavarapu et al., 2007), increases the sensitivity to HU of *rnh1Δ rnh201Δ* cells, while loss of *RAD52* is lethal in this genetic background (Figures 2D and 2E). These phenotypes may be influenced by defects in the additional processes that involve homologous recombination.

DNA Polymerase ζ Is the TLS Polymerase Replicating rNMPs-Containing DNA

To identify which translesion DNA polymerase allows the bypass of rNMPs, we combined mutations in genes coding each of the three yeast TLS polymerases, *REV1*, *REV3*/*REV7* (the catalytic and noncatalytic subunits of Pol ζ, respectively), and *RAD30* (Pol η) in *rnh1Δ rnh201Δ* cells. The experiment was performed in the absence of the *MMS2*-dependent template switch pathway, so that *rnh1Δ rnh201Δ* cells rely only on TLS to complete replication. The spot tests shown in Figure 3A reveal that *rnh1Δ rnh201Δ mms2Δ* cells carrying a deletion of *REV1* or direct inactivation of DNA polymerase ζ *(rev3Δ rev7Δ)* do not survive HU treatment and are less viable even in untreated conditions, recapitulating the total absence of TLS activities. Deletion of *RAD30* does not increase cell lethality under these conditions; on the contrary, we reproducibly observed that loss of Pol η confers an unexpected growth advantage when genomic DNA contains unrepaired rNMPs (Figure 3A), consistently with the phenotype observed in *rnh1Δ rnh201Δ TLSΔ* (Figures 2B and 2C). This unpredicted observation may be

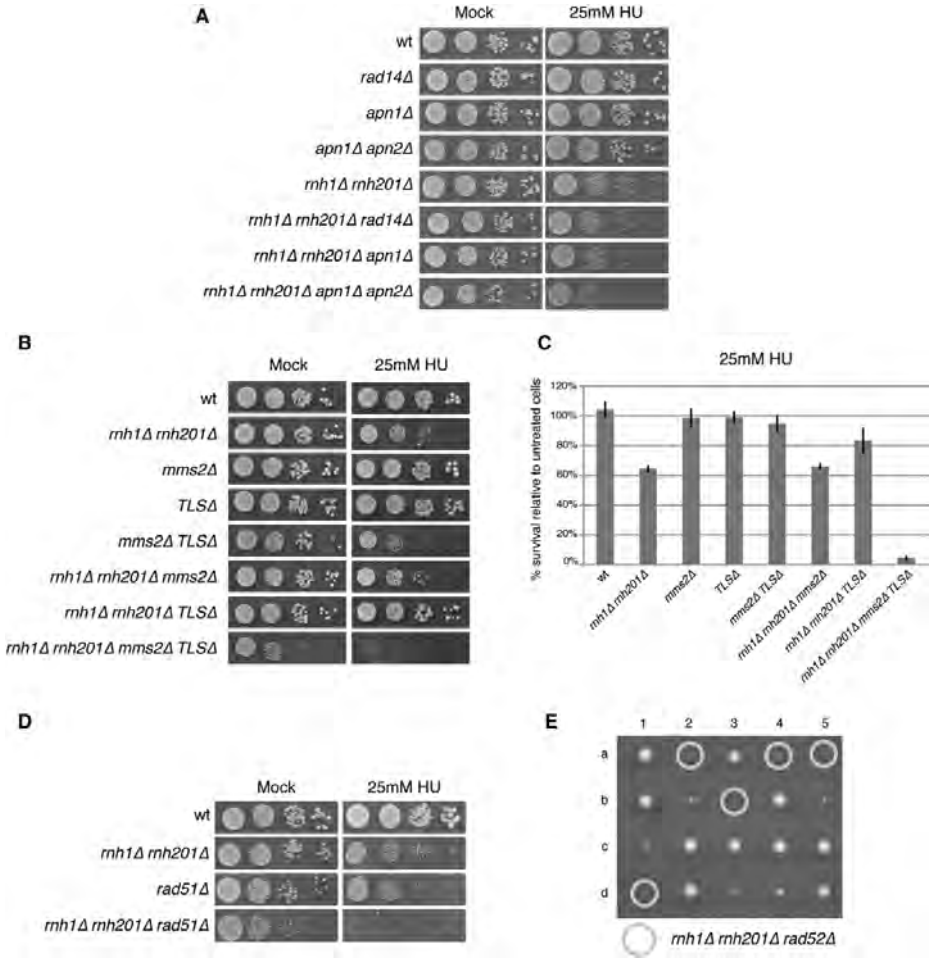

Figure 2. Postreplication Repair Is Specifically Required to Tolerate rNMPs-Containing Chromosomes

Sensitivity to sublethal doses of HU was assayed as described in Figure 1. Pictures were taken after 3 days of incubation. The contribution of NER (A), BER (A), the two branches of PRR (B), and *RAD51* (D) was tested. In (C), Quantification of cell survival was obtained as described in Figure 1H. The graph is representative of three independent experiments. Error bars describe standard deviation. It is worth noting that *mms2Δ TLSΔ* cells, despite being sensitive to HU in the spot tests, do not exhibit increased cell lethality, suggesting that the HU sensitivity derives from a very slow cell-cycle progression. In (E), tetrads derived from a cross between *rnh1Δ rnh201Δ* and *rad52Δ* were dissected on YPD plates. Five tetrads (1–5) are shown.The circles on the figure indicate the position of the original *rhn1Δ rnh201Δ rad52Δ* spores. Cells derived from such microcolonies do not grow when restreaked, revealing that a *rad52Δ* mutation is synthetic lethal with deletion of the *RNH1* and *RNH201* genes. *TLSΔ* comprises *rev1Δ rev3Δ rev7Δ rad30Δ*.

justified envisioning a competition between noneffective pol η and other PRR pathways.

Rev1 plays a noncatalytic role in supporting Pol ζ function (Lawrence and Hinkle, 1996; Lawrence, 2002) and also has a deoxycytidyl transferase activity (Nelson et al., 1996) that could insert a dCTP opposite a rNMP, allowing Pol ζ to extend. Figure 3B shows that, contrary to what was observed with *rev1Δ*, inactivating the polymerase activity of Rev1 does not significantly affect the HU sensitivity of *rnh1Δ rnh201Δ mms2Δ*. Altogether, these data indicate that cells can use Pol ζ to replicate rNMPs-containing templates in vivo and that Rev1 most likely plays a noncatalytic role to promote Pol ζ activity.

To confirm biochemically that DNA polymerase ζ is capable of bypassing rNMPs in DNA templates, we measured the rNMP bypass efficiency of purified yeast Pol ζ in vitro. Labeled substrates containing one, four, or sixteen consecutive rNMPs (Figure 4A) were incubated with purified DNA polymerase ζ or δ, and bypass efficiency was calculated after quantifying the

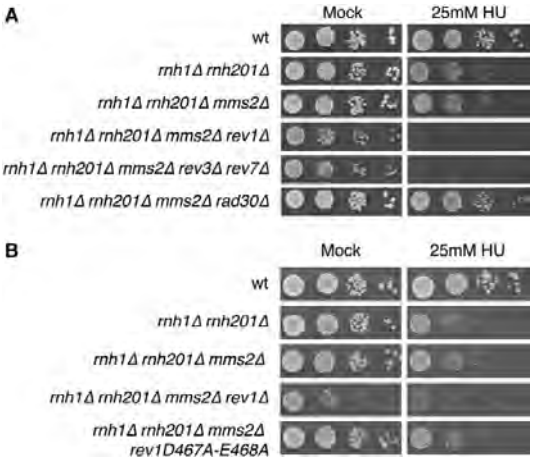

Figure 3. Pol ζ Allows Cells to Cope with Unrepaired rNMPs

The sensitivity to HU was measured as described in Figure 1: the specific contribution of each TLS polymerase (A) and the requirement of the catalytic activity of Rev1 (B) were tested.

primer extension products resulting from a single cycle of processive elongation (Figures 4B and 4D), as previously described (Nick McElhinny et al., 2010b). Consistently with the genetic observations (Figure 3A), the data indicate that Pol ζ bypasses ribonucleotides incorporated in DNA, efficiently copying DNA templates containing one (Figures 4B and 4D) or four rNMPs (Figures 4C, right, and 4D). This is in contrast with Pol δ which is somewhat less efficient in copying templates containing rC and much less efficient at copying templates containing rG, rA, rU, or four consecutive rNMPs (Watt et al., 2011) (Figures 4C and 4D). Pol δ bypass of rA or four consecutive rNMPs was stimulated several fold by adding PCNA to the reactions (see asterisks in Figure 4D), but in neither case was bypass as efficient as for Pol ζ.

We previously showed that, compared to RNase H2-proficient cells, *pol2-M644G rnh201Δ* strains (Nick McElhinny et al., 2010a) and *rnh201Δ* strains (Clark et al., 2011) have elevated rates of 2–5 base pair deletions in repetitive sequences and, recently, these deletions were shown to depend on topoisomerase 1 (Kim et al., 2011). This led to a model wherein topoisomerase 1 incises unrepaired rNMPs to create nicks in DNA with 3′-P and 5′-O ends that must be processed to allow ligation, and this processing may provide the opportunity for strand misalignments in repetitive sequences that yield the observed deletions. To determine if Pol ζ, which is relatively inaccurate (Zhong et al., 2006), might also contribute to this deletion mutagenesis, we measured the effect of deleting *REV3* on mutagenesis in the *pol2-M644G rnh201Δ* strain. Mutagenesis rates were estimated by measuring frequencies of formation of 5-FOA resistant clones, indicative of mutations leading to uracil auxotrophy. The results (Figure 4E) reveal that deleting *REV3* does not significantly (at p = 0.05; see figure legend) affect the overall rate of mutations to 5-FOA resistance, or the rates for total 2–5 base pair deletions or deletions of CA from a previously observed CACA hotspot sequence in the *URA3* gene. The lack of an effect of *rev3Δ* on mutagenesis suggests that Pol ζ does not contribute to topoisomerase 1-dependent mutagenesis resulting from unrepaired ribonucleotides incorporated during replication by Pol2-M644G. When the rate of base substitutions that might be explained by misincorporation of dCTP by Rev1p was calculated, no significant difference was observed between the *pol2-M644G* (from Pursell et al., 2007, and unpublished data), *pol2-644G rnh201Δ* (from Nick McElhinny et al., 2010a) and *pol2-M644G rnh201Δ rev3Δ* strains (from Figures 3 and S6). This supports the notion that the requirement for *REV1* in rNMPs bypass is structural rather dependent on its deoxycytidyltransferase activity.

RNase H-Defective Cells Exhibit Chronically Activated PRR Pathways

The relevance of PRR in coping with rNMPs in chromosomal DNA is evident by analyzing unperturbed mutant cells, which lack RNase H activities. FACS analysis of cycling cells suggests that *rnh1Δ rnh201Δ* cultures contain a higher fraction of S phase cells, and further inactivation of PRR pathways leads to a very sick phenotype (Figures 5A, S3A, and S3B). Indeed, these cells exhibit G2-M arrest coupled to cell lethality, as seen by Phloxine B staining of mutant colonies (Figure 5B).

Affinity-purified HIS-tagged PCNA from exponentially growing *rnh1Δ rnh201Δ* cells revealed a striking increase in PCNA ubiquitylation, compared to wild-type cells. Figure 5C shows that both mono- and polyubiquitylated forms of PCNA are abundant in cells that cannot remove rNMPs from genomic DNA. Conversely, no significant effect is observed in PCNA sumoylation (Figure 5D). Accordingly, deletion of *RAD18*, coding for the ubiquitin ligase responsible for conjugating ubiquitin to PCNA, has a synthetic effect when combined with the loss of RNase H: *rnh1Δ rnh201Δ rad18Δ* cells are exquisitely sensitive to 25 mM HU and exhibit cell lethality even in untreated conditions (Figure S3C).

All these results indicate that cells lacking RNase H have constitutively active PRR, which is crucial to tolerating the presence of rNMP-containing genomic DNA.

DISCUSSION

Yeast Cells Can Insert rNTPs into Genomic DNA

In eukaryotic cells the size of cellular dNTP pools is tightly controlled, and altered dNTP levels are responsible for increased mutagenesis and genome instability (Chabes and Stillman, 2007). Because the pools of rNTPs are much higher, DNA polymerases must be selective to correctly polymerize dNTPs during genome replication. Recent evidence has shown that during normal DNA replication in yeast, DNA polymerases incorporate rNTPs into genomic DNA. The *pol2-M644G* mutation affecting the steric gate of Pol ε increases rNTPs incorporation 10-fold (Nick McElhinny et al., 2010b). Genomic DNA isolated from *rnh201Δ* cells has a high number of alkali-sensitive sites, indicating that RNase H2 is involved in removing rNMPs from DNA (Nick McElhinny et al., 2010a).

Unrepaired rNMPs in genomic DNA will impact on cell-cycle progression since, at the next round of DNA replication, replicative polymerases must duplicate a RNA-containing DNA template. It has been shown that replicative polymerases cannot effectively replicate a template containing rNMPs (Nick McElhinny et al., 2010a; Watt et al., 2011), and this situation generates replication stress, detectable as a higher fraction of cells in S phase (Nick McElhinny et al., 2010a and Figure S1C). Combining a deletion in *RNH201*, coding for the catalytic subunit of RNase H2, with a *pol2-M644G* mutation, we found that cells became sensitive to low doses of replication stress inducing agents (i.e., HU or MMS). These data suggest that the short RNA tracts, which cannot be processed in the absence of RNase H2, cause replication stress when the cell tries to replicate them. Low levels of HU and MMS increase such stress leading to cell lethality.

Since loss of RNase H2 activity from *pol2-M644G* mutated cells does not cause cell lethality per se, additional pathways repairing rNMPs-containing chromosomes must exist. In this work we describe different mechanisms that are involved in allowing cells to cope with the presence of rNMPs in their genome.

RNase H1 Participates in the Removal from the Genome of rNMPs Introduced during DNA Replication

RNase H1 has some overlapping substrates with RNase H2 and is the preferential enzyme for processing RNA:DNA hybrids where more than four rNMPs are present. Double mutant cells, combining *rnh1Δ* with the deletion of any of the RNase H2 subunits, exhibit hypersensitivity to low levels of HU or MMS, a cell-cycle delay in G2-M, and activation of the Rad53 checkpoint kinase.

Strikingly, deletion of *RNH1*, the gene coding for RNase H1, is synthetic lethal when combined with the *pol2-M644G* mutation and RNase H2 inactivation (*rnh201Δ*), demonstrating that RNase H1 also plays a crucial role in the repair of rNMPs incorporated by replicative DNA polymerases. Our genetic analysis excludes a contribution of NER in correcting rNMPs, while a minor involvement of BER in repairing rNMP-containing chromosomes cannot be completely ruled out.

The observation that cells lacking RNase H activities are sensitive to low doses of replication stress-inducing agents may have consequences for cancer chemotherapy. In fact, many cancer cells are characterized by elevated levels of endogenous replication stress (Negrini et al., 2010) and may be thus sensitized to inhibitors of RNase H activity, which could selectively kill cells experiencing replication stress.

Recently, topoisomerase 1 has been reported to be able to process rNMPs-containing DNA and generate ssDNA breaks, which can be easily converted to chromosome breaks. We believe it unlikely that *rnh1Δ rnh201Δ* lethality in HU is due to such chromosome fragmentation, since in our experiments the *rnh1Δ rnh201Δ* double mutant and the wild-type strains exhibit a similar level of phosphorylated histone H2A (Figure S1D), suggesting the absence of double-strand breaks. Altogether, these findings indicate that high levels of unrepaired rNMPs in the chromosome hinder DNA synthesis blocking replication forks, leading to replication stress.

Either One of the PRR Pathways Is Sufficient for Tolerating rNTPs Incorporated by Replicative DNA Polymerases, and DNA Polymerase ζ Is the Enzyme Replicating rNMPs-Containing DNA

When replication-blocking lesions are present in the DNA template, replication forks stall at the site of damage and cannot proceed. Completion of replication is facilitated by PRR mechanisms, namely error-prone translesion DNA synthesis (TLS) and error-free template switch, a recombination-like pathway, requiring, respectively, mono- and polyubiquitylation of PCNA.

Strikingly, exponentially growing *rnh1Δ rnh201Δ* cells exhibit high levels of constitutive mono- and polyubiquitylated PCNA, indicative of chronic PRR activation. Either TLS or template switch can be used to complete replication over rNMPs. Indeed, a strong synthetic effect is observed when both PRR pathways are inactivated or when PCNA ubiquitylation is prevented in cells lacking RNase H activities: these cells are exquisitely sensitive to mild replication stress and are also extremely sick in untreated conditions, indicating a novel role for PRR in tolerating RNA-containing DNA templates (Figure 6).

How cells can replicate a chromosome containing rNMPs is not known. Yeast cells contain three TLS polymerases, Pol η, Pol ζ, and Rev1 (Friedberg et al., 1995). Our data show that, in the absence of a functional template switch pathway, rNMPs-containing DNA can only be replicated by the concerted action of Rev1 and Pol ζ. The fact that a catalytic *rev1* mutant is capable of rescuing the phenotype imparted by a *rev1Δ* mutation indicates that the role of Rev1 is likely to help Pol ζ to replicate rNMPs containing templates. Indeed, untreated *rnh1Δ rnh201Δ* cells lacking the template switch pathway and missing Pol ζ form fewer and smaller colonies. A similar synthetic phenotype is observed in *pol2-M644G* mutant cells lacking PRR pathways (Figure S4). In conclusion, template switch and Pol ζ are crucial to allow replication of endogenous, unrepaired rNMPs (Figure 6), and mutations increasing the rNMPs load, such as *pol2-M644G*, may saturate PRR pathways so that cell survival relies on RNase H1 and RNase H2. The crucial role of Pol ζ for replicating rNMP-containing chromosomes may be performed either by adding a dNTP opposite the rNMP, or by elongating, downstream of the damaged site, a chain created by a replicative polymerase. In vitro data confirm the genetic findings and demonstrate that Pol ζ can efficiently insert a nucleotide opposite the lesion, bypassing 1 or 4 rNMPs in the DNA template, revealing a new cognate, endogenous substrate for this essential, specialized TLS polymerase.

Recombination-dependent PRR mechanisms are less understood. Rad51 and Rad52 are involved in PRR (Gangavarapu et al., 2007) and in other recombination events and, in general, *rad52Δ* strains are more recombination defective than *rad51Δ* cells. We found that deletion of *RAD52* is synthetic lethal with loss of RNase H1 and RNase H2, and *rad51Δ* has a synthetic effect on HU sensitivity, supporting a role for recombination-dependent PRR in tolerating chromosomal rNMPs. However, defects in other recombination-dependent processes can contribute to these effects: for example, restart of blocked replication forks can proceed through recombination mechanisms (Heller and Marians, 2006; Petermann et al., 2010). Furthermore, RNase H enzymes may have diverse cellular targets in addition

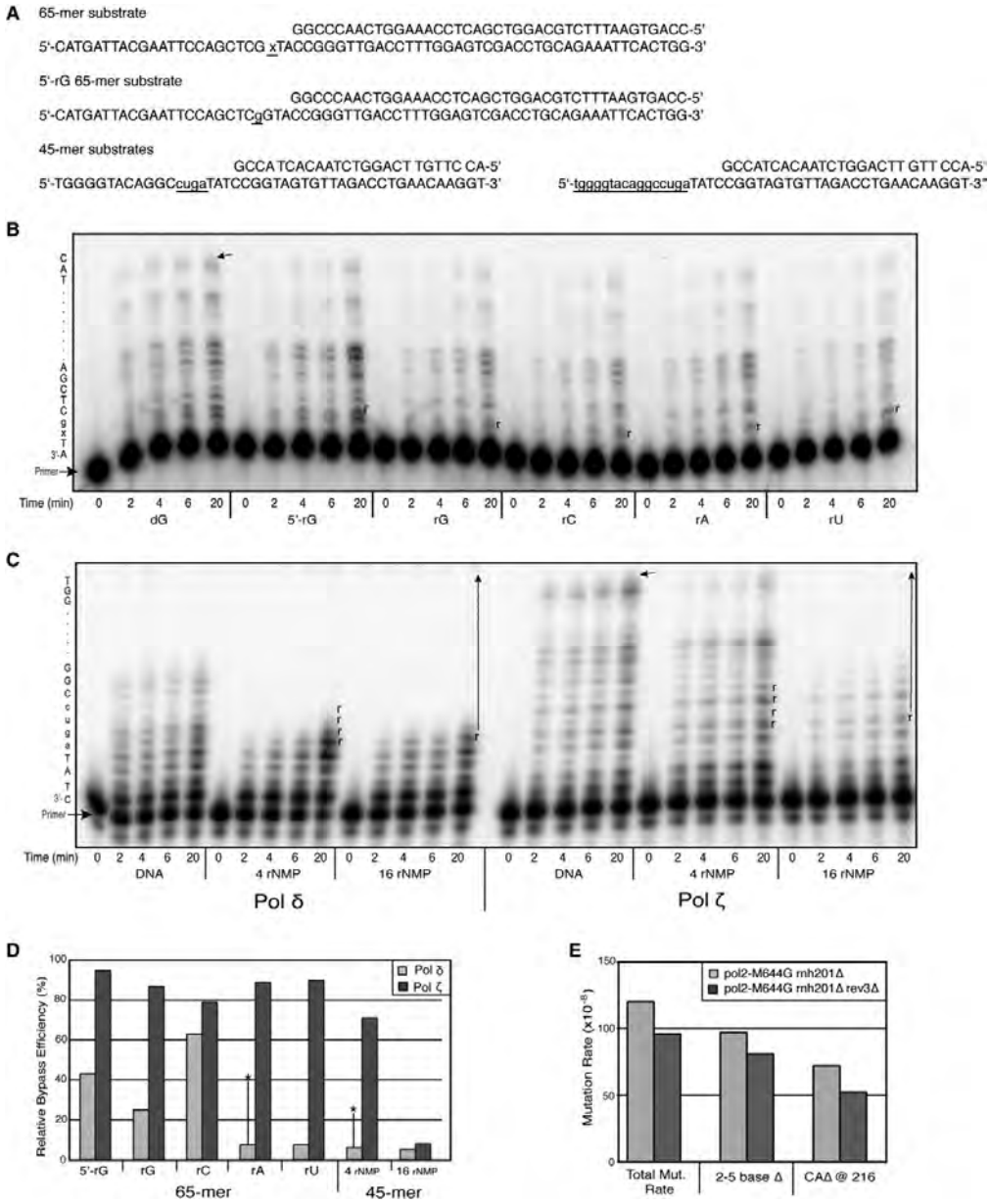

Figure 4. DNA Polymerase ζ Efficiently Bypasses rNMPs in the Template Strand

(A) Primer-template sequences. In the 65-mer substrate, "x" is the position of the single rNMP (rG, rC, rA, or rU) and "g" is the position of the 5′-rG in the DNA template. In the 45-mer substrate, the underlined lowercase nucleotides indicate the position and sequence of the rNMPs in 4- and 16-rNMP substrates, respectively.

(B and C) Phosphorimages of products generated during bypass of a single rNMP (B) and tracts of rNMPs by Pol δ and ζ (C). The template sequence is shown on the left, the arrow depicts the location of full-length product, and "r" represents the position of the rNMPs in the template. No enzyme was added to the unextended primer reaction (0 min).

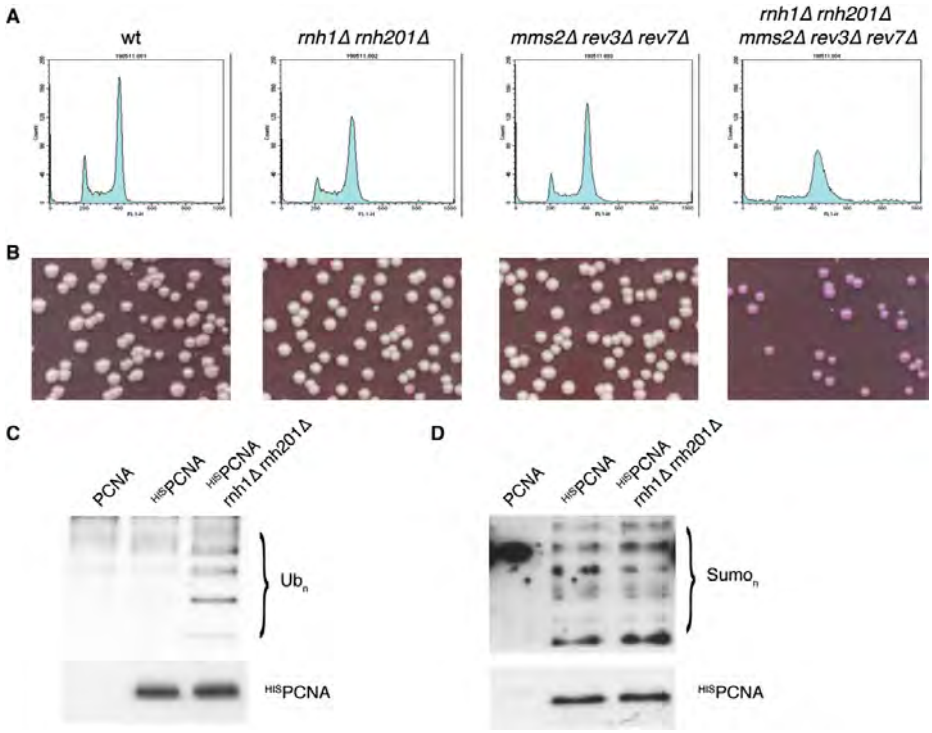

Figure 5. In the Absence of RNase H, the PRR Pathway Is Constitutively Activated and Promotes Cell Survival in an Unperturbed Cell Cycle
The role of PRR was assessed in unperturbed *rnh1Δ rnh201Δ* cultures. Exponentially growing cells lacking RNase H and defective in PRR were analyzed by FACS (A), to monitor cell cycle distribution, and by Phloxine B staining (B), to evaluate cell lethality. PCNA was affinity purified from exponentially growing unperturbed wild-type cells or from cells lacking RNase H activity. PCNA levels were estimated by western blotting with anti-HIS Ab. PCNA ubiquitylation was monitored by western blotting with anti-ubiquitin Ab (C), and PCNA sumoylation was monitored by western blotting with anti-SUMO Ab (D).

to rNTPs incorporated in genomic DNA. Among these are R-loops and Okazaki fragments; the accumulation of both these structures can have lethal outcomes and is prevented by recombination processes (Huertas and Aguilera, 2003; Ii and Brill, 2005).

Given the involvement of RNase H2 in the pathogenesis of the Aicardi-Goutières syndrome, the data reported in this work may help to understand the mechanisms underlying the disease. The reported synthetic effects between RNase H mutations, inducers of replication stress, and postreplication repair alterations, may facilitate the identification of modifier genes, whose alterations may be responsible for the phenotypic variability observed in different AGS patients carrying identical RNase H2 mutations.

EXPERIMENTAL PROCEDURES

Yeast Strains

Strains are derivatives of W303, unless otherwise indicated in Table S1, and were generated by standard genetic procedures (Adams et al., 1998). YFL1449 and YFL1376 were obtained by crossing and backcrossing five times *pol2-M644G* (Nick McElhinny et al., 2010a) or ^{HIS}PCNA (Ulrich and Davies, 2009) with SY2080.

(D) Relative bypass efficiencies for Pols δ and ζ. Images of reaction products shown in (B) and (C) were quantified, and relative bypass efficiencies were calculated as described (Stone et al., 2009). The values for Pol δ with the 65-mer substrates in the absence of PCNA have been reported previously (Watt et al., 2011) and are shown here for comparison. The asterisks indicate the relative bypass values for Pol δ for reaction mixtures containing 200 nM PCNA.
(E) Mutation rates for the *pol2-M644G rnh201Δ* and *pol2-M644G rnh201Δ rev3Δ* strains. The total mutation rates for resistance to 5-FOA were determined as described in Experimental Procedures. The 95% confidence intervals for the *pol2-M644G rnh201Δ* and *pol2-M644G rnh201Δ rev3Δ* strains were 110 to 200 and 57 to 140, respectively. For the *pol2-M644G rnh201Δ* strain, the rates for total 2–5 base pair deletions and for CA deletions at position 216–219 in *URA3* are from Clark et al. (2011). For the *pol2-M644G rnh201Δ rev3Δ* strain, rates for short deletions were calculated after sequencing the *ura3* gene in 163 independent 5-FOA resistant clones. Of these, 136 harbored 2–5 base pair deletions, 88 of which were CA deletions at the CACA hotspot at position 216–219 in *URA3* (see spectrum in Figure S6).

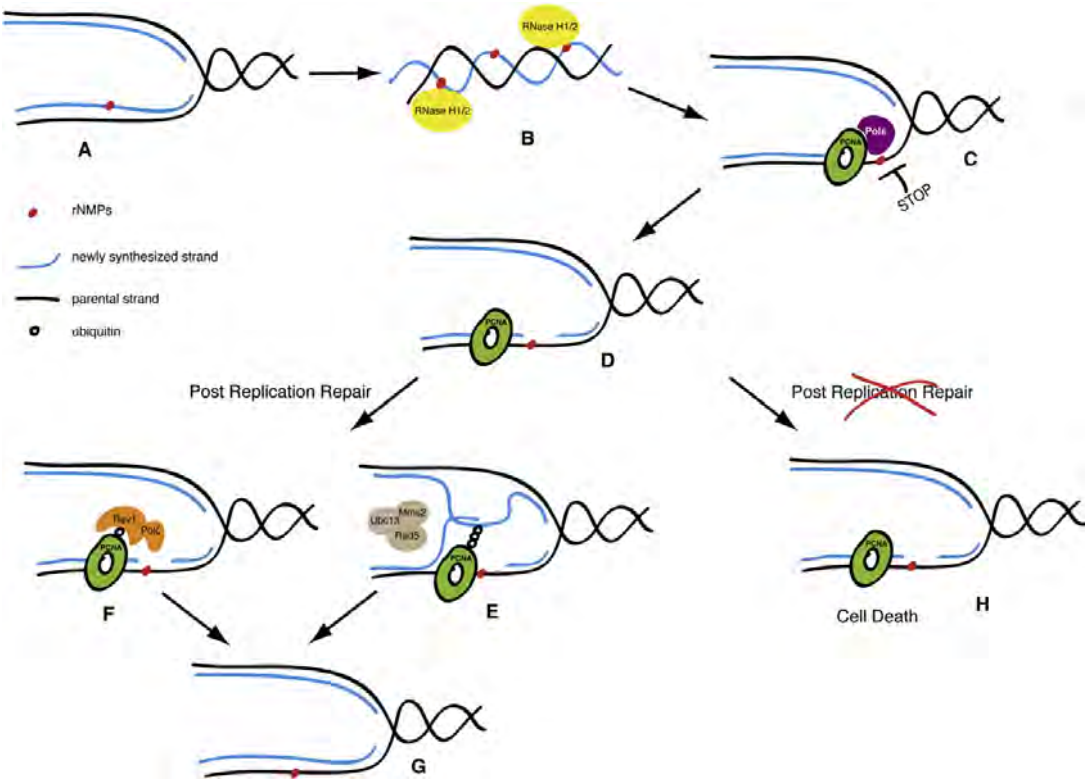

Figure 6. RNase H and Postreplication Repair Protect Cells from rNMPs Incorporated in Chromosomal DNA

During DNA synthesis, replicative polymerases can incorporate rNTPs (red dot) in place of dNTPs (A). RNase H1 and RNase H2 are required to remove rNMPs from newly replicated DNA (blue line) (B). If rNMPs persist until the following cell cycle, they will create problems at during the DNA synthesis step (C), since replicative polymerases cannot efficiently elongate the nascent strand opposite rNMPs in the template strand (black line). Replication fork restart downstream of the lesions leaves incomplete replication products for postreplication repair (D). PCNA is ubiquitylated. Either MMS2-dependent template switch mechanisms (E) or Pol ζ-dependent translesion synthesis (F) allow bypass of rNMPs and completion of replication (G). Under these conditions, inactivation of PRR causes cell lethality (H).

FACS Analysis

Cells were fixed in 70% ethanol and treated with RNase A and proteinase K. DNA was stained with Sytox Green and cell-cycle distribution was estimated by cytofluorimetric analysis with a FACScan.

SDS-PAGE and Western Blotting

To monitor protein levels and phosphorylation, TCA protein extracts were prepared and analyzed by SDS-PAGE (Sabbioneda et al., 2007); western blots were performed with anti-Rad53, anti-H2A, and anti-γH2AX antibodies.

To study PCNA posttranslational modifications, HIS-tagged PCNA was pulled down from denaturing extracts as described (Ulrich and Davies, 2009), separated on 10% SDS-Urea-PAGE, and transferred to nitrocellulose membranes. PCNA ubiquitylation and sumoylation were analyzed by western blotting with anti-ubiquitin and anti-SUMO antibodies.

Sensitivity Assay

To assess cell survival in HU and MMS, overnight yeast cultures were diluted to 1×10^6 cfu/ml, and 10-fold serial dilutions were spotted on plates containing HU or MMS at the indicated concentrations. Images were captured after 3 days' incubation at 28°C. To obtain quantitative data, exponentially growing cells were arrested in G1 with 6 μg/ml α-factor. Cultures were diluted and 100 cfu were distributed on each of three independent YPD plates (mock or 25 mM HU). After 3 days' incubation colonies were counted. The experiments were repeated three times. The graphs show the percentage of surviving cells with respect to the mock sample. Standard deviations were used to obtain error bars.

Cell Lethality Assay

Overnight yeast cultures were diluted as above, and ~100 cfu were plated on YPD containing 20 mg/l Phloxine B, with or without 25 mM HU. Images were captured after 3 days' incubation at 28°C.

Microcolony Assays

Yeast cells were grown to a concentration of 5×10^6 cells/ml and arrested in G1 with α-factor (6 μg/ml). Diluted samples were spread on YPD plates containing 25 mM HU, and single cells were separated using a micromanipulator. Plates were then incubated at 28°C and photographs were taken after 22 hr; thirty individual cells were followed for each experiment. The experiment was repeated four times, and a representative example is shown.

Cell-Cycle Analysis

Yeast cultures were grown to a concentration of 5 × 10^6 cells/ml and arrested in G1 with α-factor (6 μg/ml). Cells were released in YPD supplemented with 25 mM HU or 0.04% MMS or mock. Ninety minutes after, the release α-factor (6 μg/ml) was added back to the culture to avoid re-entry in S phase, allowing the analysis of a complete single cell cycle. Samples were collected for SDS-PAGE and FACS analysis and processed as described above. Growth curves were obtained by measuring cell concentration microscopically and normalizing each read to the initial concentration. Generation time was calculated by interpolating the growth curves.

rNMP Bypass, Mutation Rates, and Spectra

S.cerevisiae two-subunit wild-type Pol ζ (Rev3 –Rev7) and three-subunit Pol δ were expressed in yeast and purified as previously described (Burgers and Gerik, 1998; Garg et al., 2005). Oligonucleotide primer templates were prepared as described (Nick McElhinny et al., 2010b). The polymerase was added to initiate the reaction and aliquots were removed at 2, 4, 6, and 20 min. The DNA products were separated by electrophoresis through an 8% denaturing polyacrylamide gel containing 25% formamide for the 65-mer and 12% denaturing polyacrylamide gel for the 45-mer substrates. A PhosphorImager was used to visualize and quantify the DNA products. The efficiency of insertion opposite individual template positions and the bypass probability were calculated as previously described (Kokoska et al., 2003; Stone et al., 2009; Watt et al., 2011). Mutation rates and spectra were determined as described (Nick McElhinny et al., 2010a); in the relevant strains, the *URA3* reporter was inserted at the *AGP1* locus in orientation 2 as previously described (Nick McElhinny et al., 2010a).

SUPPLEMENTAL INFORMATION

Supplemental Information contains six figures, one table, and Supplemental References and can be found with this article online at doi:10.1016/j.molcel.2011.12.019.

ACKNOWLEDGMENTS

We thank H. Ulrich, A. Aguilera, and C. Santocanale for strains and reagents; J. Williams and A. Clark for comments on the manuscript; S. Sabbioneda, S. Carnevali, F. Spadaro, and the members of our laboratories for discussions. This work was supported by grants from AIRC, MIUR, and Fondazione Cariplo to P.P. and M.M.-F. and MIUR (FIRB RBFR10S3UQ) to F.L. The financial support of Telethon-Italy (grant number GGP11003) is gratefully acknowledged. F.L. was partially supported by a fellowship from Fondazione Buzzati-Traverso. Part of this work was supported by Project Z01ES065070 to T.A.K. from the Division of Intramural Research of the NIH and grant NIHGM32431 to P.M.B. Cancer Research UK, an ERC start-up grant (206281), the Lister Institute of Preventive Medicine, and the EMBO Young Investigator Program supported V.C.

Received: August 9, 2011
Revised: October 28, 2011
Accepted: December 6, 2011
Published: January 12, 2012

REFERENCES

Adams, A., Gottschling, D.E., Stearns, T., and Kaiser, C.A. (1998). Methods in yeast genetics: a Cold Spring Harbor Laboratory course manual (Plainview, NY: Cold Spring Harbor Laboratory Press).

Ayyagari, R., Gomes, X.V., Gordenin, D.A., and Burgers, P.M. (2003). Okazaki fragment maturation in yeast. I. Distribution of functions between *FEN1* AND *DNA2*. J. Biol. Chem. *278*, 1618–1625.

Ban, C., Ramakrishnan, B., and Sundaralingam, M. (1994a). A single 2′-hydroxyl group converts B-DNA to A-DNA. Crystal structure of the DNA-RNA chimeric decamer duplex d(CCGGC)r(G)d(CCGG) with a novel intermolecular G-C base-paired quadruplet. J. Mol. Biol. *236*, 275–285.

Ban, C., Ramakrishnan, B., and Sundaralingam, M. (1994b). Crystal structure of the highly distorted chimeric decamer r(C)d(CGGCGCCG)r(G).spermine complex—spermine binding to phosphate only and minor groove tertiary base-pairing. Nucleic Acids Res. *22*, 5466–5476.

Burgers, P.M., and Gerik, K.J. (1998). Structure and processivity of two forms of Saccharomyces cerevisiae DNA polymerase delta. J. Biol. Chem. *273*, 19756–19762.

Cerritelli, S.M., and Crouch, R.J. (2009). Ribonuclease H: the enzymes in eukaryotes. FEBS J. *276*, 1494–1505.

Cerritelli, S.M., Frolova, E.G., Feng, C., Grinberg, A., Love, P.E., and Crouch, R.J. (2003). Failure to produce mitochondrial DNA results in embryonic lethality in Rnaseh1 null mice. Mol. Cell *11*, 807–815.

Chabes, A., and Stillman, B. (2007). Constitutively high dNTP concentration inhibits cell cycle progression and the DNA damage checkpoint in yeast Saccharomyces cerevisiae. Proc. Natl. Acad. Sci. USA *104*, 1183–1188.

Clark, A.B., Lujan, S.A., Kissling, G.E., and Kunkel, T.A. (2011). Mismatch repair-independent tandem repeat sequence instability resulting ribonucleotide incorporation by DNA polymerase ε. DNA Repair (Amst.) *10*, 476–482.

Crow, Y.J., and Rehwinkel, J. (2009). Aicardi-Goutieres syndrome and related phenotypes: linking nucleic acid metabolism with autoimmunity. Hum. Mol. Genet. *18* (R2), R130–R136.

Crow, Y.J., Leitch, A., Hayward, B.E., Garner, A., Parmar, R., Griffith, E., Ali, M., Semple, C., Aicardi, J., Babul-Hirji, R., et al. (2006a). Mutations in genes encoding ribonuclease H2 subunits cause Aicardi-Goutières syndrome and mimic congenital viral brain infection. Nat. Genet. *38*, 910–916.

Crow, Y.J., Hayward, B.E., Parmar, R., Robins, P., Leitch, A., Ali, M., Black, D.N., van Bokhoven, H., Brunner, H.G., Hamel, B.C., et al. (2006b). Mutations in the gene encoding the 3′-5′ DNA exonuclease TREX1 cause Aicardi-Goutières syndrome at the AGS1 locus. Nat. Genet. *38*, 917–920.

Egli, M., Usman, N., and Rich, A. (1993). Conformational influence of the ribose 2′-hydroxyl group: crystal structures of DNA-RNA chimeric duplexes. Biochemistry *32*, 3221–3237.

Friedberg, E.C., Walker, G.C., and Siede, W. (1995). DNA repair and mutagenesis (Washington, DC: ASM Press).

Gangavarapu, V., Prakash, S., and Prakash, L. (2007). Requirement of RAD52 group genes for postreplication repair of UV-damaged DNA in Saccharomyces cerevisiae. Mol. Cell. Biol. *27*, 7758–7764.

Garg, P., Stith, C.M., Majka, J., and Burgers, P.M. (2005). Proliferating cell nuclear antigen promotes translesion synthesis by DNA polymerase ζ. J. Biol. Chem. *280*, 23446–23450.

Heller, R.C., and Marians, K.J. (2006). Replisome assembly and the direct restart of stalled replication forks. Nat. Rev. Mol. Cell Biol. *7*, 932–943.

Huertas, P., and Aguilera, A. (2003). Cotranscriptionally formed DNA:RNA hybrids mediate transcription elongation impairment and transcription-associated recombination. Mol. Cell *12*, 711–721.

Ii, M., and Brill, S.J. (2005). Roles of SGS1, MUS81, and RAD51 in the repair of lagging-strand replication defects in *Saccharomyces cerevisiae*. Curr. Genet. *48*, 213–225.

Jaishree, T.N., van der Marel, G.A., van Boom, J.H., and Wang, A.H. (1993). Structural influence of RNA incorporation in DNA: quantitative nuclear magnetic resonance refinement of d(CG)r(CG)d(CG) and d(CG)r(C)d(TAGCG). Biochemistry *32*, 4903–4911.

Joyce, C.M. (1997). Choosing the right sugar: how polymerases select a nucleotide substrate. Proc. Natl. Acad. Sci. USA *94*, 1619–1622.

Kim, N., Huang, S.N., Williams, J.S., Li, Y.C., Clark, A.B., Cho, J.E., Kunkel, T.A., Pommier, Y., and Jinks-Robertson, S. (2011). Mutagenic processing of ribonucleotides in DNA by yeast topoisomerase I. Science *332*, 1561–1564.

Kokoska, R.J., McCulloch, S.D., and Kunkel, T.A. (2003). The efficiency and specificity of apurinic/apyrimidinic site bypass by human DNA polymerase eta and Sulfolobus solfataricus Dpo4. J. Biol. Chem. *278*, 50537–50545.

Lawrence, C.W. (2002). Cellular roles of DNA polymerase zeta and Rev1 protein. DNA Repair (Amst.) *1*, 425–435.

Lawrence, C.W., and Hinkle, D.C. (1996). DNA polymerase zeta and the control of DNA damage induced mutagenesis in eukaryotes. Cancer Surv. *28*, 21–31.

Lazzaro, F., Giannattasio, M., Puddu, F., Granata, M., Pellicioli, A., Plevani, P., and Muzi-Falconi, M. (2009). Checkpoint mechanisms at the intersection between DNA damage and repair. DNA Repair (Amst.) *8*, 1055–1067.

Leroy, C., Mann, C., and Marsolier, M.C. (2001). Silent repair accounts for cell cycle specificity in the signaling of oxidative DNA lesions. EMBO J. *20*, 2896–2906.

Muzi-Falconi, M., Liberi, G., Lucca, C., and Foiani, M. (2003). Mechanisms controlling the integrity of replicating chromosomes in budding yeast. Cell Cycle *2*, 564–567.

Negrini, S., Gorgoulis, V.G., and Halazonetis, T.D. (2010). Genomic instability—an evolving hallmark of cancer. Nat. Rev. Mol. Cell Biol. *11*, 220–228.

Nelson, J.R., Lawrence, C.W., and Hinkle, D.C. (1996). Thymine-thymine dimer bypass by yeast DNA polymerase ζ. Science *272*, 1646–1649.

Nick McElhinny, S.A., and Ramsden, D.A. (2003). Polymerase mu is a DNA-directed DNA/RNA polymerase. Mol. Cell. Biol. *23*, 2309–2315.

Nick McElhinny, S.A., Kumar, D., Clark, A.B., Watt, D.L., Watts, B.E., Lundström, E.B., Johansson, E., Chabes, A., and Kunkel, T.A. (2010a). Genome instability due to ribonucleotide incorporation into DNA. Nat. Chem. Biol. *6*, 774–781.

Nick McElhinny, S.A., Watts, B.E., Kumar, D., Watt, D.L., Lundström, E.B., Burgers, P.M., Johansson, E., Chabes, A., and Kunkel, T.A. (2010b). Abundant ribonucleotide incorporation into DNA by yeast replicative polymerases. Proc. Natl. Acad. Sci. USA *107*, 4949–4954.

Petermann, E., Orta, M.L., Issaeva, N., Schultz, N., and Helleday, T. (2010). Hydroxyurea-stalled replication forks become progressively inactivated and require two different RAD51-mediated pathways for restart and repair. Mol. Cell *37*, 492–502.

Popoff, S.C., Spira, A.I., Johnson, A.W., and Demple, B. (1990). Yeast structural gene (APN1) for the major apurinic endonuclease: homology to Escherichia coli endonuclease IV. Proc. Natl. Acad. Sci. USA *87*, 4193–4197.

Prakash, S., Johnson, R.E., and Prakash, L. (2005). Eukaryotic translesion synthesis DNA polymerases: specificity of structure and function. Annu. Rev. Biochem. *74*, 317–353.

Pursell, Z.F., Isoz, I., Lundström, E.B., Johansson, E., and Kunkel, T.A. (2007). Yeast DNA polymerase epsilon participates in leading-strand DNA replication. Science *317*, 127–130.

Rice, G.I., Bond, J., Asipu, A., Brunette, R.L., Manfield, I.W., Carr, I.M., Fuller, J.C., Jackson, R.M., Lamb, T., Briggs, T.A., et al. (2009). Mutations involved in Aicardi-Goutières syndrome implicate SAMHD1 as regulator of the innate immune response. Nat. Genet. *41*, 829–832.

Rydberg, B., and Game, J. (2002). Excision of misincorporated ribonucleotides in DNA by RNase H (type 2) and FEN-1 in cell-free extracts. Proc. Natl. Acad. Sci. USA *99*, 16654–16659.

Sabbioneda, S., Bortolomai, I., Giannattasio, M., Plevani, P., and Muzi-Falconi, M. (2007). Yeast Rev1 is cell cycle regulated, phosphorylated in response to DNA damage and its binding to chromosomes is dependent upon MEC1. DNA Repair (Amst.) *6*, 121–127.

Sekiguchi, J., and Shuman, S. (1997). Site-specific ribonuclease activity of eukaryotic DNA topoisomerase I. Mol. Cell *1*, 89–97.

Stetson, D.B., Ko, J.S., Heidmann, T., and Medzhitov, R. (2008). Trex1 prevents cell-intrinsic initiation of autoimmunity. Cell *134*, 587–598.

Stone, J.E., Kissling, G.E., Lujan, S.A., Rogozin, I.B., Stith, C.M., Burgers, P.M., and Kunkel, T.A. (2009). Low-fidelity DNA synthesis by the L979F mutator derivative of Saccharomyces cerevisiae DNA polymerase zeta. Nucleic Acids Res. *37*, 3774–3787.

Ulrich, H.D. (2011). Timing and spacing of ubiquitin-dependent DNA damage bypass. FEBS Lett. *585*, 2861–2867.

Ulrich, H.D., and Davies, A.A. (2009). In vivo detection and characterization of sumoylation targets in Saccharomyces cerevisiae. Methods Mol. Biol. *497*, 81–103.

Wahl, M.C., and Sundaralingam, M. (2000). B-form to A-form conversion by a 3′-terminal ribose: crystal structure of the chimera d(CCACTAGTG)r(G). Nucleic Acids Res. *28*, 4356–4363.

Watt, D.L., Johansson, E., Burgers, P.M., and Kunkel, T.A. (2011). Replication of ribonucleotide-containing DNA templates by yeast replicative polymerases. DNA Repair (Amst.) *10*, 897–902.

Yang, Y.G., Lindahl, T., and Barnes, D.E. (2007). Trex1 exonuclease degrades ssDNA to prevent chronic checkpoint activation and autoimmune disease. Cell *131*, 873–886.

Zhong, X., Garg, P., Stith, C.M., Nick McElhinny, S.A., Kissling, G.E., Burgers, P.M.J., and Kunkel, T.A. (2006). The fidelity of DNA synthesis by yeast DNA polymerase zeta alone and with accessory proteins. Nucleic Acids Res. *34*, 4731–4742.

Zhu, H., and Shuman, S. (2008). Bacterial nonhomologous end joining ligases preferentially seal breaks with a 3′-OH monoribonucleotide. J. Biol. Chem. *283*, 8331–8339.

Published paper II

Crosstalk among UV-induced DNA damage checkpoint, NER and PRR.

In a study started before my entry in the Lab and published during my PhD, it was highlighted the crosstalk between PRR and DNA damage checkpoint. Indeed, it was published that in the absence of all the TLS DNA polymerases, UV irradiated G_1-arrested yeast cells are unable to recover from DNA damage checkpoint activation (Giannattasio et al 2010). Moreover, my investigation of PCNA ubiquitylation after UV irradiation uncovered a still unknown crosstalk between NER and PRR. So, I was involved in writing a review to summarize our present knowledge of the crosstalk among NER, DNA damage checkpoint and PRR, after UV DNA damage. It was hypothesized an intriguing scenario. Briefly, in response to UV irradiation, G_1 or G_2-arrested cells require NER to produce ssDNA gaps and activate DNA damage checkpoint. Moreover, it is possible that UV-induces lesion particular situations strongly affect DNA repair synthesis in particular sequence context. This is likely to correlate with the presence of closely opposing lesions (two lesions near to each other on two opposite strands). The first lesion is processed by NER but the presence of the second lesions causes the stalling of repair synthesis, the recruitment of the Exo1 nuclease that, by enlarging the gap, causes to the production of long ssDNA regions leading to the activation of the DNA damage checkpoint. Recovery from these situations requires the action of PRR: PCNA ubiquitylation and TLS DNA polymerases activities. In the case of S phase cells, the

situation is more complex. Indeed, it has been found that DNA replication could be uncoupled from S phase and DNA damage bypass (Daigaku et al., 2010; Karras and Jentsch, 2010; Diamant et al., 2011). Briefly, cells containing UV induced lesion can conclude S phase and arrest in G_2 with a gapped genome. If the PRR is artificially re-activated, these gaps can be re-filled in this phase of the cell cycle. However, no data are yet available in budding yeast on how NER may affect S phase progression of UV irradiated cells. I observed a strong delay in cell cycle progression of UV irradiated NER-deficient cells synchronized in S phase (see part III: additional file 13).

DNA Repair 10 (2011) 751–759

Contents lists available at ScienceDirect

DNA Repair

journal homepage: www.elsevier.com/locate/dnarepair

Mini review

Mind the gap: Keeping UV lesions in check

Daniele Novarina, Flavio Amara, Federico Lazzaro, Paolo Plevani*, Marco Muzi-Falconi*

Dipartimento di Scienze Biomolecolari e Biotecnologie, Università degli Studi di Milano. Via Celoria 26, 20133 Milano, Italy

ARTICLE INFO

Article history:
Available online 23 May 2011

Keywords:
UV irradiation
DNA damage checkpoint
DNA repair

ABSTRACT

Cells respond to genotoxic insults by triggering a DNA damage checkpoint surveillance mechanism and by activating repair pathways. Recent findings indicate that the two processes are more related than originally thought. Here we discuss the mechanisms involved in responding to UV-induced lesions in different phases of the cell cycle and summarize the most recent data in a model where Nucleotide Excision Repair (NER) and exonucleolytic activities act in sequence leading to checkpoint activation in non replicating cells. The critical trigger is likely represented by problematic intermediates that cannot be completely or efficiently repaired by NER. In S phase cells, on the other hand, the replicative polymerases, blocked by bulky UV lesions, re-initiate DNA synthesis downstream of the lesions, leaving behind a ssDNA tract. If these gaps are not rapidly refilled, checkpoint kinases will be activated.

Contents

1. Introduction

Cellular DNA is constantly threatened by genotoxic events arising from cellular metabolisms (e.g., free oxygen radicals, replication errors) and induced by environmental factors (e.g., ionizing and UV radiations, chemicals). To prevent the effect of endogenous and exogenous mutagenic agents and to maintain genome integrity, cells have evolved a complex response to DNA damage (DDR), which includes repair mechanisms and regulatory circuits. A key role in this response is played by signaling pathways that we will refer to as DNA damage checkpoints, surveillance mechanisms responsible for the coordination of cell cycle progression, DNA replication, transcription with DNA repair and apoptosis. Checkpoint activation temporarily halts or delays cell cycle progression, possibly providing the cell with enough time to remove DNA lesions before these are converted in secondary and more dangerous lesions (e.g., replication through a single strand gap would generate a double strand break). The checkpoints also actively stimulate the repair processes [1–9] and, in higher eukaryotes, trigger the apoptotic response, if damage cannot be dealt with successfully [10–12].

2. DNA damage checkpoint

The importance of the DNA damage checkpoint in the maintenance of genomic stability is underlined by the existence of many syndromes linked to mutations in checkpoint genes, causing increased cancer proneness or other clinical symptoms, espe-

* Corresponding author. Tel.: +39 0250315034; fax: +39 0250315044.
E-mail addresses: paolo.plevani@unimi.it (P. Plevani), marco.muzifalconi@unimi.it (M. Muzi-Falconi).

1568-7864/$ – see front matter © 2011 Elsevier B.V. All rights reserved.
doi:10.1016/j.dnarep.2011.04.030

Table 1
Checkpoint functions are evolutionarily conserved. The table shows the correspondence between various checkpoint factors in different organisms. The upstream factors are in blue, mediators are in pink and downstream effectors are in green.

S. cerevisiae	*S. pombe*	Human	*X. laevis*
Mec1	Rad3	ATR	ATR
Ddc2	Rad26	ATRIP	ATRIP
Tel1	Tel1	ATM	ATM
Rad24	Rad17	Rad17	Rad17
Rad17	Rad1	Rad1	Rad1
Mec3	Hus1	Hus1	Hus1
Ddc1	Rad9	Rad9	Rad9
Rad9	Crb2	BRCA1, 53BP1, MDC1	BRCA1, 53BP1
Mrc1	Mrc1	Claspin	Claspin
Dpb11	Rad4/Cut5	TopBP1	TopBP1
Rad53	Cds1	Chk2	Cds1
Chk1	Chk1	Chk1	Chk1

cially neurological defects [13,14]; it is thus not surprising that these pathways are extremely conserved throughout evolution (Table 1).

The DNA damage checkpoint response consists of a signal transduction cascade mainly based on phosphorylation events; the mechanistic details of the pathway have been recently discussed elsewhere [15,16], and will be just briefly summarized here to give a schematic picture to the reader. The first signaling event is carried out by the apical checkpoint kinases and is triggered after DNA damage detection. Two complexes are independently recruited at the lesion sites [17]: the human ATR/ATRIP or *Saccharomyces cerevisiae* Mec1/Ddc2 complex, and the 9-1-1 checkpoint clamp complex, composed of Rad9-Rad1-Hus1 in human or their orthologue subunits Rad17-Mec3-Ddc1 in yeast. The co-localization of these complexes is sufficient to trigger at least a partial checkpoint signaling even in the absence of actual DNA damage [18]. In *S. cerevisiae* the Mec1 apical kinase can be activated both by the Ddc1 subunit of the checkpoint clamp and by the adaptor protein Dpb11 which is recruited at the lesion through interaction with Ddc1 [19–23]. In human cells, the 9-1-1 complex is not able to directly activate ATR, but it is needed to recruit TopBP1 (the Dpb11 orthologue) which, in turn, stimulates ATR activity [24]. The apical kinases phosphorylate checkpoint mediators or adaptors, which are held close to the lesion by the interaction with post-translationally modified histone residues and with other checkpoint factors [25]. The mediators amplify the signaling cascade providing a platform to recruit effector kinases close to the apical kinases, and facilitating their activation. In budding yeast, Mec1 activates both Rad53 and Chk1 [26], while in human cells Chk2 is activated by ATM and Chk1 by ATR [27]. The prototype of checkpoint mediators is *S. cerevisiae* Rad9, which, once phosphorylated by the apical kinase, recruits Rad53 at the damage site allowing its phosphorylation by Mec1. Oligomerization of Rad9 seems to be critical to provide a scaffold for Rad53 binding, leading to a local increase in Rad53 molecules and stimulating its auto-phosphorylation; this event is responsible for full Rad53 activation [28,29]. Chk1 activation also requires Rad9, but the mechanism through which this mediator facilitates Chk1 phosphorylation by Mec1 is still poorly understood [30]. In human cells, the identity of the functional Rad9 orthologue is still debated: multiple candidates exist – i.e., MDC1 (mediator of DNA-damage checkpoint 1), 53BP1 (p53-binding protein 1) and BRCA1 (breast cancer 1 early-onset) – all characterized by the presence of tandem BRCT (BRCA1 C-terminal repeat) domains. Since these three proteins are involved in checkpoint signal transduction and each of them seems to carry out, separately and sometimes redundantly, some of Rad9 functions, they may be all considered as Rad9 orthologues [31]. Finally, effector kinases are responsible for the phosphorylation of a great number of targets, including cell cycle machinery factors and key proteins important for replication and repair [32,33].

The checkpoint response can act in at least three different phases of the cell cycle: in G1, to prevent chromosomes with problematic lesions from entering S phase, in S phase to control their replication, and in G2 (or M in some organisms) to avoid loss of genetic information due to mitotic segregation of severely damaged chromosomes. The general scheme of the checkpoint cascade is similar in all three cases, but significant differences can be found, depending on the nature of the DNA lesion and on the cell cycle phase in which the damage is detected [13,34–36]. Furthermore, in human cells the two apical kinases seem to be partly specialized in the response to different classes of DNA damaging agents. In fact, ATM (Ataxia Telangiectasia Mutated) is activated by double-strand breaks (DSBs) caused, for example, by ionizing radiation (IR), while ATR (ATM and Rad3-Related) is activated by ssDNA coated with the RPA heterotrimeric complex and mainly triggers checkpoint activation after UV irradiation or replication-stress. This specialization is possibly imputable to the different networks of physical interactions that these kinases participate to, and that are responsible for their recruitment at the sites of lesion [37–40]. The situation is somewhat complicated by the finding that ATR can be also recruited to DSBs and this binding depends upon ATM [41,42]. This separation of tasks is not found in budding yeast, where Mec1 (the ATR homologue) is the main player of checkpoint activation after all kind of DNA lesions, while Tel1 (the ATM homologue) is especially devoted to telomere maintenance. The redundant role of Tel1 in the DNA damage checkpoint is uncovered only in the absence of Mec1 [15,43].

In this review, we will focus our attention on UV-induced lesions and we will discuss the reciprocal interactions between NER, post replication repair (PRR), and the checkpoint pathway. In particular, we will discuss how NER plays a role in the activation of the checkpoint response after UV treatment, and how checkpoint kinases contribute to modulating the actual repair events.

Given the variety of DNA lesions the cell has to deal with, it was hypothesized that the first responders, among checkpoint factors, had to be recruited to a common DNA intermediate, which was later identified as long regions of ssDNA covered by RPA [44]. While ATRIP and Ddc2 directly bind RPA-covered ssDNA [44], loading of the 9-1-1 complex requires the activity of an RFC-like complex, that places it at the junction between dsDNA and 5′ ssDNA [45]. In the case of a single DSB, a large amount of evidence indicates that recombination factors are first recruited at the DSB, and then the 5′ ends of the DSB are processed through the concerted action of several proteins, including helicases and nucleases. This action generates long ssDNA tails that, on one hand will recruit checkpoint factors, and on the other will initiate repair through homologous recombination mechanisms [46]. On the other hand, extensive resection is not required when a DSB is repaired through a Non-Homologous End Joining (NHEJ) process [47]. For a long time, it was unclear how UV irradiation, which causes bulky lesions on DNA (mainly cyclobutane pyrimidine dimers (CPD) and 6,4 photoproducts (6-4PP)) responsible for inducing a distortion of the DNA helix [48], triggers the same checkpoint response in the absence of any DSB (Fig. 1).

3. Nucleotide excision repair

UV-induced DNA lesions are mainly removed through NER that efficiently identifies 6-4PPs and more slowly takes care of CPDs. The lesion recognition mechanism of NER depends upon the phys-

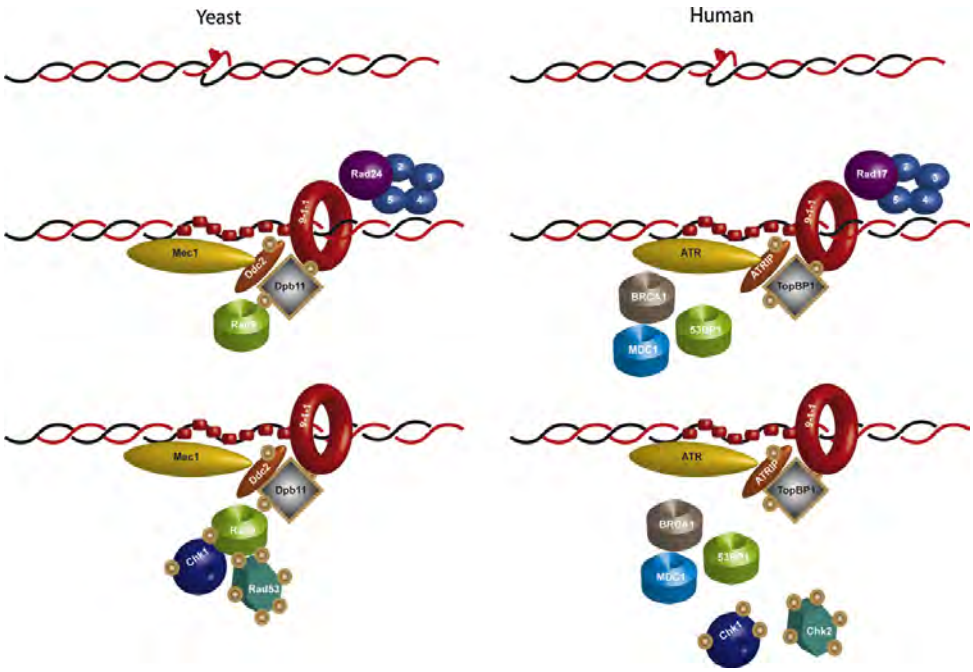

Fig. 1. The DNA damage checkpoint cascade. The DNA damage checkpoint is triggered by a ssDNA region. The left side of the figure reports the checkpoint cascade in budding yeast. RPA-covered ssDNA recruits the Mec1-Ddc2 and the 9-1-1 complexes. Phosphorylated Ddc1 interacts with Dpb11 which recruits the Rad9 mediator. Rad53 and Chk1 kinases are activated upon binding to oligomeric Rad9 and then leave chromatin to find their own targets. The right side of the figure summarizes the same signaling cascade in human cells.

ical location of the lesion, with TC-NER acting on lesions that block transcription, and GG-NER taking care of the rest of the genome [48].

NER has been reconstituted *in vitro* and the mechanism is discussed elsewhere in this issue. Briefly, once the lesion has been recognized a pre-incision complex is assembled at the damage site. Endonucleolytic incision 5′ and 3′ to the lesion produces a short gap containing ssDNA covered by RPA, which is then refilled by DNA polymerase activities.

How long this ssDNA tract is exposed for, before a DNA polymerase refills the gap is not clear, but most reports seem to agree that the refilling is extremely rapid and tightly coordinated with the incision process [49,50] (see review by Fagbemi et al. in this issue of DNA Repair).

Since UV lesions are bulky and block the progression of replicative DNA polymerases, when the replication forks collide with UV-induced lesions during the S phase of the cell cycle re-priming events may take place downstream of the lesions, leaving ssDNA gaps behind the fork. Such structures have been detected by electron microscopy on replicating UV-damaged DNA and are likely responsible for the rapid and sensitive response observed in UV-irradiated S phase cells [51]. Outside of S phase and in non cycling cells the situation is quite different. Recent analysis showed that UV lesions themselves cannot activate the checkpoint and NER plays a major role in triggering the checkpoint response, although contrasting results have also been reported [52–57].

4. NER and DNA damage checkpoint

The tight relationship between NER and the checkpoint response started to become clear when, in budding yeast, a *rad14* mutant, which is defective in assembling a competent pre-incision complex, was identified in a screen for mutations specifically inactivating the DNA damage checkpoint in response to UV irradiation, while leaving intact the DSB-induced checkpoint [55]. Furthermore, a direct interaction between Rad14 and the 9-1-1 checkpoint complex was reported, albeit its physiological significance has not been fully addressed. This work also showed that, in non cycling cells, any NER mutation affecting the incision event caused a deficient checkpoint activity, demonstrating that UV lesions *per se* are not sufficient to trigger the apical checkpoint kinase, and that their processing by a repair mechanism is necessary for recruiting the Mec1/Ddc2 and the 9-1-1 complexes to damaged chromosomes and for a prompt checkpoint response [55]. Such results are also consistent with the finding that UV irradiation in G1 of a cycling *rad14Δ* strain results in a strong arrest at the beginning of S phase [58], accompanied by the accumulation of replication-dependent ssDNA regions [51]. Altogether, it was suggested that a NER intermediate, possibly the ssDNA gapped structure generated by the double incision event may be responsible for recruiting and activating checkpoint factors. In cycling NER-deficient cells, UV irradiation would not cause a G1 delay or G2/M arrest and replication of the damaged template would lead to the accumulation of ssDNA regions resulting in Mec1 activation.

Extension of this kind of analysis to human cells derived from XP patients confirmed that lack of NER-dependent processing prevented UV-induced checkpoint activity in non cycling fibroblasts, revealing that XP cells are not only deficient in repairing UV lesions, but they are also deficient in the G1 and G2/M UV-induced checkpoint [56,57]. Interestingly, while XPC cells, defective in GG-NER, exhibit a checkpoint failure, cells obtained from Cockayne syndrome patients, which are defective in TC-NER, are instead able to activate the checkpoint, possibly thanks to the activity of GG-NER. Intriguingly, there seems to be a correlation between the capacity

of these cells to properly control G1 and G2/M transitions after UV, their genomic instability and the proneness of XP and CS patients to develop tumors [56]. In budding yeast, the analysis of mutants specifically defective in the TC-NER or in the GG-NER branches of NER, revealed that activity of either one of the sub-pathways was sufficient to trigger a checkpoint response [55]. Interestingly, although UV-induced photoproducts and DSBs are processed by different DNA repair pathways and trigger signaling responses controlled by distinct apical kinases (see above) they eventually generate the same epigenetic mark involving H2A ubiquitination [59].

The model suggesting that gapped NER intermediates are responsible for checkpoint activation in UV-irradiated cells poses a few problems: (a) the gaps are very short (~30 nt); (b) repair synthesis is very rapid, so the gaps are virtually absent; (c) it is not clear what would be the advantage of activating the checkpoint and arresting cell cycle progression, once the damage is practically repaired.

Recent work shed light on these problems, showing that normal NER-intermediates are not directly responsible for activating checkpoint kinases. In order to achieve a full and prompt checkpoint activity after UV irradiation in non cycling yeast cells, NER is necessary but not sufficient: in fact, the nuclease activity of Exo1 is also required [60,61]. Exo1 belongs to the Rad2 family of nucleases and has multiple cellular roles (see [62] for a review). This work shows that UV irradiation causes the accumulation, in yeast chromosomes, of long ssDNA regions that are dependent upon NER and Exo1 and correlate with Mec1 kinase activation. Preventing completion of repair synthesis by genetic or chemical means strongly increases accumulation of ssDNA and checkpoint activation, in agreement with a previous report [63]. The frequency of these large ssDNA gaps is much lower than the expected frequency of UV damages, suggesting that only a minor fraction of lesions undergo Exo1-dependent processing. Intriguingly, this mechanism is conserved also in human cells (Sertic et al., in preparation). These results suggest that the ~30 nt long ssDNA gaps produced by NER can be refilled by DNA polymerases or extended by Exo1; given that polymerases refill a DNA gap at a rate of about 3700 nt/min and Exo1 excises DNA at 160 nt/min, most UV lesions are normally rapidly repaired by NER. This is consistent with the observation that very low UV doses do not seem to activate the G1 checkpoint [61,64,65]; if NER can rapidly and effectively deal with a low number of lesions, there would be no point in triggering a checkpoint response. If for any reason the repair synthesis step is perturbed, Exo1 may have a kinetic opportunity to process the NER gap, generating a long ssDNA region, which recruits checkpoint factors and triggers the signaling cascade (Fig. 2). This situation may arise, for example, at higher UV doses, in case repair synthesis factors become limiting or if the refilling polymerase encounters an insurmountable block. In these conditions, repair may not be completed and the extension of the ssDNA region may meet two purposes: activating the checkpoint response and channeling the problematic lesion to a different repair pathway (e.g., recombination) [66–68].

Interestingly, translesion DNA polymerase activities (TLS) seem to counteract the generation of the UV-induced checkpoint signal [61,69]. Moreover, an unexpected role for TLS polymerases in NER was described in human cells, where DNA polymerase κ was found to be responsible for approximately 30% of the unscheduled DNA synthesis detected in UV-irradiated cells [70,71]. The actual role of TLS polymerases in NER is not completely understood and it will be interesting to determine if their activity is limited to particular regions of the genome and/or to particular configurations, such as the presence of a lesion in the template strand that may interfere with the refilling step of NER, as previously suggested in bacteria [72].

5. Closely opposing lesions

The possibility that Exo1-depedent processing may be facilitated by a polymerase blocking lesion in the template is intriguing. One instance where this might happen is when two UV lesions, one on each DNA strand, are generated in a limited region; this configuration has been defined "closely opposing UV lesions" [73–75]. Probability calculations would predict that the frequency of closely opposing lesions increases with the square of the UV dose and the chance of generating such situation in a yeast chromosome is expected to be very low. On the other hand, UV lesion formation has a strong sequence bias, and actual measurements on irradiated DNA proved that approximately 1% of all UV-induced lesions are configured as closely opposing lesions [76–78]. When NER encounters two closely spaced lesions, one on each strand, a major problem arises. NER can only process one damage at a time because the lesion needs to be in a double-stranded configuration [79]. Incision and removal of the first UV-induced dimer leaves to the refilling polymerase a gap containing a lesion in the template strand. DNA polymerase δ or ε, which normally take care of repair synthesis, cannot replicate past the template lesion and stall, strongly resembling a blocked replication fork. During S phase, such situation would be bypassed via Post Replication Repair (PRR), which entails TLS polymerases and/or template switching mechanisms. Interestingly, it was recently shown that DNA polymerase κ directly participates to NER repair synthesis in human cells [70,71] and that loss of TLS activity greatly potentiates the checkpoint response to UV irradiation in yeast G1 cells [61], suggesting that closely opposing UV lesions may indeed be at least partly responsible for checkpoint activation. These particular lesions may also contribute to explain the observation that both in wild-type yeast and bacteria cells most of the UV-induced mutagenesis depends upon a functional NER and takes place in G1 cells, while in the absence of NER the mutagenesis is S-phase specific [80,81]. Moreover, a role for TLS in G1-irradiated cells is also supported by the finding that G1 synchronized cultures of yeast mutants lacking TLS polymerases are more sensitive to UV light than asynchronous cultures, while this is not the case for strains that are TLS proficient [61].

6. Replicating UV damaged DNA

As mentioned above, in NER deficient cells, the lack of lesion removal coupled to the failure to activate the G1 DNA damage checkpoint in response to UV irradiation allows a large amount of DNA lesions to go into S phase. Here, there is no need for lesion processing to generate the checkpoint activating structures since ssDNA regions are generated by the stalling of replication forks at the polymerase blocking lesions. Blocked polymerase can leave the lesion and PCNA behind and re-initiate downstream of the lesion via a re-priming mechanism, generating numerous ssDNA gaps behind the forks, which are likely responsible for the strong activation of Mec1 during S phase in UV-irradiated cells [51,82–85]. Consistently, even at low UV doses (5 J/m^2), NER deficient yeast cells exhibit a strong cell cycle arrest at the beginning of S phase, due to Mec1 DNA damage checkpoint activation [58]. An active checkpoint leads to Rev1 phosphorylation [86,87], possibly increasing TLS activity and progressively reducing the amount of RPA-covered ssDNA, thus promoting the switch off of the checkpoint itself.

In a wild type background, elegant time lapse experiments showed that after an acute low dose of UVC light (5 J/m^2) yeast cells do not delay cell cycle progression until they proceed through S phase; for this reason this response was called post-replication checkpoint [64]. With low levels of UV-induced lesions the NER

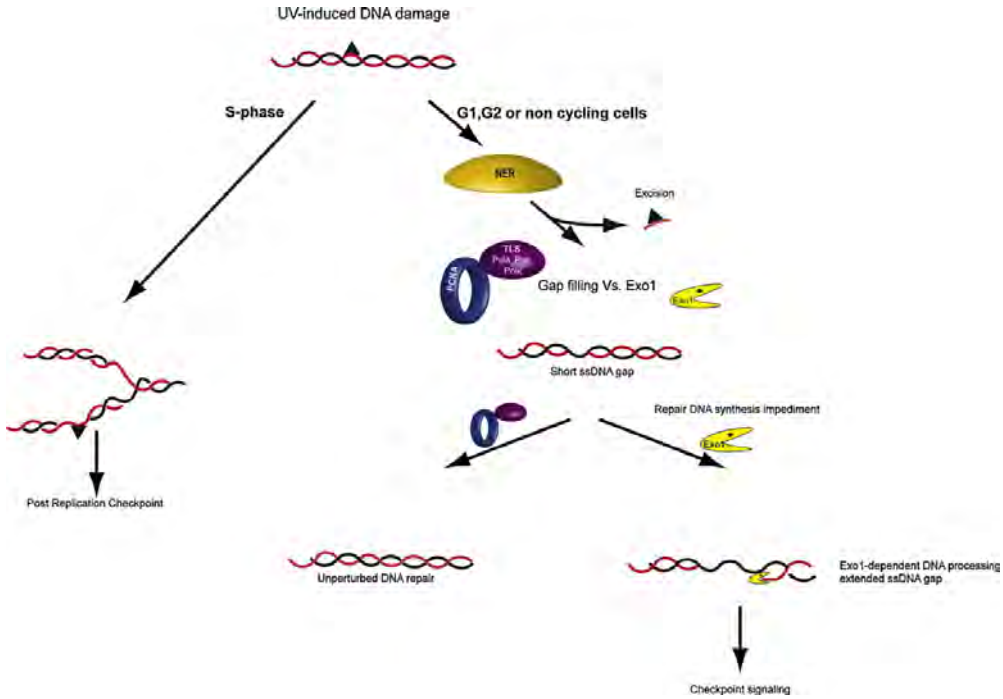

Fig. 2. UV-induced checkpoint response. In cells that are not replicating their genome (i.e., G1, G2 or non-cycling cells), NER removes UV lesions efficiently and DNA polymerases (i.e., pol δ, pol ε, TLS polymerases) begin the refilling process. If the repair reaction is impeded after the excision step, a competition between the refilling polymerases and Exo1 nuclease can take place. Problematic refilling (e.g., closely opposing lesions) allows Exo1 to further process the gapped intermediate generating long ssDNA gaps which recruit checkpoint factors and trigger the signaling. At low UV-doses G1 and G2 cells do not accumulate large ssDNA gaps since UV lesions can be efficiently removed by NER. If the damages are still present when the cell enters S phase, the replicative polymerase will be blocked by the bulky lesion and will reinitiate DNA synthesis further downstream, leaving ssDNA gaps behind the replication fork. These gaps can be refilled by post replication repair and trigger a post-replication checkpoint.

mechanism is very efficient and rapidly takes care of most lesions, so that neither the G1 or the G2 checkpoints are activated. The few lesions that are encountered by replicating polymerases in these conditions, on the other hand, block the replication fork and trigger a checkpoint response; this response may be detected in late S phase, when most replicons have completed duplication and the left-over ssDNA gaps need to be refilled (Fig. 2). An important point in this regard was made by irradiating budding yeast cells with very low ($0.18\,J\,m^{-2}\,min^{-1}$) chronic UV dose (CLUV): the only pathway necessary and sufficient to ensure cell survival was found to be the *RAD5*-dependent branch of PRR [65]. Indeed, NER deficient cells (*rad14Δ*) and DNA damage checkpoint deficient cells (*mec1Δ*) are not particularly sensitive to the CLUV treatment, contrary to the *rad18Δ* and *rad5Δ* cells, deficient in PRR [65], which irreversibly activate Mec1 DNA damage checkpoint and die in the G2 phase. In fact, S phase can be completed in the absence of PRR, but the gapped replicated DNA needs to be refilled by PRR in G2 in order to warrant cell survival [66,67].

In mammalian cells the situation is more complex, because NER acts also in S phase, where GG-NER is enhanced [88] and is stimulated by active ATR [89,90]. Indeed, ATR-deficient Seckel syndrome fibroblasts exhibit attenuation of S phase specific GG-NER and a similar effect has been detected in XPV skin fibroblasts, deficient in pol η [91]. Thus, in human cells both ATR-dependent DNA damage checkpoint and TLS influence S phase-specific GG-NER: defects in ATR or pol η may cause the abnormal persistence of ssDNA gaps opposite a template lesion and this would inhibit DNA adducts excision by GG-NER.

7. Recruitment of checkpoint factors by NER

In the last few years evidence has emerged that the role of NER in checkpoint activation is not limited to the generation of the ssDNA signal but, in addition, NER proteins seem to be involved in directly recruiting checkpoint factors to the proximity of DNA lesions.

In *S. cerevisiae*, a physical interaction was identified between Rad14 and both Ddc1 and Mec3, two subunits of the 9-1-1 checkpoint complex. Although the physiological relevance of this interaction has not been directly investigated further, association of Ddc1 and Ddc2 to UV-damaged chromosomes is lost in a *rad14Δ* strain, suggesting that the 9-1-1 complex may be initially recruited at the sites of DNA lesions by directly interacting with the key NER factor Rad14 [55].

Additional observations indicate that this mechanism is most likely conserved in higher eukaryotes. In human G1 cells the recruitment of the 9-1-1 complex onto damaged DNA is dependent on XPA and XPC proteins [92]; analogously, Cep164, a checkpoint mediator protein in the ATR signaling pathway required for Chk1 phosphorylation after UV damage, was shown to be recruited to CPD sites in a NER-dependent manner, through UV-induced physical interaction with XPA [93]. In addition, a role for NER in the activation of ATM after cisplatin treatment was discovered. Immunoprecipitation experiments revealed a physical interaction between ATM and NER factors and this association is required for ATM recruitment to DNA [94] (Fig. 3).

Combining the notion that processing of lesions by repair machineries is a pre-requisite for checkpoint activation outside of S phase, with the observation that checkpoint factors interact with

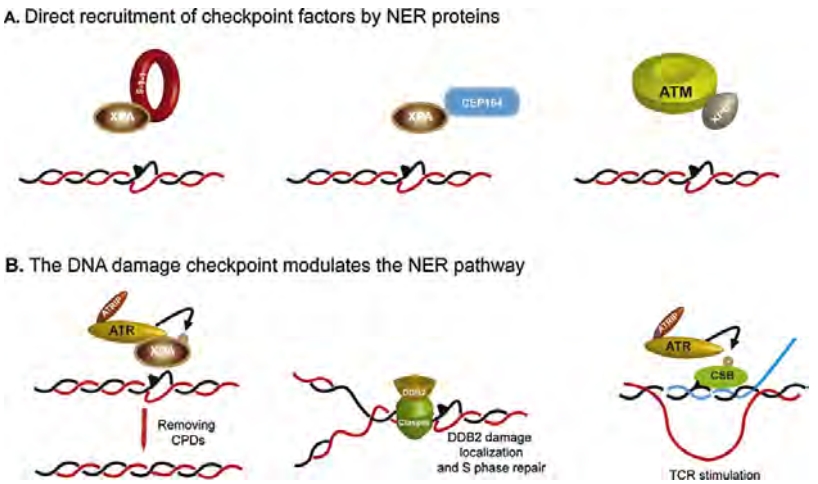

Fig. 3. Crosstalks between NER and checkpoint factors. A two-way functional interaction exists between the checkpoint machinery and the NER apparatus: some examples (discussed in the text) are shown. (A) NER factors recruit checkpoint proteins to damaged chromosomes, thus facilitating the activation of the signaling cascade. (B) DNA damage checkpoint factors modulate NER activity allowing for efficient repair of the lesions.

repair proteins depicts a model where the repair machinery, which is specialized for direct lesion recognition, increases the local concentration of checkpoint sensors on damaged chromosomal regions facilitating a robust checkpoint response.

Interestingly, a NER-independent mechanism for activating checkpoint kinases seems to exist in non cycling cells. If NER-deficient yeast cells are blocked in the G1 phase of the cell cycle, UV irradiated and held in non dividing conditions indefinitely, a delayed activation of the Mec1-dependent pathway has been reported [95,96]. Recent evidence indicates that UV-induced signaling may proceed via NER-independent mechanisms also in non-dividing mammalian cells likely through generation of DNA strand breaks [97].

8. NER modulation by checkpoint proteins

The interplay between NER and the DNA damage checkpoint is even more complex; in fact, while NER is involved in checkpoint activation, the checkpoint pathway actively stimulates NER by modulating cellular levels, localization and activity of NER factors, through transcriptional regulation, direct protein–protein interactions and post-translational modifications (Fig. 3).

The *S. cerevisiae* Rad9 gene product plays a role in the repair of both UV-damaged strands of an actively transcribed gene; this effect on NER is likely indirect and probably occurs through up-regulation of some NER genes (i.e., *RAD2*, *RAD7*, *RAD16* and *RAD23*), consistently with a previously reported Rad9-dependent stimulation of NER genes transcription [98]. Rad9 does not seem to be required for the repair of non-transcribed regions, suggesting that it is acting only when repair is coupled to transcription [8]. Along similar lines, Rad26, a NER factor critical for TC-NER, is a direct target of Mec1 kinase and its phosphorylation enhances TC-NER, possibly by stimulating its ATPase activity or by modulating its interaction with other TC-NER proteins [99]. Notably, CSB (the human orthologue of Rad26) was identified in a screen for putative ATM/ATR substrates [33], pointing to a conservation of this regulatory mechanism through evolution. Other NER factors were found in the same screening, namely XPA, XPC, RPA1 and RAD23B, but further characterization will be required to prove the significance of the interaction between ATM/ATR and the NER factors identified in the screen. Another example on the possible feedback of the checkpoint on NER is the regulation of XPA by ATR. It has been found that XPA nuclear import and its stable accumulation at nuclear foci after UV irradiation is dependent upon ATR. ATR also seems to be responsible for XPA phosphorylation after UV radiations, although this modification is not required for XPA foci formation [100–102]. Further studies will be required to firmly establish the role of ATR in the modulation of the XPA function. Finally, an S-phase specific role for the DNA damage checkpoint in regulating GG-NER was recently suggested. In particular, ATR inhibition was shown to specifically abrogate NER in S-phase, while the repair rate was unaffected in G1 and G2/M cells [89]. Another report revealed a role for the replication checkpoint mediator Claspin in regulating the DDB2 subunit of the UV-DDB factor, which is involved in the initial steps of GG-NER [103]. DDB2 is localized at the UV-induced DNA lesions, where its ubiquitination and subsequent degradation seems to control XPC recruitment and damage recognition, thus triggering the NER process [104]. Claspin knockdown affects DDB2 recruitment at damage sites and its subsequent ubiquitin-mediated degradation; in agreement with this observation, it has been shown that Claspin and DDB2 physically interact and their association is greatly enhanced upon UV irradiation [103].

9. Summary and perspectives

The complex interplay between NER and DNA damage checkpoints is not an isolate case in the DDR landscape, since in recent years a large cluster of papers highlighted the reciprocal interdependence of the checkpoint pathways and virtually all other known repair systems. It seems that, as a general rule, a two-way functional interaction exists between the checkpoint machinery and the repair apparatus. On one side, repair factors help to recruit checkpoint proteins at the damage sites onto DNA and, by modifying the primary lesions to RPA-covered ssDNA, trigger the checkpoint cascade; on the other side, once activated the checkpoint pathway stimulates the repair process mainly through direct protein–protein interactions or post-translational modifications. One of the key factors at the interface between checkpoint and repair is the 9-1-1 checkpoint clamp, and its involvement in such processes has been recently discussed [25].

The checkpoint response may be seen as a process that signals the cell that something that should have been working properly, has

instead some problem; the cell can thus deploy a set of measures to attempt to solve the problems and avoid further complications.

The data obtained with low acute UV doses suggest that if the lesions are not frequent enough to interfere with G1 or G2 processes, the cell has no way (or need) to acknowledge their presence and activate the checkpoint. Indeed, NER can easily keep these lesions under control. When these damage-containing chromosomes are replicated, though, the DNA polymerases scanning the genome will eventually detect them, and re-initiate DNA synthesis further downstream leaving behind ssDNA gaps. Since the region hosting a polymerase-blocking lesion can be almost completely replicated by an incoming fork starting from an adjacent origin, at low levels of lesions the gaps will accumulate and activate the checkpoint kinases toward the end of S phase. This event has a clear relevance since checkpoint mutants will die in this situation, and only after checkpoint activation the gaps are refilled by PRR and the lesions are actually removed from the chromosomes [61]. It has to be noted that a checkpoint response can be triggered in G1 cells, even at these low UV doses, if something interferes with completion of NER. Indeed, alterations in the refilling step of repair will sensitize G1 cells more than S phase cells [58].

At higher UV doses (>20 J/m^2), cells promptly respond also in non replicating conditions, consistently with the increased probability of repair problems arising. Repair DNA synthesis, in these situations, could be affected by the low level of dNTPs, by the formation of closely opposing lesions, by limiting level of particular factors in saturating conditions and by the higher possibility that lesions are generated in "difficult to repair" chromosomal locations. If the refilling reaction is problematic, nucleases like Exo1 have a greater chance to process the NER intermediates and elicit a checkpoint response [58].

What is surprising is what happens with chronic low UV doses (CLUV), which are supposed to best mimic sunlight exposure. Experiments performed in yeast cells have suggested that in CLUV conditions no checkpoint is activated, not even during S phase; indeed, checkpoint deficient strains do not exhibit sensitivity to CLUV treatment [62]. Even more surprisingly, NER is not important in these conditions, since NER-deficient cells are also not sensitive to CLUV. The possibility to extend these findings beyond yeast cells remains to be determined, indeed they seem to contrast with the situation observed in XP patients, who are deficient in NER and clearly hypersensitive to sunlight. In the future the actual events happening with sunlight exposure will need to be investigated.

NER is the most versatile repair system and eliminates a wide repertoire of DNA lesions, among which are UV-induced CPD and 6-4PP, that represent the main determinants in solar mutagenesis and skin cancer [105,106]. The importance of the findings summarized here may thus expand further than the problems related to exposure to UV light.

It is expected that genome-wide analysis of protein–protein interaction networks provided by high throughput screenings will progressively increase the number of known physical interactions between checkpoint proteins and repair factors, thus strengthening and expanding the model describing the functional connections between these two key genome stability pathways.

Conflicts of interest

The authors declare that there are no conflicts of interest.

Funding

Work in the authors' lab is supported by grants from AIRC, Fondazione Cariplo, MIUR and EU FP6 IP DNA Repair.

Acknowledgments

The authors apologize for the many interesting papers that they were not able to discuss or acknowledge. FP6 IP DNA Repair. F.L. is supported by Fondazione Adriano Buzzati-Traverso.

References

[1] X. Zhao, R. Rothstein, The Dun1 checkpoint kinase phosphorylates and regulates the ribonucleotide reductase inhibitor Sml1, Proc. Natl. Acad. Sci. U.S.A. 99 (2002) 3746–3751.
[2] R. Yao, Z. Zhang, et al., Subcellular localization of yeast ribonucleotide reductase regulated by the DNA replication and damage checkpoint pathways, Proc. Natl. Acad. Sci. U.S.A. 100 (2003) 6628–6633.
[3] V.I. Bashkirov, J.S. King, et al., DNA repair protein Rad55 is a terminal substrate of the DNA damage checkpoints, Mol. Cell. Biol. 20 (2000) 4393–4404.
[4] P. Ahnesorg, S.P. Jackson, The non-homologous end-joining protein Nej1p is a target of the DNA damage checkpoint, DNA Repair (Amst) 6 (2007) 190–201.
[5] S. Flott, C. Alabert, et al., Phosphorylation of Slx4 by Mec1 and Tel1 regulates the single-strand annealing mode of DNA repair in budding yeast, Mol. Cell. Biol. 27 (2007) 6433–6445.
[6] I. Morin, H.P. Ngo, et al., Checkpoint-dependent phosphorylation of Exo1 modulates the DNA damage response, EMBO J. 27 (2008) 2400–2410.
[7] W.C. Chou, H.C. Wang, et al., Chk2-dependent phosphorylation of XRCC1 in the DNA damage response promotes base excision repair, EMBO J. 27 (2008) 3140–3150.
[8] N.M. Al-Moghrabi, I.S. Al-Sharif, A. Aboussekhra, The RAD9-dependent gene trans-activation is required for excision repair of active genes but not for repair of non-transcribed DNA, Mutat. Res. 663 (2009) 60–68.
[9] A. Ciccia, S.J. Elledge, The DNA damage response: making it safe to play with knives, Mol. Cell 40 (2010) 179–204.
[10] S.W. Lowe, E.M. Schmitt, et al., p53 is required for radiation-induced apoptosis in mouse thymocytes, Nature 362 (1993) 847–849.
[11] Y. Xu, D. Baltimore, Dual roles of ATM in the cellular response to radiation and in cell growth control, Genes Dev. 10 (1996) 2401–2410.
[12] A. Hirao, Y.Y. Kong, et al., DNA damage-induced activation of p53 by the checkpoint kinase Chk2, Science 287 (2000) 1824–1827.
[13] M.B. Kastan, J. Bartek, Cell-cycle checkpoints and cancer, Nature 432 (2004) 316–323.
[14] C. Kerzendorfer, M. O'Driscoll, Human DNA damage response and repair deficiency syndromes: linking genomic instability and cell cycle checkpoint proficiency, DNA Repair (Amst) 8 (2009) 1139–1152.
[15] C.D. Putnam, E.J. Jaehnig, R.D. Kolodner, Perspectives on the DNA damage and replication checkpoint responses in *Saccharomyces cerevisiae*, DNA Repair (Amst) 8 (2009) 974–982.
[16] A. Sancar, L.A. Lindsey-Boltz, et al., Molecular mechanisms of mammalian DNA repair and the DNA damage checkpoints, Annu. Rev. Biochem. 73 (2004) 39–85.
[17] J.A. Melo, J. Cohen, D.P. Toczyski, Two checkpoint complexes are independently recruited to sites of DNA damage in vivo, Genes Dev. 15 (2001) 2809–3221.
[18] C.Y. Bonilla, J.A. Melo, D.P. Toczyski, Colocalization of sensors is sufficient to activate the DNA damage checkpoint in the absence of damage, Mol. Cell 30 (2008) 267–276.
[19] J. Majka, A. Niedziela-Majka, P.M. Burgers, The checkpoint clamp activates Mec1 kinase during initiation of the DNA damage checkpoint, Mol. Cell 24 (2006) 891–901.
[20] H. Wang, S.J. Elledge, Genetic and physical interactions between DPB11 and DDC1 in the yeast DNA damage response pathway, Genetics 160 (2002) 1295–1304.
[21] F. Puddu, M. Granata, et al., Phosphorylation of the budding yeast 9-1-1 complex is required for Dpb11 function in the full activation of the UV-induced DNA damage checkpoint, Mol. Cell. Biol. 28 (2008) 4782–4793.
[22] V.M. Navadgi-Patil, P.M. Burgers, Yeast DNA replication protein Dpb11 activates the Mec1/ATR checkpoint kinase, J. Biol. Chem. 283 (2008) 35853–35859.
[23] D.A. Mordes, E.A. Nam, D. Cortez, Dpb11 activates the Mec1-Ddc2 complex, Proc. Natl. Acad. Sci. U.S.A. 105 (2008) 18730–18734.
[24] V.M. Navadgi-Patil, P.M. Burgers, A tale of two tails: activation of DNA damage checkpoint kinase Mec1/ATR by the 9-1-1 clamp and by Dpb11/TopBP1, DNA Repair (Amst) 8 (2009) 996–1003.
[25] F. Lazzaro, M. Giannattasio, et al., Checkpoint mechanisms at the intersection between DNA damage and repair, DNA Repair (Amst) 8 (2009) 1055–1067.
[26] Y. Sanchez, J. Bachant, et al., Control of the DNA damage checkpoint by Chk1 and Rad53 protein kinases through distinct mechanisms, Science 286 (1999) 1166–1171.
[27] J. Bartek, J. Lukas, Chk1 and Chk2 kinases in checkpoint control and cancer, Cancer Cell 3 (2003) 421–429.
[28] F.D. Sweeney, F. Yang, et al., *Saccharomyces cerevisiae* Rad9 acts as a Mec1 adaptor to allow Rad53 activation, Curr. Biol. 15 (2005) 1364–1375.
[29] C.S. Gilbert, C.M. Green, N.F. Lowndes, Budding yeast Rad9 is an ATP-dependent Rad53 activating machine, Mol. Cell 8 (2001) 129–136.

[30] R.T. Blankley, D. Lydall, A domain of Rad9 specifically required for activation of Chk1 in budding yeast, J. Cell Sci. 117 (2004) 601–608.
[31] J.E. FitzGerald, M. Grenon, N.F. Lowndes, 53BP1: function and mechanisms of focal recruitment, Biochem. Soc. Trans. 37 (2009) 897–904.
[32] M.B. Smolka, C.P. Albuquerque, et al., Proteome-wide identification of in vivo targets of DNA damage checkpoint kinases, Proc. Natl. Acad. Sci. U.S.A. 104 (2007) 10364–10369.
[33] S. Matsuoka, B.A. Ballif, et al., ATM and ATR substrate analysis reveals extensive protein networks responsive to DNA damage, Science 316 (2007) 1160–1166.
[34] W. Siede, A.S. Friedberg, E.C. Friedberg, Rad9-dependent-G(1) arrest defines a second checkpoint for damaged DNA in the cell-cycle of *Saccharomyces cerevisiae*, Proc. Natl. Acad. Sci. U.S.A. 90 (1993) 7985–7989.
[35] A.G. Paulovich, L.H. Hartwell, A checkpoint regulates the rate of progression through S-phase in *Saccharomyces cerevisiae* in response to DNA-damage, Cell 82 (1995) 841–847.
[36] T.A. Weinert, L.H. Hartwell, The RAD9 gene controls the cell cycle response to DNA damage in *Saccharomyces cerevisiae*, Science 241 (1988) 317–322.
[37] K.K. Khanna, M.F. Lavin, Ionizing-radiation and UV induction of p53 protein by different pathways in ataxia–telangiectasia cells, Oncogene 8 (1993) 3307–3312.
[38] R.S. Tibbetts, K.M. Brumbaugh, et al., A role for ATR in the DNA damage-induced phosphorylation of p53, Genes Dev. 13 (1999) 152–157.
[39] C.E. Canman, D.S. Lim, et al., Activation of the ATM kinase by ionizing radiation and phosphorylation of p53, Science 281 (1998) 1677–1679.
[40] C.A. Lovejoy, D. Cortez, Common mechanisms of PIKK regulation, DNA Repair (Amst) 8 (2009) 1004–1008.
[41] A. Jazayeri, J. Falck, et al., ATM- and cell cycle-dependent regulation of ATR in response to DNA double-strand breaks, Nat. Cell Biol. 8 (2006) 37–45.
[42] K.E. Adams, A.L. Medhurst, et al., Recruitment of ATR to sites of ionising radiation-induced DNA damage requires ATM and components of the MRN protein complex, Oncogene 25 (2006) 3894–3904.
[43] D.M. Morrow, D.A. Tagle, et al., TEL1, an *S. cerevisiae* homolog of the human gene mutated in ataxia telangiectasia, is functionally related to the yeast checkpoint gene, MEC1, Cell 82 (1995) 831–840.
[44] L. Zou, S.J. Elledge, Sensing DNA damage through ATRIP recognition of RPA–ssDNA complexes, Science 300 (2003) 1542–1548.
[45] L. Zou, D. Liu, S.J. Elledge, Replication protein A-mediated recruitment and activation of Rad17 complexes, Proc. Natl. Acad. Sci. U.S.A. 100 (2003) 13827–13832.
[46] J.C. Harrison, J.E. Haber, Surviving the breakup: the DNA damage checkpoint, Annu. Rev. Genet. 40 (2006) 209–235.
[47] E. Weterings, D.J. Chen, The endless tale of non-homologous end-joining, Cell Res. 18 (2008) 114–124.
[48] E.C. Friedberg, G.C. Walker, W. Siede, DNA repair and mutagenesis, ASM Press, Washington, D.C., 2006.
[49] L. Staresincic, A.F. Fagbemi, et al., Coordination of dual incision and repair synthesis in human nucleotide excision repair, EMBO J. 28 (2009) 1111–1120.
[50] M.S. Luijsterburg, G. von Bornstaedt, et al., Stochastic and reversible assembly of a multiprotein DNA repair complex ensures accurate target site recognition and efficient repair, J. Cell Biol. 189 (2010) 445–463.
[51] M. Lopes, M. Foiani, J.M. Sogo, Multiple mechanisms control chromosome integrity after replication fork uncoupling and restart at irreparable UV lesions, Mol. Cell 21 (2006) 15–27.
[52] G. Jiang, A. Sancar, Recruitment of DNA damage checkpoint proteins to damage in transcribed and nontranscribed sequences, Mol. Cell. Biol. 26 (2006) 39–49.
[53] R.D. Bomgarden, P.J. Lupardus, et al., Opposing effects of the UV lesion repair protein XPA and UV bypass polymerase eta on ATR checkpoint signaling, EMBO J. 25 (2006) 2605–2614.
[54] M. O'Driscoll, V.L. Ruiz-Perez, et al., A splicing mutation affecting expression of ataxia–telangiectasia and Rad3-related protein (ATR) results in Seckel syndrome, Nat. Genet. 33 (2003) 497–501.
[55] M. Giannattasio, F. Lazzaro, et al., Physical and functional interactions between nucleotide excision repair and DNA damage checkpoint, EMBO J. 23 (2004) 429–438.
[56] F. Marini, T. Nardo, et al., DNA nucleotide excision repair-dependent signaling to checkpoint activation, Proc. Natl. Acad. Sci. U.S.A. 103 (2006) 17325–17330.
[57] T.M. Marti, E. Hefner, et al., H2AX phosphorylation within the G1 phase after UV irradiation depends on nucleotide excision repair and not DNA double-strand breaks, Proc. Natl. Acad. Sci. U.S.A. (2006).
[58] H. Neecke, G. Lucchini, M.P. Longhese, Cell cycle progression in the presence of irreparable DNA damage is controlled by a Mec1- and Rad53-dependent checkpoint in budding yeast, EMBO J. 18 (1999) 4485–4497.
[59] J.A. Marteijn, S. Bekker-Jensen, et al., Nucleotide excision repair-induced H2A ubiquitination is dependent on MDC1 and RNF8 and reveals a universal DNA damage response, J. Cell Biol. 186 (2009) 835–847.
[60] D. Nakada, Y. Hirano, K. Sugimoto, Requirement of the Mre11 complex and exonuclease 1 for activation of the Mec1 signaling pathway, Mol. Cell. Biol. 24 (2004) 10016–10025.
[61] M. Giannattasio, C. Follonier, et al., Exo1 competes with repair synthesis, converts NER intermediates to long ssDNA gaps, and promotes checkpoint activation, Mol. Cell 40 (2010) 50–62.
[62] P.T. Tran, N. Erdeniz, et al., EXO1-A multi-tasking eukaryotic nuclease, DNA Repair (Amst) 3 (2004) 1549–1559.
[63] M. Matsumoto, K. Yaginuma, et al., Perturbed gap-filling synthesis in nucleotide excision repair causes histone H2AX phosphorylation in human quiescent cells, J. Cell Sci. 120 (2007) 1104–1112.
[64] A.J. Callegari, T.J. Kelly, UV irradiation induces a postreplication DNA damage checkpoint, Proc. Natl. Acad. Sci. U.S.A. 103 (2006) 15877–15882.
[65] T. Hishida, Y. Kubota, et al., RAD6-RAD18-RAD5-pathway-dependent tolerance to chronic low-dose ultraviolet light, Nature 457 (2008) 612–615.
[66] G.I. Karras, S. Jentsch, The RAD6 DNA damage tolerance pathway operates uncoupled from the replication fork and is functional beyond S phase, Cell 141 (2010) 255–267.
[67] Y. Daigaku, A.A. Davies, H.D. Ulrich, Ubiquitin-dependent DNA damage bypass is separable from genome replication, Nature 465 (2010) 951–955.
[68] L. Stergiou, R. Eberhard, et al., NER and HR pathways act sequentially to promote UV-C-induced germ cell apoptosis in Caenorhabditis elegans, Cell Death Differ. 18 (2011) 897–906.
[69] A.J. Callegari, E. Clark, et al., Postreplication gaps at UV lesions are signals for checkpoint activation, Proc. Natl. Acad. Sci. U.S.A. 107 (2010) 8219–8224.
[70] T. Ogi, A.R. Lehmann, The Y-family DNA polymerase kappa (pol kappa) functions in mammalian nucleotide-excision repair, Nat. Cell Biol. 8 (2006) 640–642.
[71] T. Ogi, S. Limsirichaikul, et al., Three DNA polymerases, recruited by different mechanisms, carry out NER repair synthesis in human cells, Mol. Cell 37 (2010) 714–727.
[72] B.A. Bridges, G.M. Brown, Mutagenic DNA repair in *Escherichia coli*. XXI. A stable SOS-inducing signal persisting after excision repair of ultraviolet damage, Mutat. Res. 270 (1992) 135–144.
[73] K. Minton, E.C. Friedberg, Letter: evidence for clustering of pyrimidine dimers on opposite strands of U.V.-irradiated bacteriophage DNA, Int. J. Radiat. Biol. Relat. Stud. Phys. Chem. Med. 26 (1974) 81–85.
[74] L.H. Lam, R.J. Reynolds, Bifilar enzyme-sensitive sites in ultraviolet-irradiated DNA are indicative of closely opposed cyclobutyl pyrimidine dimers, Biophys. J. 50 (1986) 307–317.
[75] E. Sage, E. Cramb, B.W. Glickman, The distribution of UV damage in the lacI gene of *Escherichia coli* – correlation with mutation spectrum, Mutat. Res. 269 (1992) 285–299.
[76] L.H. Lam, R.J. Reynolds, A sensitive, enzymatic assay for the detection of closely opposed cyclobutyl pyrimidine dimers induced in human diploid fibroblasts, Mutat. Res. 166 (1986) 187–198.
[77] L.H. Lam, R.J. Reynolds, Repair of closely opposed cyclobutyl pyrimidine dimers in UV-sensitive human diploid fibroblasts, Mutat. Res. 166 (1986) 199–205.
[78] L.H. Lam, R.J. Reynolds, DNA sequence dependence of closely opposed cyclobutyl pyrimidine dimers induced by UV radiation, Mutat. Res. 178 (1987) 167–176.
[79] D.L. Svoboda, C.A. Smith, et al., Effect of sequence, adduct type, and opposing lesions on the binding and repair of ultraviolet photodamage by DNA photolyase and (A)BC excinuclease, J. Biol. Chem. 268 (1993) 10694–10700.
[80] F. Eckardt, S.J. Teh, R.H. Haynes, Heteroduplex repair as an intermediate step of UV mutagenesis in yeast, Genetics 95 (1980) 63–80.
[81] B.A. Bridges, R. Mottershead, $RecA^+$-dependent mutagenesis occurring before DNA replication in UV- and -γ irradiated *Escherichia coli*, Mutat. Res. 13 (1971) 1–8.
[82] W.D. Rupp, P. Howard-Flanders, Discontinuities in the DNA synthesized in an excision-defective strain of *Escherichia coli* following ultraviolet irradiation, J. Mol. Biol. 31 (1968) 291–304.
[83] A.R. Lehmann, Post-replication repair of DNA in ultraviolet-irradiated mammalian cells. No gaps in DNA synthesized late after ultraviolet irradiation, Eur. J. Biochem. 31 (1972) 438–445.
[84] L. di Caprio, B.S. Cox, DNA synthesis in UV-irradiated yeast, Mutat. Res. 82 (1981) 69–85.
[85] L. Prakash, Characterization of postreplication repair in *Saccharomyces cerevisiae* and effects of rad6, rad18, rev3 and rad52 mutations, Mol. Gen. Genet. 184 (1981) 471–478.
[86] V. Pagès, S.R. Santa Maria, et al., Role of DNA damage-induced replication checkpoint in promoting lesion bypass by translesion synthesis in yeast, Genes Dev. 23 (2009) 1438–1449.
[87] S. Sabbioneda, I. Bortolomai, et al., Yeast Rev1 is cell cycle regulated, phosphorylated in response to DNA damage and its binding to chromosomes is dependent upon MEC1, DNA Repair (Amst) 6 (2007) 121–127.
[88] A. Gospodinov, B. Anachkova, Cells synchronized in S phase show increased rate of repair of UV damaged plasmids, FEBS Lett. 572 (2004) 99–102.
[89] Y. Auclair, R. Rouget, et al., ATR kinase is required for global genomic nucleotide excision repair exclusively during S phase in human cells, Proc. Natl. Acad. Sci. U.S.A. 105 (2008) 17896–17901.
[90] Y. Auclair, R. Rouget, E.A. Drobetsky, ATR kinase as master regulator of nucleotide excision repair during S phase of the cell cycle, Cell Cycle 8 (2009) 1865–1871.
[91] Y. Auclair, R. Rouget, et al., Requirement for functional DNA polymerase eta in genome-wide repair of UV-induced DNA damage during S phase, DNA Repair (Amst) 9 (2010) 754–764.
[92] D.O. Warmerdam, R. Freire, et al., Cell cycle-dependent processing of DNA lesions controls localization of Rad9 to sites of genotoxic stress, Cell Cycle 8 (2009) 1765–1774.

[93] Y.R. Pan, E.Y. Lee, UV-dependent interaction between Cep164 and XPA mediates localization of Cep164 at sites of DNA damage and UV sensitivity, Cell Cycle 8 (2009) 655–664.
[94] S.L. Colton, X.S. Xu, et al., The involvement of ataxia–telangiectasia mutated protein activation in nucleotide excision repair-facilitated cell survival with cisplatin treatment, J. Biol. Chem. 281 (2006) 27117–27125.
[95] H. Zhang, J. Taylor, W. Siede, Checkpoint arrest signaling in response to UV damage is independent of nucleotide excision repair in *Saccharomyces cerevisiae*, J. Biol. Chem. 278 (2003) 9382–9387.
[96] M. Giannattasio, F. Lazzaro, et al., DNA decay and limited Rad53 activation after liquid holding of UV-treated nucleotide excision repair deficient *S. cerevisiae* cells, DNA Repair (Amst) 3 (2004) 1591–1599.
[97] M.G. Vrouwe, A. Pines, et al., UV-induced photolesions elicit ATR-kinase-dependent signaling in non-cycling cells through nucleotide excision repair-dependent and -independent pathways, J. Cell Sci. 124 (2011) 435–446.
[98] N.M. Al-Moghrabi, I.S. Al-Sharif, A. Aboussekhra, The *Saccharomyces cerevisiae* RAD9 cell cycle checkpoint gene is required for optimal repair of UV-induced pyrimidine dimers in both G(1) and G(2)/M phases of the cell cycle, Nucleic Acids Res. 29 (2001) 2020–2025.
[99] M. Taschner, M. Harreman, et al., A role for checkpoint kinase-dependent Rad26 phosphorylation in transcription-coupled DNA repair in *Saccharomyces cerevisiae*, Mol. Cell. Biol. 30 (2010) 436–446.
[100] X. Wu, S.M. Shell, et al., Phosphorylation of nucleotide excision repair factor xeroderma pigmentosum group A by ataxia telangiectasia mutated and Rad3-related-dependent checkpoint pathway promotes cell survival in response to UV irradiation, Cancer Res. 66 (2006) 2997–3005.
[101] S.M. Shell, Z. Li, et al., Checkpoint kinase ATR promotes nucleotide excision repair of UV-induced DNA damage via physical interaction with xeroderma pigmentosum group A, J. Biol. Chem. 284 (2009) 24213–24222.
[102] X. Wu, S.M. Shell, et al., ATR-dependent checkpoint modulates XPA nuclear import in response to UV irradiation, Oncogene 26 (2007) 757–764.
[103] M. Praetorius-Ibba, Q.E. Wang, et al., Role of Claspin in regulation of nucleotide excision repair factor DDB2, DNA Repair (Amst) 6 (2007) 578–587.
[104] M.A. El-Mahdy, Q. Zhu, et al., Cullin 4A-mediated proteolysis of DDB2 protein at DNA damage sites regulates in vivo lesion recognition by XPC, J. Biol. Chem. 281 (2006) 13404–13411.
[105] D.E. Brash, J.A. Rudolph, et al., A role for sunlight in skin-cancer – UV-induced p53 mutations in squamous-cell carcinoma, Proc. Natl. Acad. Sci. U.S.A. 88 (1991) 10124–10128.
[106] S. Tornaletti, G.P. Pfeifer, Slow repair of pyrimidine dimers at p53 mutation hotspots in skin-cancer, Science 263 (1994) 1436–1438.

Published paper III

A Systems Biology approach to describe the DDR

Since the major aim of my PhD thesis was to design a computational biology approach for PRR, I was involved in writing a short assay that will be published in the Encyclopedia of Systems Biology in 2013, by Springer-Verlag Pub. In this assay, we summarize the key concepts of intrinsic and extrinsic cell cycle checkpoints. This knowledge is important to design future investigations also in my lab to challenge the understanding of the DNA damage checkpoint through a Systems Biology approach. The rationale of the whole Encyclopedia is that Systems Biology approaches are going to contaminate any field of Life Sciences in a near future.

Cell Cycle Checkpoints

Synonyms

Adaptation; Cell cycle; DNA damage checkpoint; Recovery; Spindle checkpoint.

Definition

In this entry we describe the molecular mechanisms of the cell cycle checkpoints. We focused our attention on the DNA damage checkpoint and on the spindle assembly and spindle positioning checkpoints, controlling chromosome segregation in mitosis.

Intrinsic and Extrinsic Cell Cycle Checkpoints

The checkpoints are evolutionarily conserved surveillance mechanisms controlling the order and timing of cell cycle transitions. They are organized as signal transduction cascades blocking or slowing down cell cycle progression at specific stages. Checkpoints are triggered by sensor proteins detecting, directly or indirectly, cell cycle perturbations and transmitting the signal, through the action of protein kinases, to effector proteins that stop cell cycle progression until the signal activating the checkpoint has been turned off. These mechanisms have been highly conserved during evolution, and checkpoint defects result in genome instability, which is frequently associated to tumor development. The checkpoint controls are elicited through molecular events regulating their activation, maintenance, and inactivation resulting, respectively, in cell cycle arrest, maintenance of the arrest for a certain time and recovery of cell cycle progression.
These surveillance mechanisms can be divided into intrinsic regulatory pathways, ensuring the orderly progression of cell cycle events under physiological conditions, and extrinsic pathways that are activated in response to specific clues, such as damage to DNA or cellular structures. The intrinsic checkpoints act by controlling the activity of cell cycle dependent kinases (CDKs) mainly at the G1/S boundary and at the metaphase to anaphase transition in mitosis; such mechanisms are described in other entries of the encyclopedia.

DNA Damage Checkpoints

The DNA damage checkpoint is required for the efficient response to genotoxic stress. The checkpoint is activated when lesions in the DNA are detected and the mechanisms involved differ slightly at various cell cycle phases. DNA damage during the G1 phase activates the G1/S checkpoint preventing entry into S phase. The presence of DNA lesions while cells replicate their genome slows down the kinetics of DNA replication (intra-S checkpoint), and if the chromosomes are damaged in G2, the activation of the G2/M checkpoint avoids chromosome segregation before repair.
Precise and complete DNA replication in every cell cycle and repair of DNA lesions are critical for the maintenance of genetic stability; failures in these processes reduce cell survival and lead to cancer susceptibility. Cell cycle arrest is not the only final outcome of the DNA damage checkpoint response; indeed, it has been demonstrated that checkpoint activation regulates the choice of recombination pathways, influences transcription of DNA repair genes, stabilizes stalled replication forks and, in multicellular eukaryotes, it may promote apoptosis when the damage is irreparable.

MEC1/ATR DNA Damage Checkpoint Signaling

In Saccharomyces cerevisiae, the two main players of the DNA damage checkpoint activated in response to many DNA helix-distorting lesions are two kinases encoded by the MEC1 and RAD53 genes. They are the orthologues of ATR and CHK2 in human cells (Table 1).

Table 1 Major orthologous checkpoint proteins in budding yeast and mammalian cells

S.cerevisiae	Mammal	Function
RFA 1, 2, 3	RPA 1, 2, 3	ssDNA binding protein

MEC1/DDC2	ATR/ATRIP	Sensor (PI3K kinase)
TEL1	ATM	Sensor (PI3K kinase)
DDC1-RAD17-MEC3	RAD9-RAD1-HUS1	Sensor (9-1-1 PCNA-like clamp)
DPB11	TOPBP1	Relevant for MEC1/ATR activation
RAD9	BRCA1/53BP1	Adaptor
MRE11-RAD50-XRS2 (MRX)	MRE11-RAD50-NBS1 (MRN)	Lesion processing
SAE2	CtIP	Lesion processing
SGS1	BLM, WRN	Lesion processing
EXO1	hEXO1	Lesion processing
CHK1	CHK1	Effector kinase (S/T kinase)
RAD53	CHK2	Effector kinase(S/T kinase)

In budding yeast, MEC1 acts as the apical kinase in the checkpoint cascade and likely senses abnormal amounts of single-stranded (ss) DNA stretches covered by the replication protein A (RPA), which are generated by processing of various DNA lesions (Fig. 1).

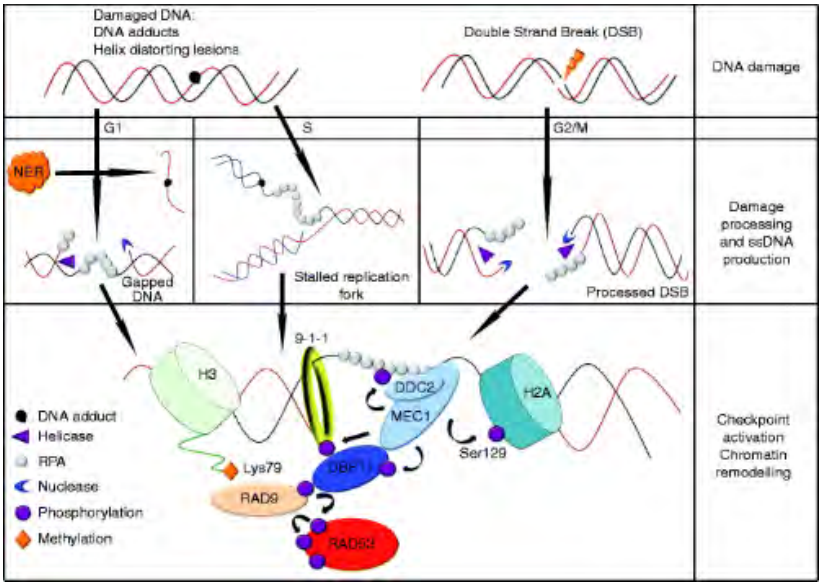

Fig. 1 DNA damage checkpoint activation

RPA-coated ssDNA is thought to recruit the apical checkpoint kinase (MEC1-DDC2 or TEL1, in budding yeast; ATR-ATRIP or ATM in mammalian cells), and the 9-1-1 complex (RAD17-MEC3-DDC1 in budding yeast) triggering the signal transduction cascade (Zou and Elledge 2003). As a consequence of this activation, MEC1 phosphorylates, directly or indirectly, a number of factors (e.g. DDC2, H2A, DDC1, RAD9, DPB11/TOPB1, RAD53/CHK2, CHK1, etc.) and these subsequent phosphorylation events are used to follow the signal through the cascade (Fig. 1). Activated RAD53/CHK2 amplifies the signal through autophosphorylation events and inhibits the cell cycle machinery by phosphorylating various targets, leading to cell cycle arrest (Harrison and Haber 2006). RAD53/CHK2 and CHK1 activation influence various DNA metabolic pathways, like homologous recombination, origin firing during S phase, nuclease activity, and gene expression.
Another essential player of checkpoint activation is represented by the 9-1-1 complex. This heterotrimeric complex show limited sequence homology to the PCNA homotrimeric clamp and it is therefore often referred to as the checkpoint clamp (Table 1 and Fig. 1). The 9-1-1 complex is loaded onto DNA by a checkpoint clamp loader, a form of replication factor-C (RFC), in which the RFC1 subunit is substituted by RAD24 (S. cerevisiae) or RAD17 (mammalian cells) (Majka and

Burgers 2003). The 9-1-1 clamp promotes checkpoint activation in vivo by influencing MEC1/ATR recruitment and its substrate specificity; the 9-1-1 clamp has a role in modulating chromatin binding of RAD9/53BP1 and subsequent RAD53/CHK2 phosphorylation events.

Checkpoint Signaling in Response to Double Strand Breaks (DSBs)

When the DNA integrity is challenged by discontinuities in the helix backbone, as those generated by double strand breaks, the checkpoint human kinase ATM is loaded near the DSBs and, together with ATR, activate the checkpoint response. ATM activation requires the presence of the MRN complex, which has a DNA tethering capacity and possesses both endo- and exo-nucleolytic activities. Although the nuclease activity of the MRX/MRN complex is not critical for checkpoint activation, the presence of a physically assembled complex and the action of other nucleases and helicases (such as EXO1 and SGS1) are important.

In S. cerevisiae TEL1, the ATM orthologue, participates only marginally in the checkpoint response induced by a single DSB, but its role becomes relevant in the presence of multiple DSBs and/or when the initiation of DSB ends processing is defective. In this organism, a single irreparable DSB triggers the MEC1 pathway, which is activated by extensive resection of the DSB DNA ends (Lazzaro et al. 2009). If the break is not rapidly repaired, nucleolytic activities produce long ssDNA regions that, via the ssDNA binding protein RPA, recruit MEC1 activating the checkpoint cascade (Fig. 1).

Chromatin Remodeling and Checkpoint Maintenance

Chromatin modifications contribute to checkpoint function. In fact, histone proteins are also modified in response to DNA damage. In S. cerevisiae, the Ser129 residue of H2A is phosphorylated in a MEC1-dependent manner in response to a variety of genotoxic treatments and the modified γH2A molecules localize near a DSB (van Attikum and Gasser 2009); the same modification occurs on the Ser139 conserved residue of the mammalian H2AX histone variant. It is assumed that RPA-coated ssDNA is required to activate the checkpoint, but the MEC1/ATR and TEL1/ATM-dependent phosphorylation of the H2A/H2AX histones (Fig. 1) is relevant for checkpoint maintenance, since in its absence the checkpoint signal is turned off prematurely. In yeast, one of the major roles of H2A phosphorylation is the recruitment of chromatin remodeling complexes near the DNA lesions. Another histone modification important for the activation of the DNA damage checkpoint is methylation of Lys79 of histone H3 (H3-Lys79Me) by the specific methyl transferase DOT1. In fact, the main mediator proteins in the checkpoint cascade (RAD9 in S. cerevisiae and 53BP1 in mammals) can be recruited near a chromatin damaged site through two parallel pathways. The first one is dependent upon H3-Lys79 methylation, while the second pathway acts through the function of the DPB11/TOPB1 adaptor proteins (Fig. 1).

Turning Off the DNA Damage Checkpoint Signal

In cells with repairable DNA damage, the checkpoint arrest is maintained until repair is completed. Then, cells can resume the cell cycle turning off the checkpoint signal in a process known as recovery. Instead, if an irreparable lesion is present, cells eventually override the cell cycle arrest in a process called adaptation. In mammals, it has been proposed that adaptation to damage is linked to cancerogenesis and, likely, this event is normally prevented by inducing the apoptotic pathway. Inactivation of the RAD53 kinase is required to recover from checkpoint-mediated cell cycle arrest in S. cerevisiae. Various protein phosphatases, including PTC2, PTC3, PPH3, and GLC7, have been found to be important for checkpoint inactivation. Interestingly, their relative contribution to the recovery process seems to be influenced by the type of genotoxic stress causing checkpoint activation (DSBs, alkylating agents, hydroxyurea). The same phosphatases act on phosphorylated γH2A and, not surprisingly, homologous phosphatases influence checkpoint inactivation also in human cells.

While it was somehow expected that reversal of checkpoint signaling would involve the action of phosphatases acting on the master effector kinases of the cascade, it was interesting to learn that POLO-like kinases (such as PLK1 and CDC5) also play an important role in switching off the checkpoint. It is likely that recovery and adaptation, being two sides of the same coin, are going to share common players and mechanisms. However, genetic screenings in budding yeast revealed that some mutations allow to distinguish between the two processes. For example, the cdc5-ad allele and deletions of certain recombination genes (such as KU70/80, TID1 and RAD51) prevent the adaptation process without affecting recovery.

S. cerevisiae Spindle Assembly and Spindle Position Checkpoints

Chromosome segregation at mitosis is controlled by two surveillance mechanisms: the spindle assembly and the spindle positioning checkpoints. Accurate segregation requires bipolar attachment of sister chromatids to the mitotic spindle, which is mediated by a proper connection between kinetochores and spindle microtubules. Kinetochore capture and microtubules bi-orientation are stochastic processes taking a variable amount of time to complete. During that time individual chromosomes may be detached from the microtubules or be connected only to one spindle pole. The spindle assembly checkpoint (SAC) delays the metaphase to anaphase transition until the sister chromatids are properly attached to the spindle in a bipolar orientation. In budding yeast, cell cycle arrest at the G2/M transition is mediated by inhibition of the CDC20-anaphase promoting complex (APC) ubiquitin ligase, thus preventing proteolysis of the securin PDS1 until complete bi-orientation is achieved (Fig. 2).

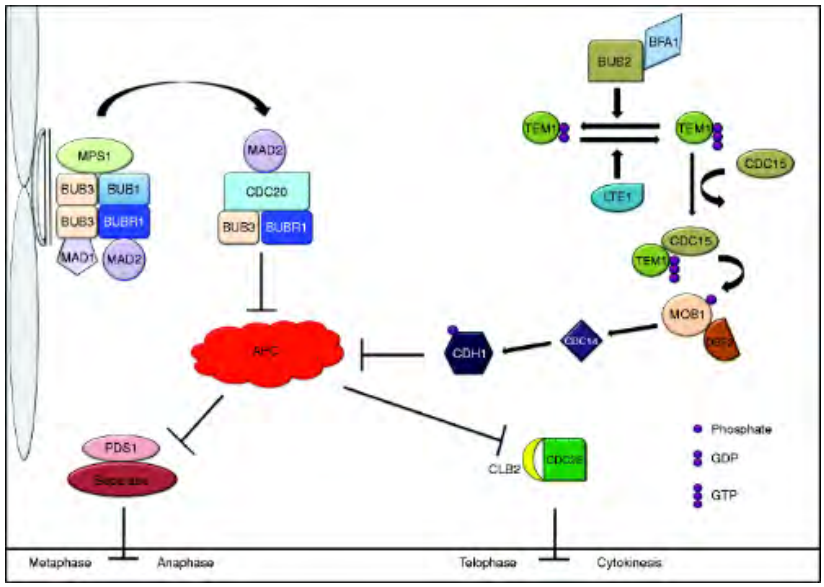

Fig. 2 The spindle assembly and spindle positioning checkpoints

Checkpoint proteins (MAD1, MAD2, BUB1, BUBR1, BUB3, and MPS1) all accumulate at unattached kinetochores and form various complexes, many of which can inhibit the APC (Fang et al. 1998) (Fig. 2). APC is a multiprotein complex that targets several proteins for degradation during mitosis through the associated specificity factor CDC20. Securin and cyclins are ubiquitylated by CDC20-APC; therefore, to delay anaphase onset in the presence of spindle defects, the checkpoint must block CDC20-APC mediated PDS1 degradation. Experimental evidence suggests that in response to spindle defects, MAD2 exchanges from a MAD1/MAD2 complex to a CDC20/MAD2 complex sequestering CDC20 away from the APC and blocking PDS1 degradation (Fig. 2).

In S. cerevisiae, spindle misorientation is detected by the spindle positioning checkpoint (SPOC) which prevents mitotic exit. The target of this control is the mitosis exit network (MEN), and more specifically the activation of the TEM1 GTPase (Adames et al. 2001). TEM1 cycles between GDP- and GTP-bound states, regulated by the putative guanine nucleotide exchange factor (GEF) LTE1 and the two-component GTPase activating protein (GAP) BFA1/BUB2. The last one recruits TEM1 to the bud-directed spindle pole, where TEM1 is kept inactive until the pole crosses the neck into the bud. GTP-TEM1 then binds to the protein kinase CDC15, which phosphorylates and activates the protein kinase DBF2. MOB1 binds to DBF2 and, in a poorly understood manner, MOB1/DBF2 stimulates the release of the CDC14 phosphatase from the nucleolus and contributes to cytokinesis. CDC14 dephosphorylates CDH1, leading to the activation of CDH1-APC complex, which triggers cyclin degradation and exit from mitosis. A possible crosstalk between the SAC and SPOC is likely, but not yet fully demonstrated (Lew and Burke 2003).

Summary

The maintenance of genome stability is an essential process, which needs a careful control. Indeed, all eukaryotic cells evolved surveillance mechanisms, called checkpoints, sensing the presence of DNA damage in the genome or alterations in cellular structures controlling chromosome segregation in mitosis. DNA integrity can be challenged by lesions caused by a variety of chimico-physical agents, or by replication stress caused by special DNA structures or by a limited supply of deoxyribonucleotides. The DNA integrity checkpoint is a signal transduction cascade conserved from yeast to man and the apical factors in the pathway are protein kinases. The spindle assembly checkpoint controls the status of kinetochore/microtubule attachment delaying exit from mitosis until all kinetochores have formed correct bipolar connections with the spindle. In budding yeast, and likely in all eukaryotes, the alignment of the mitotic spindle with the axis of cell polarity is controlled by another surveillance mechanism, called the spindle positioning checkpoint.

Cross-References

DNA Damage
DNA Repair
Histones
Kinetochores
Mitosis
Protein Kinases
Phosphatases

References

Adames NR, Oberle JR, Cooper JA (2001) The surveillance mechanism of the spindle position checkpoint in yeast. J Cell Biol 153(1):159–168

Fang G, Yu H, Kirschner MW (1998) Direct binding of CDC20 protein family members activates the anaphase-promoting complex in mitosis and G1. Mol Cell 2(2):163–171

Harrison JC, Haber JE (2006) Surviving the breakup: the DNA damage checkpoint. Annu Rev Genet 40:209–235

Lazzaro F, Giannattasio M, Puddu F, Granata M, Pellicioli A, Plevani P, Muzi-Falconi M (2009) Checkpoint mechanisms at the intersection between DNA damage and repair. DNA Repair 8:1055–1067

Lew DJ, Burke DJ (2003) The spindle assembly and spindle position checkpoints. Annu Rev Genet 37:251–282

Majka J, Burgers PM (2003) Yeast Rad17/Mec3/Ddc1: a sliding clamp for the DNA damage checkpoint. Proc Natl Acad Sci USA 100:2249–2254

van Attikum H, Gasser SM (2009) Crosstalk between histone modifications during the DNA damage response. Trends Cell Biol 19:207–217

Zou L, Elledge SJ (2003) Sensing DNA damage through ATRIP recognition of RPA-ssDNA complexes. Science 300:1542–1548

Cell Cycle Checkpoints

Flavio Amara	Dipartimento di Scienze Biomolecolari e Biotecnologie, Università di Milano, Milan, Italy
Dr. Marco Muzi-Falconi	Dipartimento di Scienze Biomolecolari e Biotecnologie, Università di Milano, Milan, Italy
Dr. Paolo Plevani	Dipartimento di Scienze Biomolecolari e Biotecnologie, Università di Milano, Milan, Italy

DOI:	10.1007/SpringerReference_306217
URL:	http://www.springerreference.com/index/chapterdbid/306217
Part of:	Encyclopedia of Systems Biology
Editors:	-
PDF created on:	February, 04, 2012 16:36

Submitted manuscript

The results shown previously in the "main results" section of my thesis were essential to design the key experiments extensively described in the submitted manuscript. In the manuscript are presented the most relevant results obtained during my PhD that I tried to rationalize by considering a variety of data coming from different branches of Life Sciences, Bioinformatics and Molecular and Cellular Biology.

In vivo and in silico analysis of PCNA ubiquitylation in the activation of the Post Replication Repair pathway in S. cerevisiae

Flavio Amara[1,♯] , Riccardo Colombo[2,♯] , Paolo Cazzaniga[3] , Dario Pescini[4] , Attila Csikász-Nagy[5] , Marco Muzi Falconi[1] , Daniela Besozzi*[6] , Paolo Plevani*[1]

[1]Dipartimento di Bioscienze, Università degli Studi di Milano, Milano, Italy
[2]Dipartimento di Informatica, Sistemistica e Comunicazione, Università degli Studi di Milano-Bicocca, Milano, Italy
[3]Dipartimento di Scienze Umane e Sociali, Università degli Studi di Bergamo, Bergamo, Italy
[4]Dipartimento di Statistica, Università degli Studi di Milano-Bicocca, Milano, Italy
[5]The Microsoft Research - Università degli Studi di Trento, Centre for Computational and Systems Biology, Rovereto (Trento), Italy
[6]Dipartimento di Informatica, Università degli Studi di Milano, Milano, Italy

Email: Flavio Amara*- flavio.amara@unimi.it; Riccardo Colombo - riccardo.colombo@disco.unimib.it; Paolo Cazzaniga - paolo.cazzaniga@unibg.it; Dario Pescini - dario.pescini@unimib.it; Attila Csikász-Nagy - csikasz@cosbi.eu; Marco Muzi Falconi - marco.muzifalconi@unimi.it; Daniela Besozzi*- besozzi@di.unimi.it; Paolo Plevani*- paolo.plevani@unimi.it;

*Corresponding author

♯These authors contributed equally to this work.

Abstract

Background: The genome of living organisms is constantly exposed to several damaging agents that induce different types of DNA lesions, leading to cellular malfunctioning and onset of many diseases. To maintain genome stability, cells developed various repair and tolerance systems to counteract the effects of DNA damage. Here we focus on Post-Replication Repair (PRR), the pathway involved in the bypass of DNA lesions induced by sunlight exposure and UV radiation. PRR acts through two different mechanisms, activated by mono- and poly-ubiquitylation of the DNA sliding clamp, called Proliferating Cell Nuclear Antigen (PCNA).

Results: We developed a novel protocol to measure the time-course ratio between mono-, di- and tri-ubiquitylated PCNA isoforms on a single western blot, which were used as the wet readout for PRR events in wild type and mutant *S. cerevisiae* cells exposed to acute UV radiation doses. Stochastic simulations of PCNA ubiquitylation dynamics, performed by exploiting a novel mechanistic model of PRR, well fitted the experimental data at low UV doses, but evidenced divergent behaviors at high UV doses, thus driving the design of further experiments to verify new hypothesis on the functioning of PRR. The model predicted the existence of a UV dose threshold for the proper functioning of the PRR model, and highlighted an overlapping effect of Nucleotide Excision Repair (the pathway effectively responsible to clean the genome from UV lesions) on the dynamics of PCNA ubiquitylation in different phases of the cell cycle. In addition, we showed that ubiquitin concentration can affect the rate of PCNA ubiquitylation in PRR, offering a possible explanation to the DNA damage sensitivity of yeast strains lacking deubiquitylating enzymes.

Conclusions: We exploited an *in vivo* and *in silico* combinational approach to analyze for the first time in a Systems Biology context the events of PCNA ubiquitylation occurring in PRR in budding yeast cells. Our findings highlighted an intricate functional crosstalk between PRR and other events controlling genome stability, and

evidenced that PRR is more complicated and still far less characterized than previously thought.

Background

The genome of living organisms is constantly exposed to several exogenous and endogenous damaging agents – environmental chemicals, ultraviolet (UV) light, ionizing radiation, reactive oxygen species – that can result in DNA lesions potentially leading to cellular malfunctioning, aging and the onset of several diseases, including cancer and neurodegeneration [1, 2]. Since the maintenance of genome stability is a pivotal task for cell survival and division, cells have developed various repair and tolerance systems to counteract the effects of DNA damage, which altogether rely on the crosstalk between the biochemical processes involved in DNA metabolism and in cell cycle progression. According to the type of DNA lesion and the cell cycle stage at which the damage occurs, cells exploit the activation of specific DNA-damage tolerance (DDT) pathways. In this work, we aim to investigate the functioning of Post-Replication Repair (PRR), a DDT pathway involved in the recognition of the most abundant mutagenic and cytotoxic DNA lesions induced by sunlight exposure and UV radiation [3–6].

The cellular pathway that is effectively responsible to clean the genome from these UV adducts is Nucleotide Excision Repair (NER). Briefly, NER excides short DNA patches ($\sim$ 30 nucleotides long) containing UV lesions and promotes the filling of the generated single-stranded DNA (ssDNA) gap [7, 8]. It is generally assumed that NER acts in the G1 and G2 phases of the cell cycle, as the NER excision activity can result dangerous during S phase because it might generate breaks and gaps near the incoming replication forks [9]. On the other hand, during the S phase of the cell cycle the DNA replication machinery stalls in front of a UV-induced lesion, because of the inability of the replicative DNA polymerases to incorporate nucleotides opposite a UV adduct. To avoid prolonged stalling and the possible collapse of the replication fork, eukaryotic cells activate the PRR pathway, whose role is not to repair but instead to *bypass* the UV-induced DNA lesions, allowing the replisome to complete genome replication over the damaged template. This way, cells can complete S phase and postpone DNA repair at the G2/M transition.

Notwithstanding the relevance of genome integrity and the ever increasing body of data that is continuously produced in this field, a global view of the crosstalk between the numerous DNA repair pathways is still lacking. Recently, a number of studies based on wet experiments, as well as computational modeling and bioinformatics tools, started to investigate these mutual relationships, in order to understand how regulative mechanisms and proteins modifications occurring in each pathway are able to influence the other pathways to coordinate either the detection, the repair or the bypass of the different DNA lesions, in a finely orchestrated manner with cell cycle progression and cellular metabolism [10–16].

In addition, a number of mathematical models were recently defined to analyze in details specific processes that govern the machinery of DNA damage and repair in different organisms. For instance, in bacteria some works investigated the dynamics of double-strand breaks (DSBs) formation and analyzed the relation between bacterial death rate and the concentration of endogenous damaging agents [17], or tried to explain the UV-induced SOS response in *E. coli* incorporating mutagenesis by error-prone DNA polymerases [18]. In eukaryotes, several models were proposed to analyze different regulatory mechanisms, such as, e.g., the detection of DSBs depending on ATM (ataxia telangiectasia mutated) autophosphorylation [19], or the imbalance between DNA damage and repair processes in the formation of DNA adducts due to oxidative estrogen metabolism [20]. Most of these models focused on NER and Base Excision Repair (BER) pathways in human and mammalian cells (see for example [21–24]), though no mathematical model was developed up to now to elucidate the mechanisms governing the PRR pathway.

Experimental works concerning this complicated and not well characterized pathway determined that the bypass of UV adducts promoted by PRR involves two different sub-pathways: the first may be error-prone and is related to Translesion DNA

Synthesis (TLS), while the second is error-free and acts through Template Switching (TS) processes. The key event driving the activation of these sub-pathways is a post-translational modification of the sliding clamp Proliferating Cell Nuclear Antigen (PCNA), a protein acting as scaffold for the binding of replicative DNA polymerases and several other proteins involved in DNA replication, repair and cell cycle regulation [3, 25, 26]. In particular, in *Saccharomyces cerevisiae* it is known that the mono-ubiquitylation of PCNA drives the PRR pathway to TLS, while PCNA poly-ubiquitylation directs PRR to the error-free sub-pathway. A major issue in the study of PRR is to understand how the dynamics of PCNA ubiquitylation might influence the choice between TLS and TS, or whether there exists a damage-related threshold able to regulate the crosstalk between these sub-pathways.

In this paper, we focus on the analysis of the events of PCNA ubiquitylation occurring in PRR by exploiting a bottom-up Systems Biology approach, based on data-driven modeling and model-driven experiments. This was carried out through an integrate and cyclic workflow consisting in laboratory experiments based on genetic and molecular biology protocols on the one side, and mathematical modeling and computational analysis on the other side. In particular, experimental measurements of the ratio between mono- and poly-ubiquitylated PCNA were used as the wet readout of cells response to acute UV irradiation, carried out through a systematic *in vivo* characterization of the dynamics of PCNA ubiquitylation after UV irradiation of *S. cerevisiae* cells. For this purpose, we developed a specific experimental protocol that allows the detection of mono- and poly-ubiquitylated PCNA isoforms on a single western blot, unlike other previously devised methods which could only allow the measurement of the amount of di- to N poly-ubiquitylated PCNA isoforms – albeit not the mono-ubiquitylated one – on the same film (see, e.g., [27]). These laboratory measurements were systematically compared with the outcome of stochastic simulations, performed by exploiting a novel mechanistic model of PRR that describes in details the molecular interactions involved in the mono- and poly-ubiquitylation steps of PCNA, and which takes into account the estimated number of induced DNA lesions at different UV doses.

In this context, the choice of a stochastic computational framework was motivated by several aspects related to the pathway under investigation. First of all, the molecular amounts of most species involved in PRR are low, and we also evidenced quite large noise in the experimental measurements; therefore, a stochastic approach was more suitable to capture the possible noise effects in the emergent dynamics of PCNA ubiquitylation. Secondly, the mechanistic approach based on the stochastic formulation of chemical kinetics [28] that we exploited to define the mathematical model of PRR, allows to give a detailed description of the molecular interactions occurring in PRR events, and also to test different interaction topologies by minimizing the model revision from time to time.

In addition, the definition of the mathematical model benefited from a preliminary bioinformatic process based on three-dimensional protein structure modeling, to establish the actual spatio-temporal cascade of PRR interactions, and on a successive computational phase based on parameter sweep analysis, to test the reliability of the chosen model parameterization.

The integration of *in vivo* and *in silico* data allowed us to make predictions on the functioning of PRR in living cells and to drive the design of further laboratory experiments, aimed at improving the knowledge of the pathway. In particular, our results suggest the existence of a UV dose threshold for the proper functioning of our PRR model in response to UV-induced damages, corroborated by a fine concordance of the balance of mono- and poly-ubiquitylated PCNA isoforms between wet measurements and simulation outcomes at UV doses below 30 J/m^2. Above this threshold, we obtained an unexpected discrepancy between *in vivo* and *in silico* data, which allowed us to postulate an overlapping effect of NER on the dynamics of PCNA ubiquitylation (altering the actual response of PRR in irradiated cells), and the relevance of NER not only in G1 and G2 phases but also during the S phase of the cell cycle, in agreement with some previous observations [29]. In addition, our results showed that the concentration of free ubiquitin in the nuclear compartment can affect the rate of PCNA ubiquitylation, offering a possible explanation to the DNA damage sensitivity of yeast strains lacking deubiquitylating enzymes [30].

After providing a detailed description of the biochemical processes involved in the PRR pathway in budding yeast cells, we present the experimental procedures and the computational methods exploited in this Systems Biology work. Then, we show

the computational results related to the definition of the mathematical model and discuss the biological insights concerning PRR, achieved thanks to the combined crosstalk of *in silico* simulations and laboratory experiments. Finally, we conclude the paper with some final remarks and open questions for future research.

Post Replication Repair in S. cerevisiae

PRR is the most complicated and least characterized DDT pathway [3] involved in the bypass of the most abundant mutagenic and cytotoxic DNA lesions induced by sunlight exposure and UV radiation, namely, pyrimidine cyclobutane dimers (CPDs) and 6-4 photoproducts (6-4 PPs) [4–6]. The key event process taking place in PRR for the bypass of these UV lesions is the ubiquitylation at lysine 164 (K164) of the sliding clamp named Proliferating Cell Nuclear Antigen (PCNA) [3,25,26]. PCNA is a ring-shaped homotrimeric protein, which encircles and slides along double-stranded DNA molecules localizing and tethering a plethora of other proteins (such as polymerases) to DNA. PCNA ubiquitylation in response to UV-induced DNA damage does not mediate proteasomal-induced degradation: rather, K164 PCNA ubiquitylation signals the presence of a non-replicable UV lesion in the genome [31,32].

The ubiquitylation process of PCNA requires three consecutive steps: (1) ubiquitin activation, (2) ubiquitin trans-thio-esterification, and (3) PCNA ubiquitin conjugation. While the first two steps are common to other cellular pathways, the third step is carried out by proteins that are specific of PRR. In *S. cerevisiae*, the step of ubiquitin activation is mediated by Uba1, which is the unique ubiquitin activating enzyme (also known as E1) in budding yeast. This process, requiring ATP consumption, is fully conserved in eukaryotes and it requires at least 20 biochemical reactions on the whole [33]. Once activated, the ubiquitin moves from the E1 enzyme to the ubiquitin conjugating enzyme (also known as E2) through a trans-thio-esterification reaction. In *S. cerevisiae*, the PRR pathway includes two different E2 enzymes which are able to receive an activated ubiquitin from Uba1: Rad6 and Ubc13. The latter enzyme, Ubc13, works in a complex with an ubiquitin conjugating enzyme variant (UEV), called Mms2 [34, 35]. The key event in the activation of PRR actually consists in the capability of transferring the ubiquitin from an E2 enzyme to PCNA, through the action of an ubiquitin ligase enzyme (also known as E3). In *S. cerevisiae* cells there exist two different E3 enzymes, Rad18 and Rad5, which drive the ubiquitin transfer to PCNA from the E2 Rad6 and Ubc13-Mms2, respectively. Each E3 enzyme has its own function and specificity within the PRR pathway, and the kind of ubiquitylation they carry out on PCNA drives the next steps of the DNA damage bypass process in different ways.

On the whole, the ubiquitylation process within the PRR pathway involves five actors (see Figure 1): two E2 enzymes (Rad6 and Ubc13-Mms2), two E3 enzymes (Rad18 and Rad5) and one target (PCNA) [25]. The way the E2 and E3 enzymes work together to induce the covalent modification of PCNA was recently characterized *in vitro* by using purified *S. cerevisiae* proteins [36], suggesting that the most probable mechanism of PCNA ubiquitin conjugation after UV-induced DNA damage consists in the following step-wise process. After stalling of the replication machinery, the formation of RPA protein-coated ssDNA at level of the UV lesion leads to recruitment of the Rad18-Rad6 complex and the subsequent mono-ubiquitylation of PCNA at K164 [37]. This mono-ubiquitylation can be further extended by Rad5 and Ubc13-Mms2, which carry another ubiquitin moiety. Then, the Rad5-Ubc13-Mms2 complex can further bind to di-ubiquitylated PCNA and, in a step-wise process, it leads to tri-ubiquitylation and, rarely, to tetra-ubiquitylation of PCNA [38]. This limited PCNA poly-ubiquitylation is obtained through the formation of K63-linked ubiquitin chains and this linkage specificity is the major signal for UV lesion bypass.

It is effectively the balance between the mono- and poly-ubiquitylated modification states of PCNA that is able to influence the distinct modes of UV lesion bypass: mono-ubiquitylation drives the PRR towards Translesion DNA Synthesis (TLS), while K63 poly-ubiquitylation drives it to Template Switching (TS). Regarding TLS, PCNA mono-ubiquitylation enhances the binding affinity of particular DNA polymerases, called TLS polymerases (Pol-η, Rev1 and Pol-ζ in budding yeast), which are able to substitute the stalled replicative polymerases in a process called "polymerase switch" [39]. TLS polymerases are able to host the UV lesion within their active site and to incorporate a nucleotide in front of the lesion, while the replicative polymerases Pol-δ and Pol-ε are unable to bypass the DNA damage. Depending on which TLS polymerase binds PCNA,

two different kinds of UV lesion bypass are possible. In fact, TLS can be further divided into two sub-branches: the "error-free TLS", taking place when Pol-η incorporates the right nucleotide opposite a CPD, and the "error-prone TLS", occurring when Pol-η incorporates a wrong nucleotide opposite a 6-4 PP and then stalls. In this case, Pol-η is replaced by Pol-ζ which, in cooperation with Rev1, is able to carry on the replication, though generating mutations on the genome [40, 41]. Therefore, PCNA mono-ubiquitylation and TLS are potentially mutagenic and may cause genome instability. Conversely, the TS sub-pathway allows to bypass UV lesions in an error-free way, because it exploits the invasion of the undamaged DNA sister filament to overcome replication fork stalling, without the intervention of TLS polymerases (a process also known as recombination-based UV lesion bypass). This branch of PRR is enhanced by PCNA K63-linked poly-ubiquitylation, but the molecular details of the whole process are largely unknown.

A relevant issue in the investigation of PRR is related to the regulation of the dynamics of PCNA ubiquitylation in response to UV-induced damages, since the balance between its mono- and poly-ubiquitylated isoforms is supposed to control the crosstalk between the TLS and TS sub-pathways. Therefore, we propose hereby a detailed mechanistic model of the enzymatic processes involved in PCNA ubiquitylation related to the PRR pathway, in order to monitor the formation of mono- versus poly-ubiquitylated PCNA isoforms after UV irradiation, and to better understand the cellular response to UV-induced DNA damages.

Methods

Experimental procedures

S. cerevisiae *strains, media and growing conditions*

All *S. cerevisiae* strains used in this work are isogenic to DF5 genetic background (*his3-Δ200 leu2-3,112 lys2-801 trp1-1 ura3-52*) and deletion mutants were constructed by one-step PCR strategy [42] and confirmed by PCR [43]. All strains are carrying the ^{HIS}*POL30* allele, expressing HIS tagged PCNA protein. All strains were grown in liquid YPD following standard genetic procedures [43]. The complete list of strains used in this work is given in Table 1.

UV irradiation

Yeast cells were grown to a concentration of $\sim 10^7$ cells/ml, plated on YPD agar and irradiated with different doses (5 to 75 J/m^2) of UV-C light (254 nm). Immediately after irradiation, cells were resuspended in liquid medium and samples collected at various time points – taken between 0 h and 5 h after irradiation – were analyzed. In order to avoid variations due to newly synthesized proteins which may affect experimental reproducibility and alter the comparison with the computational modeling, we added 10 μg/ml of cycloheximide (CHX), a protein synthesis inhibitor, after UV irradiation of logarithmically growing cells. This CHX dose inhibits protein synthesis to $\sim 90\%$ within 15 min [44] and stops cell cycle progression, as shown in histogram and density plots reported in Additional File 1.

Fluorescence activated cell sorter (FACS) analysis

Cell cycle progression was monitored by measuring DNA content by FACS analysis, as previously described [45]. By this analysis we established the percentage of G1, S and G2 cells in a cell population.

In vivo *detection of ubiquitylated PCNA and signal quantification*

Ubiquitylated PCNA represents a small percentage of total PCNA in the cells, and quantitative detection of the modified PCNA isoforms requires their enrichment. This was achieved by using yeast strains carrying the ^{HIS}*POL30* allele and a well established pull-down protocol [46]. Before pull-down of ubiquitylated PCNA, cell lisates were normalized to the sample containing the lower amount of proteins determined with the BioRad Assay. Proteins were separated by PAGE on 10% SDS-urea [47] and then transferred onto a nitrocellulose membrane at 4 °C. After transfer, nitrocellulose membranes were treated at 120 °C for 30 min. Ubiquitylated PCNA was detected with polyclonal anti-Ub antibody, and unmodified PCNA was detected with a monoclonal anti-HIS antibody (Cell Signaling). The signal corresponding to ubiquitylated PCNA was quantified by ImageJ software [48]. The PCNA ubiquitylation signal was normalized to the unmodified PCNA signal and analyzed as the ratio between mono-, di- and tri-ubiquitylated PCNA, as described in Additional File 2.

Model parameterization

In order to gain insights into the functioning of a biological system, it is fundamental to identify the system structure (i.e. its main components and their respective interactions), as well as the set of parameters involved, which are needed to perform simulations and to conduct a quantitative analysis of the system response under different conditions. Here, we present a mechanistic model of the PRR pathway, defined according to the stochastic formulation of chemical kinetics [28], which requires to specify the set of molecular species occurring in the pathway and their respective interactions, formally described as a set of biochemical reactions.

The parameterization of this model is given by the values of the stochastic constants associated to the reactions, the molecular amounts of the species initially present in the system, and the number of lesions per genome corresponding to any given UV irradiation dose. We describe hereafter the methods used to calibrate the values of the parameters of the PRR model, and to analyze the PCNA ubiquitylation dynamics in response to UV-induced damages.

Molecular species amounts

In vivo data related to PRR protein concentrations were retrieved from [49], the Saccharomyces Genome Database (SGD) [50], and from VonDerHaar curated database [51], which represent the primary sources for the identification of the amount of proteins within yeast cells.

Since the model describes a process taking place inside the nucleus, the molecular amounts of the PRR proteins that are localized both in the nucleus and in the cytoplasm have to be scaled to the nuclear portion volume. To this aim, since we could not retrieve any additional information about the precise cellular localization (related to, e.g., concentration gradients or buffering mechanisms) of all the proteins involved in PRR, we assumed a uniform distribution within the cell. Then, we calculated the nuclear amount of these proteins as a fraction of their whole cellular amount (as reported in the protein databases), proportional to the nuclear volume of the cell. In *S. cerevisiae*, the nuclear volume corresponds to 7% of the total cell volume for exponential growing cells, as derived through microscopy techniques [52].

The derived molecular amounts (expressed as number of molecules per cell) of the proteins occurring in the initial state of the PRR model are reported in Table 2.

Reaction constants

In the context of computational modeling, the general lack of experimental measurements of *in vivo* kinetics usually challenge the definition of a homogeneous set of values for reaction constants. As a matter of fact, the available literature on PRR is almost characterized by qualitative descriptions of the pathway; the only kinetic constant that we could assess from literature corresponds to the process of poly-ubiquityl chain extension on mono-ubiquitylated PCNA, showing a $K_{\mathrm{cat}} = (3.0 \pm 0.04)\ \mathrm{min}^{-1}$ [53]. This value was transformed into the stochastic constant of the corresponding reaction in the model described later on (see also Table 5, reaction 16).

All other stochastic constants were manually tuned by exploiting the time-courses of mono-, di- and tri-ubiquitylated PCNA isoforms derived from western blots of the experiments performed at 5 J/m^2, considered as reference dose for parameter calibration. The choice of the initial parameterization at 5 J/m^2 was then corroborated by comparing the outcome of stochastic simulations with the *in vivo* dynamics of PCNA ubiquitylation at 10 J/m^2 UV dose.

Number of DNA lesions

The number of DNA lesions (CPD plus 6-4 PP) generated on the genome after different UV dose exposition was determined by using literature data [54,55]. These measurements, reported in Table 3, were exploited to derive the linear regression equations required to estimate the correlation between the radiation dose used in our laboratory experiments, and the corresponding number of lesions induced on *S. cerevisiae* genome.

In particular, we derived the equations $y = 200.248\ x$ and $y = 222.22\ x$, by using data reported in [54] and [55], respectively (where y is the number of genomic lesions induced by the UV dose x). Afterwards, a χ^2 cross-validation test was applied over the two datasets. The result of the cross-validation indicated that the best coefficient is that related to the data reported in [54], being $\chi^2 = 0.049$ for the dataset from [54], and $\chi^2 = 129.79$ for the dataset from [55]. Therefore, the first equation was applied to estimate the number of genomic lesions induced

by the various UV doses considered in our laboratory experiments. These values, reported in Table 4, represent an important input parameter for the mechanistic model of PRR, and are necessary to investigate its response under different UV irradiation conditions.

Simulations setup

The model presented here was simulated and analyzed with the software BioSimWare [56]. All stochastic simulations were performed by using the tau-leaping algorithm [57], which represents one of the most efficient methods for simulating the temporal evolution of biochemical systems. This method is an approximated but accurate version of the stochastic simulation algorithm (SSA) [28], since it allows to select and execute in parallel several reactions per step – instead of executing the reactions in a sequential manner, as it is done with SSA – thus speeding up the computation.

In particular, the efficiency of tau-leaping was exploited to carry out a parameter sweep analysis (PSA), with the aim of investigating the effect of varying the value of molecular amounts, the number of DNA lesions and the value of reaction constants on the dynamics of the PRR pathway. PSA was performed using a computational tool that generates a set of different initial conditions for the model and then automatically executes the corresponding stochastic simulations. With this tool, the value of each analyzed parameter varies within a specified range (with respect to a fixed reference value). To be more precise, the sweep analysis varies a single parameter from time to time, considering a linear (logarithmic, respectively) sampling of values within the specified range in the case of molecular amounts (reaction constants, respectively). The logarithmic sampling allows to uniformly span different orders of magnitude of the value of the chosen parameter using a reduced but fine-grained set of samples, therefore efficiently analyzing the dynamics of the system in a broad range of experimental conditions.

In this work, the PSA executed to check the reliability of the values of the stochastic constants and of the molecular amounts, that is, the parameterization used in the PRR model, was set as follows:

- the value of each stochastic constant was varied of 3 orders of magnitude above and 3 below the reference value (given in Table 5);
- the value of the molecular amounts initially present in the system was varied in a range between 0 and twice the reference value (given in Table 2), thus mimicking the biological conditions ranging from the deletion to a 2-fold overexpression of the initial species.

The results obtained from PSA confirmed the reliability of the chosen parameterization of the model, as shown further on.

All stochastic simulations were performed on a personal computer with a CPU Intel Core i5 M 520 @ 2.40 GHz, 4 GB RAM running Linux (Ubuntu 11.04). The PSA was performed on a personal computer with a CPU Intel Core2 @ 2.66 GHz, 2 GB RAM running Linux (Ubuntu 10.04). The mean duration time to execute one run of the tau-leaping algorithm to simulate the dynamics of the PRR model over 5 h (i.e. the time interval considered during laboratory experiments to measure the time-courses of PCNA ubiquitylation) is about 1 min for low UV doses and a dozen of minutes for high UV doses, using the initial values of molecular amounts given in Table 2 and the stochastic constants reported in Table 5.

Representation of simulation outcomes and comparison with experimental data

The consistency of the PRR model was validated by comparing the outcome of stochastic simulations with the experimental measurements carried out on the wild type (WT) yeast strain at various UV doses. To this aim, by considering the western blots at each UV irradiation dose, we first quantified the values of mono-, di- and tri-ubiquitylated PCNA ratios (denoted by $\div\text{PCNA}^{\text{Ub}_\text{u}}_{exp}$, where $u = 1, 2, 3$ corresponds to the three ubiquitylated isoforms), together with the respective mean $\mu(\div\text{PCNA}^{\text{Ub}_\text{u}}_{exp})$ and standard deviation $\sigma(\div\text{PCNA}^{\text{Ub}_\text{u}}_{exp})$ of each PCNA isoform. This quantification is described in details in Additional File 2.

Then, from the outcome of stochastic simulations we derived the molecular amounts of PCNA isoforms (denoted by $\#\text{PCNA}^{\text{Ub}_\text{u}}_{sim}$, where $u = 1, 2, 3$ corresponds to the three ubiquitylated isoforms). In particular, to tame the effect of stochastic fluctuations that are inherent in these computational analysis, we exploited the outcomes of a set of independent simulations (performed with the same initial conditions) to calculate the mean $\mu(\#\text{PCNA}^{\text{Ub}_\text{u}}_{sim})$ and standard

deviation $\sigma(\#\mathrm{PCNA}_{sim}^{\mathrm{Ub_u}})$ of PCNA amounts.
Afterwards, since we had to compare different kinds of measurements – namely, ratios of modified PCNA derived from laboratory experiments on the one side, and molecular amounts of modified PCNA obtained from stochastic simulations on the other side – we introduced two different strategies (see details in Additional File 3) for the graphical representation and comparison of the experimental and the computational results:

1. the first strategy, called "normalized representation" (NR), consists of stacked bar graphs: for each sample analyzed within the time interval of 0-5 h, the stacked bars corresponding to the normalized ratios of mono-, di- and tri-ubiquitylated PCNA isoforms obtained from stochastic simulations (denoted by $\div\mathrm{PCNA}_{sim}^{\mathrm{Ub_u}}$) are plotted side by side to the experimental bars $\div\mathrm{PCNA}_{exp}^{\mathrm{Ub_u}}$ (which, as stated above, are already expressed as ratios);

2. in the second strategy, called "units representation" (UR), the molecular amounts derived from stochastic simulations $\#\mathrm{PCNA}_{sim}^{\mathrm{Ub_u}}$ are compared to the western blot quantifications which, in this case, were specifically transformed into molecular quantities (denoted by $\#\mathrm{PCNA}_{exp}^{\mathrm{Ub_u}}$).

We stress the fact that the NR allows a direct comparison between the experimental and simulation results, by considering the ratio of the three ubiquitylated isoforms of PCNA with respect to the total amount of modified PCNA measured in the system. Anyway, this strategy does not give any knowledge on the actual amount of modified PCNA, and it does not allow to clearly evidence the switch-off of PCNA ubiquitylation signal as long as the DNA lesions get processed, which can be instead directly represented by using the UR.
In what follows, we will use both NR and UR to give alternative representations of experimental measurements and simulations outcomes in WT and mutant yeast cells, in order to compare the variation of modified PCNA ratios, as well as to clearly display the dynamics of modified PCNA amounts.

Results and discussion

In this section we present the results achieved from the integration between laboratory work and computational analysis, together with a discussion of the emergent issues concerning PRR. We start by presenting the identification of the spatio-temporal cascade of proteins aggregation involved in PRR, as well as the stoichiometry of the corresponding protein complexes, which was performed through a structural modeling approach. These information were exploited, together with experimental data and the available knowledge on the molecular processes occurring during PRR, to define a novel mathematical model of PCNA ubiquitylation involved in the bypass of UV-induced DNA lesions.
Afterwards, we present the biological insights on PRR achieved from the comparison between laboratory experiments and stochastic simulations of the PRR model, at both low and high UV doses, and we discuss, in particular, the effects of the estimated number of UV-induced DNA lesions and of the intracellular levels of ubiquitin on the system dynamics. We show how a divergent behavior between wet data and computational outcomes at high UV doses led to the design of new laboratory experiments, that allowed us to suggest novel aspects about the functioning of PRR in living cells.

Structural modeling of uncharacterized protein-protein complexes

Protein ubiquitylation is a multistep process carried out by the concerted action of activating (E1), conjugating (E2) and ligating (E3) enzymes, which can possibly support the generation of poly-ubiquitin chains [58]. In eukaryotes, all ubiquitin-associated pathways are characterized by a crescent complexity, since there exist more E2s than E1s, and more E3s than E2s; therefore, the number of proteins potentially involved in each step increases, as well as the specificity of binding to the next substrate [59]. In budding yeast, there is a unique E1 enzyme (Uba1), eleven E2 enzymes and more than fifty E3 enzymes [60], a few of which are directly involved in PRR. In order to clarify the spatio-temporal cascade of aggregation among the enzymes involved in the mono- and poly-ubiquitylation of PCNA, as well as to deduce the stoichiometry of the respective protein complexes, we exploited a bioinformatic approach based on three-dimensional (3D) modeling to perform the structural reconstruction of the hypothetical structures of the E1-E2 and E2-E3 enzyme complexes involved in PRR.
To this aim, we considered the known 3D structures

of proteins involved in PRR to deduce the 3D structure of their uncharacterized molecular complexes. More precisely, we exploited the published crystallographic structures of the proteins of our interest that were available on Protein Data Bank (PDB) and the PDB viewer software [61] (the PDB accession code for protein complexes analyzed in this work are listed in Additional File 4).
This approach showed that each of the three steps of PCNA ubiquitylation occurring in the PRR pathway is characterized by specific protein complexes, and that there exists a mutual exclusivity in the formation of these complexes. More specifically, following the procedure described in [62, 63], we constructed the E1-E2 and E2-E3 complexes involved in the mono-ubiquitylation of PCNA and in its poly-ubiquitylation through chain elongation. Our results suggest that:

- the E1-E2 and E2-E3 complexes (Uba1-Rad6 and Rad6-Rad18, respectively) involved in PCNA mono-ubiquitylation are mutually exclusive (see Additional Files 5 and 6) and that the mechanism of PCNA mono-ubiquitylation – from ubiquitin activation to its covalent linkage on PCNA – consists in a step-wise process, as also suggested by previously published results [36, 64];

- the E1-E2 and E2-E3 complexes (Uba1-Ubc13 and Ubc13-Rad5, respectively) involved in PCNA poly-ubiquitylation are mutually exclusive (see Additional Files 6 and 7). Moreover, the analysis of the hypothetical complex Uba1-Ubc13-Mms2 – involving the ubiquitin conjugating enzyme variant Mms2, which works together with Ubc13 – suggests that also the two complexes Uba1-Ubc13 and Ubc13-Mms2 are mutually exclusive: Ubc13 needs to be charged with ubiquitin by Uba1 before binding Mms2. Also in this case, our results support previous data [36, 64], which argue for a distributive/step-wise sequence of events for PCNA poly-ubiquitylation, starting from ubiquitin activation to its covalent linkage on mono-ubiquitylated PCNA.

These results highlight the modularity of the whole process of PCNA ubiquitylation and allowed us to address the definition of the mathematical model of PRR on the most relevant biological process only, that is, PCNA ubiquitin conjugation. In particular, we could neglect the whole cascade of reactions involved in the ubiquitin activation process, and reduce to two simple reactions the detailed biochemical steps related to the ubiquitin trans-thioesterification process, as described in the following section.

The PCNA ubiquitylation model

Model assumptions

Wet laboratory experiments, combined with the knowledge built upon an accurate literature analysis, led us to the following major assumptions in the development of the model of PCNA ubiquitylation:

1. a stepwise formation of the ubiquitin chain on PCNA;

2. a limited extension of the ubiquitin chain on PCNA;

3. a generic mechanism for the switch-off of the ubiquitylation signal.

These assumptions are motivated on the following bases:
1. A stepwise formation of the ubiquitin chain is strongly motivated by *in vitro* assays [36]. In this context, the addition of a single unit of ubiquitin at a time for PCNA mono-ubiquitylation and K63-linked chain elongation, through multiple cycles of enzymatic catalysis mediated by E1, E2 and E3 enzymes, displays the following biochemical scheme for ubiquitin recruitment:

$$\begin{aligned} E_1{:}U + E_2 &\rightarrow E_1 + E_2{:}U \\ E_3 + PCNA{:}U_i &\rightarrow E_3{:}PCNA{:}U_i \\ E_2{:}U + E_3{:}PCNA{:}U_i &\rightarrow E_2{:}U{:}E_3{:}PCNA{:}U_i \\ E_2{:}U{:}E_3{:}PCNA{:}U_i &\rightarrow E_2{:}E_3{:}PCNA{:}U_{i+1} \\ E_2{:}E_3{:}PCNA{:}U_{i+1} &\rightarrow E_2 + E_3 + PCNA{:}U_{i+1} \end{aligned}$$

where the classical formalism $X + Y$ is used to denote an interaction between the generic molecular species X and Y, while $X{:}Y$ denotes a molecular complex. More precisely, the notation $PCNA{:}U_i$ here comprehensively represents that a DNA lesion has been identified by the sliding clamp (for $i = 0$), and describes as well the mono-ubiquitylated (for $i = 1$) and poly-ubiquitylated (for $i > 1$) isoforms of PCNA. Enzymes E2 and E3 correspond to Rad6 and Rad18 for mono-ubiquitylation, and to Ubc13

and Rad5 for poly-ubiquitylation, while E1 represents Uba1 in both cases. We remark that, in what follows, the effective role of enzyme E1 will not be formally considered, since the processes of ubiquitin activation and trans-thio-esterification can be widely reduced by deriving other simple reactions that describe the load of ubiquitin moieties on the E2 enzymes.

2. The assumption of limiting to the third unit the elongation of the K63-linked ubiquitin chains on PCNA was taken because the detection of tetra-ubiquitylated PCNA is not technically reproducible. Moreover, N-ubiquitylated PCNA rarely appears after DNA damage [38]. Notwithstanding this choice, simulation outcomes show the capability of our model to discriminate between the mono- and the poly-ubiquitylation contributions in the functioning of PRR, as discussed later on.

3. The last assumption is motivated by the fact that our laboratory experiments conducted at low doses of UV irradiation show the switch-off of PCNA ubiquitylation signal (see, e.g., the western blots in Figure 2A and Figure 3A), as also previously evidenced in [27]. This switch-off mechanism has not been precisely characterized yet. At present, there are no evidences for the activity of enzymes acting on PCNA deubiquitylation in yeast; however, even if we are not able to detect the real enzymatic mechanisms occurring *in vivo* in the PRR pathway, the results of our experimental setup report unmistakably the presence and the related global effect of the signal switch-off.

Definition of the mechanistic model

The information collected from literature, together with our assumptions, led to the development of the model of the PRR pathway depicted in Figure 1, and to the formulation of the biochemical reactions reported in Table 5. The mechanistic model consists of 21 molecular species (7 of which appear in the initial state of the system, as reported in Table 2) and 25 reactions, which can be clustered into four functional modules whose detailed description is reported hereby.

PCNA mono-ubiquitylation. The first module, consisting of reactions 1 to 10 in Table 5, describes the process of PCNA mono-ubiquitylation. Reaction 1 models the identification of the UV-induced lesion (denoted by L) by means of PCNA proteins sliding on the DNA strand; this reaction is assumed to be non reversible. We denote by the symbol $PCNA_{\text{on}}$ the PCNA clamp whenever it hits the DNA lesion (see also Figure 1, parts (b) and (c)). Reactions 2 and 3 illustrate the formation and separation of the Rad18 dimer, whereas reaction 4 resumes the simplified ubiquitin loading mechanism of Rad6, excluding the direct intervention of the E1 enzyme Uba1. Reactions from 5 to 10 describe the formation of the first ubiquitylated isoform of PCNA ($PCNA_{\text{on}}$:U), due to the concerted action of the E2 Rad6 and E3 Rad18 enzymes, as described in the general biochemical scheme presented above (see also Figure 1, parts (d)-(f)).

PCNA di-ubiquitylation. The second module, consisting of reactions 11 to 17 in Table 5, describes the molecular mechanisms leading to the addition of the second ubiquitin moiety on the mono-ubiquitylated PCNA. Similarly to reaction 4, reaction 11 resumes the simplified ubiquitin loading mechanism of Ubc13-Mms2, excluding the direct intervention of the E1 enzyme Uba1. Reactions from 12 to 17 describe the formation of the di-ubiquitylated isoform of PCNA ($PCNA_{\text{on}} : U : U$), due to the concerted action of the E2 Ubc13-Mms2 and E3 Rad5 enzymes, as described in the general biochemical scheme presented above (see also Figure 1, parts (h)-(k)). In particular, reaction 12 and its reverse 13 model the binding of the mono-ubiquitylated isoform ($PCNA_{\text{on}} : U$) to the E3 Rad5, while reactions 14 and 15 give rise to the formation of the heterotrimer $Ubc13 : U : Mms2$. Reactions 16 and 17 describe the dissociation of the complex $Ubc13 : U : Mms2 : Rad5 : PCNA_{\text{on}} : U$, while the ubiquitin moiety is transferred to $PCNA_{\text{on}}$:U, thus inducing the formation of $PCNA_{\text{on}}$:U:U.

PCNA tri-ubiquitylation. The third module, consisting of reactions 18 to 22 in Table 5, describes the molecular mechanisms leading to the addition of the third ubiquitin moiety on the di-ubiquitylated PCNA, leading to $PCNA_{\text{on}} : U : U : U$ (see also Figure 1, dotted steps between parts (k) and (l)). Once more, these reactions resemble the biochemical scheme previously presented. In particular, reaction

18 models the capability of Rad5 to reassociate with the di-ubiquitylated isoform $PCNA_{\text{on}}$:U:U, though we chose not to model the reverse reaction (equivalent to reaction 13, releasing Rad5 from $PCNA_{\text{on}}$:U) to mark the biological difference between mono- and poly-ubiquitylation effects in PRR. Reactions 19-22 correspond to reactions 14-17, except for the fact that in this case $PCNA_{\text{on}}$ carries two linked ubiquitin moieties instead of a single one.

Ubiquitylation signal switch-off. The fourth module, consisting of reactions 23 to 25 in Table 5, describes a generic mechanism for signal switch-off (denoted by $PCNA_{\text{off}}$) of all three PCNA ubiquitylated isoforms, as suggested by experimental data and explained in our third assumption (see also Figure 1, parts (g), (m), (n)). These reactions also include a recycling mechanisms of ubiquitin moieties that, once released from PCNA, are made again available as input of the system and can be reloaded on Rad6 (reaction 4) and on $Ubc13$:$Mms2$ (reaction 13). We highlight here that these two reactions represent an important part of the model, as they influence the sensitivity of the model to free ubiquitin amounts, as discussed later on.

A previous definition of the model included an additional module describing the formation and disassociation of $Ubc13:U:Mms2$ and $Ubc13:Mms2$ complexes. After a careful verification that the system dynamics was not affected by the removal of this module, we chose to substitute this set of reactions with a congruous initial amount of the complex $Ubc13:Mms2$ (assumed to be already formed and available in the initial state of the system), in order to speed up the simulations. The initial amount of this complex was set to the minimum value between the amounts of the two proteins (Ubc13, Mms2) necessary for its formation, as reported in Table 2. For the sake of completeness, the set of removed reactions and the comparison of the simulated dynamics obtained by using the two versions of the model are reported in Additional File 8.

The SBML version of the model is downloadable from the BioModels database [65, 66] under ID=XXXXX (FOR REFEREES: OUR FINAL, ACCEPTED VERSION WILL BE SUBMITTED THERE).

Kinetics of PCNA ubiquitylation at low and high doses of UV irradiation

The levels of mono-, di- and tri-ubiquitylated PCNA measured *in vivo* after UV irradiation of WT yeast cells were used as the biological readout to validate the mechanistic model of PRR. As a matter of fact, the generally accepted PRR model assumes that K164 mono-ubiquitylation is a marker of the PRR error-prone/error-free TLS sub-pathway, while K164 di- and tri-ubiquitylation are a marker of the PRR error-free TS sub-pathway [25]. In order to derive time-series measurements of all ubiquitylated PCNA isoforms at the same time points and in the same yeast cells, we developed an experimental protocol that allows to detect both mono- and poly-ubiquitylated PCNA isoforms on a single western blot. This method represents indeed a relevant advantage with respect to other protocols previously devised for PCNA ubiquitylation [27], which could only allow the measurements of di- to N-ubiquitylated isoforms on the same film, without the mono-ubiquitylated one.

In [67], it was shown that physiological UV-induced responses of PRR are obtained by exposing cells to Chronic-Dose of UV light (CLUV) for 6-9 h (0.18 J/m^2 min^{-1}). However, we did not conducted laboratory experiments under these conditions since our experimental resolution does not allow the detection of PCNA ubiquitylation in chronically UV irradiated yeast cells. Indeed, in our laboratory experiments these irradiation doses are below the threshold for the detection of PCNA ubiquitylation; on the contrary, with our method the ubiquitylation signal becomes measurable at *acute* treatment with UV doses of 5 J/m^2, at least, because of a technical limit of detection of the western blot technique. For this reason, we produced western blot time-courses as previously described by exposing cells either to low UV doses (5 and 10 J/m^2) or to high UV doses (50 and 75 J/m^2).

Concerning the experiments at the lower UV irradiation doses, the PCNA ubiquitylation signal in response to 5 J/m^2 undergoes a quick increase, reaching its maximal value after about 30 min, as shown by experimental results (Figure 2A). Afterwards, the signal intensity decreases resulting barely detectable after 2 and 3 h because of the signal switch-off. Moreover, at 5 J/m^2 the system is character-

ized by an intense PCNA poly-ubiquitylation signal, with respect to the mono-ubiquitylated PCNA isoform, which results into the activation of the TS subpathway. This behavior is well reproduced by means of computational simulations, which mimic the PRR functioning in response to an estimated number of 1001 lesions (see Table 4). The match between experimental and computational results is clearly shown in Figure 2B, where we plot the dynamics of mono- and poly-ubiquitylated PCNA. Moreover, the simulated amounts of mono-, di- and tri-ubiquitylated PCNA isoforms well fit the experimental data, as reported in Figure 2C, where the average dynamics of the three PCNA isoforms is compared with the experimental measures, plotted by using the units representation (UR) (as explained in Additional File 3). This can also be seen in Figure 2D, where we compare the normalized stacked bars of the ratio of ubiquitylated PCNA isoforms obtained from stochastic simulations with those measured through wet experiments (here plotted using the normalized representation (NR), as explained in Additional File 3).

Analogous results were obtained at a UV dose of 10 J/m^2, corresponding to an estimated number of 2002 lesions in the model (Table 4), as shown in Figure 3. These analyses indicate that the computational model is able to correctly reproduce the *in vivo* dynamics of PCNA ubiquitylation at low UV doses. In particular, the model accurately reproduces the experimental ratio between mono- and poly-ubiquitylated PCNA (Figure 2B and Figure 3B), which corresponds to the activity of the potentially mutagenic lesion bypass sub-pathway and of the error-free lesion bypass sub-pathway, respectively. In addition, the model correctly reproduces the switching-off of the UV lesion bypass signal at low UV doses.

The response of the model at low UV doses (namely, 10 J/m^2) was also analyzed through a PSA, carried out on the values of all reaction constants and of all initial molecular amounts. The most interesting results are presented in Additional Files 9-12.

Concerning the experiments at the higher, non physiological UV doses of 50 J/m^2 and 75 J/m^2, we observed a divergence between *in vivo* PCNA ubiquitylation measurements and the computational outcomes. At these UV doses, the simulated dynamics of mono-, di- and tri-ubiquitylated PCNA reach a stable steady state (see Figure 4B-C for 50 J/m^2, Figure 5B-C for 75 J/m^2), corresponding to a saturation-like trend. This is in contrast with the observed *in vivo* measurements, where we can evidence a dose-dependent increase of the mono-ubiquitylated PCNA isoform with respect to the sum of di- and tri-ubiquitylated PCNA isoforms (see Figure 4A for 50 J/m^2, Figure 5A for 75 J/m^2), reaching about 50% of the bypass signal after 5 h at 75 J/m^2. This dose-dependent increase of mono-ubiquitylated PCNA is indeed biologically relevant, since it might correlate with the UV dose-dependent induced mutagenesis that was previously observed by others [68].

After an extensive and careful verification that this divergent behavior was not due to the model layout (for either the topological structure of molecular interactions or the chosen parameterization), we hypothesized that the difference between the experimental and the computational outcomes might be due to an overestimation of the number of bypassed UV lesions at 50 J/m^2 and 75 J/m^2 UV doses, corresponding to 10012 and 15018 lesions, respectively. To clarify the reason why we obtained a divergent behavior of the model at low and high UV doses, we designed further laboratory experiments, as discussed in the next sections.

Determination of UV dose-dependent threshold for the validation of the PRR model

To test *in vivo* the possible overestimation of the number of DNA lesions actually processed by PRR at high UV doses, we performed a time-course experiment using a yeast strain carrying a deletion of the *RAD14* gene (*rad14*Δ strain, see Table 1). This gene codifies for a well-characterized protein of the NER pathway, which is responsible for the repair, rather than the bypass, of UV-induced lesions in the genome. It is well established that the deletion of this master NER gene in yeast essentially abrogates excision and repair of UV lesions by NER in the genome [69]. Therefore, by inactivating NER all DNA lesions should be processed by other response mechanisms to UV-induced damage, including PRR, and we should be able to test whether the *in vivo* dynamics of PCNA ubiquitylation in these saturating conditions match the computational dynamics obtained at high UV doses.

As shown in Figure 6A, *RAD14* deletion causes a clear modification of the *in vivo* dynamics of PCNA ubiquitylation with respect to the WT strain at a UV dose of 75 J/m^2. Indeed, in *rad14*Δ cells we

observed a dramatic decrease in the intensity of the signal, and we obtained a ratio between mono- and poly-ubiquitylated PCNA isoforms that well matches the computational results (Figure 6B-C). This validation experiment therefore supports our hypothesis that the computational model cannot properly reproducing the measured PRR response *in vivo* at high UV doses because of an overestimation of the bypassed DNA lesions.

As a consequence, considering the result obtained on the *rad14*Δ strain and taking into account the different behaviors of the model at low and high UV doses in the WT strain, we tried to identify the UV dose threshold which ensures the proper functioning of the model. To this aim, we carried out additional wet experiments on WT strain cells irradiated at UV doses between 10 J/m^2 and 50 J/m^2, in order to detect the UV-dose dependent threshold that ensures a good match between *in vivo* measurements and computational results. As shown in Figure 7A-B, the model reproduces a proper dynamics at 20 J/m^2, while its behavior starts to diverge from *in vivo* measurements at 30 J/m^2 (Figure 7C-D). Therefore, we can conclude that at UV doses below 30 J/m^2 our model is capable to mimic *in vivo* data or, stated otherwise, it is able to correctly describe the mono- and poly-ubiquitylation processes of PCNA taking place in the PRR pathway *in vivo*.

So, the next question we asked ourselves was: what kind of processes are actually occurring in living yeast cells, that are able to induce this contrasting behavior responses at acute low and high UV irradiation doses?

Crosstalk between PRR and NER

As previously discussed, the trend of steady state dynamics of mono- and poly-ubiquitylated PCNA obtained with stochastic simulations resemble the biochemical kinetics of saturation, meaning that all PCNA molecules occurring in the system get involved in the lesion bypass processes. Therefore, we hypothesized a saturation of PRR *in vivo* because of an overestimation of the number of processed lesions in our experimental system. We reproduced this saturation *in vivo* by deleting the *RAD14* gene, which dramatically affected the dynamics of PCNA ubiquitylation after UV irradiation *in vivo*. More precisely, in NER-deficient cells we obtained, *in vivo*, a comparable steady state of mono- and poly-ubiquitylated PCNA species with respect to the computational results at high UV doses.

Altogether, these findings highlight a poorly characterized crosstalk between PRR and NER. Indeed, an optimal lesion bypass PRR activity, at least correlated to PCNA ubiquitylation, seems to depend on NER functionality. Therefore, to better characterize the effects of NER on UV-induced damage, we also evaluated whether its role may be important for proper S phase progression. It was shown that UV irradiation with 5 J/m^2 of a G1 arrested *rad14*Δ strain causes a cell cycle block at the G1/S transition [29]. When we UV irradiated (10 J/m^2) a S phase synchronized *rad14*Δ cell population, the lack of NER strongly impaired correct S phase progression, suggesting an under estimated function of NER also during S phase (see Additional File 13).

A possible explanation of our findings is that, on the one side, we are overestimating the number of lesions bypassed by PRR in the computational model while, on the other side, *in vivo* PRR needs the contribution of the NER pathway to work properly. Considering such experimental data, it is likely that the number of lesions, which represents an important input parameter of our model, is actually dependent on the action of NER and on the combined crosstalk between these two pathways. Unfortunately, it is presently impossible to measure the exact number of lesions processed by NER and PRR *in vivo*, but we are currently working on a bioinformatic strategy based on DNA sequence analysis to predict the correct number of lesions to be used as input value of our model at any given UV irradiation dose, in a similar way to the approach presented in [70].

Influence of ubiquitin concentration

As a further investigation of the functioning of the PRR pathway, we tested the influence of ubiquitin concentration on the performance of the computational model and the effect of *in vivo* reduction of free ubiquitin concentration. In living cells, ubiquitin is usually kept at stable levels through homeostatic mechanisms. The main actors in this process are deubiquitylating enzymes (DUBs), which recycle ubiquitin moieties from ubiquitylated proteins. The reduction of free ubiquitin in the cell can potentially impair PRR as well as all ubiquitin-related pathways, such as protein degradation/proteasome, cell cycle, DNA repair, chromatin remodeling, etc. Therefore, it is likely that the free cellular level of ubiquitin could act as a limiting factor for PRR,

given the competition with other molecular processes. To verify this hypothesis, we carried out a PSA to explore the influence of the level of free ubiquitin on PCNA ubiquitylation dynamics. The simulation results evidenced that the model is sensitive to this variation, as shown in Figure 8A-B, which report the dynamics of PCNA mono-ubiquitylation and poly-ubiquitylation obtained from a PSA carried out on the initial amount of ubiquitin. As clearly shown in the plots, for amounts of ubiquitin lower than the reference value (around 8700 molecules/cell, see Table 2), the amounts of mono- and poly-ubiquitylated PCNA isoforms decrease. On the other hand, by increasing the number of ubiquitin present inside the system, the dynamics show an initial peak in the number of mono- and poly-ubiquitylated PCNA, suggesting that higher amounts of free available ubiquitin might lead the system to a faster bypass of all DNA lesions with respect to the standard conditions.

The possible occurrence of similar effects *in vivo* was investigated through *ad hoc* experiments in living cells. Indeed, it was previously shown that the deletion of *DOA1*, a gene codifying a DUB essential for ubiquitin homeostasis, causes a dramatic reduction of the free ubiquitin pool in budding yeast log phase cells [71]. This reduction correlates with sensitivity to DNA damaging and replication stress agents (such as UV, methyl methanesulfonate (MMS), hydroxyurea) and abolishes PCNA ubiquitylation in the presence of MMS [30, 71].

Since the reduction of free ubiquitin in *doa1*Δ cells is so strong to impair both sensitivity to UV damage and PCNA ubiquitylation after DNA damage, we tested a less extreme *in vivo* situation. Namely, we considered *DOA4*, a gene codifying another DUB whose deletion was shown to cause, in log phase yeast cells, a 3-fold reduction of free ubiquitin and a weak sensitivity to UV-induced damage [30, 72, 73]. We thus tested *in vivo* the effect of *DOA4* deletion on the dynamics of PCNA ubiquitylation at 20 J/m^2, a dose compatible with the threshold under which our model behaves properly (Figure 7A-B). As shown in Figure 8C, the deletion of *DOA4* and the related reduction of the ubiquitin pool cause *in vivo* a reduction of about 65% of PCNA ubiquitylation in our *doa4*Δ yeast strain. This is in agreement with our computational analysis, as shown in Figure 8A-B, which report the dynamics of PCNA mono-ubiquitylation and poly-ubiquitylation obtained at a UV dose of 20 J/m^2.

We can therefore conclude that the level of free ubiquitin occurring in the system is one of the most sensitive parameters of the PRR model, and suggests that the ubiquitin pool needs to be actively maintained at a constant level since any change in its intracellular concentration has a large influence in downstream processes. This is in agreement both with previous results and with our model-driven experimental verification on *doa4*Δ yeast strain.

Conclusions

In this paper we proposed a novel computational model describing the PRR pathway in *S. cerevisiae*, involved in UV-induced DNA damage bypass. As wet readout of PRR activity in wild type and mutants yeast cells, in response to different doses of UV irradiation, we considered the intracellular levels of mono-, di- and tri-ubiquitylated PCNA on the K164 residue. In fact, the generally accepted biological model of PRR assumes that K164 mono-ubiquitylation is a marker of the PRR error-prone/error-free TLS sub-pathway, while K164 di- and tri-ubiquitylation are a marker of the PRR error-free TS sub-pathway [25]. The comparison between experimental measurements and computational outcomes showed that our model correctly describe the functioning of PRR response at UV doses lower than 30 J/m^2, approximately. On the contrary, at higher UV doses the dynamics of PCNA ubiquitylation obtained from computational simulations is characterized by a quick saturation, reaching a stable steady state for all the analyzed PCNA isoforms. In the attempt to better understand these results, we found that NER, the repair pathway known to fix UV-induced lesions during the G1 (see [74], Figure S1-C) and G2 [75] phases of the cell cycle, is required also for a proper S phase progression in response to UV irradiation.

This NER connection suggests intricate functional crosstalks between PRR and other pathways controlling genome stability. Indeed, in addition to NER, PRR was shown to be functionally linked to homologous recombination genes [76] and to the DNA damage checkpoint, which seems to affect the error-free sub-pathway but not the error-prone sub-pathway [77]. Moreover, it was recently found that defects in DNA ligase I (codified by *CDC9* gene) leads to mono-ubiquitylation of PCNA on the K107 residue, rather than on K164 [78]. This PCNA modification

requires the E2 variant Mms2 in conjunction with Ubc4 and the E3 Rad5, and occurs before full checkpoint activation [78]. Accumulation of DNA nicks in response to high UV doses and saturation of other downstream actors of PRR, such as DNA ligase I, may also cause K107 ubiquitylation after the DNA damage-specific ubiquitylation on K164. We might therefore speculate that, in the PCNA homotrimer, each monomer can be modified at least on two different residues at the same time, by different modifiers. The PRR pathway can thus be more complicated and less far characterized than previously thought. We are presently working on the experimental characterization of these new PRR aspects, with the aim of gaining new biological insights into the effective functioning of PRR *in vivo*, and of retrieving additional information to improve the computational model presented here.

Another intriguing aspect that we predicted by means of computational analysis and then verified by means of *ad hoc* designed experiments, is the relevance of ubiquitin concentration on the DNA damage response in yeast and, in particular, on the PRR pathway. Ubiquitin is usually kept at stable levels through homeostatic mechanisms involving DUBs, which recycle ubiquitin moieties from ubiquitylated proteins. The reduction of free ubiquitin in the cell can potentially impair all ubiquitin-related pathways. Indeed, deletion of some DUBs in budding yeast causes a UV sensitivity that seems to correlate with the extent of free ubiquitin reduction [30, 71]. We thus explored the effect of variations in the level of free ubiquitin in PCNA ubiquitylation dynamics, through a parameter sweep analysis. We found that the model is sensitive to variation of free ubiquitin concentrations; in particular, a 3-fold reduction of free ubiquitin, obtained *in vivo* by deleting the *DOA4* gene, causes a 65% reduction of PCNA ubiquitylation in response to 20 J/m^2 UV irradiation.

An aspect of PRR that is still to be elucidated concerns the fate of K164 mono- and poly-ubiquitylated PCNA after its activity on DNA damage bypass. Through dedicated laboratory experiments we tried many solutions to inhibit the hypothetical yet still unknown steps of signal switch-off; for instance, we carried out the deletion of the RCF1-like proteins (Rad24, Elg1 and Ctf18), in order to block the unloading of PCNA from chromatin, as well as of other DUBs like Ubp15 – the homologous of the specific PCNA DUBs Upb21 and Ubp22 in *Schizosaccharomyces pombe* [79] – and Ubp10. Anyway, we did not find any biochemical prove of the perturbation of PCNA ubiquitylation switch-off at the low acute UV irradiation dose we tested (5 J/m^2, data not shown), that represents the condition for which we can evidence the ubiquitylation signal switch-off. Whenever novel insights will be learned in relation to the fate of ubiquitylated PCNA in response to UV-induced damages, a further refinement of our computational model could be performed, in order to describe in details the molecular interactions involved in the effective mechanism of the ubiquitylation signal switch-off.

Finally, a further challenging aspect emerging from our analysis is the presence of the slight discrepancy between the experimental and computational ratios of di- and tri-ubiquitylated PCNA isoforms found, e.g., at 10 J/m^2. This could be due to an overestimation of the number of bypassed lesions, as previously discussed, but another and more interesting hypothesis to explain this finding is the possible presence of two different modifications on a single monomer of PCNA at the same time. In fact, PCNA can be covalently modified also on K127 residue by SUMO [80] and on K107 by ubiquitin [78]. At the present moment, we cannot exclude the possibility of different combinations of simultaneous modifications of PCNA, which give origin to distinct hybrid molecules; however, since these complexes are characterized by the same molecular mass, they are very hard to discriminate with standard laboratory techniques. This hypothesis and the novel biological insights gained with our Systems Biology approach indeed open new research perspectives on PRR, that are worth to be thoroughly investigated.

In conclusion, we used a combination of genetic, biochemical, structural and computational approaches to investigate the molecular mechanisms of PCNA ubiquitylation involved in the activation of the PPR pathway in vivo. PRR mechanisms are well conserved from yeast to man and it is well established that PRR defects are linked to increased genome instability and cancerogenesis. The original computational model of PRR presented here might be extended in the future to other eukaryotic cells by integrating novel knowledge coming from further experimental data, or used as a basic component within a modular computational approach to analyze the crosstalk with other pathways involved in genome stability.

Competing interests

The authors declare that they have no competing interests

Authors contributions

FA, MMF, DB and PP conceived the study. FA developed the experimental setup and performed the laboratory work. RC defined the model and conducted the computational analyses. DB, PC, DP, FA and RC wrote the manuscript. DB, PC and DP contributed key ideas, supervised the computational work and critically revised the manuscript. MMF and PP contributed key ideas, supervised the laboratory work and assisted in manuscript preparation. ACN critically read the manuscript and provided valuable advices during the progress of the whole work. All authors read and approved the final manuscript.

Acknowledgements

We thank Helle D. Ulrich for yeast strains and antibodies critical for this study, Giancarlo Mauri for providing access to the computational resources used to perform the simulations, Ivan Mura for discussion and Francesca Spadaro for help in some experiment. This work was supported by Fondazione Cariplo "Progetto NOBEL – Genetic and Epigenetic Control of Genome Stability" and by a AIRC grant to MMF.

References

1. Hoeijmakers J: **Genome maintenance mechanisms for preventing cancer.** *Nature* 2001, **411**:366–374.
2. Rolig RL, McKinnon PJ: **Linking DNA damage and neurodegeneration**. *Trends Neurosci* 2000, **23**:417–424.
3. Moldovan G, Pfander B, Jentsch S: **PCNA, the maestro of the replication fork**. *Cell* 2007, **129**(4):665–679.
4. Sinha RP, Hader DP: **UV-induced DNA damage and repair: a review**. *Photochem Photobiol Sci* 2002, **1**:225–236.
5. Mitchell D, Karentz D: **The induction and repair of DNA photodamage in the environment**. In *Environmental UV Photobiology*. Edited by Young A, Bjorn L, Moan J, Nultsch W, Plenum, New York, NY, USA 1993:345–377.
6. Friedberg E, Walker G, Siede W: *DNA repair and mutagenesis*. ASM Press, Washington DC 1995.
7. Lazzaro F, Giannattasio M, Puddu F, Granata M, Pellicioli A, Plevani P, Muzi-Falconi M: **Checkpoint mechanisms at the intersection between DNA damage and repair**. *DNA Repair* 2009, **8**(9):1055–1067.
8. Novarina D, Amara F, Lazzaro F, Plevani P, Muzi-Falconi M: **Mind the gap: Keeping UV lesions in check**. *DNA Repair* 2011, **10**(7):751–9.
9. Ulrich HD, Walden H: **Ubiquitin signalling in DNA replication and repair**. *Nat Rev Mol Cell Biol* 2010, **11**(7):479–489.
10. Pan X, Ye P, Yuan DS, Wang X, Bader JS, Boeke JD: **A DNA integrity network in the yeast *Saccharomyces cerevisiae***. *Cell* 2006, **124**(5):1069–1081.
11. Lisby M, Barlow JH, Burgess RC, Rothstein R: **Choreography of the DNA damage response**. *Cell* 2004, **118**(6):699–713.
12. Milanowska K, Rother K, Bujnicki J: **Databases and bioinformatics tools for the study of DNA repair**. *Mol Biol Int* 2011, **2011**:Article ID 475718.
13. Qu Z, MacLellan WR, Weiss JN: **Dynamics of the cell cycle: checkpoints, sizers, and timers**. *Biophys J* 2003, **85**(6):3600–3611.
14. Iwamoto K, Tashima Y, Hamada H, Eguchi Y, Okamoto M: **Mathematical modeling and sensitivity analysis of G1/S phase in the cell cycle including the DNA-damage signal transduction pathway**. *BioSystems* 2008, **94**(1-2):109–17.
15. Iwamoto K, Hamada H, Eguchi Y, Okamoto M: **Mathematical modeling of cell cycle regulation in response to DNA damage: Exploring mechanisms of cell-fate determination**. *BioSystems* 2011, **103**(3):384–391.
16. Csikász-Nagy A: **Computational systems biology of the cell cycle**. *Brief Bioinform* 2009, **10**(4):424–434.
17. Karschau J, de Almeida C, Richard MC, Miller S, Booth IR, Grebogi C, de Moura AP: **A matter of life or death: modeling DNA damage and repair in bacteria**. *Biophys J* 2011, **100**(4):814–821.
18. Krishna S, Maslov S, Sneppen K: **UV-induced mutagenesis in *Escherichia coli* SOS response: A quantitative model**. *PLoS Comput Biol* 2007, **3**(3):e41.
19. Mouri K, Nacher JC, Akutsu T: **A mathematical model for the detection mechanism of DNA double-strand breaks depending on autophosphorylation of ATM**. *PLoS ONE* 2009, **4**(4):e5131.
20. Crooke PS, Parl FF: **A mathematical model for DNA damage and repair**. *J Nucleic Acids* 2010, **2010**:Article ID 352603.
21. Sokhansanj BA, Rodrigue GR, Fitch JP, Wilson III DM: **A quantitative model of human DNA base excision repair. I. mechanistic insights**. *Nucleic Acids Res* 2002, **30**(8):1817–1825.
22. Politi A, Moné MJ, Houtsmuller AB, Hoogstraten D, Vermeulen W, Heinrich R, van Driel R: **Mathematical modeling of nucleotide excision repair reveals efficiency of sequential assembly strategies**. *Mol Cell* 2005, **19**(5):679–690.
23. Kesseler KJ, Kaufmann WK, Reardon JT, Elston T, Sancar A: **A mathematical model for human nucleotide excision repair: damage recognition by random order assembly and kinetic proofreading**. *J Theor Biol* 2007, **249**(2):361–375.
24. Luijsterburg MS, von Bornstaedt G, Gourdin AM, Politi AZ, Moné MJ, Warmerdam DO, Goedhart J, Vermeulen W, van Driel R, Höffer T: **Stochastic and reversible assembly of a multiprotein DNA repair complex ensures accurate target site recognition and efficient repair**. *J Cell Biol* 2010, **189**(3):445–463.
25. Hoege C, Pfander B, Moldovan G, Pyrowolakis G, Jentsch S: **RAD6-dependent DNA repair is linked to modification of PCNA by ubiquitin and SUMO**. *Nature* 2002, **419**:135–141.
26. Zhang W, Qin Z, Zhang X, Xiao W: **Roles of sequential ubiquitination of PCNA in DNA-damage tolerance**. *FEBS Letters* 2011, **585**(18):2786–94.
27. Daigaku Y, Davies AA, Ulrich HD: **Ubiquitin-dependent DNA damage bypass is separable from genome replication**. *Nature* 2010, **465**(7300):951–5.
28. Gillespie DT: **Exact stochastic simulation of coupled chemical reactions**. *J Phys Chem* 1977, **81**(25):2340–2361.

29. Neecke H, Lucchini G, Longhese M: **Cell cycle progression in the presence of irreparable DNA damage is controlled by a Mec1- and Rad53-dependent checkpoint in budding yeast**. *EMBO J* 1999, **18**(16):4485–97.

30. Gong J, Siede W: **Influence of deubiquitinating enzymes on mutagenesis in *Saccharomyces cerevisiae***. *Internet J Microb* 2011, **9**(2).

31. Zhao S, Ulrich H: **Distinct consequences of posttranslational modification by linear versus K63-linked polyubiquitin chain**. *P Natl Acad Sci USA* 2010, **107**(17):7704–9.

32. Essers J, Theil AF, Baldeyron C, van Cappellen WA, Houtsmuller AB, Kanaar R, Vermeulen W: **Nuclear dynamics of PCNA in DNA replication and repair**. *Mol Cell Biol* 2005, **25**(21):9350–9359.

33. Haas A, Rose I: **The mechanism of ubiquitin activating enzyme. A kinetic and equilibrium analysis**. *J Biol Chem* 1982, **257**(17):10329–37.

34. Hofmann RM, Pickart CM: **Noncanonical *MMS2*-encoded ubiquitin-conjugating enzyme functions in assembly of novel polyubiquitin chains for DNA repair**. *Cell* 1999, **96**:645–653.

35. Vandemark AP, Hofmann RM, Tsui C, Pickart CM, Wolberger C: **Molecular insights into polyubiquitin chain assembly: crystal structure of the Mms2/Ubc13 heterodimer**. *Structure* 2001, **105**:711–720.

36. Parker J, Ulrich HD: **Mechanistic analysis of PCNA poly-ubiquitylation by the ubiquitin protein ligases Rad18 and Rad5**. *EMBO J* 2009, **28**:3657–3666.

37. Davies A, Huttner D, Daigaku Y, Chen S, HD HU: **Activation of ubiquitin-dependent DNA damage bypass is mediated by replication protein A**. *Mol Cell* 2008, **29**(5):625–36.

38. Windecker H, Ulrich HD: **Architecture and assembly of poly-SUMO Chains on PCNA in *Saccharomyces cerevisiae***. *J Mol Biol* 2008, **376**:221–231.

39. Friedberg E, Lehmann A, Fuchs R: **Trading places: how do DNA polymerases switch during translesion DNA synthesis?** *Mol Cell* 2005, **18**:499–505.

40. Johnson RE, Haracska L, Prakash S, Prakash L: **Role of DNA polymerase η in the bypass of a (6-4) TT photoproduct**. *Mol Cell Biol* 2001, **21**(10):3558–3563.

41. Nelson JR, Lawrence CW, Hinkle DC: **Thymine-thymine dimer bypass by yeast DNA polymerase**. *Science* 1996, **272**:1646–1649.

42. Longtine MS, Mckenzie III A, Demarini DJ, Shah NG, Wach A, Brachat A, Philippsen P, Pringle JR: **Additional modules for versatile and economical PCR-based gene deletion and modification in *Saccharomyces cerevisiae***. *Yeast* 1998, **14**(10):953–961.

43. Longhese M, Fraschini R, Plevani P, Lucchini G: **Yeast pip3/mec3 mutants fail to delay entry into S phase and to slow DNA replication in response to DNA damage, and they define a functional link between Mec3 and DNA primase**. *Mol Cell Biol* 1996, **16**(7):3235–3244.

44. Hanna J, Leggett D, Finley D: **Ubiquitin depletion as a key mediator of toxicity by translational inhibitors**. *Mol Cell Biol* 2003, **23**(24):9251–9261.

45. Lazzaro F, Novarina D, Amara F, Watt DL, Stone JE, Costanzo V, Burgers PM, Kunkel TA, Plevani P, Muzi-Falconi M: **RNase H and Postreplication Repair protect cells from ribonucleotides incorporated in DNA**. *Mol Cell* 2012, **45**:99–110.

46. Ulrich HD, Davies AA: **In vivo detection and characterization of sumoylation targets in *Saccharomyces cerevisiae***. *Methods Mol Biol* 2009, **497**(II):81–103.

47. Hafiz A: *Principles and Reactions of Protein Extraction, Purification, and Characterization*. CRC Press 2004.

48. Abramoff M, Magelhaes P, Ram S: **Image processing with ImageJ**. *Biophotonics International* 2004, **11**(7):36–42.

49. Ghaemmaghami S, Huh W, Bower K, Howson R, Belle A, Dephoure N, et al.: **Global analysis of protein expression in yeast**. *Nature* 2003, **425**(6959):671–672.

50. **SGD project. "Saccharomyces Genome Database"** (May 2011), [http://www.yeastgenome.org/].

51. VonDerHaar T: **A quantitative estimation of the global translational activity in logarithmically growing yeast cells**. *BMC Syst Biol* 2008, **2**(87).

52. Jorgensen P, Edgington N, Schneider B, Rupes I, Tyers M, Futcher B: **The size of the nucleus increases as yeast cells grow**. *Mol Biol Cell* 2007, **18**:3523–3532.

53. Carlile CM, Pickart CM, Matunis MJ, Cohen RE: **Synthesis of free and Proliferating Cell Nuclear Antigen-bound polyubiquitin chains by the RING E3 ubiquitin ligase Rad5**. *J Biol Chem* 2009, **284**(43):29326–29334.

54. Resnick M, Setlow J: **Repair of pyrimidine dimer damage induced in yeast by ultraviolet light**. *J Bacteriol* 1972, **109**(3):979–986.

55. Fäth W, Brendel M: **UV-induction of thymine-containing dimers in *Saccharomyces cerevisiae***. *Z Naturforsch C* 1975, **30**(6):811–7.

56. Besozzi D, Cazzaniga P, Mauri G, Pescini D: **BioSimWare: a software for the modeling, simulation and analysis of biological systems**. In *Membrane Computing, 11th International Conference, CMC 2010, Jena, Germany, August 24-27, Revised selected papers*. Edited by Gheorghe M, Hinze T, Păun G, Rozenberg G, Salomaa A, LNCS 6501 2010:119–143.

57. Cao Y, Gillespie DT, Petzold L: **Efficient step size selection for the tau-leaping simulation method**. *J Chem Phys* 2006, **124**(4):044109.

58. Grabbe C, Husnjak K, Dikic I: **The spatial and temporal organization of ubiquitin networks**. *Nat Rev Mol Cell Biol* 2011, **12**(5):295–307.

59. Weissman A: **Themes and variations on ubiquitylation**. *Nat Rev Mol Cell Biol* 2001, **2**(3):169–78.

60. Bergink S, Jentsch S: **Principles of ubiquitin and SUMO modifications in DNA repair**. *Nature* 2009, **458**:461–467.

61. Guex N, Peitsch M: **SWISS-MODEL and the Swiss-PdbViewer: an environment for comparative protein modeling**. *Electrophoresis* 1997, **18**(15):2714–23.

62. Lee I, Schindelin H: **Structural insights into E1-catalyzed ubiquitin activation and transfer to conjugating enzymes.** *Cell* 2008, **134**(2):268–278.

63. Ulrich HD: **Protein-protein interactions within an E2-RING finger complex**. *J Biol Chem* 2003, **278**(9):7051–7058.

64. Eletr ZM, Huang DT, Duda DM, Schulman BA, Kuhlman B: **E2 conjugating enzymes must disengage from their E1 enzymes before E3-dependent ubiquitin and ubiquitin-like transfer**. *Nat Struct Mol Biol* 2005, **12**(10):933–934.

65. Li C, Donizelli M, Rodriguez N, Dharuri H, Endler L, Chelliah V, Li L, He E, Henry A, Stefan MI, Snoep JL, Hucka M, Le Novère N, Laibe C: **BioModels Database: An enhanced, curated and annotated resource for published quantitative kinetic models.** *BMC Syst Biol* 2010, **4**:92.

66. **BioModels Database.** (July 2012), [http://www.ebi.ac.uk/biomodels-main/].

67. Hishida T, Kubota Y, AMCarr, Iwasaki H: **RAD6–RAD18–RAD5-pathway-dependent tolerance to chronic low-dose ultraviolet light**. *Nature* 2009, **457**(7229):612–615.

68. Abdulovic A, Jinks-Robertson S: **The in vivo characterization of translesion synthesis across UV-induced lesions in *Saccharomyces cerevisiae*: insights into Pol zeta- and Pol eta-dependent frameshift mutagenesis.** *Genetics* 2006, **172**(3):1489–98.

69. Prakash L, Prakash S: **Three additional genes involved in pyrimidine dimer removal in *Saccharomyces cerevisiae*: RAD7, RAD14 and MMS19**. *Mol Gen Genet* 1979, **176**(3):351–359.

70. Teng Y, Bennett M, Evans KE, Zhuang-Jackson H, Higgs A, Reed SH, Waters R: **A novel method for the genome-wide high resolution analysis of DNA damage**. *Nucleic Acids Res* 2011, **39**(2):e10.

71. Lis E, Romesberg F: **Role of Doa1 in the *Saccharomyces cerevisiae* DNA Damage Response.** *Mol Cell Biol* 2006, **26**(11):4122–33.

72. Swaminathan S, Amerik A, Hochstrasser M: **The Doa4 deubiquitinating enzyme is required for ubiquitin homeostasis in yeast**. *Mol Cell Biol* 1999, **10**(8):2583–2594.

73. Amerik A, Hochstrasser M: **Analysis of the deubiquitinating enzymes of the yeast *Saccharomyces cerevisiae***. *Biol Chem* 2000, **381**(9-10):981–992.

74. Giannattasio M, Follonier C, Tourrière H, Puddu F, Lazzaro F, Pasero P, Lopes M, Plevani P, Muzi-Falconi M: **Exo1 competes with repair synthesis, converts NER intermediates to long ssDNA gaps, and promotes checkpoint activation**. *Mol Cell* 2010, **40**:50–62.

75. Aboussekhra A, Al-Sharif I: **Homologous recombination is involved in transcription-coupled repair of UV damage in *Saccharomyces cerevisiae***. *EMBO J* 2005, **24**(11):1999–2010.

76. Santa Maria S, Gangavarapu V, Johnson R, Prakash L, Prakash S: **Requirement of Nse1, a subunit of the Smc5-Smc6 complex, for Rad52-dependent postreplication repair of UV-damaged DNA in *Saccharomyces cerevisiae***. *Mol Cell Biol* 2007, **27**(23):8409–8418.

77. Gangavarapu V, Santa Maria S, Prakash S, Prakash L: **Requirement of replication checkpoint protein kinases Mec1/Rad53 for postreplication repair in yeast**. *mBio* 2011, **2**(3):e00079–11.

78. Das-Bradoo S, Nguyen H, Wood J, Ricke R, Haworth J, Bielinsky A: **Defects in DNA ligase I trigger PCNA ubiquitylation at Lys 107**. *Nat Cell Biol* 2010, **12**:74–79.

79. Holmes RM: **Deubiquitinating enzymes and post-replication repair in *Schizosaccharomyces pombe***. *PhD thesis*, University of Sussex 2010.

80. Parker J, Bucceri A, Davies A, Heidrich K, Windecker H, Ulrich HD: **SUMO modification of PCNA is controlled by DNA**. *EMBO J* 2008, **27**:2422–2431.

81. Notenboom V, Hibbert RG, van Rossum-Fikkert SE, Olsen JV, Mann M, Sixma TK: **Functional characterization of Rad18 domains for Rad6, ubiquitin, DNA binding and PCNA modification**. *Mol Carcinog* 2007, **35**(17):5819–5830.

82. Bailly V, Lamb J, Sung P, Prakash S, Prakash L: **Specific complex formation between yeast RAD6 and RAD18 proteins: a potential mechanism for targeting RAD6 ubiquitin-conjugating activity to DNA damage sites.** *Genes Dev* 1994, **8**(7):811–820.

83. Jentsch S, McGrath J, Varshavsky A: **The yeast DNA repair gene Rad6 encodes a ubiquitin-conjugating enzime**. *Nature* 1987, **329**(10):131–134.

84. Ulrich HD, Jentsch S: **Two RING finger proteins mediate cooperation between ubiquitin-conjugating enzymes in DNA repair**. *EMBO J* 2000, **19**(13):3388–3397.

85. Bailly V, Prakash S, Prakash L: **Domains required for dimerization of yeast Rad6 ubiquitin-conjugating enzyme and Rad18 DNA binding protein**. *Mol Cell Biol* 1997, **17**(8):4536–4543.

86. Hibbert RG, Huang A, Boelens R, Sixma TK: **E3 ligase Rad18 promotes monoubiquitination rather than ubiquitin chain formation by E2 enzyme Rad6.** *Proc Natl Acad Sci* 2011, **1**:1–7.

87. Worthylake D, Prakash S, Prakash L, Hill C: **Crystal structure of the *Saccharomyces cerevisiae* ubiquitin-conjugating enzyme Rad6 at 2.6Å resolution**. *J Biol Chem* 1998, **273**(11):6271–6276.

88. Hofmann R, Pickart C: **In vitro assembly and recognition of Lys-63 polyubiquitin chains**. *J Biol Chem* 2001, **276**(30):27936–43.

89. Eddins MJ, Carlile CM, Gomez KM, Pickart CM, Wolberger C: **Mms2–Ubc13 covalently bound to ubiquitin reveals the structural basis of linkage-specific polyubiquitin chain formation**. *Nat Struct Mol Biol* 2006, **13**(10):915–920.

Figures

Figure 1 - Graphical representation of the PRR pathway

The diagram shows the main steps of the PRR pathway concerning the covalent modification of PCNA (mono- and poly-ubiquitylation) in response to UV-induced damage. UV radiation can induce lesions on DNA (represented as a gray triangle in (**a**)), which cause the stall of the replication fork when PCNA hits a lesion (denoted by $PCNA_{\text{on}}$)(**b**, **c**). Afterwards, PCNA is mono-ubiquitylated ($PCNA_{\text{on}}:U$) by the combined activity of E2 Rad6 and E3 Rad18 (**d**, **e**, **f**). At this stage, mono-ubiquitylated PCNA can activate the Translesion DNA Synthesis sub-pathway (TLS), leading to lesion bypass (represented as an orange triangle in (**g**)), and eventually to the ubiquitylation signal switch-off ($PCNA_{\text{off}}$). On the other hand, mono-ubiquitylated PCNA can undergo further ubiquitylation events through the combined action of E2 Ubc13-Mms2 and E3 Rad5 (**h**, **i**, **j**), adding a single ubiquitin moiety per step (**k**, **l**). Di- and tri-ubiquitylated PCNA isoforms are denoted by $PCNA_{\text{on}}{:}U{:}U$ (**k**) and $PCNA_{\text{on}}{:}U{:}U{:}U$ (**l**), respectively. Poly-ubiquitylated PCNA promotes lesion bypass (represented as an orange triangle in (**m**) and (**n**)) through the Template Switching sub-pathway (TS) and, eventually, the ubiquitylation signal switch-off.

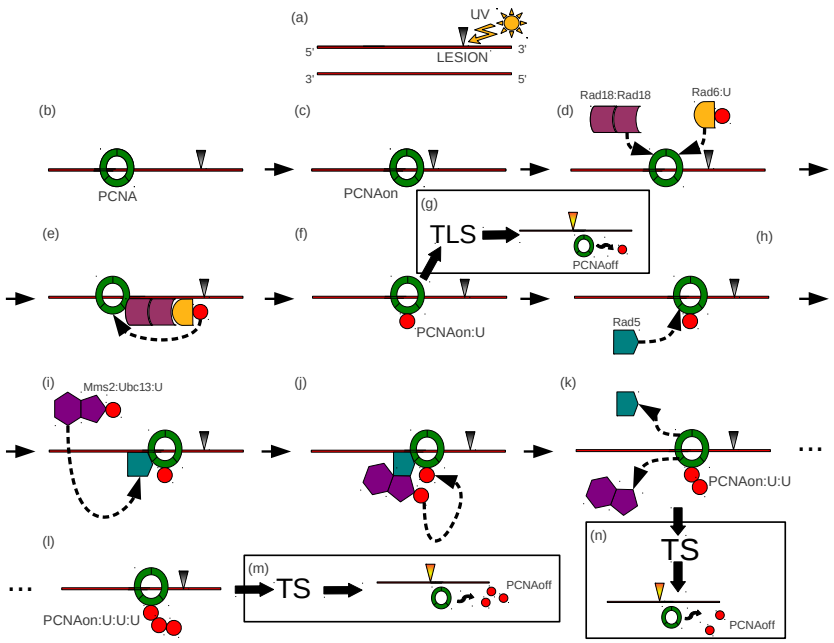
(a)
UV
LESION
5'
3'
3'
5'
(b)
PCNA
(c)
PCNAon
(d)
Rad18:Rad18
Rad6:U
(e)
(f)
PCNAon:U
(g)
TLS
PCNAoff
(h)
Rad5
(i)
Mms2:Ubc13:U
(j)
(k)
PCNAon:U:U
(l)
PCNAon:U:U:U
(m)
TS
PCNAoff
(n)
TS
PCNAoff

Figure 1:

Figure 2 - Comparison between experimental and simulation results of PCNA ubiquitylation dynamics obtained on wild type yeast cells at 5 J/m^2 UV dose

The figure shows the experimental measurements on WT yeast cells irradiated at 5 J/m^2 UV dose and the comparison with the corresponding simulation results. (**A**) Representative image of a western blot showing a time-course measurement of mono-, di- and tri-ubiquitylated PCNA isoforms (top part, denoted by α-Ub) and of non modified PCNA (bottom part, denoted by α-His), sampled from 0 to 5 h after UV irradiation. The experiment was repeated 3 times. (**B**) Average dynamics of mono-ubiquitylated PCNA (blue line) and of poly-ubiquitylated PCNA (orange line), obtained from 100 independent stochastic simulations, executed starting from the same initial conditions (see Table 2 for molecular amounts and Table 5 for reaction constants) and with an estimated number of DNA lesions equal to 1001. (**C**) Comparison between the mean dynamics of mono-, di- and tri-ubiquitylated PCNA isoforms emerging from 100 independent stochastic simulations, and the mean value of experimental data $\mu(\#\text{PCNA}_{exp}^{\text{Ub}_\text{u}})$, together with the respective standard deviation $\sigma(\#\text{PCNA}_{exp}^{\text{Ub}_\text{u}})$. Colored areas indicate the amplitude of stochastic fluctuations around the mean value $\mu(\#\text{PCNA}_{sim}^{\text{Ub}_\text{u}})$. Data are plotted by using the units representation (see Additional File 3). (**D**) Comparison between the ratio of experimental ($\div\text{PCNA}_{exp}^{\text{Ub}_\text{u}}$, left bars) and simulated ($\div\text{PCNA}_{sim}^{\text{Ub}_\text{u}}$, right bars) ubiquitylated PCNA isoforms at every sampled time point where experimental measurements yield a detectable amount of modified PCNA. Mean and standard deviation bars of both experimental and simulated ratios are plotted by using the normalized representation (see Additional File 3).

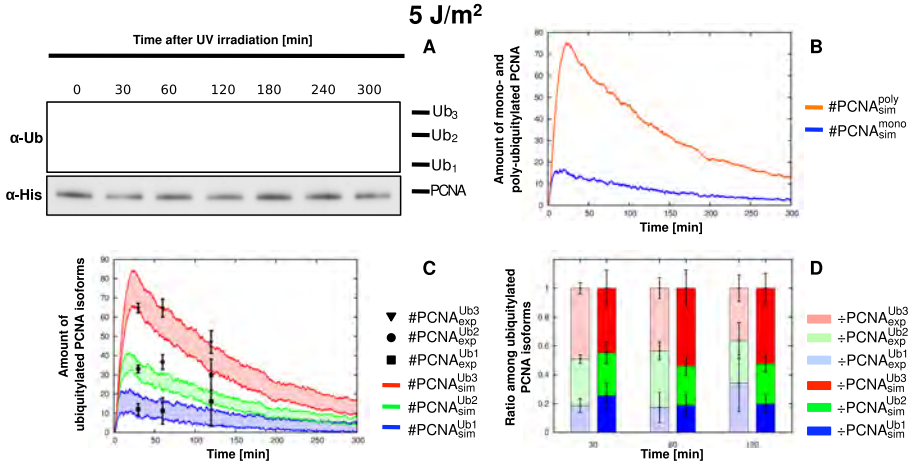

Figure 2:

Figure 3 - Comparison between experimental and simulation results of PCNA ubiquitylation dynamics obtained on wild type yeast cells at 10 J/m^2 UV dose

The figure shows the experimental measurements on WT yeast cells irradiated at 10 J/m^2 UV dose and the comparison with the corresponding simulation results. (**A**) Representative image of a western blot showing a time-course measurement of mono-, di- and tri-ubiquitylated PCNA isoforms (top part, denoted by α-Ub) and of non modified PCNA (bottom part, denoted by α-His), sampled from 0 to 5 h after UV irradiation. The experiment was repeated 3 times. (**B**) Average dynamics of mono-ubiquitylated PCNA (blue line) and of poly-ubiquitylated PCNA (orange line), obtained from 100 independent stochastic simulations, executed starting from the same initial conditions (see Table 2 for molecular amounts and Table 5 for reaction constants) and with an estimated number of DNA lesions equal to 2002. (**C**) Comparison between the mean dynamics of mono-, di- and tri-ubiquitylated PCNA isoforms emerging from 100 independent stochastic simulations, and the mean value of experimental data $\mu(\#\mathrm{PCNA}_{exp}^{\mathrm{Ub_u}})$, together with the respective standard deviation $\sigma(\#\mathrm{PCNA}_{exp}^{\mathrm{Ub_u}})$. Colored areas indicate the amplitude of stochastic fluctuations around the mean value $\mu(\#\mathrm{PCNA}_{sim}^{\mathrm{Ub_u}})$. Data are plotted by using the units representation (see Additional File 3). (**D**) Comparison between the ratio of experimental ($\div\mathrm{PCNA}_{exp}^{\mathrm{Ub_u}}$, left bars) and simulated ($\div\mathrm{PCNA}_{sim}^{\mathrm{Ub_u}}$, right bars) ubiquitylated PCNA isoforms at every sampled time point where experimental measurements yield a detectable amount of modified PCNA. Mean and standard deviation bars of both experimental and simulated ratios are plotted by using the normalized representation (see Additional File 3).

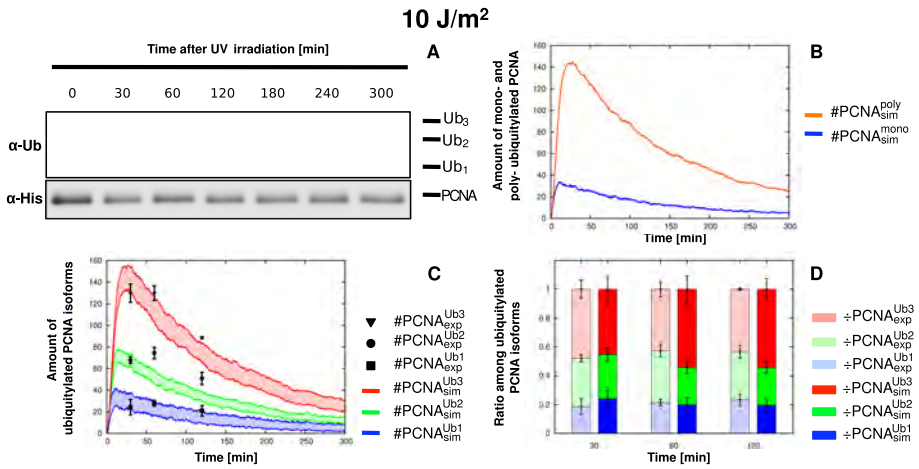

Figure 3:

Figure 4 - Comparison between experimental and simulation results of PCNA ubiquitylation dynamics obtained on wild type yeast cells at 50 J/m^2 UV dose

The figure shows the experimental measurements on WT yeast cells irradiated at 50 J/m^2 UV dose and the comparison with the corresponding simulation results. (**A**) Representative image of a western blot showing a time-course measurement of mono-, di- and tri-ubiquitylated PCNA isoforms (top part, denoted by α-Ub) and of non modified PCNA (bottom part, denoted by α-His), sampled from 0 to 5 h after UV irradiation. The experiment was repeated 3 times. (**B**) Comparison between the mean dynamics of mono-, di- and tri-ubiquitylated PCNA isoforms emerging from 10 independent stochastic simulations, and the mean value of experimental data $\mu(\#\mathrm{PCNA}_{exp}^{\mathrm{Ub_u}})$, together with the respective standard deviation $\sigma(\#\mathrm{PCNA}_{exp}^{\mathrm{Ub_u}})$. Stochastic simulations were executed starting from the same initial conditions (see Table 2 for molecular amounts and Table 5 for reaction constants) and with an estimated number of DNA lesions equal to 10012. Colored areas indicate the amplitude of stochastic fluctuations around the mean value $\mu(\#\mathrm{PCNA}_{sim}^{\mathrm{Ub_u}})$. Data are plotted by using the units representation (see Additional File 3). (**C**) Comparison between the ratio of experimental ($\div\mathrm{PCNA}_{exp}^{\mathrm{Ub_u}}$, left bars) and simulated ($\div\mathrm{PCNA}_{sim}^{\mathrm{Ub_u}}$, right bars) ubiquitylated PCNA isoforms at every sampled time point. Mean and standard deviation bars of both experimental and simulated ratios are plotted by using the normalized representation (see Additional File 3).

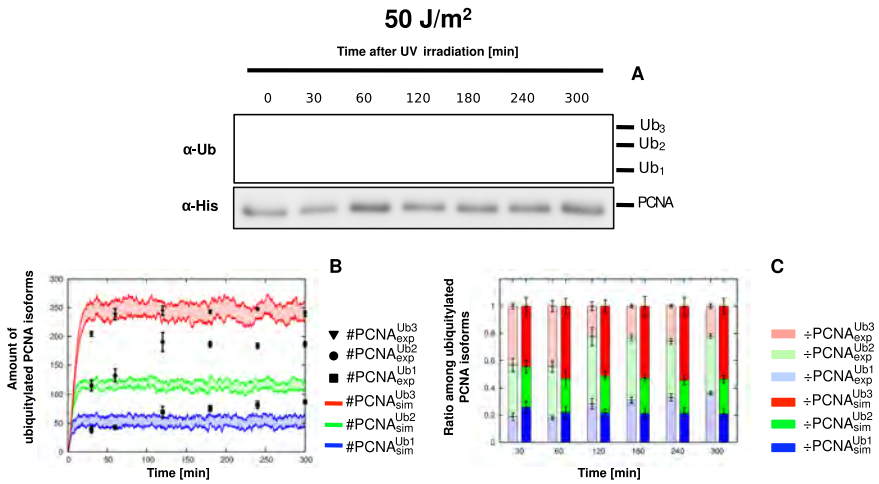

Figure 4:

Figure 5 - Comparison between experimental and simulation results of PCNA ubiquitylation dynamics obtained on wild type yeast cells at 75 J/m^2 UV dose

The figure shows the experimental measurements on WT yeast cells irradiated at 75 J/m^2 UV dose and the comparison with the corresponding simulation results. (**A**) Representative image of a western blot showing a time-course measurement of mono-, di- and tri-ubiquitylated PCNA isoforms (top part, denoted by α-Ub) and of non modified PCNA (bottom part, denoted by α-His), sampled from 0 to 5 h after UV irradiation. The experiment was repeated 3 times. (**B**) Comparison between the mean dynamics of mono-, di- and tri-ubiquitylated PCNA isoforms emerging from 10 independent stochastic simulations, and the mean value of experimental data $\mu(\#\mathrm{PCNA}_{exp}^{\mathrm{Ub_u}})$, together with the respective standard deviation $\sigma(\#\mathrm{PCNA}_{exp}^{\mathrm{Ub_u}})$. Stochastic simulations were executed starting from the same initial conditions (see Table 2 for molecular amounts and Table 5 for reaction constants) and with an estimated number of DNA lesions equal to 15018. Colored areas indicate the amplitude of stochastic fluctuations around the mean value $\mu(\#\mathrm{PCNA}_{sim}^{\mathrm{Ub_u}})$. Data are plotted by using the units representation (see Additional File 3). (**C**) Comparison between the ratio of experimental ($\div\mathrm{PCNA}_{exp}^{\mathrm{Ub_u}}$, left bars) and simulated ($\div\mathrm{PCNA}_{sim}^{\mathrm{Ub_u}}$, right bars) ubiquitylated PCNA isoforms at every sampled time point. Mean and standard deviation bars of both experimental and simulated ratios are plotted by using the normalized representation (see Additional File 3).

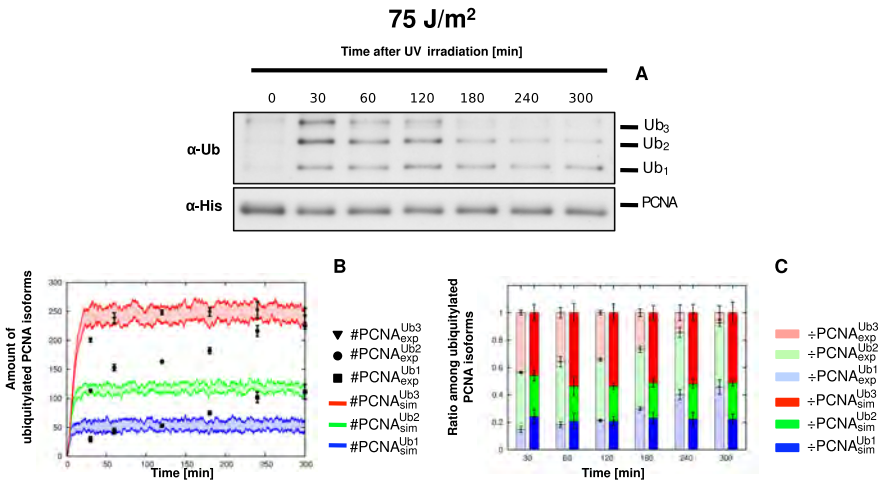

Figure 5:

Figure 6 - Prediction of bypassed DNA lesions overestimation and validation results on rad14Δ background yeast cells at 75 J/m^2 UV dose

The figure shows the experimental measurements on *rad14Δ* background yeast cells irradiated at 75 J/m^2 UV dose and the comparison with the corresponding simulation results. (**A**) Western blots showing a comparison between time-course measurements executed on WT cells (left part) and *rad14Δ* background cells (right part), of mono-, di- and tri-ubiquitylated PCNA isoforms (top part, denoted by α-Ub) and of non modified PCNA (bottom part, denoted by α-His), sampled from 0 to 5 h after UV irradiation. As the aim of this experiment was not to carry out a precise quantification of the PCNA ubiquitylated isoforms, but only to verify the prediction of computational analysis, it was conducted with a single repetition. (**B**) Comparison between the values of experimental data ($\#\text{PCNA}^{\text{mono}}_{exp}$, $\#\text{PCNA}^{\text{poly}}_{exp}$) and the mean dynamics ($\#\text{PCNA}^{\text{mono}}_{sim}$, $\#\text{PCNA}^{\text{poly}}_{sim}$) of mono- and poly-ubiquitylated PCNA isoforms emerging from 10 independent stochastic simulations, where $\#\text{PCNA}^{\text{poly}}_{exp}$, $\#\text{PCNA}^{\text{poly}}_{sim}$ represent the sum of mono-, di- and tri-ubiquitylated PCNA amounts obtained from experimental data and simulation outcomes, respectively. Stochastic simulations were executed starting from the same initial conditions (see Table 2 for molecular amounts and Table 5 for reaction constants) and with an estimated number of DNA lesions equal to 15018. Colored areas indicate the amplitude of stochastic fluctuations around the mean values $\mu(\#\text{PCNA}^{\text{mono}}_{sim})$, $\mu(\#\text{PCNA}^{\text{poly}}_{sim})$. Data are plotted by using the units representation (see Additional File 3). (**C**) Comparison between the ratio of experimental ($\div\text{PCNA}^{\text{mono}}_{exp}$ and $\div\text{PCNA}^{\text{poly}}_{exp}$, left bars) and simulated ($\div\text{PCNA}^{\text{mono}}_{sim}$ and $\div\text{PCNA}^{\text{poly}}_{sim}$, right bars) ubiquitylated PCNA isoforms at every sampled time point. Mean and standard deviation bars of both experimental and simulated ratios are plotted by using the normalized representation (see Additional File 3).

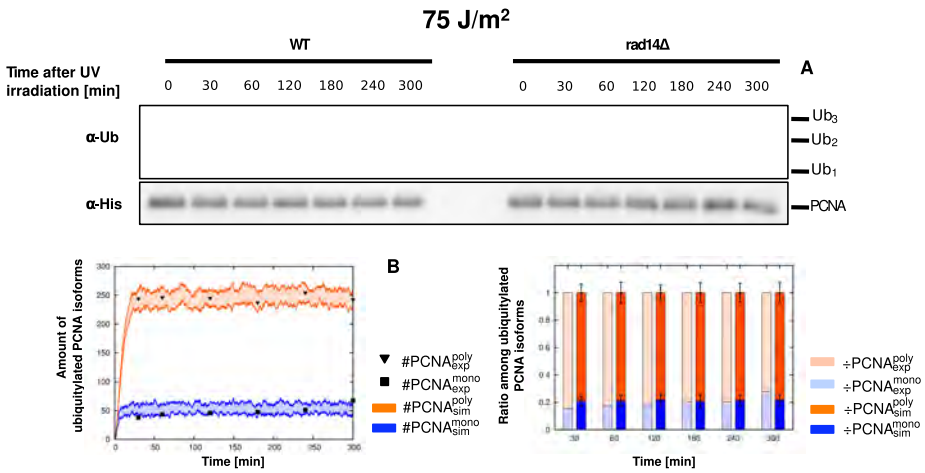

Figure 6:

Figure 7 - Prediction of UV dose-dependent threshold and validation results on wild type yeast cells at 20 J/m² and 30 J/m² UV doses

The figure shows the experimental measurements on WT cells irradiated at 20 J/m^2 UV dose (top part) and at 30 J/m^2 UV dose (bottom part), as well as the comparison with the corresponding simulation results. As the aim of these experiments was not to carry out a precise quantification of the PCNA ubiquitylated isoforms, but only to verify the prediction of computational analysis, they were conducted with a single repetition. (**A-C**) Comparison between the value of western blot quantification $\#\mathrm{PCNA}_{exp}^{\mathrm{Ub_u}}$ deriving from a single experiment, and the dynamics of mono-, di- and tri-ubiquitylated PCNA isoforms $\#\mathrm{PCNA}_{sim}^{\mathrm{Ub_u}}$ emerging from 10 independent stochastic simulations, executed starting from the same initial conditions (see Table 2 for molecular amounts and Table 5 for reaction constants), with an estimated number of DNA lesions equal to 4005 (**A**) and 6007 (**B**). Colored areas indicate the amplitude of stochastic fluctuations around the mean value $\mu(\#\mathrm{PCNA}_{sim}^{\mathrm{Ub_u}})$. Data are plotted by using the units representation (see Additional File 3). (**B-D**) Comparison between the ratio of experimental ($\div\mathrm{PCNA}_{exp}^{\mathrm{Ub_u}}$, left bars) and simulated ($\div\mathrm{PCNA}_{sim}^{\mathrm{Ub_u}}$, right bars) ubiquitylated PCNA isoforms at every sampled time point. Mean and standard deviation bars of simulated results are plotted by using the normalized representation (see Additional File 3).

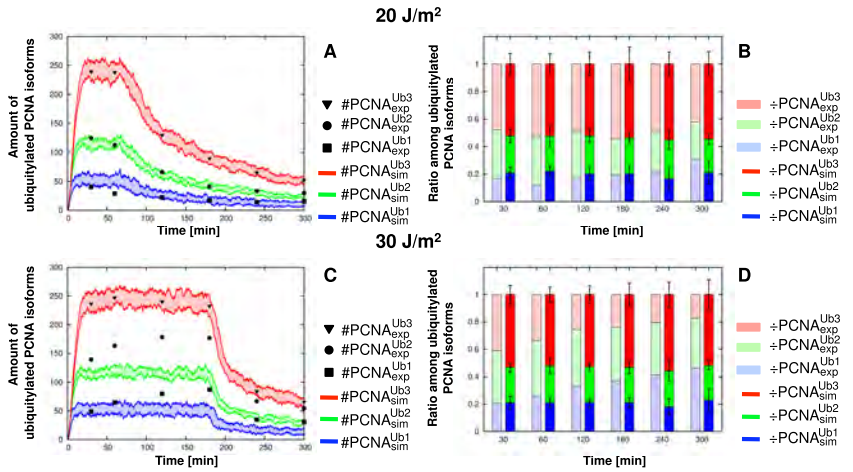

Figure 7:

Figure 8 - Influence of free ubiquitin concentration and validation results on doa4Δ background yeast cells at 20 J/m^2 UV dose

The figure shows the simulated dynamics of PCNA mono-ubiquitylation (**A**) and poly-ubiquitylation (**B**) at a UV dose of 20 J/m^2, obtained from a PSA executed on the initial amount of ubiquitin, which is varied in the interval [870, 17396] molecules – mimicking the biological conditions ranging from a 10-fold reduction (corresponding to the severely impaired condition of *doa1*Δ yeast cells) to a 2-fold overexpression of the total amount of free ubiquitin in WT cells (see the reference value in Table 2). In the plots, the thick lines correspond to the dynamics obtained with the reference value for ubiquitin amount. The simulations show that for ubiquitin amounts lower than the reference value, the amounts of mono- and poly-ubiquitylated PCNA decrease, as also observed experimentally in *doa4*Δ cells (**C**, right part). On the other hand, by increasing the ubiquitin amount present inside the system, the dynamics show an initial peak in the amount of mono- and poly-ubiquitylated PCNA, suggesting that high amounts of ubiquitin might lead the system to a faster bypass of all lesions with respect to the physiological reference value. (**C**) Western blot showing a comparison between time-course measurements in WT yeast cells (left part) and *doa4*Δ yeast cells (right part), of mono-, di- and tri-ubiquitylated PCNA isoforms (top part, denoted by *α-Ub*) and of non modified PCNA (bottom part, denoted by *α-His*), sampled at 30 min after UV irradiation. As the aim of these experiments was not to carry out a precise quantification of the PCNA ubiquitylated isoforms, but only to verify the prediction of computational analysis, they were conducted with a single repetition.

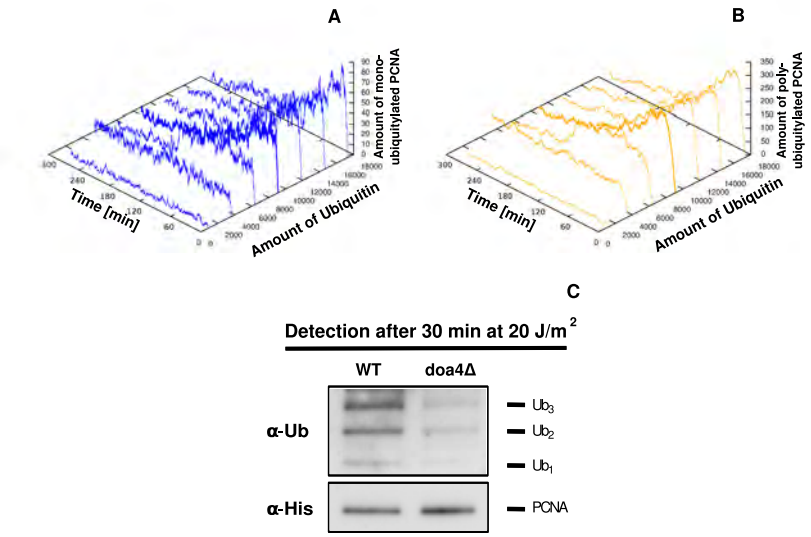

Figure 8:

Tables

Table 1 - Yeast strains used in this study

Wild type (WT) and mutant budding yeast strains used in this study.

Table 1: Yeast strains used in this study

Strain name	Genotype	Reference
WT	(DF5) *pol30*Δ::URA3 LEU2::YIplac128-His_6-*POL30*	[38]
*rad14*Δ	(DF5) *pol30*Δ::URA3 LEU2::YIplac128-His_6-*POL30 rad14*Δ::KanMX6	This study
*doa4*Δ	(DF5) *pol30*Δ::URA3 LEU2::YIplac128-His_6-*POL30 doa4*Δ::KanMX6	This study

Table 2 - Molecular amounts of initial species in the PRR model

The molecular amounts of the proteins initially occurring in the PRR model are here expressed as number of molecules per cell. Data in the second column were collected from log phase growing yeast cells, retrieved from the reference database reported in the third column. The amount of ubiquitin is calculated as the sum of molecular amounts deriving from the four genes encoding for ubiquitin in yeast cells (namely, UBI1, UBI2, UBI3, UBI4). The fourth column reports the derived molecular amounts of proteins localized both in the nucleus and in the cytoplasm, scaled according to the 7% fraction of nuclear volume with respect to the total yeast cell volume [52]. This column specifies the molecular amounts of proteins occurring in the initial state of the system; the proteins marked with the asterisk (Ubc13, Mms2) occur in the system as complex $Ubc13{:}Mms2$, whose initial amount is fixed at the minimum value between the amounts of the two proteins (namely, 193 molecules/cell).

Table 2: Molecular amounts of initial species in the PRR model

Protein	Total amount	Reference	Nuclear amount
Rad5	1520	[50]	1520
Rad6	2770	[50]	194
Rad18	206	[50]	206
Ubc13*	8970	[50]	628
Mms2*	2760	[50]	193
PCNA	22440 (7480 trimers)	[51]	7480 trimers
Ubiquitin	124260	[50, 51]	8698

Table 3 - Experimental measurements of DNA lesions per genome at different UV irradiation doses

Number of DNA lesions per genome induced by different UV irradiation doses in yeast cells.

Table 3: Experimental measurements of DNA lesions per genome at different UV irradiation doses

UV irradiation dose (J/m^2)	Number of lesions	Reference
0.1	22	[55]
1	200	[54]
29	6000	[54]
108	24000	[55]
150	30000	[54]

Table 4 - Estimation of the number of DNA lesions per genome
Evaluation of the number of DNA lesions (y) at different UV irradiation doses (x), determined using the linear regression equation $y = 200.248\,x$.

Table 4: Estimation of the number of DNA lesions per genome

UV irradiation dose (J/m^2)	**Estimated number of lesions**
5	1001
10	2002
20	4005
30	6007
50	10012
75	15018

Table 5 - Mechanistic model of the PRR pathway in yeast
The mechanistic model for the PRR pathway, developed according to the stochastic formulation of chemical kinetics, consists of 25 reactions among 21 molecular species. Each reaction is described by a set of reagents and a set of products, and is characterized by a stochastic constant (c_i, $i = 1, \ldots, 25$), here expressed in sec^{-1}. The following notation was used in writing the reactions: (i) $X + Y$ represents an interaction between the molecular species X and Y; (ii) X:Y describes a molecular complex between species X and Y. Data reported in the last column specify the literature references from which we retrieved the information used to define the corresponding reaction.

Reaction	Reagents	Products	Constant c_i [sec^{-1}]	Reference
1	$PCNA + L$	$PCNA_{\text{on}}$	1.5×10^{-8}	This study
2	$Rad18 + Rad18$	$Rad18{:}Rad18$	1×10^{-2}	[81, 82]
3	$Rad18{:}Rad18$	$Rad18 + Rad18$	1×10^{-3}	[81, 82]
4	$Rad6 + U$	$Rad6{:}U$	2.5×10^{-7}	[83]
5	$PCNA_{\text{on}} + Rad18{:}Rad18$	$Rad18{:}Rad18{:}PCNA_{\text{on}}$	1×10^{5}	[25, 36]
6	$Rad18{:}Rad18{:}PCNA_{\text{on}}$	$PCNA_{\text{on}} + Rad18{:}Rad18$	1×10^{3}	[25, 36]
7	$Rad6{:}U + Rad18{:}Rad18{:}PCNA_{\text{on}}$	$Rad18{:}Rad18{:}PCNA_{\text{on}}{:}Rad6{:}U$	3.51×10^{-2}	[25, 36, 84–87], this study
8	$Rad18{:}Rad18{:}PCNA_{\text{on}}{:}Rad6{:}U$	$Rad6{:}U + Rad18{:}Rad18{:}PCNA_{\text{on}}$	1×10^{-2}	[25, 36, 84–87], this study
9	$Rad18{:}Rad18{:}PCNA_{\text{on}}{:}Rad6{:}U$	$Rad6 + Rad18{:}Rad18{:}PCNA_{\text{on}}{:}U$	1×10^{-2}	[25, 36, 86]
10	$Rad18{:}Rad18{:}PCNA_{\text{on}}{:}U$	$Rad18{:}Rad18 + PCNA_{\text{on}}{:}U$	1	[25, 36, 86]
11	$Ubc13{:}Mms2 + U$	$Ubc13{:}U{:}Mms2$	1×10^{5}	[35, 63, 88], this study
12	$PCNA_{\text{on}}{:}U + Rad5$	$Rad5{:}PCNA_{\text{on}}{:}U$	5×10^{-6}	[36]
13	$Rad5{:}PCNA_{\text{on}}{:}U$	$PCNA_{\text{on}}{:}U + Rad5$	5×10^{-3}	[36]
14	$Ubc13{:}U{:}Mms2 + Rad5{:}PCNA_{\text{on}}{:}U$	$Ubc13{:}U{:}Mms2{:}Rad5{:}PCNA_{\text{on}}{:}U$	7.8×10^{-2}	[25, 36, 63, 84], this study
15	$Ubc13{:}U{:}Mms2{:}Rad5{:}PCNA_{\text{on}}{:}U$	$Rad5{:}PCNA_{\text{on}}{:}U + Ubc13{:}U{:}Mms2$	1×10^{-10}	[25, 36, 63, 84]
16	$Ubc13{:}U{:}Mms2{:}Rad5{:}PCNA_{\text{on}}{:}U$	$Ubc13{:}Mms2 + Rad5{:}PCNA_{\text{on}}{:}U{:}U$	5×10^{-2}	[36, 53, 88, 89]
17	$Rad5{:}PCNA_{\text{on}}{:}U{:}U$	$Rad5 + PCNA_{\text{on}}{:}U{:}U$	7.5×10^{-6}	This study
18	$PCNA_{\text{on}}{:}U{:}U + Rad5$	$Rad5{:}PCNA_{\text{on}}{:}U{:}U$	5×10^{-6}	This study
19	$Ubc13{:}U{:}Mms2 + Rad5{:}PCNA_{\text{on}}{:}U{:}U$	$Ubc13{:}U{:}Mms2{:}Rad5{:}PCNA_{\text{on}}{:}U{:}U$	7.8×10^{-2}	[25, 36, 63, 84], this study
20	$Ubc13{:}U{:}Mms2{:}Rad5{:}PCNA_{\text{on}}{:}U{:}U$	$Rad5{:}PCNA_{\text{on}}{:}U{:}U + Ubc13{:}U{:}Mms2$	1×10^{-10}	[25, 36, 63, 84]
21	$Ubc13{:}U{:}Mms2{:}Rad5{:}PCNA_{\text{on}}{:}U{:}U$	$Ubc13{:}Mms2 + Rad5{:}PCNA_{\text{on}}{:}U{:}U{:}U$	5×10^{-3}	[36, 53, 88, 89]
22	$Rad5{:}PCNA_{\text{on}}{:}U{:}U{:}U$	$Rad5 + PCNA_{\text{on}}{:}U{:}U{:}U$	5×10^{-3}	This study
23	$PCNA_{\text{on}}{:}U$	$U + PCNA_{\text{off}}$	3×10^{-8}	This study
24	$PCNA_{\text{on}}U{:}U$	$U + U + PCNA_{\text{off}}$	8×10^{-4}	This study
25	$PCNA_{\text{on}}{:}U{:}U{:}U$	$U + U + U + PCNA_{\text{off}}$	1×10^{5}	This study

Table 5: Mechanistic model of the PRR pathway in yeast

PART III

Additional Files

Additional file 1 — Histogram and density plots of CHX effect on protein synthesis and cell cycle progression of UV irradiated cells

Additional file 2 — Determination of mono- and poly-ubiquitylated PCNA ratio using western blots: elaboration and representation of densitometry quantification

Additional file 3 — Methods for the representation of simulation outcomes and comparison with experimental data

Additional file 4 — PDB accession codes for protein complexes analyzed through 3D structural modeling

Additional file 5 — Structural modeling of Uba1-Rad6 and Rad6-Rad18 complexes involved in PCNA mono-ubiquitylation

Additional file 6 — Hypothetical yeast E1-E2 and E2-E3 complexes involved in PCNA mono- and poly-ubiquitylation obtained through structural modeling of PRR complexes

Additional file 7 — Structural modeling of Uba1-Ubc13 and Ubc13-Rad5 complexes involved in PCNA poly-ubiquitylation

Additional file 8 — List of reactions involved in the formation of $Ubc13{:}Mms2$ complex and simulation results

Additional file 9 — Effects of the variation of the initial amount of PCNA

Additional file 10 — Effects of the modulation of the binding between Rad6 and ubiquitin (reaction constant c_4) and of PCNA mono-ubiquitylation (reaction constant c_9)

Additional file 11 — Effects of the modulation of the dissociation of mono-ubiquitylated PCNA from Rad18 dimer (reaction constant c_{10}) and of the association of Rad5 with mono-ubiquitylated PCNA (reaction constant c_{12})

Additional file 12 — Effects of the modulation of the formation of di-ubiquitylated (reaction constant c_{16}) and of tri-ubiquitylated (reaction constant c_{22}) PCNA isoforms

Additional file 13 — FACS analysis of wild type and rad14Δ background cells irradiated at 10 J/m^2 UV dose

ADDITIONAL FILE 1

Histogram and density plots of CHX effect on protein synthesis and cell cycle progression of UV-irradiated cells

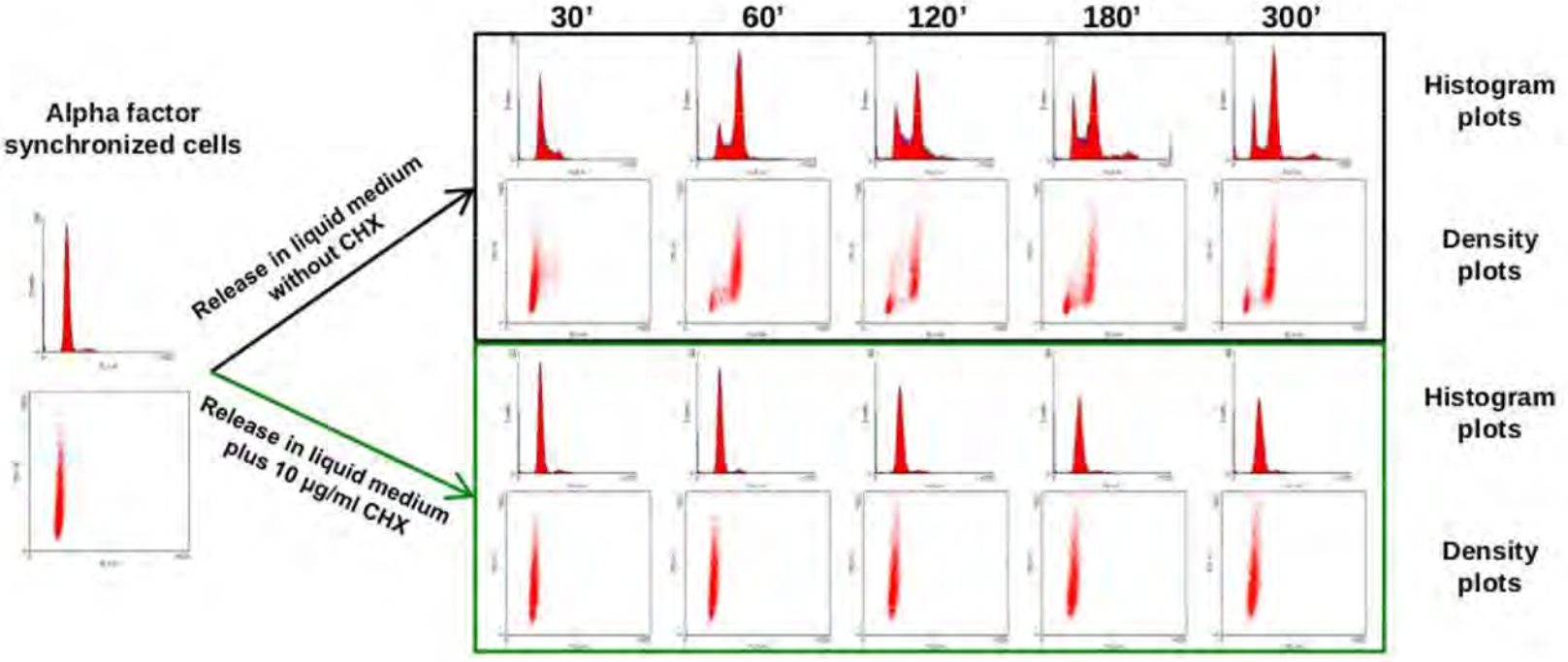

Cells were synchronized through 6 μg/ml of alpha factor and then released in liquid medium without CHX (top graphics) or with 10 μg/ml CHX (bottom graphics).
In the histogram plots, the left peak corresponds to G1 cells, the right peak corresponds to G2 cells, while S phase cells are in the middle; in the density plots, the left cloud corresponds to G1 cells, the right cloud corresponds to G2 cells, S phase cells are in the middle. Both histogram and density plots at 240 min are not shown, since they are exactly equal to those taken at 180 min and 300 min.
This experiment confirmed that 10 μg/ml CHX are sufficient to stop cell cycle progression.

ADDITIONAL FILE 2
Determination of mono- and poly-ubiquitylated PCNA ratio using western blots: elaboration and representation of densitometry quantification

To quantify the values of mono-/poly-ubiquitylated PCNA ratio from time-course experiments, the ubiquitylation signal of mono- and poly-ubiquitylated PCNA isoforms was normalized with respect to the unmodified PCNA signal obtained on western blots. The whole process was carried out for each UV irradiation dose considered in this work (5, 10, 50, 75 J/m^2), taking into account all the experiments replicates (3, unless otherwise specified), in order to derive the mean and standard deviation of mono-/poly-ubiquitylated PCNA ratio.
The quantification procedure consisted in the following steps.

1. The initial data are represented by two different types of western blot film for each experiment: "film A", corresponding to the measurement of the unmodified PCNA (see, e.g., top part of blot in Figure 2A), and "film B", corresponding to ubiquitylated PCNA (see, e.g., bottom part of blot in Figure 2A). Seven time measurements $t_1, \ldots, t_7$ – taken at 0, 30, 60, 120, 180, 240, 300 min, respectively – appear on each film. Both films were scanned and quantified by means of the NIH densitometry software ImageJ [1], yielding the initial quantifications $w_1, \ldots, w_7$ of unmodified PCNA (film A), and $w_{1,1}, \ldots, w_{1,7}$, $w_{2,1} \ldots, w_{2,7}$, $w_{3,1}, \ldots, w_{3,7}$ of mono-, di- and tri-ubiquitylated isoforms of PCNA (film B), respectively, for each sampled time point $t_1, \ldots, t_7$.

2. To obtain the correct measurements of unmodified PCNA and of mono-, di- and tri-ubiquitylated PCNA isoforms from western blots, we had to determine the value of the background of each film, which was quantified by using ImageJ, for any given UV dose and for each replicate of the experiments. Let us call α and β the background values for film A and B, respectively. Then, for each time point t_i ($i = 1, \ldots, 7$), we processed the previously quantified values of unmodified (w_i) and mono-, di- and tri-ubiquitylated PCNA isoforms ($w_{u,i}$, where $u = 1, 2, 3$) with respect to α and β as follows:
$$w'_i = \begin{cases} w_i - \alpha & \text{if } w_i - \alpha > 0, \\ 0 & \text{otherwise,} \end{cases}$$
and, for every $u = 1, 2, 3$,
$$w'_{u,i} = \begin{cases} w_{u,i} - \beta & \text{if } w_{u,i} - \beta > 0, \\ 0 & \text{otherwise.} \end{cases}$$

3. The measurements derived at Step 2 for film B need to be normalized with respect to the measurements of the corresponding film A, for any given UV dose and for each replicate. To this aim, we first evaluated the normalization coefficient γ_i for each time point t_i ($i = 1, \ldots, 7$) of film A:
$$\gamma_i = \frac{w'_i}{\max\limits_{i=1,\ldots,7}\{w'_i\}},$$
and then, for each time point t_i and for every $u = 1, 2, 3$, we derived the normalized values of mono-, di- and tri-ubiquitylated isoforms of PCNA on film B with respect to the corresponding values of unmodified PCNA on film A (namely, the value γ_i):
$$w''_{u,i} = \frac{w'_{u,i}}{\gamma_i}.$$

4. Finally, for each western blot film we computed the percentage of the mutual signal intensity of each isoform of poly-ubiquitylated PCNA with respect to the total amount of poly-ubiquitylated PCNA measured on the same film. By taking into account the normalized values of the western blot of all replicates of the experiments, we then evaluated the mean and standard deviation of mono-, di- and tri-ubiquitylated isoforms of PCNA – denoted by $\mu(\div\text{PCNA}^{\text{Ub}_u}_{exp})$ and $\sigma(\div\text{PCNA}^{\text{Ub}_u}_{exp})$, respectively – that were finally used to compare the results of the computational analysis with the experimental data.

[1] Abramoff M, Magelhaes P, Ram S: **Image processing with ImageJ**. *Biophotonics International* 2004, 11(7):36–42.

ADDITIONAL FILE 3
Methods for the representation of simulation outcomes and comparison with experimental data

For the validation of the PRR model, we compared the outcome of stochastic simulations with the experimental measurements. Since we had to compare different kinds of measurements – namely, *ratios* of modified PCNA derived from laboratory experiments on the one side, and *molecular amounts* of modified PCNA obtained from stochastic simulations on the other side – we introduced two strategies, called *normalized representation* and *units representation*, for the graphical representation of experimental and computational results.

To this aim, we first quantified the ratio of mono-, di- and tri-ubiquitylated PCNA from western blot experiments for each UV irradiation dose (denoted by $\div\text{PCNA}_{exp}^{\text{Ub}_u}$, where $u = 1, 2, 3$ corresponds to the three ubiquitylated isoforms), as described in Additional File 2. Then, we derived the molecular amounts of mono-, di- and tri-ubiquitylated PCNA (denoted by $\#\text{PCNA}_{sim}^{\text{Ub}_u}$, where $u = 1, 2, 3$ corresponds to the three ubiquitylated isoforms) generated during the stochastic simulations. These values were determined by summing up the molecular amounts of all complexes in which mono-, di- and tri-ubiquitylated PCNA isoforms appeared in the system during the simulations (see Table 5 in the paper). In order to take into account the effects of stochastic fluctuations, a set of independent stochastic simulations were performed to compute the mean $\mu(\#\text{PCNA}_{sim}^{\text{Ub}_u})$ and standard deviation $\sigma(\#\text{PCNA}_{sim}^{\text{Ub}_u})$ of these modified PCNA amounts. Moreover, in both representations the values of di- and tri-ubiquitylated forms of simulated PCNA were represented as the sum of $\#\text{PCNA}_{sim}^{\text{Ub}_1}+\#\text{PCNA}_{sim}^{\text{Ub}_2}$ and $\#\text{PCNA}_{sim}^{\text{Ub}_1}+\#\text{PCNA}_{sim}^{\text{Ub}_2}+\#\text{PCNA}_{sim}^{\text{Ub}_3}$, respectively, to be correctly compared with the corresponding experimental measurements.

1. The *normalized representation* (NR) strategy consists of stacked bar graphs: for each sampled time point $t_1, \ldots, t_7$ within the measurement interval 0-5 h, the stacked bars corresponding to the normalized values of the computational outcomes (denoted by $\div\text{PCNA}_{sim}^{\text{Ub}_u}$) are plotted side by side to the experimental bars $\div\text{PCNA}_{exp}^{\text{Ub}_u}$ (which are already expressed as ratios, as described in Additional File 2). With NR, the "normalized stacked bars" corresponding to the computational outcomes were derived as follows: we first run a stochastic simulation of the model and acquired the values of $\#\text{PCNA}_{sim}^{\text{Ub}_u}$ occurring at times points $t_1, \ldots, t_7$; then, for each t_i, we derived and plotted the three bar portions $\div\text{PCNA}_{sim}^{\text{Ub}_u}$ corresponding to the normalized values of mono-, di- and tri-ubiquitylated PCNA ratios occurring during the simulation. We remark that the NR allows a direct comparison between the experimental and simulation results, by considering the ratio of the three ubiquitylated isoforms of PCNA with respect to the total amount of modified PCNA measured in the system. Nonetheless, this strategy does not give any information related to the molecular amounts of the mono-, di- and tri-ubiquitylated isoforms of PCNA obtained through stochastic simulations.

2. The *units representation* (UR) strategy overcomes the drawback of NR, since it allows to directly compare the outcomes of stochastic simulations with the western blot quantifications which, in this case, are specifically transformed into molecular quantities. To this aim, the experimental measured ratios $\div\text{PCNA}_{exp}^{\text{Ub}_u}$ were converted into molecular amounts (i.e., number of molecules per cell) by exploiting the results of stochastic simulations: by considering the values of $\#\text{PCNA}_{sim}^{\text{Ub}_u}$ obtained at each time instants t_i during a simulation, we computed the value $S = \sum_{u=1,2,3} \#\text{PCNA}_{sim}^{\text{Ub}_u}$ at time t_i, $i = 1, \ldots, 7$. Then, we evaluated the quantities

$$\begin{aligned}
\#\text{PCNA}_{exp}^{\text{Ub}_1} &= \div\text{PCNA}_{exp}^{\text{Ub}_1} \times S,\\
\#\text{PCNA}_{exp}^{\text{Ub}_2} &= (\div\text{PCNA}_{exp}^{\text{Ub}_1} + \div\text{PCNA}_{exp}^{\text{Ub}_2}) \times S,\\
\#\text{PCNA}_{exp}^{\text{Ub}_3} &= (\div\text{PCNA}_{exp}^{\text{Ub}_1} + \div\text{PCNA}_{exp}^{\text{Ub}_2} + \div\text{PCNA}_{exp}^{\text{Ub}_3}) \times S.
\end{aligned}$$

   The variables $\#\text{PCNA}_{exp}^{\text{Ub}_u}$ represent the experimental measurements transformed from percentages (i.e., ratio of each modified isoform of PCNA with respect to the total amount of modified PCNA experimentally measured) into units (i.e., number of molecules of each modified isoform of PCNA with respect to the total molecular amounts of modified PCNA occurring in the simulation). So doing, the UR of the experimental results can be directly compared to the simulation outcomes. The UR allows to evidence the different dynamics emerging from the system and, in particular, it clearly represents the switch-off of the ubiquitylation signal as long as the DNA lesions get processed. This kind of information is not shown with the NR of the simulated and experimental ratios, since the NR does not give any knowledge on the actual amount of modified PCNA corresponding to the height of the stacked bars.

Finally, we stress the fact that whilst the NR is a direct display of the experimental measurements, the UR is markedly related to the computational outcomes and, as such, it hinges upon the parameterization used to run the stochastic simulations. This means that if we change the parameters (either the initial molecular amounts or the stochastic constants, or both) and run a new simulation, the computational results, and hence also the values $\#\text{PCNA}_{exp}^{\text{Ub}_u}$, vary. Therefore, the UR graphs cannot give a certain knowledge on the actual cellular amounts of mono- and poly-ubiquitylated isoforms of PCNA, but nevertheless it provides useful hints on the system dynamics.

We also remark that additional sources of uncertainty, possibly able to impair the direct comparison between the experimental data and the simulation outcomes, and that can be even more evidenced with both NR and UR representation methods, are due to two factors: on the one hand, the discrepancy between the amounts of some key regulatory molecules that are effectively occurring *in vivo* and those considered in simulations; on the other hand, the simplification of complex biochemical processes – taking place through a cascade of multiple reactions – reduced to a single reaction or a set of few reactions. In the PRR model, an example of such simplification is related to the ubiquitin activation step mediated by Uba1, a biochemical process consisting in about 20 biochemical reactions which was modeled as a single reaction (see reaction 4, Table 5, and the discussion in section "The PCNA ubiquitylation model" within the paper). Model simplification is a common and essential practice both for developing models at an appropriate level of abstraction and for reducing the computational costs, notwithstanding the fact that the presence of multiple step processes modeled as single reactions can amplify the discrepancy between the values of the experimental and simulated standard deviations, as previously shown in [1,2].

[1] Pedraza J, Paulsson J: **Effects of molecular memory and bursting on fluctuations in gene expression.** *Science* 2008, 319(5861):339–343.

[2] Csikász-Nagy A, Mura I: **Role of mRNA gestation and senescence in noise reduction during the cell cycle.** *Stud Health Technol Inform* 2011, 162:236–43.

ADDITIONAL FILE 4
PDB accession codes for protein complexes analyzed through 3D structural modeling

PDB accession codes for proteins and protein complexes analyzed through the structural modeling approach (see also Additional Files 5 and 7).

Protein/complex	PDB accession code
UBA3-Ubc12	1Y8X
Uba1	3CMM
Rad6	1AYZ
UbcH7-c-CBL(RING)	1FVB
Ubc13-Mms2	2GMI

ADDITIONAL FILE 5
Structural modeling of Uba1-Rad6 and Rad6-Rad18 complexes involved in PCNA mono-ubiquitylation

Following the procedure published in [1], we constructed the hypothetical yeast E1-E2 complex Uba1-Rad6 (Figure A, Additional File 6) by using as template the crystallized complex UBA3(UFD)-Ubc12(core) formed by the catalytic subunit of the human E1 UBA3-NAE1 and the human E2 Ubc12. These two proteins share high structural conservation with yeast Uba1 (UFD domain) and Rad6, respectively [1]. Then, we superimposed the published 3D structures of yeast Uba1 and Rad6 on the UBA3(UFD)-Ubc12(core) template, and we finally deleted the human proteins from the workbench, obtaining the hypothetical Uba1-Rad6 yeast complex. This complex was analyzed by Protein Interfaces, Surfaces and Assemblies (PISA) server [2] to identify the residues through which Rad6 interacts with Uba1. We determined that 9 residues of Rad6 (Met10, Arg11, Asp12, Phe13, Lys14, Arg15, Met16, Lys17, Glu18 of N-term alpha helix H1), which resulted to be involved in the interaction with Uba1, were experimentally found to be involved also in the interaction with Rad18 [3]. This result suggests the mutual exclusivity of the two yeast complexes Uba1-Rad6 and Rad6-Rad18.

We further confirmed this prediction by constructing the hypothetical yeast complex Rad6-Rad18(RING). For this purpose we used the human E2 UbcH7-c-CBL(RING) complex as 3D template, which is the crystallized complex between the human E2 UbcH7 and the RING domain of human c-CBL. We superimposed the yeast Rad6 structure on this template and, after deleting the UbcH7 structure from the virtual workbench, we started the threading task. Based on the sequence alignment between yeast Rad18(RING) and human c-CBL(RING), we manually threaded the yeast Rad18(RING) onto the fold of human c-CBL(RING), which was then deleted from the virtual workbench. The resulting hypothetical structure of yeast Rad6-Rad18(RING) complex (Figure B, Additional File 6) was analyzed by PISA server, obtaining the putative residues of yeast Rad6 interacting with yeast Rad18. Our predictions were then compared with previous experimental data [3], which confirmed that we correctly predicted 6 residues of the yeast Rad6 (Met10, Arg11, Asp12, Phe13, Lys14, Lys17 of N-term alpha helix H1) interacting with Rad18(RING).

The structural modeling analysis carried out on these two hypothetical yeast complexes E1-E2 Uba1-Rad6 and E2-E3 Rad6-Rad18 allowed us to deduce that the two complexes are mutually exclusive, and that the mechanism of PCNA mono-ubiquitylation, from ubiquitin activation to its covalent linkage on PCNA, is a step-wise process, as previously suggested in [4, 5].

[1] Lee I, Schindelin H: **Structural insights into E1-catalyzed ubiquitin activation and transfer to conjugating enzymes.** *Cell* 2008, **134**(2):268–278.

[2] Krissinel E, Henrick K: **Inference of macromolecular assemblies from crystalline state**. *J Mol Biol* 2007, **372**(3):774–797.

[3] Bailly V, Prakash S, Prakash L: **Domains required for dimerization of yeast Rad6 ubiquitin-conjugating enzyme and Rad18 DNA binding protein**. *Mol Cell Biol* 1997, **17**(8):4536–4543.

[4] Eletr ZM, Huang DT, Duda DM, Schulman BA, Kuhlman B: **E2 conjugating enzymes must disengage from their E1 enzymes before E3-dependent ubiquitin and ubiquitin-like transfer**. *Nat Struct Mol Biol* 2005, **12**(10):933–934.

[5] Parker J, Ulrich HD: **Mechanistic analysis of PCNA poly-ubiquitylation by the ubiquitin protein ligases Rad18 and Rad5**. *EMBO J* 2009, **28**:3657–3666.

ADDITIONAL FILE 6

Hypothetical yeast E1-E2 and E2-E3 complexes involved in PCNA mono- and poly-ubiquitylation obtained through structural modeling of PRR complexes

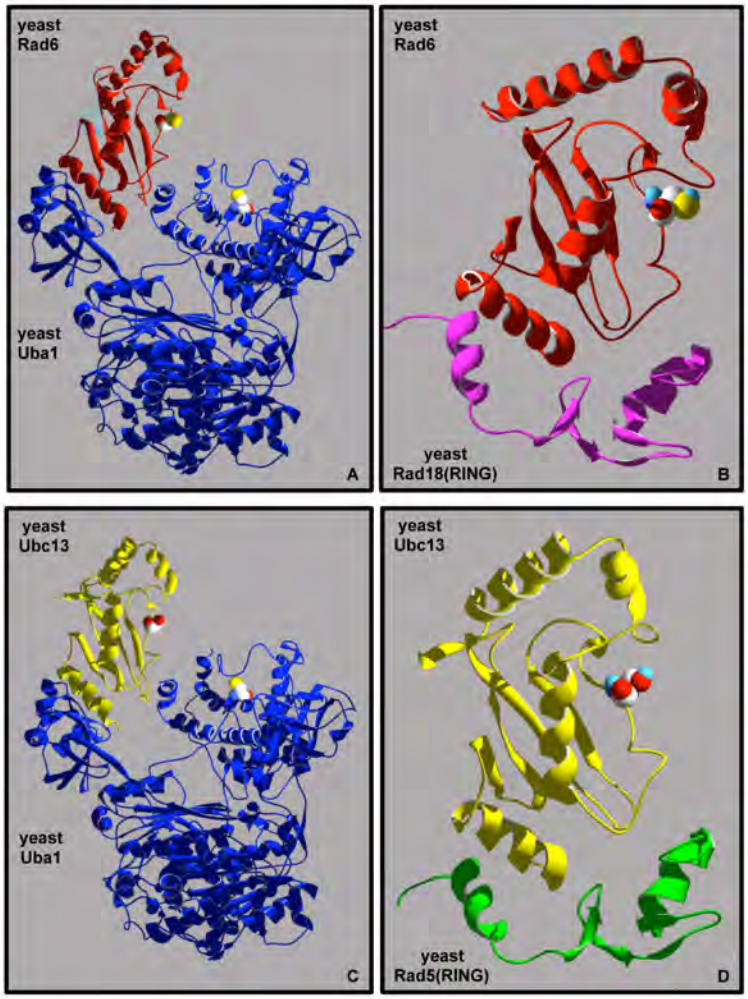

(A) Hypothetical yeast E1-E2 complex Uba1(blue)-Rad6(red).
(B) Hypothetical yeast E2-E3(RING) complex Rad6(red)-Rad18(RING)(magenta).
(C) Hypothetical yeast E1-E2 complex Uba1(blue)-Ubc13(yellow).
(D) Hypothetical yeast E2-E3(RING) complex Ubc13(yellow)-Rad5(RING)(green).

The active sites of the proteins are rendered in solid 3D, namely, Cys600 for Uba1, Cys88 for Rad6, Cys87 for Ubc13.

ADDITIONAL FILE 7
Structural modeling of Uba1-Ubc13 and Ubc13-Rad5 complexes involved in PCNA poly-ubiquitylation

Following the procedure published in [1], we constructed the hypothetical yeast Uba1-Ubc13 and Uba1-Ubc13-Mms2 complexes using the template UBA3(UFD)-Ubc12(core), in combination with the Uba1 structure and the published crystallographic structure of yeast Ubc13-Mms2 complex.
We constructed and analyzed the hypothetical yeast Uba1-Ubc13 complex (Figure C, Additional File 6) through the Protein Interfaces, Surfaces and Assemblies (PISA) server [2], identifying the Ubc13 residues involved in the interaction with Uba1. At least two residues of Ubc13 (Lys6 and Lys10 of N-term alpha helix H1), which interact with Uba1, were previously found to be necessary also for the interaction with the E3 enzyme Rad5 [3]. This result suggests the mutual exclusivity between the two complexes Uba1-Ubc13 and Ubc13-Rad5. Moreover, from the analysis of the hypothetical complex Uba1-Ubc13-Mms2, we determined that there are unrealistic contacts between Uba1 and Mms2, deducing that also Uba1-Ubc13 and Ubc13-Mms2 are mutually exclusive: Ubc13 needs to be charged with ubiquitin by Uba1 before binding Mms2.
We confirmed the mutual exclusivity of Uba1-Ubc13 and Ubc13-Rad5 by constructing the hypothetical yeast complex Ubc13-Rad5(RING), exploiting the same approach described in Additional File 5. We used the human E2 UbcH7-c-CBL(RING) complex as main template (this was previously used also by H.D. Ulrich to design mutations on the putative surface of Ubc13-Rad5 [3]). On this template we first superimposed the structure of yeast Ubc13 and then deleted UbcH7 from the virtual workbench; based on the sequence alignment between human c-CBL(RING) and yeast Rad5(RING), we manually threaded the primary sequence of yeast Rad5 onto the fold of human c-CBL(RING). The resulting structure (Figure D, Additional File 6) was analyzed by PISA server. Through this analysis, we assessed that our predictions are in perfect agreement with previously published experimental data [3], confirming that the yeast Uba1-Ubc13 and Ubc13-Rad5 complexes are mutually exclusive.
Our deductions are in good agreement with all published data, which support a distributive/step-wise sequence of events for PCNA poly-ubiquitylation, from ubiquitin activation to its covalent linkage on mono-ubiquitylated PCNA [4, 5].

References

[1] Lee I, Schindelin H: **Structural insights into E1-catalyzed ubiquitin activation and transfer to conjugating enzymes.** *Cell* 2008, **134**(2):268–278.

[2] Krissinel E, Henrick K: **Inference of macromolecular assemblies from crystalline state**. *J Mol Biol* 2007, **372**(3):774–797.

[3] Ulrich HD: **Protein-protein interactions within an E2-RING finger complex**. *J Biol Chem* 2003, **278**(9):7051–7058.

[4] Eletr ZM, Huang DT, Duda DM, Schulman BA, Kuhlman B: **E2 conjugating enzymes must disengage from their E1 enzymes before E3-dependent ubiquitin and ubiquitin-like transfer**. *Nat Struct Mol Biol* 2005, **12**(10):933–934.

[5] Parker J, Ulrich HD: **Mechanistic analysis of PCNA poly-ubiquitylation by the ubiquitin protein ligases Rad18 and Rad5**. *EMBO J* 2009, **28**:3657–3666.

ADDITIONAL FILE 8
List of reactions involved in the formation of $Ubc13{:}Mms2$ complex and simulation results

Table 1 reports the list of biochemical reactions involved in the formation of $Ubc13{:}Mms2$ complex, which were removed from an initial version of the model.
Figure 1 shows the average dynamics of mono-ubiquitylated PCNA (blue line) and poly-ubiquitylated PCNA (red line) at 5 J/m^2 UV dose, obtained with (dashed lines) and without (solid lines) the set of reactions given in Table 1. In both cases, the average dynamics were evaluated by considering 100 independent stochastic simulations, executed starting from the same initial conditions and with an estimated number of DNA lesions equal to 1001. The initial conditions for dashed line dynamics are given in Table 1 hereafter, together with Tables 2 and 5 in the paper, while for solid line dynamics they are reported in Tables 2 and 5 in the paper.

Table 1: Removed reactions

Reaction	Reagents	Products	Constant [sec^{-1}]	Reference
1	$Ubc13 + Mms2$	$Ubc13{:}Mms2$	$1.82{\times}10^{-1}$	[1–4]
2	$Ubc13{:}Mms2$	$Ubc13 + Mms2$	98	[1–4]
3	$Ubc13{:}U{:}Mms2$	$Ubc13{:}Mms2 + U$	$1.82{\times}10^{-1}$	[1–4]

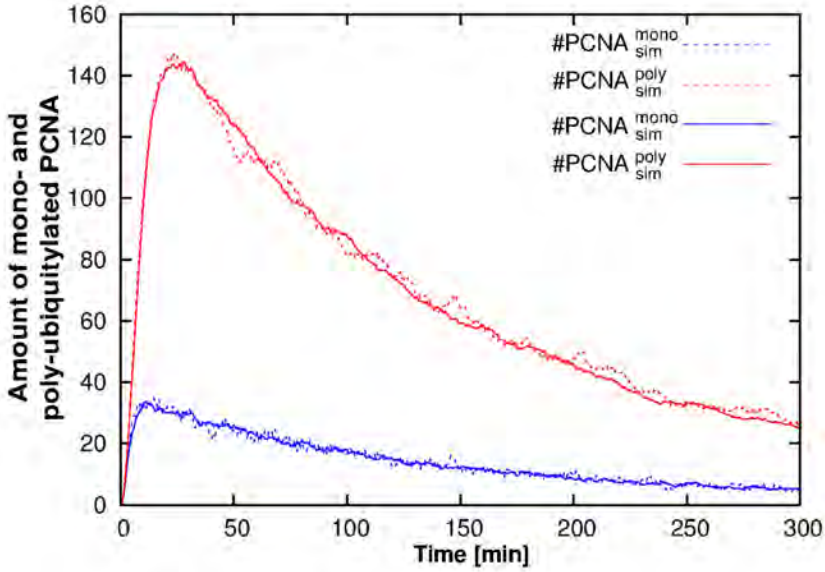

Figure 1: Comparison between the simulated dynamics of PCNA ubiquitylation obtained with (dashed lines) and without (solid lines) the set of removed reactions

[1] Hoege C, Pfander B, Moldovan G, Pyrowolakis G, Jentsch S: **RAD6-dependent DNA repair is linked to modification of PCNA by ubiquitin and SUMO**. *Nature* 2002, **419**:135–141.

[2] Parker J, Ulrich HD: **Mechanistic analysis of PCNA poly-ubiquitylation by the ubiquitin protein ligases Rad18 and Rad5**. *EMBO J* 2009, **28**:3657–3666.

[3] Ulrich HD: **Protein-protein interactions within an E2-RING finger complex**. *J Biol Chem* 2003, **278**(9):7051–7058.

[4] Ulrich HD, Jentsch S: **Two RING finger proteins mediate cooperation between ubiquitin-conjugating enzymes in DNA repair**. *EMBO J* 2000, **19**(13):3388–3397.

ADDITIONAL FILE 9
Effects of the variation of the initial amount of PCNA

The figure shows the simulated dynamics of the ubiquitylated PCNA isoforms resulting from a PSA on the amount of PCNA initially present inside the system; simulations were executed assuming an UV dose equal to 10 J/m^2. The molecular amount of PCNA was varied in the interval $[0, 14960]$, mimicking the biological effect ranging from the deletion to a 2-fold overexpression of the DNA sliding clamp. The reference dynamics, obtained by using the value of PCNA equal to 7480 molecule, is marked with a red arrow in the plots.
The simulations show that for amounts of PCNA lower than the reference value, the amount of modified PCNA isoforms is strongly reduced and we no longer observe the signal switch-off within 300 min of simulation. Conversely, by incrementing the amount of PCNA, we observe an increase in the initial peak of all PCNA isoforms and the subsequent signal switch-off.

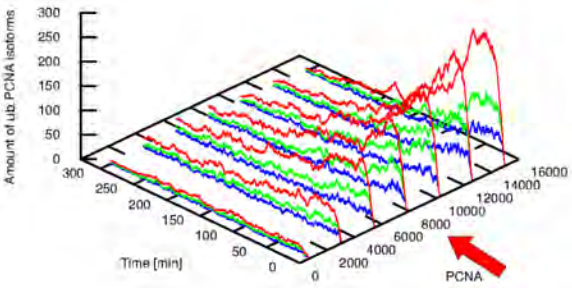

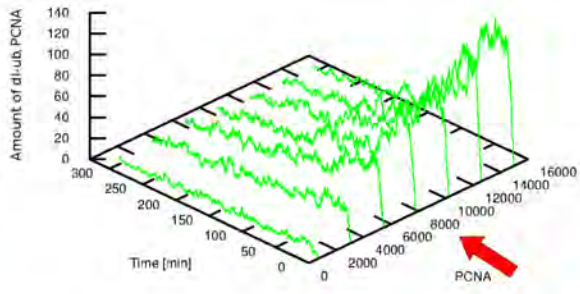

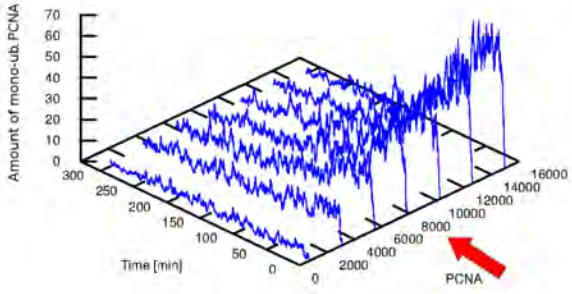

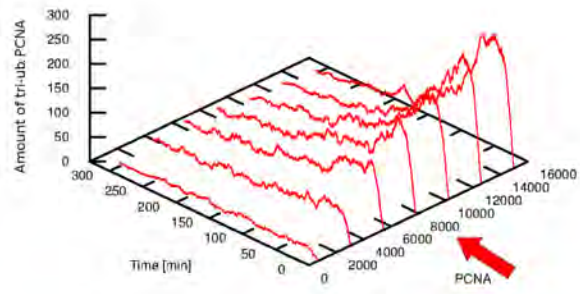

ADDITIONAL FILE 10

Effects of the modulation of the binding between Rad6 and ubiquitin (reaction constant c_4) and of PCNA mono-ubiquitylation (reaction constant c_9)

The figure shows the simulated dynamics of the ubiquitylated PCNA isoforms resulting from two PSA, the first executed on the value of the reaction constant that modulates the binding between Rad6 and ubiquitin (top frame), and the second executed on the reaction constant that rules PCNA mono-ubiquitylation (bottom frame). All simulations were executed assuming an UV dose equal to 10 J/m^2.

The two varied parameters and the corresponding sweep ranges are: (1) constant c_4 within the interval $[2.5 \times 10^{-10}, 2.5 \times 10^{-4}]$; (2) constant c_9 within the interval $[1 \times 10^{-5}, 10]$. The dynamics corresponding to the reference values (see Table 5) are marked with a red box. These two reactions are involved in the ubiquitin transfer process: reaction 4 loads the ubiquitin on Rad6, while reaction 9 transfers the ubiquitin from Rad6 to PCNA. In both cases, for values of the reaction constant lower than the reference value, we observe low amounts of all modified PCNA isoforms. Conversely, by increasing the value of the constant, that is, by enhancing the binding affinity between Rad6 or ubiquitin and the formation of mono-ubiquitylated PCNA, the obtained dynamics are comparable with the reference one, since we observe the same initial increase in the amount of all PCNA isoforms and the following ubiquitylation signal switch-off.

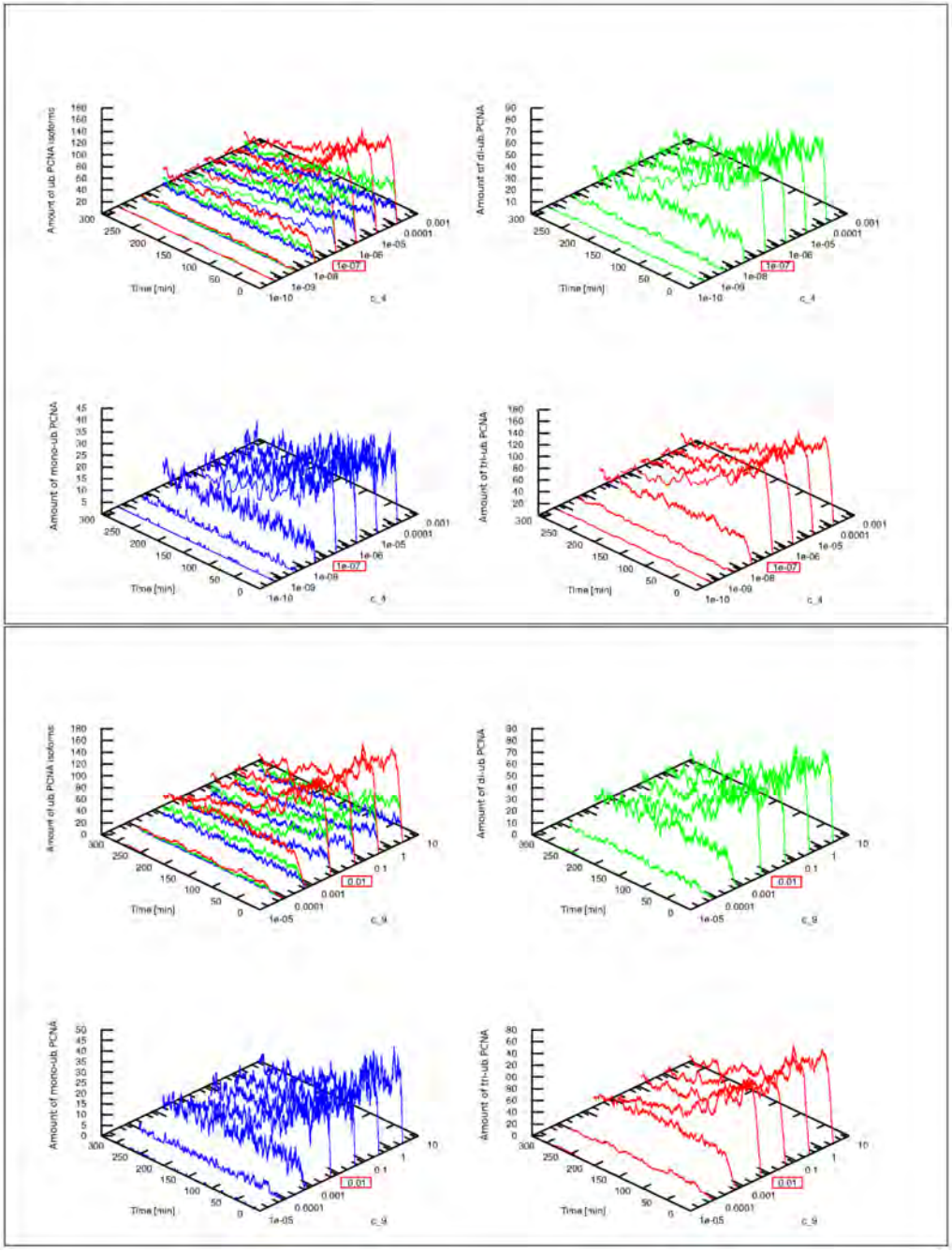

ADDITIONAL FILE 11

Effects of the modulation of the dissociation of mono-ubiquitylated PCNA from Rad18 dimer (reaction constant c_{10}) and of the association of Rad5 with mono-ubiquitylated PCNA (reaction constant c_{12})

The figure shows the simulated dynamics of the ubiquitylated PCNA isoforms resulting from two PSA, the first executed on the value of the reaction constant that modulates the dissociation of mono-ubiquitylated PNCA from Rad18 dimer (top frame), and the second executed on the association constant of Rad5 with mono-ubiquitylated PCNA (bottom frame). All simulations were executed assuming an UV dose equal to 10 J/m^2.

The two varied parameters and the corresponding sweep ranges are: (1) constant c_{10} within the interval $[1 \times 10^{-3}, 1 \times 10^{3}]$; (2) constant c_{12} within the interval $[5 \times 10^{-9}, 5 \times 10^{-3}]$. The dynamics corresponding to the reference values (see Table 5) are marked with a red box.

For values of reaction constant c_{10} lower or equal to 1×10^{-3} we observe an accumulation of the mono-ubiquitylated PCNA isoform, since this constant rules the dissociation activity of mono-ubiquitylated PCNA from Rad18 dimer. Conversely, for higher values of this constant, the resulting dynamics is comparable to the reference one, suggesting that the reaction able to modulate the amount of mono- and poly-ubiquitylated PCNA isoforms is upstream to reaction 10.

Very low values of constant c_{12} (equal or lower than 1×10^{-8}) induce an accumulation of the mono-ubiquitylated PCNA isoform in the system, while keeping the amount of the other PCNA isoforms around zero. This is due to the fact that reaction 12 forms the trimer $Rad5{:}PCNA_{on}{:}U$, which is a control point for the switch between PCNA mono- and poly-ubiquitylation. On the other hand, higher values of this constant result in a dynamics comparable to the reference one.

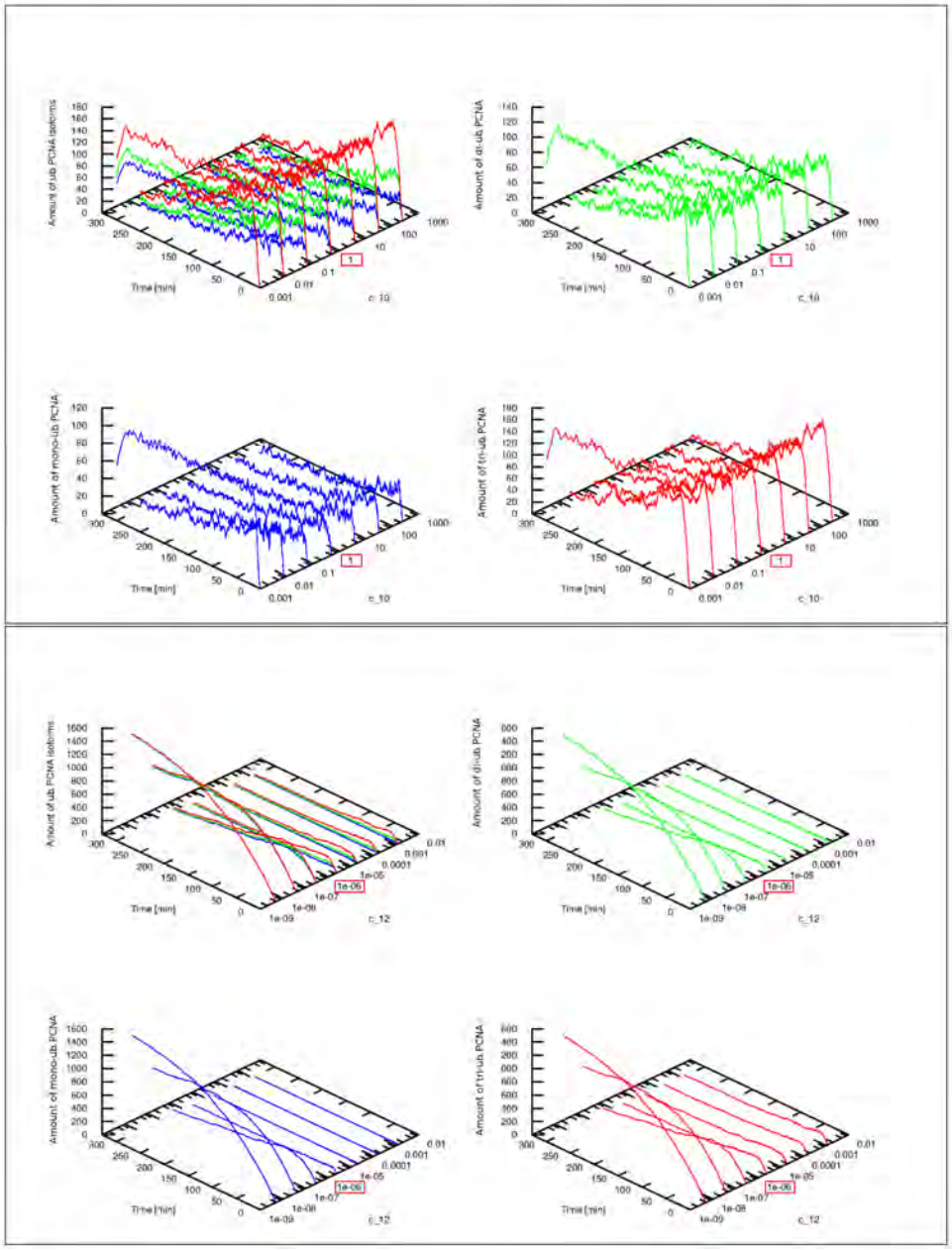

ADDITIONAL FILE 12

Effects of the modulation of the formation of di-ubiquitylated (reaction constant c_{16}) and of tri-ubiquitylated (reaction constant c_{22}) PCNA isoforms

The figure shows the simulated dynamics of the ubiquitylated PCNA isoforms resulting from two PSA, the first executed on the value of the reaction constant that modulates the formation of di-ubiquitylated PCNA isoform (top frame), and the second one executed on the reaction constant related to the formation of tri-ubiquitylated PCNA isoform (bottom frame). All simulations were executed assuming an UV dose equal to 10 J/m^2.

The two varied parameters and the corresponding sweep ranges are: (1) constant c_{16} within the interval $[5 \times 10^{-5}, 50]$; (2) constant c_{22} within the interval $[5 \times 10^{-6}, 5]$. The dynamics corresponding to the reference values (see Table 5) are marked with a red box.

For values of reaction constant c_{16} lower or equal to 1×10^{-3} we observe an accumulation of mono-ubiquitylated PCNA, since the rate of formation of di-ubiquitylated PCNA is very low. Conversely, for higher values of this constant, the resulting dynamics are comparable to the reference one.

At very low values of reaction constant c_{22} (equal or lower than 1×10^{-4}), the tri-ubiquitylated PCNA isoform accumulates in the system, pushing the amount of the other two isoforms around zero. By lowering constant c_{22}, the system reduces the production of the complex $PCNA_{on}{:}U{:}U{:}U$; however, the high signal of tri-ubiquitylated PCNA isoform is due to the accumulation of $Rad5{:}PCNA_{on}{:}U{:}U{:}U$, whose level, in turn, rises because this complex cannot undergo degradation. On the other hand, higher values of constant c_{22} result in a dynamics comparable to the reference one, probably for the combined interplay with reaction 25.

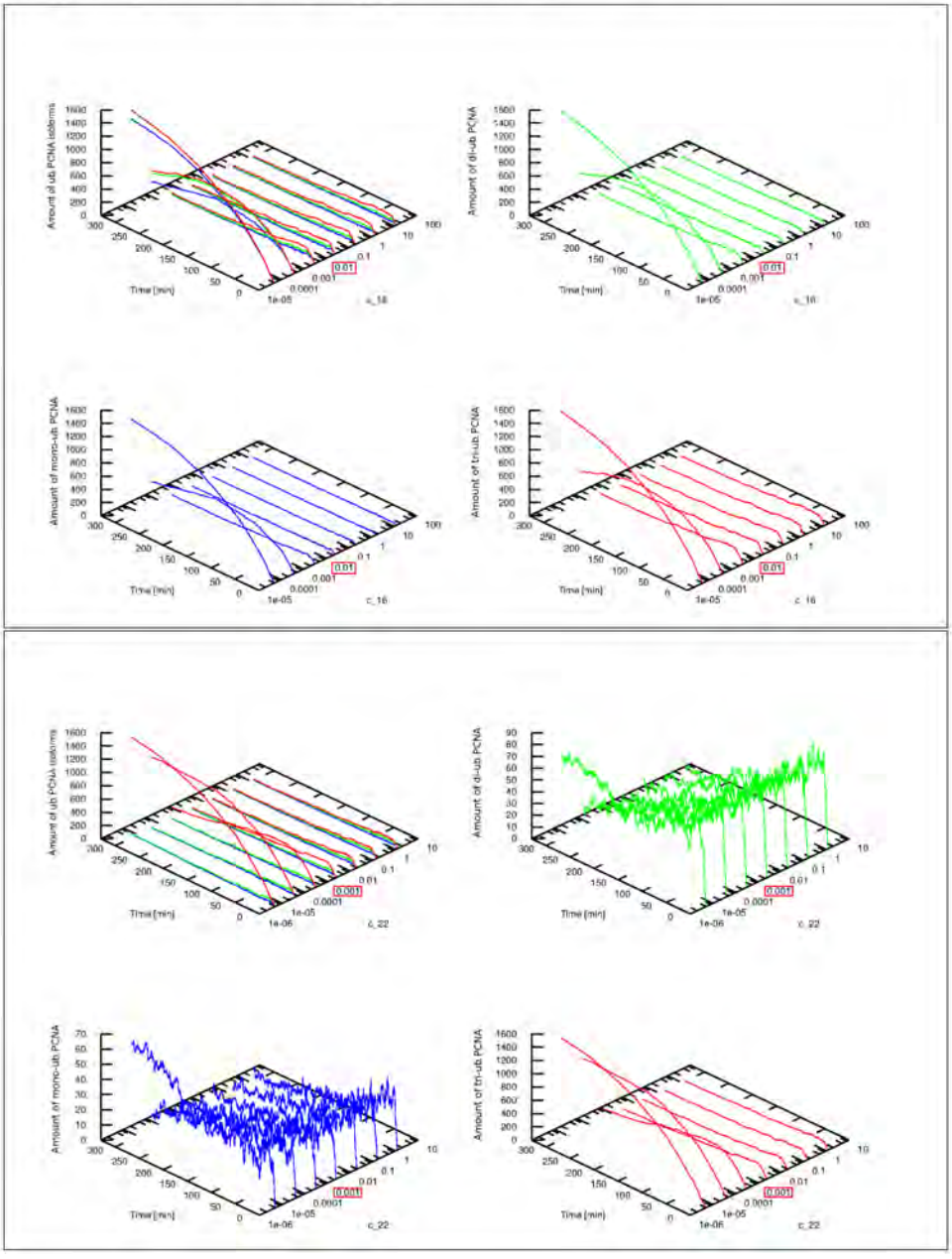

ADDITIONAL FILE 13

FACS analysis of wild type and *rad14*Δ background cells irradiated at 10 J/m^2 UV dose

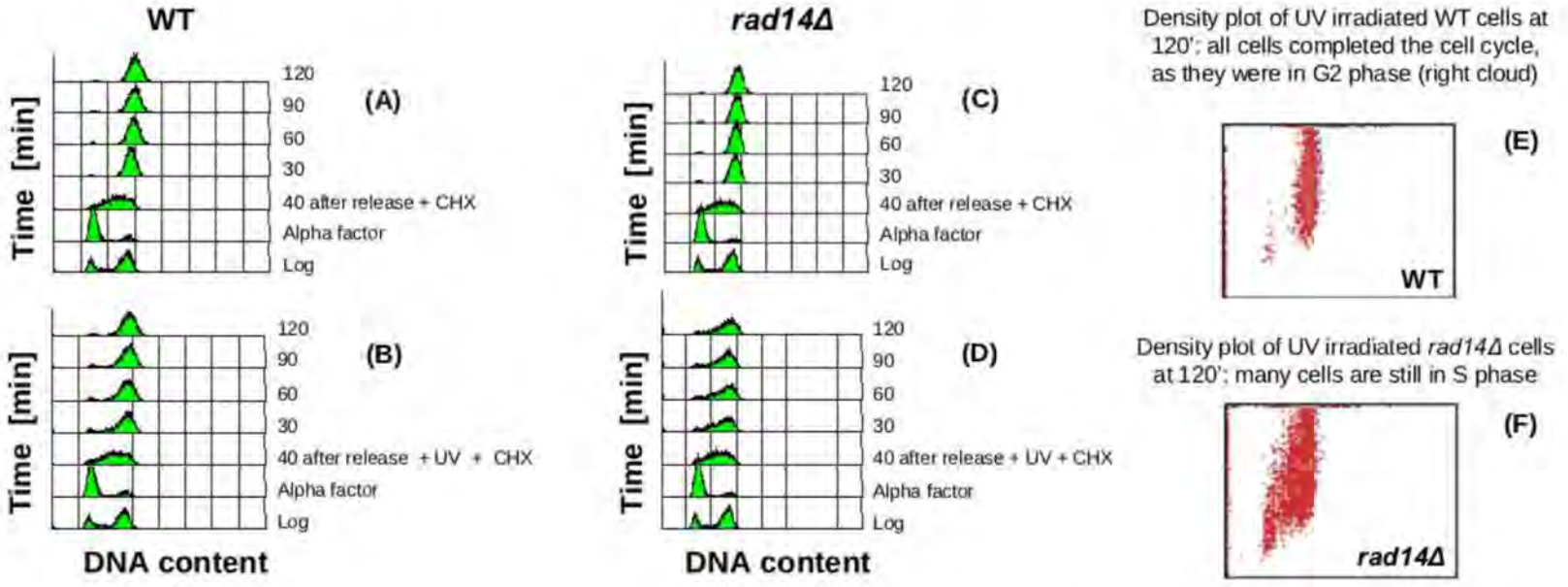

WT and *rad14*Δ cells were synchronized through 6 μg/ml of alpha factor. Cells were released in liquid medium till more than 80% of both cell populations were in S phase (about 30 minutes). Cells were then harvested and half of both populations were UV irradiated at 10 J/m^2 and released in liquid medium plus 10 μg/ml of CHX, while the other half was released in liquid medium plus 10 μg/ml of CHX without UV irradiation. Non irradiated cells of both populations completed the cell cycle within two hours (**A** and **C**) and UV irradiated WT cells completed the cell cycle with no difficulties (**B** and **E**). On the contrary, S phase UV irradiated *rad14*Δ cells had many troubles to complete the cell cycle and at two hours after UV irradiation many of them were still in S phase (**D** and **F**).
This experiment shows that UV irradiated *rad14*Δ cells in S phase show the same defect of UV irradiated *rad14*Δ cells in G1 phase [1], suggesting that NER must "clean" the genome from UV adducts also in S phase for the completion of DNA replication.

[1] Neecke H, Lucchini G, Longhese M: **Cell cycle progression in the presence of irreparable DNA damage is controlled by a Mec1- and Rad53-dependent checkpoint in budding yeast.** *EMBO J* 1999, 18(16):4485–97.